Exp 531

MEASUREMENT OF THE LIFETIMES OF THE CHARMED D^+, F^+ MESONS AND Λ_c^+ CHARMED BARYON

DISSERTATION

Presented in Partial Fulfillment of the Requirements

for the Degree of Doctor of Philosophy

in the Graduate School of The Ohio State University

By

Steven Michael Errede, B.Sc., M.Sc.

* * * * * * * * * * * * * *

The Ohio State University

1981

Reading Committee:

Katsumi Tanaka

Noel R. Stanton

Neville W. Reay

Approved By:

Neville W. Reay

Advisor

Department of Physics

AAB2019

MEASUREMENT OF THE LIFETIMES OF THE CHARMED D^+, F^+ MESONS

AND Λ_c^+ CHARMED BARYON

By

Steven Michael Errede, Ph.D.

The Ohio State University, 1981

Professor Neville W. Reay, Advisor

An experiment was performed in the 350 GeV wide-band neutrino beam at the Fermi National Accelerator Laboratory using a high-precision, high-efficiency hybrid emulsion/neutrino spectrometer, with which the mean lifetimes of the D^+, D^0 and F^+ mesons and Λ_c^+ baryon were measured.

1829 neutrino interactions were reconstructed with a vertex within the emulsion fiducial volume, 1242 of which were subsequently found in the emulsion. In 49 of the found neutrino events a charmed particle, produced at the primary vertex was observed to decay within the emulsion volume.

The mean lifetimes of charmed particles were determined from the reconstructed decays of 5 D^+, 15 D^0, 3 F^+ mesons: and 8 Λ_c^+ baryons:

$$\tau_{D^+} = 10.3^{+10.3}_{-4.2} \times 10^{-13} \text{ sec}$$

$$\tau_{D^0} = 2.3^{+0.8}_{-0.5} \times 10^{-13} \text{ sec}$$

$$\tau_{F^+} = 2.0^{+1.8}_{-0.8} \times 10^{-13} \text{ sec}$$

$$\tau_{\Lambda_c^+} = 2.3^{+1.0}_{-0.6} \times 10^{-13} \text{ sec}$$

The charmed particle masses measured in this experiment were:

$$M_{D^+} = 1851 \pm 20 \text{ MeV}/c^2$$

$$M_{D^0} = 1856 \pm 15 \text{ MeV}/c^2$$

$$M_{F^+} = 2042 \pm 33 \text{ MeV}/c^2$$

$$M_{\Lambda_c^+} = 2265 \pm 30 \text{ MeV}/c^2$$

A candidate event for the production and decay of a long-lived neutral charmed baryon was observed, with a decay mode, mass and lifetime of

Decay Mode	Mass (MeV/c^2)	Decay Time ($\times 10^{-13}$ sec)
$NB \rightarrow p\pi^- K_S^0$	2450 ± 15	77.2 ± 0.9
	or	
$NB \rightarrow pK^- K_S^0$	2647 ± 11	83.4 ± 0.9

The probability of this event being due to background nuclear interactions is less than 3.1×10^{-4} events.

ACKNOWLEDGEMENTS

It is difficult within the confines of a few pages, to do honorable justice and thank all those who have helped me to arrive at this point in my life, and also those who contributed (directly and indirectly) to the sucess of this experiment. It stands without question that none of this would have been possible without the total human effort of all people involved; in particular I wish to thank all of the members of the E-531 collaboration (whose names are listed below); I also wish to thank the neutrino department and accelerator division at Fermilab for the support given during the course of this experiment, and the U.S. Department of Energy and the National Science Foundation for the funding of this endeavor.

However, I wish to especially thank my advisor, Bill Reay, who through his guidance, expertise and wisdom has helped me to grow in a multitude of ways, teaching me many valuable lessons in experimental physics and instilling in me a much greater appreciation for the art and rigors of making a physical measurement. I will use the knowledge gained from him as a sound experimental foundation on which to continue to grow.

I wish to thank Ron Sidwell for his guidance and encouragement throughout the analysis of the data for this experiment. His positive suggestions and constructive criticism were of great help in the completion of this thesis.

I wish to thank Noel Stanton, Kurt Reibel, Jim Prentice, Taek Soon Yoon and John Trischuk for their efforts on behalf of my education while on this experiment. I have enjoyed interacting with them and also learning from them much experimental physics during this period.

Special thanks go to David Bailey, Taka Kondo, Mike Gutzwiller, Dale Pitman, Shuichi Kuramata, Phil Davis, Sergio Conetti, Jean Fischer, Steve Bracker and John Martin for many hours of enjoyable interactions, discussions and pleasantries.

I wish to thank Profs. Kiyoshi Niu, Osamu Kusumoto and Goro Fujioka for their kind hospitality while I was visiting Japan, and also Jacques and Joan Hebert for their hospitality while I was visiting Ottawa. I also wish to thank Kimio Niwa, Kaoru Hoshino, Hiroshi Fukushima, Toshio Hara, Hiroshi Shibuya, and Yutaka Noguchi as well as Chiaki Yokoyama, T.Omori and Motoaki Miyanishi for many memorable and enjoyable experiences and discussions. I wish to thank my advisor for his kind permission to go to Ottawa and to Japan for the purposes of the measurement of Event 671-8147 and discussion of the data from the first run of E-531. As a consequence of these visits, I have a much greater understanding, appreciation and respect for the emulsion of this experiment, and for the hard work and the skill of the "emulsionists".

I thoroughly enjoyed working under the expert direction of Chuck Rush and the people in the electronics lab at OSU during the early stages of this experiment on the drift chamber electronics, and with the OSU technicians, particularly Nino Richards, on the construction of the upstream drift chambers. I enjoyed many stimulating conversations with John Heimaster concerning the intricacies of the drift chamber readout, amongst many other topics.

Likewise, I very much enjoyed working with Paul Gallo, Tony Kiang and Chuck Serritella.

Much appreciation and thanks goes to Gavin Stairs for the design and construction of the drift chamber and emulsion stands.

Much appreciation and thanks goes to the professional skills and expertise of the Fermilab surveyors; I especially wish to thank Dick Hunckler and Tom Schuhow for excellence in their efforts.

Much appreciation and thanks goes to Barry McLeod for his excellence in design and construction of the emulsion processing facility at Ottawa, and for his efforts in the mass quantities of emulsion processing.

The sucess of this experiment is in no small way due to them.

For the analysis part of this experiment, I wish to thank Greg Donaldson (SLAC) for providing us with DELCO and Mk.II data on the likelihood functions for the D^+ D^0 lifetime ratios, and Jim Hanlon (IIT) for providing us with E-545 data on the neutrino event rate at the 15' B.C. for the 350 GeV horn-focussed neutrino beam.

I wish to thank Profs. Chris Quigg (FNAL), Harry Lipkin (FNAL, ANL, Weitzmann Inst.), Jonathan Rosner (Univ. Minn.) Shuzo Ogawa and Shoji Sawada (Nagoya Univ.) for many useful, elucidating and enjoyable discussions regarding the neutral charmed baryon candidate (Event 635-4949), and also the rest of the data from this experiment.

I also wish to thank Profs. Chris Quigg and Bj. Bjorken and also Lou Voyvodic for much help and encouragement during the time I have been at Fermilab.

Thanks go to Elaine Moore for her word processing expertise in the typing of this thesis, and to Robin Sidwell for her expertise in the technical drawing sector.

Finally, I wish to thank my wife, Deborah Mills Errede for her support, patience and understanding over the past year. Her steadfast love and encouragement helped bring this "marathon" to completion.

Members of the E-531 Collaboration

Aichi University:	N.Ushida
Fermilab:	T.Kondo
Kobe University:	G.Fujioka, H.Fukushima, Y.Takahashi, S.Tatumi, C.Yokoyama, Y.Homma, Y.Tsuzuki
Korea University:	S.Bahk, C.Kim, J.Park, J.Song
McGill University:	D.Bailey, S.Conetti, J.Fischer, J.Trischuk
Nagoya University:	H.Fuchi, K.Hoshino, M.Miyanishi, K.Niu, K.Niwa, H.Shibuya, Y.Yanagisawa
Ohio State University:	S.Errede, M.Gutzwiller, S.Kuramata, N.W.Reay*, K.Reibel, T.A.Romanowski, R.A.Sidwell, N.R.Stanton
Okayama University:	K.Moriyama, H.Shibata
Osaka City University:	T.Hara, O.Kusumoto, Y.Noguchi, M.Teranaka
Osaka City Prefecture:	H.Okabe, J.Yokota
University of Ottawa:	J.Harnois, C.Hebert, J.Hebert, S.Lokanathan, B.McLeod
Institute for Cosmic Ray Research, (Tokyo)	S.Tasaka
University of Toronto:	P.Davis, J.Martin, D.Pitman, J.D.Prentice, P.Sinervo, T.S.Yoon
Yokohama National University	H.Kimura, Y.Maeda

* Spokesperson

VITA

December 24, 1952	Born - Newark, N.J., USA.
June,1975	B.Sc., with distinction University of Minnesota
Fall,1975	Graduate Teaching Assistant The Ohio State University
Fall,1977	Graduate Research Associate The Ohio State University
Fall,1977	M.Sc. The Ohio State University
August,1981	Ph.D. The Ohio State University High Energy Physics

TABLE OF CONTENTS

Page

ACKNOWLEDGEMENTS ii

VITA vi

LIST OF TABLES xii

LIST OF FIGURES xiv

INTRODUCTION 1

Chapter

I. EXPERIMENT E-531 4

1. Experimental Pre-History 4

2. Motivation for Experimental Apparatus 6

3. The Single Horn Wide-Band Neutrino Beam 7

4. Spatial-Temporal Requirements for the Detector .. 8

5. The Emulsion Target 11

6. The Anti-Coincidence Counters 13

7. The Time of Flight (TOF) System 14

8. Particle Identification 16

9. The Drift Chambers 17

10. The SCM-104 Magnet 22

11. The Lead Glass Array 25

12. The Hadron Calorimeter 27

13. The Muon Counters and Muon Identification 29

14. Data-Taking on Experiment E-531 30

15. The Trigger Electronics and Data Aquisition 32

16. The On-line Equipment Monitoring System 34

TABLE OF CONTENTS

II. DATA ANALYSIS
DETERMINATION OF CHARMED PARTICLE LIFETIMES

1. A Brief Overview 35

2. Charged Particle Track and Vertex Reconstruction 36

3. Event Finding in Emulsion 40

4. Charm Search; Scanning Criteria 44

5. Charm Decay Scanning Efficiencies 45

6. Discussion of Event Finding and Charm Search ... 51

7. Calculation of Nuclear Interaction Backgrounds . 52

8. Charmed Particle Event Reconstruction 58

9. Momentum Measurement and Particle Identification in Emulsion 61

10. Kinematic Fits to Charmed Particle Decays 62

11. Calculation of Particle Mean Lifetimes 65

12. Charm Candidate Event Sample 67

13. Determination of the D^+ Lifetime 69

14. Determination of the F^+ Lifetime 75

15. Determination of the Λ_c^+ Lifetime 78

16. Ambiguous Charm Decay Candidates 80

III. LONG-LIVED NEUTRAL CHARMED BARYON CANDIDATE
Event 635-4949 NB $\rightarrow p\ \pi^-K^-K_s^0$ 89

IV. SUMMARY OF EXPERIMENTAL RESULTS 105
Discussion of Experimental Results 107

V. CONCLUSIONS 113

TABLE OF CONTENTS

APPENDIXES 114
A. Charm Candidate Events 114

D^+ Decay Candidates 115

Event 512-5781 $D^+ \rightarrow K^-\pi^+\underline{\pi}^+\pi^0$ 115

Event 546-1439 $D^+ \rightarrow K^-\pi^+\underline{\mu}^+(\nu_\mu)$ 115

Event 580-4508 $D^- \rightarrow \underline{K}^+\pi^-\underline{e}^-(\bar{\nu}_e)$ 116

Event 598-1759 $D^+ \rightarrow K^-K^+\underline{\pi}^+\underline{\pi}^0$ 117

Event 663-7758 $D^+ \rightarrow K^-\underline{e}^+\pi^+(\nu_e)$ 118

F^+ and Λ_c^+ Background in D^+ Decays 119

F^+ Decay Candidates 121

Event 527-3682 $F^- \rightarrow \underline{\pi}^+\underline{\pi}^-\pi^-\underline{\pi}^0$ 121

Event 597-1851 $F^+ \rightarrow \underline{K}^+\underline{\pi}^+\underline{\pi}^-K_L^0$ 122

Event 638-9417 $F^+ \rightarrow \underline{K}^+K^-\pi^+\underline{\pi}^0$ 123

Λ_c^+ Decay Candidates 124

Event 476-4449 $\Lambda_c^+ \rightarrow \underline{p}\ \underset{\sim}{\pi}^+\underset{\sim}{\pi}^-(K_L^0)$ 124

Event 498-4985 $\Lambda_c^+ \rightarrow \underline{\Lambda}^0\underline{\pi}^+\underline{\pi}^-\underline{\pi}^+$ 125

Event 499-4713 $\Lambda_c^+ \rightarrow \underline{\Sigma}^0\pi^+$ 125

Event 549-4068 $\Lambda_c^+ \rightarrow \underset{\sim}{p}\ K^-\underset{\sim}{\pi}^+(\pi^0)$ 126

Event 567-2596 $\Lambda_c^+ \rightarrow \underline{p}\ K_L^0$ 127

Event 602-2032 $\Lambda_c^+ \rightarrow \underline{p}\ \underset{\sim}{\pi}^+\underset{\sim}{\pi}^-(K_S^0)$ 127

Event 610-4088 $\Lambda_c^+ \rightarrow \underline{\Lambda}^0\underline{\pi}^+\underset{\sim}{\pi}^-\underset{\sim}{\pi}^+$ 128

Event 650-6003 $\Lambda_c^+ \rightarrow \underline{\Lambda}^0\underline{\pi}^+\underset{\sim}{\pi}^-\underset{\sim}{\pi}^+$ 128

Calculation of Nuclear Interaction Backgrounds
for Charmed Baryons Produced
in Neutrino Interactions 130

TABLE OF CONTENTS

Ambiguous Charm Decay Candidates 132

Event 493-1235 $D^+ \to \pi^+\pi^+\pi^-K_L^0$,

$F^+ \to \pi^+\pi^+K^-K_L^0$, $\Lambda_c^+ \to \pi^+\pi^-K^-n$ 132

Event 502-354 $Y^{++} \to \underline{\Lambda}^0\pi^+h^+\pi^0(\pi^0)$

$\Sigma_c^{++} \to \Lambda_c^+\pi^+$, $\Lambda_c^+ \to \underline{\Lambda}^0\pi^+\pi^0(\pi^0)$ 132

Event 522-2107

$D^+ \to \pi^+\underline{\pi}^+K^-(\pi^0)$, $F^+ \to K^+\underline{\pi}^+K^-(\pi^0)$

$\Lambda_c^+ \to p\underline{\pi}^+K^-(\pi^0)$ 133

Event 529-271 $D^+ \to \pi^+\pi^0(K_L^0)$,

$F^+ \to K^+(K_L^0)$, $F^+ \to K^+\pi^0(K_L^0)$ 134

Event 533-7152 $D^+ \to \pi^+\pi^0(K_L^0)$, $F^+ \to K^+(K_L^0)$ 134

Event 547-3192 $F^+ \to \pi^+\pi^-\pi^+(\pi^0)$ 134

Event 563-5269 $D^+ \to \pi^+(K_L^0)$, $F^+ \to K^+(K_L^0)$ 135

Event 656-2631 $D^+ \to \pi^+K^-\pi^+\pi^0$,

$F^+ \to K^+K^-\pi^+\pi^0$, $\Lambda_c^+ \to p\,K^-\pi^+$ 135

Event 665-2113 $D^+ \to \underline{\pi}^+\underset{\sim}{\pi}^-\underset{\sim}{\pi}^+(K^0)$ 136

$F^+ \to \underline{\pi}^+\underset{\sim}{\pi}^-\underset{\sim}{\pi}^+(\pi^0)$, $\Lambda_c^+ \to \underline{\pi}^+\underset{\sim}{\pi}^-\underset{\sim}{\pi}^+(\Lambda^0)$

Event 665-4023 $C^+ \to h^+h^-h^+(?)$ 137

Event 670-12 $\Lambda_c^+ \to K^+p\pi^-(\pi^0)$ 137

Event 671-2642 $D^+ \to \underline{\pi}^+K^-\pi^+(\pi^0)$

$F^+ \to \underline{\pi}^+\pi^-\pi^+(\pi^0)$, $\Lambda_c^+ \to \underline{\pi}^+\pi^-\pi^+(\Lambda^0)$ 138

TABLE OF CONTENTS

B. Charged Charm Candidate Event Summary Sheets 139

C. Summary of Kinematic Fits of π^0 Observed in Charmed Particle Decays 143

D. summary of Kinematic Fits of Λ^0 and K^0_S Observed in Charmed Particle Decays 144

E. Investigation of Systematic Shifts in Kinematic Fits of Charmed Particle Decays 145

LIST OF REFERENCES 147

LIST OF TABLES

Table	Title	Page
1.	Drift Chamber and Emulsion Target Survey: Spatial Resolution	10
2.	Charged Particle Background in Emulsion	41
3.	Charged Decay Scanning Efficiencies	50
4.	Neutral Decay Scanning Efficiencies	50
5.	Summary of Emulsion Scanning Results	57
6.	Summary of D^+ Decay Candidates	70
7.	Summary of D^+ Kinematic Fits	70
8.	Summary of F^+ Decay Candidates	76
9.	Summary of F^+ Kinematic Fits	76
10.	Summary of Λ_c^+ Decay candidates	79
11.	Summary of Λ_c^+ Kinematic Fits	79
12.	Summary of Ambiguous Charm Decay Candidates (Constrained Events)	82
13.	Summary of Kinematic Fits of Ambiguous Charm Decays (Constrained Events)	82
14.	Summary of Ambiguous Charm Decay Candidates (Unconstrained Events)	86
15.	Summary of Kinematic Fits for Event 635-4949	91
16.	Composition and Nuclear Activity of Fuji ET-7B Emulsion	94
17.	Kinematic Variables for Event 635-4949	98

LIST OF TABLES

18. Nuclear Interaction Background Calculation for Charmed Baryons 130

19. Summary of π^0 Kinematic Fits 143

20. summary of Λ^0 and K^0_S Kinematic Fits 144

21. Monte Carlo Results of Kinematic Fits 145

22. Investigation of Systematic Shifts in Kinematic Fits 146

23. Charmed Candidate Event Summary Sheets 222

LIST OF FIGURES

Figure	Title	Page
1.	Meson and Baryon SU(4) Multiplets	162
2.	Neutrino Production of Charm	163
3.	Plan and Elevation View of E-531	164
4.	The Fermi National Accelerator	165
5.	350 GeV Accelerator Cycle and Trigger Timing	166
6.	350 GeV Wide-Band Single Horn Neutrino Beam	167
7.	Neutrino Energy Spectrum, Charm Candidate Event Distribution	168
8.	Detail of Emulsion Target and Upstream Drift Chambers (Beam View)	169
9.	Detail of Emulsion Target and Emulsion Modules (Downstream View)	170
10.	Elevation View of Emulsion Target	171
11.	ΔX, ΔY of Tracks at Changeable Sheet	172
12.	TOF Counters	173
13.	TOF II Δt and ΔY for Muon Overlap Events	174
14.	TOF Particle Identification: $1+(m/P)^2$ vs. Momentum P	175
15.	Particle Mass from TOF	176
16.	Upstream Drift Chamber Cell Configuration	177
17.	Upstream Drift Chambers: Efficiency vs. E-Field	177
18.	Downstream Drift Chambers	178

LIST OF FIGURES

19. Drift Chamber Fast Amplifier/Discriminator 179

20. Drift Chamber Pulse Height Spectrum - Minimum Ionizing Muons 180

21. Drift Chamber Readout System Electronics 181

22. Drift Chamber Resolution 182

23. Lead Glass Array 183

24. Lead Glass Energy Response and Resolution 184

25. Lead Glass Pulse Height Spectrum, M-5 Tests, 30 GeV/c Negatives 185

26. Hadron Calorimeter 186

27. Hadron Calorimeter Response to Minimum Ionizing Muons 187

28. Muon Detection Array 188

29. ΔY of Back Muon Counters 189

30. Neutrino and Muon Trigger Electronics 190

31. Example of On-line Display of a Neutrino Interaction 191

32. Reconstructed Events vs. Z 192

33. Found Neutrino Events vs. Z 193

34. Event Finding Efficiency vs. Z 194

35. Charm Candidate ν-Event Distribution and Relative Charm ν-Event Finding Efficiency 195

36. Predicted vs.Found Events: Vertex Localizations 196

LIST OF FIGURES

37. Charged Track Following Efficiency (Horizontal Emulsion) 197

38. Track Reconstruction Efficiency vs. Emission Angle 198

39. Angular Distribution of Minimum Ionizing Background Tracks in Emulsion 199

40. NH and NS Distributions for Neutrino Events ... 200

41. Emulsion Track Angular Resolution 201

42. Charged and Neutral Charm Decay Scanning Efficiencies; Flight Lengths of Charmed Particles 202

43. Charm Production Angle 203

44. I/I_0 vs. $P\beta$ 204

45. χ^2, C.L., ΔPx, ΔPy, ΔP Distributions for Charm Decays 205

46. Charmed Particle Masses 206

47. Photo-Micrographs of Event 546-1339 and Event 527-3682 207

48. -1 C Curves for Events With a Missing Neutral 208

49. F^+ Background for Semi-leptonic D^+ Decays: $F^+ \rightarrow \pi^+\pi^-\ell^+(\nu_\ell)$ Decay Diagrams 209

50. D^+, D^0, F^+, Λ_c^+ ln $\mathscr{L}(\tau)$ vs. τ 210

51. D^+, D^0 Lifetime Ratio: 1 and 2 S.D. Contours 211

52. Likelihood Function $\xi(R)$ for D^+, D^0 Lifetime Ratio 212

LIST OF FIGURES

53. Likelihood Functions $\xi(R)$ for D^+, D^0 Lifetime Ratio: Mk.II and DELCO 213

54. Combined Likelihood Functions $\Xi(R)$ for D^+, D^0 Lifetime Ratio: E-531 and Mk.II; E-531, Mk.II and DELCO. 214

55. Λ_c^+ Decay: $\Lambda^0-\pi^\pm$, $(p-\pi^\pm)(K^{\pm,0}-\pi^\pm)$ Mass Combinations 215

56. $\Lambda_c^+-\pi^{\pm,0}$ Mass combinations 215

57. Event 635-4949 216

58. -1 C Curve for $V^0 \rightarrow p\pi^-$(V1-V2) 217

59. ΔPx, ΔPy vs. $Mv^0(Pv^0)$ 218

60. ϕ of Decay Particles 219

61. Charmed Particle Momentum Spectrum 220

62. Weak Decays of Charmed Mesons and Baryons 221

INTRODUCTION

Throughout the history of particle physics, determination of the lifetimes of unstable particles has played an important role in the advancement of man's understanding as to the nature of the fundamental interactions between elementary particles, and how such interactions are responsible for their decay.

The canonical example of such a role is the discrepancy between the theoretical [1] and measured [2,3] π^0 lifetime, which differ by a factor of nine unless "color" (the concept of strong charge quantization) is incorporated in the theory.

$$\Gamma^{thy}(\pi^0 \to \gamma\gamma) = 7.87(N_c/3)^2 \text{ (eV)}$$

$$\Gamma^{exp}(\pi^0 \to \gamma\gamma) = 7.95 \pm 0.05 \text{ (eV)}$$

Where N_c is the number of colors.

Another outstanding example is neutral K_L^0, K_S^0 meson system, which have lifetimes of [160]:

$$\tau_{K_L^0} = 5.183 \pm 0.040 \times 10^{-8} \text{ sec}$$

$$\tau_{K_S^0} = 0.892 \pm 0.002 \times 10^{-10} \text{ sec}$$

The prediction of the existence of two particle states with (almost) degenerate mass and opposite parities, composed of orthogonal linear combinations of (equal) amounts of K^0, $\bar{K}^0$ [4], and the subsequent discovery of the K_L^0 in 1956 [5], set the stage for the prediction [6] and discovery [7] of parity violation in the weak interactions in 1957 and the discovery of CP violation in the K^0- $\bar{K}^0$ system in 1964 [8,9].

The concept of weak mixing between mass eigenstates has been of fundamental importance in the understanding of the $K^0 - \bar{K}^0$ system, and has formed the theoretical basis for all mixing phenomena (e.g. mixing between the d, s, and b quarks [10,11,187]; the conjectured mixing between ν_e, ν_μ and ν_τ neutrinos [12-16]; and neutron - anti-neutron oscillations, as predicted by some grand unified theories of quark-lepton unification [17-19]).

From the prediction of charm in 1964 by J.D.Bjorken and S.L.Glashow as "a new quantum number, violated only by the weak interaction" [20], many new particle states were expected, consisting of a charmed quark, c , in combination with lighter u, d and s quarks. The classic 1974 paper on charm by M.K.Gaillard, B.W.Lee and J.L.Rosner enumerated these states [21], as shown by the SU(4) weight diagrams in Fig.1 for the lowest-lying meson ($q\bar{q}$) and baryon (qqq) particle states. The spin-0 charmed iso-doublet D^+, D^0 mesons are composed of $c\bar{d}$, $c\bar{u}$ quark-antiquark pairs, respectively, while the iso-singlet F^+ meson is composed of a $c\bar{s}$ pair. Charmed baryons are composed of cqq quark triplets, e.g. the Λ_c^+ is composed of cud quarks in an iso-singlet spin 1/2 state.

The existence of charm as described by the Weinberg-Salam model of electro-weak interactions [22-24], along with the GIM mechanism [25] explained many phenomena not previously understood in the framework of the SU(3) quark model, such as the $K_L^0 - K_S^0$ mass difference [26,35], and the apparent absence of strangeness-changing neutral currents in weak interaction processes (the measured decay rates of $K_L^0 \to \mu^+\mu^-$ [27,28] and $K^+ \to \pi^+\nu_\ell\bar{\nu}_\ell$ [29] were found to be significantly less than those from SU(3) predictions [30-34]).

One of the characteristic signatures for the production and decay of charm is that, as a fundamental quantum number, only the weak interaction is responsible for the "transmutation" of charm (via the weak charged current) to other lighter (s and d) quarks. Hence, as a consequence of the nature of the weak interactions, the lifetimes of charmed particles were expected to be long (compared to lifetimes associated with strong interactions, $\mathcal{O}(10^{-22}$ sec). Early calculations [20,21,36-40] for the lifetimes of charmed particles were on the order of few $\times 10^{-13}$ sec based on "naive" free quark decay calculations and estimates of the charmed quark mass, as determined from the $K_L^0 - K_S^0$ mass difference [35].

$$\Gamma(c \to s\alpha\bar{\beta}) \simeq \frac{G_F^2}{192\pi^3} M_c^5 \qquad \alpha\bar{\beta} = q\bar{q}' \text{ or } \ell_\ell^+\nu$$

$$\Gamma^{tot} = \Gamma(c \to \text{all}) = 2\Gamma_{SL} + 3\Gamma_{NL}$$

(for 2 leptons e, μ and three quark colors)

For Mc = 1.5 GeV/c , the lifetime for charm is

$$\tau_{charm} = 1/\Gamma^{tot}_{charm} \simeq 5\text{-}6 \times 10^{-13} \text{ sec}$$

with a predicted semi-leptonic branching ratio of 20%.

Thus, for lifetimes in this range, it was expected that the decays of charmed particles would be capable of being visibly observed [21,42]; for charmed particle momenta of a few GeV/c, corresponding flight lengths on the order a few hundred microns were anticipated, since $L = \gamma\beta c\tau = pc\tau/M$.

In addition, differences in the lifetimes of the various charmed particles were expected by some authors [21,41-44]. In particular, the D^+ lifetime was expected to be longer than the other charmed D^0 and F^+ mesons on the basis of the structure of the effective weak non-leptonic Hamiltonian for charmed meson decay, due to the (renormalization) effects of the strong interactions upon the weak decay process [21,35-37,41-44].

CHAPTER I

EXPERIMENT E-531

EXPERIMENTAL PRE-HISTORY

The first candidate for the production and decay of particles carrying the quantum numbers of charm was observed in 1971 by K. Niu et al. in a cosmic ray-emulsion chamber experiment [45]. The decay times were measured to be 2.2 and 3.6 x 10^{-14} sec with masses on the order of 2 GeV/c . Immediately thereafter, this event was interpreted as the associated production and decay of a pair of charged charmed particles by T. Hayashi et al. [46]. By 1975, ten candidate charm decays had been reported in cosmic ray emulsion exposures [47,48].

An interesting historical comment here is that earlier evidence for charm production in high energy cosmic ray interactions existed in the literature; however the two events, one observed in 1951 by M. Kaplon et al. [49], and the other in 1956 by K. Nishikawa [50] were not then understood to be due to (associated) charm production. They were subsequently re-analyzed by S. Kuramata et al. and found to be consistent with charm production [51,52].

In November 1974 the ψ/J was simultaneously discovered at Brookhaven, by J.J.Aubert et al.[53] and at SPEAR, by J.E.Augustin et al. [54]. The mass and the width of the ψ/J were consistent with the characteristics expected for a meson with "hidden" charm, i.e. a meson composed of a $c\bar{c}$ pair. Conclusive evidence for the existence of charm came with the observation of the D^{+}, D^{0} mesons in the Mk.I detector at SPEAR in the spring of 1976 [55-58].

Soon after the discovery of the ψ/J other experimental evidence for the existence of (naked) charm was seen. In a bubble chamber experiment, an apparent violation of the $\Delta S = -\Delta Q$ rule was observed in one event [73]; opposite sign di-lepton ($\mu^{-}\mu^{+}$ and $\mu^{-}e^{+}$) events were observed in neutrino interactions [101-104], along with the observation of associated strange particles in such events [71-75]; all of these phenomena were consistent with what was expected for the production and decay of charmed particles in neutrino interactions.

The first example of the visible (i.e. short track) production and decay of charm in neutrino interactions was observed in emulsions in the fall of 1976 by E.H.S.Burhop et al. at Fermilab (experiment E-247) [59]. Visible evidence for the production and decay of charm was also observed in interactions of 400 GeV protons in emulsion by several groups [60-62]. Two other experiments were performed at CERN; one a hybrid emulsion-bubble chamber ν-experiment (WA-17) [64-66], the second a hybrid emulsion-spectrometer photoproduction experiment (the Ω-spectrometer) [67-70], have also reported their results on visible charm production and decay. Other experiments with neutrino interactions in bubble chambers have observed further μμ, μe and associated strange particle phenomena [76-80,105-108]; along with evidence for D^+, D^0, Λ_c^+ and Σ_c^{++} production in neutrino interactions [81-84]. e+e- experiments [53-58,85,139-144], photoproduction experiments [86-91], hadro-production (p-p collision) experiments [92-95] and a streamer chamber experiment [95] have reported on various aspects of charm production, decay modes and masses of the D^+, D^0, F^+ and Λ_c^+, Σ_c^{++} baryons. Several bubble chamber experiments have reported observation of visible charm decays [97-100,232].

Three hybrid emulsion-spectrometer / bubble chamber experiments (E-531, E-553, E-564) ran simultaneously in the wide-band neutrino beam at Fermilab. Two of the three experiments have reported [109-116] preliminary results. With few exceptions, the events with visible decays of charmed particles observed in experiments prior to 1978 (and even after E-531) were not fully reconstructable, in that many of the charm decays had missing neutrals, and/or the experiments suffered from severe scanning biases, resulting in contradictory measurements for the mean lifetimes ranging from 10^{-14} sec [60]. to 10^{-12} sec [96-100] for the same species of charmed particle. Hence the great need for a definitive, unbiased determination of the mean lifetime for each species of charmed particle, the identity of which had to be known on an event-by-event basis. This was the purpose of experiment E-531.

MOTIVATION FOR EXPERIMENTAL APPARATUS

The wide-band neutrino beam at Fermilab was chosen for this experiment as charm was believed to be copiously produced in neutrino interactions (as much as 10% of the total charged-current cross-section) for neutrino energies well above charm threshold ($\sim$2-3 GeV). As stated earlier, neutrino-induced opposite sign di-lepton events were indicative of these expectations [71-80,101-108]. Production of charmed particles in neutrino interactions is believed to occur via processes as shown by the Feynman diagrams of Fig.2.

Nuclear emulsion was the natural choice for a target, as flight lengths of weakly decaying particles ranging from a few microns to a few centimeters are capable of being observed, corresponding to (proper) decay times of 10^{-15} to 10^{-10} secs, respectively. The use of a neutrino beam for the production of charmed particles was complementary to this choice of target; for neutrinos leave no trace of their passage through the emulsion target unless they interact. Hence the backgrounds for such an experiment are inherently low, the major sources of which are from cosmic rays, beam-associated muons and (low energy) neutrons.

To locate the neutrino interactions occurring within the emulsion target, over 2000 man-years would be required to search the entire target volume without the aid of external particle detectors. To minimize the scanning time required for finding events, twelve high precision drift chambers located downstream of the emulsion target were used to pinpoint the interaction vertex. To further augment event finding, a large-area emulsion "changeable sheet" (changed every few days during the experiment), located immediately downstream of the emulsion target, served as a low-background high-resolution detector, coupling drift chamber tracks to the events located in the emulsion. (It should be noted that world data for neutrino interactions in emulsion consisted of only a handful of events prior to E-531 [59,64-66].)

Additional information such as the momentum, charge and particle type were required for every particle produced in a given neutrino interaction. Therefore, the downstream detector was designed to perform not only as a high precision locating device, but also as a high-acceptance neutrino spectrometer. A wide-gap analyzing magnet, along with eight additional drift chambers for momentum analysis; a TOF (Time-Of-Flight) system for charged particle identification; a lead glass array (for detection of high-energy photons and electron identification); a

rudimentary calorimeter to measure hadronic energy, and two planes of scintillation counter hodoscopes embedded in steel for muon identification were thus incorporated into the detector to meet these requirements. Fig.3 shows the plan and elevation views of the experimental apparatus.

THE SINGLE HORN WIDE-BAND NEUTRINO BEAM

Protons were accelerated to 350 GeV in the main ring of the accelerator at Fermilab (Fig.4) and resonantly extracted at the end of the 7 sec machine cycle in a fast spill mode (1 msec FWBase), See Fig.5. The extracted protons were transported to the ν-target via a standard FODO (Focus-Open-Defocus-Open) system. The ν-target consisted of one interaction length (30 cm) of BeO, located 954 m upstream of the experiment. An average of 1.5×10^{13} protons were incident on the neutrino target per pulse. To increase the intensity of the neutrino beam, a (pulsed) magnetic horn located 5.3 m downstream of the neutrino target was used. Charged secondaries exiting from the ν-target with production angle greater than 1.8 mrad were focussed (de-focussed, depending on charge sign) by the single horn, run at an excitation current of 80 kA, providing a transverse momentum kick of 0.170 GeV/c [117,118].

The tertiary neutrino beam ($\sim 3.5 \times 10^9$ ν's/m^2 per pulse at the detector) was generated from the decay in flight of secondary pions and kaons in the 410 m long decay space downstream of the production target. (Thus the mean flight path for neutrinos to our emulsion target was 749 m.) The layout of the single horn wide-band neutrino beam is shown in Fig.6. The (Monte Carlo corrected) neutrino energy spectrum is shown in Fig.7. The neutrino energy peaks at approximately 25 GeV. The Monte Carlo corrections to the observed neutrino energy spectrum are small, except at low energies, where corrections of 3-4 are made to account for non-negligible thick target effects, multiple re-scattering within the horn, and the acceptance of the spectrometer at low energies. See Ref.[120] for further details.

Normally, the accelerator ran at 400 GeV energy. However, due to the proximity of the experiment to the production target, the stopping power of the earth and steel shielding in the neutrino berm was not sufficient to range out the background muons at 400 GeV. In order to be successful in finding neutrino interactions in the emulsion, and thus find the decays of charmed particles, an upper limit on the integrated muon flux of 50,000 muons/cm^2 for the emulsion target was set by the emulsion experts, based on past experience in scanning for events. Initial tests at

400 GeV measured unacceptably high muon fluxes in excess of of 6000 muons/m^2/pulse. Thus, the machine energy was lowered to 350 GeV, resulting in a factor of 13.3 reduction in the background muon flux ($\sim$450 muons/m^2/pulse) with only a 26% reduction in the neutrino event rate. The machine cycle time was reduced from 10.0 seconds to 7.0 seconds, resulting in improved machine reliability and an increase in the number of protons delivered to the neutrino target. Early on into the run, an additional 18.3 m of concrete shielding was installed upstream of our experiment, resulting in a further reduction of 2.0 in the background muon flux. A muon spoiler system, consisting of two large toroids and four small toroids (which covered the center holes of the large toroids), reduced the flux a factor of 3.0 from energy loss in the toroid mass, with an additional reduction in the muon flux of a factor of 2.2 when energized. Unfortunately, operation of the toroids resulted in an unacceptable increase in the muon flux at the 15' bubble chamber (5-60 μ's/m^2/10^{13} protons), and were therefore not used for two-thirds of the experiment.

SPATIAL-TEMPORAL REQUIREMENTS FOR THE DETECTOR

The key to the sucess of this experiment was in the ability to locate events in the emulsion. The equipment associated with event location and reconstruction was required not only to be highly accurate, but also mechanically and thermally stable. (The positions of each piece of apparatus were also required to be accurately known, especially the emulsion target and the drift chambers.) Hence the emulsion and drift chambers were mounted on a 3.5 ton, 1.5 m x 2.75 m x 0.3 m granite block/optical bench. The emulsion target, upstream and downstream drift chamber arrays were supported by precision aluminum stands bolted to the granite block as shown in Fig.8. The drift chamber and emulsion stands were designed to expand smoothly with fluctuations in the ambient temperature, in a controlled and measureable manner. The positions of the emulsion target and each drift chamber with respect to the surface of the granite block were continuously monitored throughout the data-taking via a LVDT (Linear Variable Differential Transformer) gauging system, having a (least count) spatial resolution of 15 μm. The ambient temperature and the emulsion temperature were continously monitored with solid state temperature sensors positioned at various locations on the emulsion target.

To minimize the degradation of spatial resolution due to the effects of thermal fluctuations, the ambient temperature was maintained at 20 ± 5°C with the emulsion target region maintained at 10.0 ± 2.5°C (via an air conditioner) throughout the experiment.

Considerable effort was expended in obtaining the necessary survey information for all of the equipment and detectors in the experiment, with particular attention given to the emulsion and drift chambers, to ensure that accurate and consistent spatial information was obtained. The accuracy with which this was achieved is summarized in Table 1.

The survey data for the drift chambers was input to a tuning program, which used muon straight-through tracks to obtain improved knowledge of the location of the drift chambers. The position resolution achieved via this method (125 μm) was sufficient to ensure high efficiency in finding events, and the data from the LVDT gauging system was therefore not used except as an "indicator" for the tuning program. The envelope of temporal variation of critical equipment, as measured by the LVDT sensors was less than 120 μm (FWHM) over the entire run.

The location of each emulsion module in relation to the changeable sheet was known through use of collimated Fe-55 X-ray sources embedded in the four corners of each emulsion module. Sixteen X-ray "guns" on the emulsion target mount coupled the changeable sheet directly to the drift chamber coordinate system with comparable resolution (See Figs.8, 9 and 10).

TABLE 1.

DRIFT CHAMBER and EMULSION TARGET SURVEY:
SPATIAL RESOLUTION

DRIFT CHAMBERS:	Resolution (FWHM)
Upstream drift chamber sense wires (relative to each other)	10 μm
Downstream drift chamber sense wires (relative to each other)	25 μm
Position of drift chambers (optical survey) (relative to support rods)	50 μm
Position of support rods (optical survey) (relative to granite block)	50 μm
Position of drift chamber planes (in beam direction)	250 μm
EMULSION TARGET:	
X-Y-Z of emulsion modules (relative to hexcell plate)	100 μm
Emulsion modules (X-ray) (relative to changeable sheet)	50 μm
Changeable sheet (X-ray) (relative to hexcel plate)	50 μm
Hexcel plate (optical survey) (relative to granite block)	50 μm

THE EMULSION TARGET

The emulsion target consisted of 22.9 liters (88.4 kg.) of Fuji ET-7B nuclear emulsion packaged in 42 modules, 39 of which were in position in the experiment at any given time during the running period. (Three modules were processed half-way through the run.) The emulsion modules were mounted on a precision-made aluminum hexcel plate, with the modules located downstream of the plate. The plate was supported by a precision stand, bolted to the surface of the granite block. The stand was designed such that the lower left-hand corner of the hexcel plate was fixed, while the other corners were free to expand transverse to the beam direction.

Horizontal and Vertical Emulsion Modules

Two types of emulsion modules were used in the experiment, 12 "horizontal" modules (9.1 liters, total volume) and 27 "vertical" modules (13.8 liters, total volume). Each horizontal emulsion module consisted of 188 pellicles of pure emulsion, 600 μm thick, exposed with the emulsion plane parallel to the beam direction. The vertical emulsion modules consisted of 68 sheets of emulsion, each sheet composed of a 70 μm thick polystyrene base coated on both sides with 330 μm of emulsion, exposed with the emulsion plane perpendicular to the beam direction. (See Figs.8, 9 and 10.)

The Changeable Sheet

The changeable sheet consisted of a 800 μm thick lucite base coated on both sides with 75 μm of emulsion, located immediately downstream of the emulsion modules. The purpose of the changeable sheet was to act as an ultra-high spatial resolution detector; single tracks from neutrino interactions in the emulsion modules were located on the changeable sheet from drift chamber predictions with a spatial resolution in X and Y (as shown in Fig.11) of

$$\Delta X^{CS} = -50\ \mu m \qquad \sigma^{CS}_{\Delta X} = 300\ \mu m$$

$$\Delta Y^{CS} = -150\ \mu m \qquad \sigma^{CS}_{\Delta Y} = 320\ \mu m$$

The X and Y offsets from predicted vs. found track coordinates are compatible with survey resolution although the Y offset, which is relatively large, may be due to a slight sagging of the changeable sheet with respect to the hexcel plate.

The observed spatial resolution of the drift chamber tracks at the changeable sheet is in good agreement with the quadrature sum (300 μm) of the intrinsic drift chamber resolution (125 μm), the projected spatial resolution at the changeable sheet (270 μm) from the angular resolution of the upstream drift chambers (0.6 mrad) and the emulsion measurement resolution (50 μm FWHM) (see below).

Track candidates found on the changeable sheet were followed into the vertical emulsion modules with high efficiency (96 ± 2%), with a spatial resolution of 50 μm (FWHM). Once a track was found on the changeable sheet (typically after 10 minutes of scanning time), the event would be found in the emulsion module within one hour, on average. Fig.10 demonstrates the use of the changeable sheet.

THE ANTI-COINCIDENCE COUNTERS

The anti counters were used in the experiment to prevent triggering the detector on interactions caused by charged particles present in the ν-beam, notably muons. The anti array consisted of seven scintillation counters, with an Amperex 56AVP phototube on each end, covering an area of 3.1 m^2, located 1.3 m upstream of the emulsion target as shown in Fig.3.

Due to the short distance of the anti counters from the emulsion target, the timing of the anti relative to the rest of the ν trigger had to be set extremely close to prevent loss of real neutrino events from the anti firing on "backsplash" (electrons and/or hadrons ejected backwards from ν-interactions). Backsplash occurred in approximately 15% of the neutrino triggers, as determined from TDC spectra for the anti counters from neutrino interactions.

Jitter in the anti counters due to the position of the hits in the paddles (8 nsec FWHM) was removed through the use of a Lecroy 624 octal meantimer.

The anti efficiency ($A \cdot \mu'/\mu'$) was 89 ± 1%, (less than unity due to dead time losses of 5 ± 1%, inefficiencies of 2 ± 1% and also geometrical losses of approximately 3 ± 1% due to wide angle tracks). The anti "overkill" ($A{:}\mu'/\mu'$) was 13 ± 2% during the experiment. The logical variable

$$\mu' \equiv TOF_{\geq 1}\ I \quad TOF_{\geq 1}\ II$$

The notation "." (":") denotes the logical AND with the two counters in (out) of time with each other.)

THE TIME OF FLIGHT SYSTEM

The TOF system served the dual purpose of triggering the rest of the detector on neutrino interactions and measuring the flight time of charged particles. Knowledge of a particle's path through the detector and its momentum (obtained from drift chamber track information) used in conjunction with TOF information allowed determination of particle type, as discussed in the next section.

The TOF system consisted of a single start counter, TOF I, located 15.5 cm downstream of the emulsion target, and a picket fence array, TOF II, consisting of thirty counters located downstream of the magnet, 2.84 m from the emulsion target. The constrcuction and dimensions of the TOF counters are given in Fig.12 (see also Fig.3). The TOF I counter was composed of Pilot-F scintillator, viewed by twelve RCA 8575 phototubes through 90° curved adiabatic light guides, 0.68 m^2 in area. The TOF II counters consisted of two types, 16 narrow counters 7.0 cm wide, and 14 wide counters 10.2 cm wide, overlapped 0.6 cm (0.2 cm) for the narrow (wide) counters. The TOF II counters were 1.5 m in length and 2.5 cm thick Pilot-F scintillator coupled to Amperex XP-2230 phototubes used in conjunction with Winston cones (the wide counters also used adiabatic light guides). The attenuation length for TOF I and both types of TOF II counters was 1.0 m The signals from the TOF counters were split in a 4:1 ratio, 1/5 to a 10-bit (1024 count) Lecroy LRS 2249A ADC (0.25 pC/count) and 4/5 to a 10-bit Lecroy LRS 2228A TDC (50 psec/count).

Considerable effort went into maintaining and monitoring the stability of the TOF system throughout the experiment. The ambient temperature was maintained to within ±5°C throughout the running period, to minimize phototube gain variations from temperature fluctuations. The (LRS R24 HV4032) high voltage power supplies used for the TOF system kept drifts in the phototube voltages to less than ±1 volt on each tube. The operating voltages in the TOF system were never changed during the experiment; the pulse heights were allowed to drift, the effects of which were corrected for later, off-line.

The gain and response time of each individual phototube was monitored through the use of a conventional N_2 (nitrogen) laser system. Laser light was focussed onto a block of scintillator; the scintillation light was distributed to all TOF phototubes via a fiber optics system attached to the light guides of the TOF I counters, and to the centers of the TOF II counters.

The overall system stability was quite high, as only small systematic corrections on the order of few per cent were made to the TOF data over the entire running period.

The calibration of the TOF counters was obtained from 2.0×10^5 muon triggers taken during the experiment. Only those muon events with a reconstructed track passing through a single TOF counter with minimum ionizing pulse height were used for calibration.

The measured time resolution of the TOF I counter was

$\sigma_{TOFI}(\mu H)$ = 900 psec (muon triggers, hardware start)

$\sigma_{TOFI}(\mu c)$ = 450 psec (muon triggers, corrected)

$\sigma_{TOFI}(\nu_c)$ = 300 psec (neutrino triggers, corrected)

The resolution of TOF I was degraded due to poor light collection and the finite "spot-size" of the tracks from the neutrino interaction as they passed through TOF I. The typical spot-size was 5.0 cm in diameter, corresponding to a time difference of 300 psec.

The measured time resolution for the TOF II counters, using muon "overlap" events (where the muon passed through two adjacent counters) was obtained by summing the (pulse height) corrected times for both tubes on a given counter, computing the flight times for each, and then taking the time difference between counters (left-right). The corresponding spatial resolution is computed using the measured speed of light in the scintillator (61.4 psec/cm).

$\sigma^n_{TOFII}(t)$ = 100 psec ($\sigma^n_{TOFII}(y)$=1.7 cm) (narrow counters)

$\sigma^w_{TOFII}(t)$ = 150 psec ($\sigma^w_{TOFII}(y)$=2.5 cm) (wide counters)

The measured spatial resolution for the TOF II counters, using muon overlap events was obtained by taking the difference in the (pulse height) corrected times for each tube, computing a position coordinate and then taking the difference between counters (left-right):

$\sigma^n_{TOFII}(y)$ = 1.6 cm ($\sigma^n_{TOFII}(t)$ = 98 psec) (narrow counters)

$\sigma^w_{TOFII}(y)$ = 2.0 cm ($\sigma^w_{TOFII}(t)$ = 126 psec) (wide counters)

The time resolution and spatial resolution for the narrow TOF II counters are shown in Fig.13 for muon overlap events.

PARTICLE IDENTIFICATION

Particle identification was achieved from the use of TOF information in conjunction with drift chamber momentum and track length information.

From $L = \beta c t_{TOF}$ and $P_{trk} = \gamma\beta m$ we have the relation:

$$m = \sqrt{(ct_{TOF}/L)^2 - 1}\, P_{trk}$$

Where: L = track length

$\beta = v/c$

$\gamma = 1/\sqrt{1-\beta^2}$

t_{TOF} = TOF flight time

P_{trk} = particle momentum

From the measured TOF time resolution, the one S.D. (68% C.L.) separation points occur at 3.25 (2.65)GeV/c for π/K identification and 5.47 (4.46) GeV/c for K/p for the narrow (wide) TOF II counters (See Fig.14). The start time for each event was obtained by incorporating the flight times for all reconstructed up-to-down tracks (with suitable weights) in a least squares fit to the start time. The mass of secondary particles (as determined from TOF information) is shown in Fig.15 for "clean" tracks, defined as those tracks passing through a given TOF II counter having minimum ionizing pulse height and no other tracks present.

A more detailed discussion of the TOF system is contained in Ref.[120].

THE DRIFT CHAMBERS

The drift chambers performed several functions in the experiment, the primary function being to locate events in the emulsion target. The second purpose of the drift chambers (equally important) was to obtain momentum information on charged tracks. Therefore, the drift chambers were required not only to have high track efficiency but also the ability to detect and resolve multiple tracks associated with neutrino interactions occurring only a few tens of centimeters upstream.

The Upstream Drift Chambers

Twelve upstream drift chambers were arranged in four groups of three chambers. Each triplet of chambers consisted of a U-X-V arrangement. Alternating triplets were shifted by a half of one cell width, to reduce the number of spurious track combinations caused by the inherent left-right ambiguity associated with the use of drift chambers. The U (V) chambers were rotated 60° clockwise (anti-clockwise) (looking along the beam direction) with respect to the orientation of the X-chambers, which had vertical wires. (See Fig.8). A Monte Carlo program was used to deterimine the optimal spacing and orientation of the drift chambers. The use of 60° stereo for the upstream drift chambers preserved the rotational invariance associated with neutrino interactions in the emulsion target.

The first chamber was spaced off from the downstream face of the emulsion by 15.0 cm because of spatial constraints from TOF I, and also to reduce "shadowing" effects, i.e. one or more tracks obscuring another track in a given view (U,X or V). The effects of shadowing were measured to be less than 10% at the first upstream drift chamber, for neutrino interactions. The distance between consecutive drift chamber planes was 4.66 ± 0.02 cm.

The construction of the upstream drift chambers was the same for all three types, U,X and V. The active area of each drift chamber was 1.7 m^2. (128 cm x 128 cm). Each drift chamber had thirty-two sense wires, spaced 4.0 cm apart (≡ cell size), with field shaping wires between each of the sense wires. The sense wires were 20 μm diameter gold plated tungsten, strung with 50 grams of tension. The cathode plane wires (and field shaping wires) were 75 μm diameter copper plated beryllium, wound (strung) with 200 grams of tension on G-10 frames. The cathode planes were 6.35 mm apart, with 2 x 21 cathode wires/cell, with 2 mm spacing between adjacent cathode wires. Each chamber was a

separate system, independent of the operation and performance of the other chambers. The gas windows for each chamber consisted of aluminized mylar, 25 μm of aluminum on 50 μm of mylar, and performed the dual function of gas containment and R.F. shielding. The entire chamber was R.F. shielded, as the drift chamber amplifiers were extremely sensitive.

The operating voltages for the upstream drift chambers were Vmax=3100v, Vmin=1700v, generating an electric field of

$$E = (V_{max} - V_{min})/\text{cell size} = 700 \text{ V/cm}.$$

The cell configuration for the upstream drift chambers is shown in Fig.16. The efficiency as a function of electric field is shown in Fig.17, for a gas mixture of 50% argon-50% ethane.

The Downstream Drift Chambers

The eight downstream drift chambers were arranged in two groups of four, as shown in Figs.3 and 18. The first quartet consisted of X-V-U-Xs chambers, the second quartet of X-Vs-Us-Xs chambers, where s denotes a chamber shifted by 1/2 of a cell. The U (V) chambers were rotated 10° clockwise (anti-clockwise) with respect to the X-chambers The active area was 2.5 m^2 (118.1 cm x 213.4 cm) for the X chambers, and 2.6 m^2 (118.1 cm x 223.5 cm) for the U and V chambers. The distance between consecutive planes was 5.08 cm.

The construction of the downstream drift chambers was not the same for the three types of chambers. The X (U,V) chambers had 40 (44) 20 μm diameter gold plated tungsten sense wires each, spaced 5.08 cm apart with 75 μm diameter copper plated beryllium field-shaping wires in between the sense wires. The sense and field wires were corrected to be 2.540 ± 0.005 cm apart as they were strung. The cathode planes consisted of copper spark chamber foils, i.e. 125 μm diameter copper wire flattened to 25 μm high x 375 μm wide, laminated to a 62.5 μm thick mylar sheet. The drift chamber frames were made of G-10, bolted together in halves, with a silicone-rubber O-ring for a gas seal. The gas windows were made of aluminized mylar, 25 μm of aluminum on 62.5 μm of mylar. The entire chamber was R.F. shielded.

Nominal operating voltages for the downstream drift chambers were Vmax=3700v, Vmin=1800v, generating an electric field of 750v/cm. The gas used for the downstream drift chambers was the same mixture as that used for the upstream drift chambers. Further details of the downstream drift chambers appear in Ref.[121,122].

The Drift Chamber Readout System

The signals from the drift chambers were 100X amplified with a fast amplifier (See Fig.19), designed such that the pulse shape into the fast discriminator maximized single and multiple-track resolution by elimination of ringing on the trailing edge of the pulse, and by selective "Fourier-filtering" of various frequency components of the pulse. The nominal pulse height from minimum ionizing muons was 100 mV at the input of the discriminator, with a FWHM of 30 nsec (see Fig.20). The discriminator threshold was set to 15mV to reduce time jitter from pulse height variations (0.1 nsec). The drift chamber pulse height had a weak angular dependence for tracks with $\theta \leq 500$ mrad (30°); the pulse height decreased rapidly for tracks with angles greater than this, in addition to suffering large statistical fluctuations. Cross talk between drift chamber cells was less than 0.1%

The NIM pulses from the discriminators were sent to a multi-hit capability time-digitization system, similar in deSign to one of the W.Sippach (Nevis Labs) drift chamber readout systems [129], employing a four-bit phase code and a three-bit gray code, driven by a $83\frac{1}{3}$ MHz. clock and utilizing MECL 10000 logic. The four bit phase code allowed interpolation of the basic 24 nsec clock cycle to 1.5 nsec intervals, while the three bit gray code was used for error detection and correction purposes. The (multiple) hits from each of the wires in the drift chambers were continuously digitized, (with 1.5 nsec least count resolution, equivalent to 75 μm in space) with the time digitization of hits on one wire occurring independently of the operation of all other time recorder channels. The digitized time data was stored in local 18-word deep registers (one "hit" per word) within each time recorder. When the apparatus was triggered by a ν-interaction (or otherwise), hit data stored in the time recorder registers was "frozen", converted to a time difference between the start (drift chamber hit) and stop (trigger) time by the time encoder, read out and stored in larger (256 word deep) local memories, with the time recorders re-activated at the end of this process. Thus, several events could be recorded during the fast spill, with the drift chamber event data read out by the computer through CAMAC at the end of the spill. A block diagram of the drift chamber readout electronics is shown in Fig.21.

Drift Chamber Resolution and Operation

The single track spatial resolution, obtained from the composite residuals (i.e. deviations of drift chamber hits from fitted tracks) from muon triggers is shown in Fig.22 for the upstream and downstream drift chambers for a typical "tuning run". The spatial resolution of the drift chambers, averaged over the entire experiment is

$$\sigma_{up}(x) = 125\ \mu m \qquad (\sigma_{dn}(x) = 175\ \mu m)$$

corresponding to an angular resolution of

$$\sigma_{up}(\theta) = 0.6\ \text{mrad} \qquad (\sigma_{dn}(\theta) = 0.8\ \text{mrad})$$

for the 12 upstream (8 downstream) drift chambers.

The minimum (maximum) time recorder dead time between hits on one wire was 24 (48) nsec (corresponding to one (two) $83\frac{1}{3}$MHz. clock cycle(s)). the mean dead time was 36 nsec, corresponding to the average time required to reset the input flip-flop of the time recorder input after receiving a hit. The mean pulse width from the drift chamber discriminators was 30 nsec, although variations in pulse-height caused the discriminator pulse width (time-over-threshold) to vary from 20 nsec to 40 nsec. The minimum measured dead time, obtained from time correlation studies of drift chamber hits in ν-events, was measured to be 30 nsec with a mean dead time of 36 nsec corresponding to a mean two track resolution (for one view) of 1.8 ± 0.3 mm

The drift chamber track efficiencies (as distinct from hit efficiencies, which were higher) were well above 90% throughout the experiment. The effect of the fringe field of the magnet (< 1 KG at the last upstream drift chamber) had no observable effect on the operation of the drift chambers nearest to the magnet aperture; no significant changes (i.e. < 2%) in the drift velocities or efficiencies were measured for these chambers.

Drift Chamber Calibration

Calibration of the drift chambers was achieved through the use of a tuning program, to which the drift chamber survey data was input, along with 2.0×10^5 tracks from muon triggers taken during the run. The tuning program optimized various parameters associated with the location of hits (discussed below), which resulted in a significant (2-fold) improvement in track resolution and track reconstruction efficiency. The data was broken up into short time periods

of approximately ten runs each, in which the values for a set of drift chamber operating parameters were optimized. The values of the parameters changed by less than 5% from their mean values over the entire run. The positions of the drift chambers, as determined by the tuning program changed by less than 125 μm during the course of the experiment, and in general, tracked the position information as obtained by the LVDT system.

The parameters of the tuning program were:

1. Drift velocity v_d = 50 μm/nsec in 50% argon-50% ethane gas

2. Position of the first wire in each drift chamber (to which all other wires in were referenced)

3. Non-linear drift velocity correction near the sense wires, to correct for field non-linearities in this region.

4. Sense wire offsets, to account for deviations in the spacing between sense wires in the upstream drift chambers. The location of each sense wire relative to the first sense wire in each drift chamber was known to 10 μm FWHM from survey measurements. Wire corrections were in the form of translations and rotations done on a per-wire basis. Offsets were typically 100 μm, rotations were typically 0.1 mrad. Offset corrections could by done directly on the raw hit data, while rotation corrections could be done only after the tracks had been reconstructed (to first order).

5. A correction was made to take into account the finite propagation time of the signal along the sense wire.

6. Angle corrections were made on the hit data, once the track had been reconstructed to first order.

7. Drift chamber stop time for each drift chamber.

The values determined for the drift chamber parameters were then input to the neutrino event reconstruction programs, for the set of runs covered by a particular tune.

THE SCM-104 MAGNET

The SCM-104 magnet (on loan to Fermilab from Argonne National Laboratory) was used for momentum analysis of charged particles. As the magnetic field both inside and outside the magnet aperture was highly non-uniform, an extensive field map of the field region between the magnet poles and outside was made. 50,000 data points were taken in the region between the magnet pole tips, on a lattice of 2.54 cm cubes. For the region far from the pole tips of the magnet, a parametrization in the form of a polynomial for the spatial dependence of the magnetic field was used. Agreement between the measured data and the parametrization was within 5% for the measured fringe field region. The magnet current was kept within 0.5% of its nominal value of 2400 A throughout the experiment.

For tracks passing through the magnet aperture, the track reconstruction programs used the quintic spline method for determination of the track parameters, i.e. the track slopes, intercepts and 1/P. As a simplification (for the purposes of discussion), the momentum of a charged particle (in the thin lens approximation) is given by:

$$P = 0.03\int Bdl/\theta_B = 0.186/\theta_B$$

Where $\langle\int Bdl\rangle$ = 6.2 kG-m (At 2400 Amps.)

θ_B = bend angle (in radians)

Pt kick = 0.186 GeV/c. (At 2400 Amps.)

The momentum resolution of the drift chambers was estimated to be

$$\delta P/P = [(0.009)^2 + (0.005P)^2]^{1/2} \text{ For 20 drift chambers.}$$

Where the first term is the contribution from multiple Coulomb scattering in the drift chambers, the second term is the contribution from the intrinsic drift chamber spatial (and therefore angular) resolution. The values obtained from calculations on the momentum resolution contributions are in good agreement with Monte Carlo studies.

For tracks not passing through the magnet aperture, it was possible to utilize the fringe field of the magnet for momentum analysis, although the measured momentum resolution was considerably reduced.

$$\delta P/P = 0.35\ P\ (\text{Sigma})\ \ (\ 0\ \text{mrad} < \theta < 300\ \text{mrad})$$

$$\delta P/P = 0.50\ (\text{Sigma})\ \ (\ 300\ \text{mrad} < \theta < 600\ \text{mrad})$$

$$\delta P/P = 0.75\ (\text{Sigma})\ \ (\ \theta > 600\ \text{mrad})$$

See Ref.[123] for further information on the momentum resolution.

Checks on the Momentum Calibration

No direct calibration of charged particle momentum with a particle beam of known momentum was possible. The momentum calibration was inferred from previous experiments at Argonne National Lab in which the SCM-104 magnet was used.

A check on the momentum calibration came from use of TOF identified protons in which the centroid of the inverse momentum difference Q ($Q \equiv 1/P$) was measured to be:

$$\Delta Q = Q_{DCH} - Q_{TOF} = 0.001 \pm 0.005$$

$$\delta Q_{TOF} = \frac{1}{M}\frac{1}{\sqrt{1-\beta^2}}\frac{1}{\beta^2} \qquad \Delta\beta \simeq \frac{0.014}{\beta\sqrt{1-\beta^2}}\frac{1}{M}$$

$$\delta Q_{DCH} = [(0.010 Q_{DCH})^2 + (0.005)^2]^{1/2}$$

The mass of the proton determined from "clean" tracks in TOF II counters was

$$Mp = P_{DCH}/(\beta/\sqrt{1-\beta^2})_{TOF} = 939 \pm 4\ \text{MeV}/c^2.$$

Another check on the momentum calibration came from work done in Ref.[120], where it was found that the μ^+/μ^- ratio for neutrino events was brought into agreement with the Monte Carlo μ^+/μ^- ratio, for a shift in Q of $\Delta Q \simeq 0.005$. Another check on the momentum resolution and momentum calibration of the drift chambers was obtained from the Q distribution of muons taken with the magnet off. $\langle Q \rangle = 0.011 \pm 0.005$. The origin of the non-zero value of $\langle Q \rangle$ in this case is not fully understood.

It is not inconceivable that small systematic shifts in the drift chamber parameters would be such as to cause an effective 2 mrad rotation between upstream and downstream drift chambers. A physical rotation of this magnitude between upstream and downstream drift chamber arrays would be readily apparent, and was not observed. The width of the Q distribution is consistent with the calculated intrinsic momentum resolution.

An investigation of the effects of such a shift on the kinematic fits on charm decays found little observable effect, the largest observable effect was on the 2-C masses, on the order of 5% in the worst case. Little effect was observed for shifts in the momentum, decay time, p-perp balance and correspondingly the χ^2 and C.L. for each event.

The K_S^0 mass was measured in a partial sample of of neutrino events ($\sim$50% of the total data) in which a V^0 search was made. From ten reconstructed events with a V^0 reconstructed in the drift chambers, having two (opposite charged) up-to-down tracks, the K^0 mass was measured to be:

$$M_{K_S^0} = 504.5 \pm 1.0 \text{ MeV}/c^2$$

This value for the K_S^0 mass is 1.4% above the true K_S^0 mass, 497.7 ± 0.1 MeV/c^2 [160]. To supress background due to interactions in the drift chambers an asymmetry cut of

$$|P_{\pi+}/P_{\pi-}| > 0.2$$

and flight length cut of $L/\gamma\beta c\tau > 0.15$ were made.

Another check on the momentum calibration came from the collective determination of the charmed particle masses (from 2-C constrained fits), which were found to have an overall, systematic shift of 0.7 ± 0.6% (13 ± 11 MeV) below the true values of the D^+, D^0 and Λ_c^+ masses.

Thus, it can be seen that the momentum calibration, as determined from the above methods, is accurate to within $\sim$1%.

THE LEAD GLASS ARRAY

The lead glass array was used for detection of high energy photons and identification of electrons, and consisted of 68 blocks arranged in nine rows of eight columns, with the four corners removed. (See Figs.3 and 23.)

Two types of lead glass blocks were used in the array, each type was 19 cm x 19 cm square. There were 56 short blocks, 30.5 cm (11 R.L.) in length, and twelve long blocks, of 35.6 cm (14 R.L.) length. The long blocks were placed in the center of the array to optimize shower energy resolution. Each block had a 12.7 cm diameter EMI 9815 phototube mounted on its downstream face.

Signals from each of the phototubes were 10X amplified, split in a 1:20 ratio and fed into two 0.25 pC./channel ADC'S. The high gain ADC tracked the minimum ionizing peak from muons; the low gain ADC recorded the pulse height from E.M. showers associated with ν-events. The phototube voltages were set up for 30 ADC counts/GeV in the electron ADC, for a maximum measureable energy of 35 GeV per block. The angular resolution associated with gamma detection by the lead glass array, for 19 cm x 19 cm blocks was $\sigma_\theta = 0.015$ rad. The location and size of the lead glass blocks was such that γ's from symmetric π^0 decay could not be resolved for $P_{\pi^0} > 4.25$ GeV/c.

A Neon flasher/fiber optics light transmission and distribution system facilitated set-up and equalization of phototube gains, as well as gain monitoring during the course of the experiment. Flasher triggers were taken once per machine cycle, between spills.

Lead Glass Calibration

Calibration of the lead glass array was achieved through several means. One block of each type was calibrated in the M-5 test beam at Fermilab. Electron and minimum ionizing triggers were taken at various beam energies from 5 to 30 GeV/c. The response and resolution for each type of block, shown in Fig.24 were measured to be:

E(long block) = 467 ± 15MeV/ minimum ionizing track

E(short block) = 392 ± 15MeV/ minimum ionizing track

$$\delta E/E = 0.15/\sqrt{E} \text{ (sigma)}$$

The pulse height spectrum for 30GeV/c negative particles is shown in Fig.25. The electron peak is clearly visible. The lead glass blocks are approximately 0.7 hadronic interaction lengths thick. Approximately 1% of the hadrons (at any momentum) are capable of depositing energy within 3 S.D. of the pulse height for electrons of the same momenta. As muon tracks and charged hadrons from ν-interations illuminate the lead glass block faces uniformly, the pulse height dependence must be averaged over the entire block. As the response of a lead glass block was not constant for off axis and non-normal tracks (see Ref.[124] for a typical lead glass spatial response spectrum), it was necessary that the M-5 test beam results be modified to take into account such an effect. The ratio R of the minimum ionizing pulse height from on-axis tracks (as measured in the M-5 test beam) to that for tracks spread uniformly over the block faces is $R = 1.20 \pm 0.12$. Further consistency checks on the lead glass calibration were obtained from the ratio of lead glass energy to charged track momentum for spectrometer - identified electrons associated with neutrino interactions, for which the ratio R was found to be $R = 1.09 \pm 0.06$. Emulsion - identified electrons from e+e- pairs found by scanback of spectrometer tracks were also used in a similar study, in which $R = 1.16 \pm 0.16$. The average value of R; determined from the above studies was $R = 1.17 \pm 0.10$; thus the energy responses for the long and short blocks were decreased accordingly, to

E(long block) = 397 ± 13 MeV/ minimum ionizing track

E(short block) = 333 ± 13 MeV/ minimum ionizing track

These results are also in good agreement with the results obtained for the lead glass array (short blocks only) at Argonne, used in the Charged-Neutral Spectrometer (ANL E-420,428), where the energy calibration was measured to be:

E(short block) = 325 ± 10MeV/ minimum ionizing track

$$\delta E/E = 0.09/\sqrt{E} \text{ (sigma)}$$

The lead glass energy resolution attained in experiments at Argonne was significantly better than for this experiment, as it was possible to calibrate each lead glass block in the array on a run-by-run basis from decay. This was not possible for E-531, which had a total of 2100 events occurring over a period of three months.

A further check on the calibration of the lead glass

was obtained from "clean" π^0 candidates from ν events with charm decays, (see Table 18). Candidate π^0's from charm events were obtained from those events where all the energy deposited in the lead glass array was accounted for in terms of the charged tracks incident upon the array; "clean" π^0 candidates were obtained from gamma candidates (blocks with no charged track incident upon the block). The π^0 mass was measured to be 134.8 ± 5.9 MeV/c using 20 clean π^0 candidates from charm decay ν-events.

THE HADRON CALORIMETER

A hadron calorimeter was included in the experimental apparatus to provide crude information on the total hadronic energy from ν-interactions. The calorimeter consisted of twenty counters arranged in five planes of four counters per plane, sandwiched between 10 cm thick steel plates. (See Figs.3 and 26.) Each counter consisted of a single piece of NE110 or NE114 scintillator (ten counters of each type 1.3 cm thick) viewed by a single 12.7 cm diameter Amperex 58DVP phototube, through an adiabatic light guide and Winston cone. The attenuation length was measured to be 5 m for both types of scintillator.

The signals from each of the calorimeter counters were split in a 1:7 ratio and fed into two 1024 channel 0.25 pC/channel ADC'S. The high gain ADC monitored the minimum ionizing peak from muon triggers for calibration purposes, while the low gain ADC recorded the hadronic energy from neutrino interactions.

Hadron Calorimeter Calibration

Calibration of the calorimeter was indirect as no hadron beam was available in place. As the construction of our calorimeter was identical (in granularity and material) to the calorimeter discussed in Ref.[126], their results were used to calibrate our calorimeter. The energy response and resolution for the calorimeter was thus:

$$E(cal) = \frac{N}{2a}(1+\sqrt{1+4ab/N})$$

$$\delta E/E = 1.1/\sqrt{E}\ (\text{sigma})$$

N = # of equivalent singly ionizing particles
a = 5.428 equivalent singly ionizing particles/GeV
b = 0.721 GeV

The non-linear term provided a "boost" in the low energy region to correct for increased absorbtion losses at low energies. (No additional corrections were made, such as for light attenuation effects in the scintillator ($\sim$30% from end-to-end), nor for for angular effects, leakage out the back and sides of the calorimeter ($\sim$5-10% effects).

The response of the calorimeter to minimum ionizing muons is shown in Fig.27. Minimum ionizing tracks deposited 1.75 GeV peak (2.08 GeV mean) hadron equivalent energy in traversing the hadron calorimeter (50.8 cm of steel, equivalent to $dE/dX = 0.6$ GeV). The calorimeter counters saturated at 13.7 GeV, implying a saturation threshold of 40 GeV per calorimeter row. The calibration of the calorimeter was checked using the data from 31 charm candidate events, was found to be $\delta E/E = (0.8 \pm 0.2)/\sqrt{E}$ (sigma), consistent with the above estimate.

THE MUON COUNTERS AND MUON IDENTIFICATION

Muon identification was obtained by penetration of charged tracks through steel. Tagging of muons was achieved with two crossed planes of counters embedded in the steel at depths of 1.2 and 2.3 m, corresponding to energy thresholds of 1.9 and 3.4 GeV/c, respectively. (Including matter from lead glass and calorimeter steel.)

The front muon counter plane consisted of 36 horizontal counters (arranged in two vertical columns of 18 counters each), the back plane consisted of 40 vertical counters (arranged in two horizontal rows of 20 counters each). (See Figs.2 and 28.) Each counter consisted of a 1.5 m long NE 114 scintillator, coupled through an adiabatic light guide and Winston cone to a single Amperex 56AVP phototube at one end. The signals from each muon counter were split in a 2:3 ratio, 2/5 sent to an ADC and 3/5 sent to a TDC.

Muon Counter Calibration

The muon counters were calibrated with 2.0×10^5 muon triggers taken during the run. Track information from the drift chambers was used to predict the location of the muon as it passed through each counter plane. Calibration events were restricted to those events with minimum ionizing pulse height in a single TOF II counter. The values for the parameters associated with the (pulse height) corrected time, such as the speed of light in the scintillator ($v^{-1} = 62.2$ psec/cm), and the t_0 for each counter were determined by histogramming the time spreads for each counter. The average muon counter time resolution was

$$\sigma_\mu(t) = 0.8 \text{ nsec}$$

corresponding to a position resolution of

$$\sigma_\mu(y) = 129 \text{ cm}$$

The ΔY distribution for the back muon counters is shown in Fig.29.

There were several types of muon tags, "muon fronts" (MUF), "muon backs" (MUB) and "muon front-backs" (MUFB), corresponding to which muon counters had been hit. A charged particle in an event was identified as a muon if the measured positions of the hits in the muon counters in the front and/or back planes were within 2.5 S.D. of the predicted X-Y position of the track from downstream drift chamber information, including multiple scattering effects

in the calorimeter and muon steel. From Ref.[127], punchthrough from energetic hadrons at the front muon counter plane was less than 1%, for hadrons with momenta less than 5 GeV/c. The measured overall muon detection efficiency for MUF, MUB, MUFB was 95 ± 1%, 94 ± 1% and 89 ± 1.5%, respectively. The muon detection efficiencies are less than unity due to timing and pulse height cuts (~2% effect) and geometrical inefficiencies (~3% effect, due to counter overlap and edge effects). (The MUFB inefficiency, i.e. neither hodoscope firing, is 0.3%.) The acceptance of the muon counter array from geometry and threshold (range) requirements as determined from a Monte Carlo of neutrino interactions in the emulsion target, was found to be 82 ± 4% for the 350 GeV/c wide-band beam. The losses due to muons going wide of the muon identification system are less significant than losses due to threshold requirements. The net muon detection efficiency was therefore 74 ± 5%. The efficiency and acceptance corrected CC+NC/CC ratio for 1242 found events is 1.40 ± 0.10, in good agreement with the world average of 1.301 ± 0.007 [128].

The measured $\bar{\nu}_\mu/\nu_\mu$ C.C. ratio is 7.5 ± 2.0%, in agreement with Monte Carlo predictions [120].

DATA-TAKING on EXPERIMENT E-531

Data-taking started on November 18, 1978 and ended on February 7, 1979. Over 1250 hours of running time with 155 shifts were logged, with less than 100 hours of equipment-related downtime. 183 data tapes were written. 7.2×10^{18} protons were incident on the ν-target during this period, from which a total flux of 1.7×10^{15} ν's/m^2 (A_{tot} = 0.49 m^2) passed through the emulsion target. Over 900,000 muon triggers, 68,000 neutrino and 140 anti-neutrino triggers were taken during this period. (Several data-taking runs were made with the horn polarity reversed.) The majority of the neutrino triggers were muon-induced, due to the anti efficiency (89 ± 1%), and also due to the fact that adjacent TOF II counters were allowed to trigger the apparatus (for the purpose of calibration of TOF II counters). Thus, approximately one out of every 30 neutrino triggers was real, i.e. there was approximately one real neutrino interaction per 100 machine cycles (one interaction every 11 minutes).

The data-taking can be broken up into three major periods, corresponding to three different experimental running conditions.

Beginning: Runs 475-517 (high muon background)
15% of data

Middle: Runs 518-614 (concrete shielding installed)
55% of data

End: Runs 630-672 (toroids on)
30% of data

Event Yield

The expected event yield was obtained via two methods, one a calculation which extrapolated the measured event rate at the 15' B.C. the Wonder Building; the other modelled the neutrino beam, using Monte Carlo techniques. The measured event rate from experiment E-545 (a ν-liquid deuterium experiment which ran coincident with E-531 in the same 350 GeV wide-band ν-beam, located 1400 m from the ν-target) was $2.24 \pm 0.18 \times 10^{-2}$ events/ton/10^{13} protons on target for $E\nu > 10$ GeV [119]. Extrapolating this rate to the Wonder Building, taking into account the increase in the neutrino flux density (a factor of 2.0), the trigger acceptance of E-531 (0.93), the fractional live time (0.80), the number of protons on target for E-531 (7.2×10^{18}) and the mass of the emulsion target (0.1 tons), the expected event yield is:

$$N_{EV}^{\nu} = 2545 \pm 500 \text{ Events}$$

For the Monte Carlo program, the number of neutrino events N_{EV}^{ν} was obtained by integrating the neutrino flux over the energy range of the neutrino beam:

$$N_{EV}^{\nu} = M_{TGT}^{EMUL} \int_0^{350} \sigma(E_\nu) \mathcal{F}_\nu(E_\nu) \delta E_\nu$$

With $\sigma(E_\nu) = 0.63\ E_\nu \times 10^{-38} cm^2/\text{nucleon/GeV}$ for ν_μ [160].

and $\sigma(E_{\bar{\nu}}) = 0.30\ E_{\bar{\nu}} \times 10^{-38} cm^2/\text{nucleon/GeV}$ for $\bar{\nu}_\mu$

The calculated Monte Carlo event yield (i.e. the number of events recorded on magnetic tape, taking into account the effects of dead time losses, acceptance losses, etc.) is:

$$N_{ev}^{\nu} = 2260 \pm 450 \text{ Events}$$

The details of the Monte Carlo calculations for the neutrino beam and event yield are contained in Refs.[120,118].

THE TRIGGER ELECTRONICS AND DATA AQUISITION

Four triggers were used in this experiment, the ν-trigger and three calibration triggers; the muon trigger, the laser/flasher and sensor triggers.

The neutrino trigger used in the experiment was very nearly that used for measuring total cross sections. There were no requirements on minimum energy deposition or demanding a muon be present in the event. Requirements for the ν-trigger were that the event occur within the fast spill; no charged track into the apparatus; at least twice minimum ionizing in TOF I; and at least two tracks pass through TOF II. Thus, the logical statement for the ν-trigger is:

$$\nu \equiv G_{\nu} \cdot \bar{A} \cdot \text{TOF I } (\geq 2 \text{ M.I.}) \cdot \text{TOF II } (\geq 2 \text{ trks.})$$

The live time for the ν-trigger was measured to be 73, 79 and 82% for the beginning, middle and end running periods, with a mean live time of 80%. The ν-trigger was gated on during the fast spill by the background muons associated with the ν-beam, obtained from the integrated signal from the summed outputs of the muon counters. (The detector was gated on in this manner, rather than through the use of timing signals, as undesirably large fluctuations occurred in the timing of the fast spill with respect to these signals.)

The muon trigger required that the event occur within the last 5% of the neutrino spill (to limit the number of muon triggers and thus the loss of neutrino events); at least one minimum ionizing track exit from the target; and at most one track pass through TOF II. The logical statement for the muon trigger is therefore:

$$\mu \equiv G_{\mu} \cdot \text{TOF I}(\geq 1 \text{ M.I.}), \text{ TOF II}(\equiv 1 \text{ track})$$

An average of five muon triggers were taken per spill. Because the muons associated with the neutrino beam were predominantly positive, the beam-right side of the apparatus downstream of the magnet was illuminated by muons more often than the beam-left side. In an effort to spread out the muon triggers more evenly, pairs of TOF II counters directly in front of the nine lead glass columns were OR'ed together with the four calorimeter rows, such that multiple muon triggers could be taken during this part of the spill, thus improving the statistics for each counter.

For a given spill, all counter ADC'S and TDC'S were gated on and latched by a neutrino trigger. For spills with

multiple ν-events (or ν with μ) occurring during the spill, all counter information was lost for the events following the first trigger. The drift chamber system however, was capable of stacking multiple events in local memory (e.g. ten neutrino events or fifty muon events), the hit data for the events being read out at the end of the spill, and written onto magnetic tape by a Data General Eclipse computer. The electronics associated with the neutrino and muon triggers is shown in Fig.30. The timing of various equipment and phenomena occurring within or during the fast spill is shown in Fig.5.

A typical neutrino interaction, as it appeared in an on-line display of the experiment is shown in Fig.31.

In addition to ν and μ triggers, laser/flasher triggers were also taken between spills for on-line calibration and gain monitoring of TOF and the lead glass. The responses of the TOF counters to the laser pulse, and the lead glass array to the neon flasher, were recorded in their respective ADC'S and TDC'S, and then read out.

In a similar manner, LVDT sensor triggers were also taken between spills, where the ADC'S for the position sensors and equipment monitoring system were read out, along with all other ADC'S and TDC'S (to obtain pedestal data). The timing of the laser/flasher and sensor triggers came from timing signals provided by the laboratory, synchronized to the machine cycle, shown in Fig.5.

THE ON-LINE EQUIPMENT MONITORING SYSTEM

Critical equipment and delicate hardware were monitored continuously throughout the experiment to minimize the irrecoverable loss of data from equipment malfunction. All high voltage and low voltage power supplies for the drift chambers, scintillation counters, etc., along with analog voltages representing Vmax, Vmin, Idch, Disc.Level for each drift chamber, the Hall probe for the SCM-104 magnet, the gas pressure for the argon-ethane gas supply, and five temperature sensors for the emulsion target were monitored. The values of each monitored device were checked once between each spill by the computer. If the value of the monitored device was found to differ from its nominal value by more than ±10% for more than three machine cycles, an audible and visual trip monitor signal was given by the computer, with a message indicating which device had failed. Use of this system was instrumental in improving the quantity and quality of the recorded data.

Emulsion Radiation Protection System

Another experiment downstream of the Wonder Building operated a nearby hadron beamline (the N-5/N-7 beamline) simultaneously with our experiment. Concern over the possibilty of irradiation of our emulsion target from beam scraping, beam aborts, etc. prompted installation of a beam interlock for the N-5/N-7 beam with TOF I singles rates during both the fast and slow beam spills. Rates in excess of twice the nominal rates caused an immediate shutdown of this beamline. This precaution was well taken, as the monitoring system was activated several times during the course of the experiment.

CHAPTER II

DATA ANALYSIS

DETERMINATION OF CHARMED PARTICLE LIFETIMES

A Brief Overview:

The analysis of the data took place in several stages, starting from the data recorded on magnetic tape. A "tuning" program aligned and calibrated the drift chambers for the entire running period. Programs were developed for TOF calibration and particle identification, calibration of the lead glass and hadron calorimeter, and calibration of the muon counters and muon identification, as discussed above.

The second stage in the data analysis consisted of reconstruction of charged tracks and vertices for ν events. Reconstruction programs successfully reconstructed a total of 2100 events with a vertex in the target volume. Fiducial cuts around emulsion module edges and posts reduced the sample to 1829 events.

The ν event track and vertex information was used to locate events in the emulsion by volume scanning and track following methods. Of the 1821 events predicted in the emulsion, 1242 events were found, for a net finding efficiency of 68%. All found events were searched for visible decays. Decays of charged particles were located by following charged tracks out from the primary vertex, and by "scanback" of spectrometer tracks (following spectrometer tracks not observed at the primary vertex back into the emulsion). Neutral decays were searched for by volume scanning methods, and by scanback of spectrometer tracks. 27.7 m of hadronic track length was scanned, in which 89 nuclear interactions (96 expected), 53 single-prong or "kink" events (of which 5 are consistent with charm decay) and 23 charged multi-prong (trident) charm decay candidates were found, along with 21 neutral multi-prong charm decay candidates. Background from hadronic interactions for charmed charged decays is less than 3.3 (0.6) events, and less than 0.3 (0.03) events for neutral charm decays (the numbers in parentheses denote the number of charmed candidate events with parent momentum above a momentum cut of 4.0 GeV/c).

The third stage of analysis involved the synthesis of all counter and emulsion data for each charm decay candidate. The identity of the decaying particle was determined from counter, emulsion and kinematical information. The (proper) decay time was determined for each charmed particle.

The final step in the lifetime analysis was to determine the mean lifetime for each species of charmed particle from the fitted, unambiguous decay candidates, using the maximum likelihood method.

CHARGED PARTICLE TRACK RECONSTRUCTION and VERTEX RECONSTRUCTION.

Several track and vertex reconstruction programs were used to analyze neutrino events. A program written by Prof. Taek Soon Yoon was used in the early stages of analysis. Another independent program utilizing a different approach to track reconstruction was written by Prof. Noel R. Stanton. Both TSY and NRS programs are discussed here (although only qualitatively) to elucidate different approaches to the difficult problem of track and vertex reconstruction.

TSY Program

The first step in the TSY program was to estimate the location of the vertex, obtained by histogramming the Z = 0 intecept of lines drawn through pairs of hits in any two upstream drift chamber planes for U, X and V views to obtain the average <U>, <X> and <V> intercepts at Z = 0.

Tracks were then reconstructed in the downstream drift chambers, starting with downstream X chambers. Four hits were demanded in these drift chambers in a "straight" line, with a tolerance of 0.75 mm (Tolerance = deviation of hit from fitted line.) The fitted track was then used to predict the X coordinates of the expected hits in the downstream U and V drift chambers. If the U - V hits were found to match the expected hits in X, then a Y coordinate for each U and V hit could be obtained from the relations:

$$U = X\cos\theta_u + Y\sin\theta_u$$

$$V = X\cos\theta_v + Y\sin\theta_v$$

$$\theta_u = -\theta_v = 60^\circ \text{ for upstream drift chambers}$$

$$\theta_u = -\theta_v = 10^\circ \text{ for downstream drift chambers}$$

Note: For the upstream drift chambers

$$X = U - V \; ; \; Y = 1/\sqrt{3}(U + V)$$

The above relations also hold for track slopes.

The Y values for the U - V hits were checked for consistency with a straight line in Y-space. The hits for all 4 + 4 and 4 + 3 hit track candidates were then "erased" and the procedure repeated for tracks with downstream X segments with 3 hits. The downstream tracks were projected to the middle of the magnet, where "roads" were made from the intersections of the tracks with the magnet midplane to the vertex. The road "widths" were ±2.5 cm at the vertex and ±0.65 cm at the magnet midplane. A search for tracks within these roads was then performed, in which upstream track segments having 4 or 3 hits in one view were obtained. The upstream X track segment was used in conjunction with upstream U and V hits from respective U and V track segments to obtain Y coordinates for these hit combinations. The Y values were then histogrammed and a peak in the resulting distribution sought for. The hit combinations were permuted (e.g. the U track segment combined with X and V hits, etc.) to obtain a set of Y-values, and the process repeated. The "best" track candidate was chosen on the basis of χ^2 and number of hits. More than one upstream track candidate was allowed for the same downstream track candidate. A quintic spline fit was then performed on these tracks, the fitted track parameters being dX/dZ, dY/dZ, Xint, Yint and Q = 1/P. Tracks identified as a muon or having high momentum were used to obtain a better estimate of the vertex.

The fitted vertex location was obtained from a least squares fit of the reconstructed tracks to a common vertex. The effects of multiple scattering in the emulsion were included in the fitting procedure.

NRS Program

The NRS program made two passes through the data for a given event. The first pass track finder searched through the track data in an effort to reconstruct a muon track (MUFB or MUF), or failing that, a stiff hadron. Track segments were reconstructed in the downstream drift chambers first, and matched with track segments found in the upstream drift chambers, at the magnet midplane, in a manner similar to that of the TSY program. The first pass track-finding routine then searched for all tracks which passed close to this "leading" track within the emulsion volume, looking for high momentum tracks first. A trial vertex was determined from the intersection of two or more stiff tracks. The

upstream track segments were searched for within "roads" determined by the postion of the downstream track segment at the magnet midplane and the trial vertex. Sucessively softer tracks were then searched for, which originated from the region of the trial vertex. Templates were used for reconstructing soft tracks, which allowed for track curvature in the fringe field of the magnet. No attempts were made to reconstruct up-only tracks, i.e. tracks which did not pass through the magnet aperture. If only the "leading" track was found, and no other, the hits for this track were "erased", as it was possible for the reconstruction program to have "locked in" on a spurious or bad track. The track finding procedure was repeated again before the event was abandoned.

Each of the tracks reconstructed in the first pass were assigned a weight reflecting its credibility in determining a vertex. High weights were assigned for tagged muons, high momentum, good χ^2 and few missing hits. The tracks were then fit to one or more vertices using these weights. An average fitted stop time was obtained for these tracks, and used for tracks found in the second pass.

The second pass track finder utilized the same procedures as in the first pass, except that the search was limited to tracks passing close to the vertices that were found in the first pass. Tracks found in the first pass were kept, but were assigned a low weight (corresponding to 2.5 missing hits) to encourage finding better versions of these tracks in the second pass, using the improved stop time and vertex locations. Improved vertex locations were obtained using the reconstructed tracks and their weights found in the second pass.

The measured event reconstruction efficiencies were 73 ± 8% (80 ± 9%) for the TSY (NRS) programs (determined by hand scanning methods, for events within the emulsion fiducial region and near the edges of the emulsion). Comparison of the two programs on an event-by-event basis, particularly where one program succeeded and the other program failed, resulted in improved reconstruction efficiencies. The final version of the NRS program, which became the primary data source for event finding in the emulsion, had an event reconstruction efficiency of 95 ± 5%, based on the same sample of events. This number does not take into account correlated losses, where both the TSY and (original) NRS programs failed to reconstruct a particular event. Such losses are believed to be small, as the product of the inefficiencies of the individual programs matches that of the inefficiency of the final NRS program. Note that the reconstruction efficiency, as determined from the

15' B.C. extrapolation is 83 ± 17%, while the reconstruction efficiency as determined from the Monte Carlo of the neutrino energy spectrum, is 80 ± 10% for E_ν > 10 GeV, 90 ± 10 % for E_ν > 30 GeV.

The mean number of tracks reconstructed per event was 3.9 for this program. The mean processing time per event was 15 seconds on an Amdahl 470 V6 computer. The number of events reconstructed as a function of Z is shown in Fig.32. The 25% decrease in the number of reconstructed events from the downstream to upstream edge of the target is consistent with the measured reconstruction efficiency, and is due to the effects of multiple scattering, nuclear interactions and increased numbers of events with associated electromagnetic showers from gamma conversions within the emulsion, which result in higher multiplicity events. Such events are more difficult to reconstruct, with correspondingly more computer time used and less reliability associated with each track. A "timer" was used in the event reconstruction program to prevent inordinately large amounts of time spent on such events.

The drift chamber track reconstruction efficiency vs. emission angle θ is shown in Fig.38 (for horizontal events). Tracks from events found in the emulsion are "matched up" with spectrometer tracks (according to criteria discussed below). The first distribution shown is the raw track reconstruction efficiency, and includes all factors responsible for track non-reconstruction, such as the production momentum spectrum and angular distribution of charged secondaries from neutrino interactions; multiple scattering, nuclear interactions and decays in the emulsion; as well as the dependence on the intrinsic drift chamber hit (and track) reconstruction efficiency with angle. The second distribution is the acceptance of the spectrometer as a function of emission angle θ, as defined by the 6-th downstream drift chamber and the magnet aperture. The third distribution is the normalized track reconstruction efficiency as a function of emission angle (i.e. the ratio of the raw efficiency to the acceptance). The mean track reconstruction efficiency (averaged over all track momenta) is in excess of 85 ± 5% for tracks with θ < 200 mrad, falling to zero at 600 mrad.

Analyzer and Refit Reconstruction Programs

Another reconstruction program, written by Michael Gutzwiller [123] was used for on-line and off-line display of the event spectrometer data (See Fig.31). This program was of fundamental use in reconstruction of charm decay candidate events, as the spectrometer data could be displayed visually on a crt screen, or hardcopies made for each event. The "Refit" program was also of fundamental utility in the analysis of event data. This program attempted to reconstruct all tracks associated with the event, utilizing the emulsion track slope and vertex location information in reconstruction of events. In addition, the Refit program provided TOF, lead glass, calorimeter and muon counter information. The event reconstruction programs are discussed in greater detail in Ref.[123].

EVENT FINDING IN EMULSION

After the emulsion modules were removed from the experiment, they were processed at the University of Ottawa, in Ottawa, Ontario, Canada. The emulsion processing procedure is discussed in detail in Ref.[122]. The horizontal pellicles were stuck to gelatin-coated lucite before processing. Bubble and blister damage was found to affect less than 4% of the pellicles. The most significant processing-related problem was a 1-2 μm thick surface blackening of all pellicles and plates, which was removed by carefully abrading away this layer using tissue paper and alcohol. The shrinkage factor after processing was about 330 μm/165 μm = 2.0. Shrinkage occurred only in the unconstrained dimension of the emulsion pellicles or plates, as the lucite plate (for horizontal emulsion) and plastic base (for vertical) emulsion prevented shrinkage in the other dimension.

The emulsion quality was excellent. The grain density for electron tracks from the decays of stopping muons was measured to be $I_h = 28.4 \pm 0.7/100$ μm ($I_v = 31.3 \pm 1.2/100$ μm) for the horizontal (vertical) emulsion. The variation of grain density from pellicle to pellicle, plate to plate was less than 3%. Track fading in the emulsion was measured to be 10% (6% with respect to the changeable sheets, $I_{cs} = 32.3$ grains/100 μm) over a period of three months.

The backgrounds observed in the emulsion are listed in Table 2. The angular distribution for minimum ionizing background tracks in the emulsion is shown in Fig.39. The zenith $\cos\theta$ dependence of cosmic rays is clearly seen, along with beam associated muons.

TABLE 2

CHARGED PARTICLE BACKGROUNDS IN EMULSION

BACKGROUND	HORIZONTAL EMULSION	VERTICAL EMULSION
Fog Density: (per 1000 μm^3)	1.44±0.06	1.20±0.10
Nuclear Stars: (per cm^3)	141 ± 35	110 ± 20
Cosmic Rays: (per mm^2)	30 ± 5	30 ± 5
Beam Associated Muons: (per mm^2)	130 ± 20 (5° 1/2 cone)	225 ± 23 (20° 1/2 cone)
Compton Electrons: (x 1000 per mm^3)	7.7 ± 0.9	4.3 ± 0.4
All M.I. Tracks: (x 1000 per mm^3)	1.9 ± 0.1	4.1 ± 0.3

Note: All volumes are pre-processing volumes. (the emulsion shrinks by a factor of 2.0 in the unconstrained dimensions when processed.)

The measured densities of Compton electrons and fog grains are subjective, scanner-dependent quantities, and are uncertain by factors of 2-5.

To facilitate event finding in the emulsion, various referencing/survey methods were used. The horizontal emulsion modules were marked with X-rays at Argonne National Laboratory before processing, in such a way that that the relative positions of each pellicle with respect to any other pellicle could be determined from X-ray marks. Each horizontal pellicle was also imprinted with an optical grid of 500 μm by 500 μm squares on the side of the pellicle stuck to the glass plate. The vertical emulsion used no optical grid; rather, one corner of each of the emulsion plates (precision punched during construction of the vertical emulsion modules) was designated as the origin for the local (plate) coordinate system.

Due to the effects of distortion and warpage along edges of the emulsion, fiducial cuts of 3.0 (2.5) mm from the edges and around post holes were made for the horizontal (vertical) emulsion. Additional cuts were made in X and Y to exclude the regions of G-10 in the horizontal modules. These fiducial cuts caused a reduction of 12% (13%) in the number of events predicted in the horizontal (vertical) emulsion.

Event Search

Volume Scanning and Track Followback Methods

Several methods were used for locating events. For the volume scanning method, a region of

$$4 \text{ mm} \times 4 \text{ mm} \times 20 \text{ mm} = 320 \text{ mm}^3,$$

centered on the predicted vertex location was searched for the event vertex.

The counter resolution associated with event localization for the horizontal and vertical emulsion is shown in Fig.36. The distributions are the same for events found in both types of emulsion modules:

$$\sigma_x \simeq 370 \text{ um}, \quad \sigma_y \simeq 290 \text{ um}, \quad \sigma_z \simeq 1.4 \text{ mm}$$

$$\langle \Delta X \rangle = 235 \ \mu\text{m}, \quad \langle \Delta Y \rangle = 645 \ \mu\text{m}, \quad \langle \Delta Z \rangle = -75 \ \mu\text{m}$$

The origin of the offsets in the X and Y event localizations are not fully understood. The offsets in X and Y are not consistent with survey resolution, and with independent survey measurements made before, during and after the experiment.

The number of found events vs. Z for the volume

scanning and track followback methods (i.e. horizontal and vertical emulsion) are shown in Fig.33. These distributions should be compared with the number of reconstructed events vs. Z.

The measured efficiency for finding events by the volume scanning method was 51 ± 2%. The volume scanning method was used primarily by the horizontal emulsion group. The vertical emulsion group used the "track followback" method. Track candidates were first located on the changeable sheet, and then followed into the emulsion stack. The efficiency associated with this process is 96 ± 2% for locating tracks on the changeable sheet, and 90 ± 2% for following a track back to the primary vertex in the emulsion, for a net efficiency of 87 ± 2%.

The event finding efficiencies vs. Z for the volume scanning method and the track following method (shown in Fig.34) were obtained from the ratios of found to predicted events in the horizontal and vertical emulsion respectively, at a given value of Z. The volume scanning method shows a drop in both the upstream and downstream regions of emulsion, due to fiducial cuts around the edges of emulsion pellicles and also due to the effects of multiple scattering in the emulsion, which tend to decrease the accuracy of the vertex predictions, more for events occurring in the upstream portion of the emulsion target than for the downstream portion. Low energy neutrino interactions suffer from these effects more so than do high energy neutrino interactions.

The horizontal group also attempted to use the track followback method, but found it difficult because of the high muon background, and because of distortion effects at the downstream edge of the emulsion pellicles. Subsequently, another track followback technique was developed by the horizontal group; tracks with $dX/dZ < 0.050$ rad and $dY/dZ > 0.050$ rad were followed directly from drift chamber predictions into the horizontal emulsion. The finding efficiency was 80 ± 25% for events satisfying these criteria, which comprise 62.5 ± 12.5% of all found neutrino events, hence a net efficiency of 50 ± 28%. This method was more sucessful due to the decrease in the number of minimum ionizing background tracks away from the beam direction (See Fig 39.) The volume scanning method suffered from significant scanning biases, in that events with a large number of "black" NH tracks were found more readily than for those events which had few black tracks, particularly "white stars" (NH = 0 events) as is apparent in the NH and NS distributions for found events in horizontal and vertical emulsion, shown in Fig.40. NH

specifies the number of heavily ionizing (black) evaporation tracks from the break-up of the struck nucleus, and NS is the number of "shower" or minimum ionizing tracks produced in the interaction.

Emulsion Track Angular Resolution

The angular resolution of emulsion tracks was determined from measurements on individual tracks. Momentum cuts of $P(trk) \geq 4$ GeV/c and $Z \geq 2.5$ cm were used to minimize the effects of multiple scattering in the emulsion. Plots for $\Delta dX/dZ$ and $\Delta dY/dZ$ are shown in Fig.41 for the horizontal and vertical emulsion. The results, after unfolding the drift chamber resolution ($\theta^{rms}_{dch} = 0.6$ mrad) and the effects of multiple scattering in the emulsion ($\theta^{rms}_{m.s.} = 0.0017$ for $P_{trk} \geq 4.0$ GeV/c), such that

$$\theta^{emul^2}_{trk} = \theta^{obs^2}_{trk} - (\theta^{rms^2}_{dch} + \theta^{rms^2}_{m.s.})$$

$$0.5\sigma_x = \sigma_y = 0.0033 + 0.02\theta \text{ rad (Horizontal)}$$

$$\sigma_x = \sigma_y = 0.0015 + 0.01\theta \text{ rad (Vertical)}$$

CHARM SEARCH; SCANNING CRITERIA

Charged Decays

The search for decays of charged charmed particles required that for each event all charged tracks be followed from the primary vertex for 6.0 mm or until the track exited the emulsion stack, and also satisfied the following criteria:

Horizontal Emulsion	Vertical Emulsion
$X', Y' \leq 20°$ (365 mrad)	$X', Y' \leq 200$ mrad
$\Delta X'$, or $\Delta Y' \leq 15$ mrad	$\Delta X'$, or $\Delta Y' \leq 15$ mrad
$I/I_0 \leq 4$	

Where X', Y' are the X and Y slopes, and $\Delta X'$, $\Delta Y'$ are the differences between counter and emulsion measurements of track slopes.

Neutral Decays

The search for the decays of neutral charmed particles required that for each event a volume be scanned for decays downstream of the primary vertex, with:

Horizontal Emulsion
A volume of size $\Delta X = \Delta Y = 600$ μm
and length $\Delta Z = 1000$ μm

Vertical Emulsion
A cylindrical volume of radius $r = 200$ μm
and length $\Delta Z = 1000$ μm

Scanback

Tracks with $P > 700$ MeV/c which extrapolate to within 2.0 mm of the primary vertex, which are not (initally) observed in the emulsion (i.e. tracks with $\Delta dX/dZ$, $\Delta dY/dZ \geq 15$ mrad, defined as "not observed") were searched for in the changeable sheet and "scanned back" to their origin in the emulsion (most often a gamma conversion, or nuclear interaction). Implementation of the scanback technique for the horizontal emulsion met with limited success for the same reasons as for the track followback technique. (Note that the methods of track-followback and scanback are "symmetric" operations in the process of event finding. A priori, scanners have no knowledge where the tracks originate. Tracks (chosen essentially at random) many times lead to the decay vertices first; hence scanback for the primary vertex was carried out in these events.) Particular care was taken when NH = 0, NS = 2,4,6,... prong events were found, for this reason. The ability to scanback tracks in the emulsion is a unique feature associated with this experiment and is an important factor in determining the mean lifetimes of charmed particles, as is discussed further, below.

CHARM DECAY SCANNING EFFICIENCIES

The ability to detect particle decays was not independent of the distance from the primary vertex. The scanning efficiency decreased near the primary vertex due to the obscuration of decays by other minimum ionizing (NS, or shower) tracks from the primary vertex, and also due to finite "diameter" size effects at the primary vertex. Far away from the primary vertex, the overall scanning efficiency decreased due to the fact that scanback of spectrometer tracks was possible only in the vertical emulsion. The scanning efficiencies of horizontal and vertical emulsion for charged and neutral charm decays were

determined in various ways, for several distance regions in the emulsion.

Scanning Efficiency Near the Primary Vertex

The effects of geometrical obscuration of decays from shower tracks were determined from knowledge of the angular distribution and also the number distribution of NS tracks, and by defining a detection criterion, that two tracks are resolvable as distinct entities for track separations greater than 3 μm (for grain sizes $d \simeq 0.7$ μm). Thus, the scanning efficiency due to geometrical effects is the fraction of tracks capable of being detected as distinct (i.e. separate) at a given distance from the primary vertex.

The scanning efficiency due to the finite "diameter" associated with the primary vertex was determined from the empirical dependence of the diameter on the number of NH and NS tracks present in the event, The diameters for 320 neutrino interactions (chosen at random) were measured to obtain the following analytic form:

$$D \doteq (NH + NS/2)/4 + 1.80 \quad (\mu m)$$

for diameters $D \geq 3$ μm with the observed NH and NS distributions as shown in Fig.40.

Charged Track Following Efficiency

The scanning efficiency as a function of follow length is shown in Fig.37 for the horizontal emulsion. (The track following efficiency for the vertical emulsion is similar to the horizontal emulsion over the angular regions scanned and for track follow lengths < 6 mm). The track following efficiency is the ratio of the number of tracks followed for a given distance, to the total number of followed tracks. Away from the primary vertex, the track following efficiency for multi-prong charged decays is approximately 95 ± 5% for tracks with $\theta < 200$ mrad and follow length less than 6 mm 90% of all charged tracks were followed the full 6.0 mm (or more).

Neutral Decay Volume Scanning Efficiency

The (volume) scanning efficiency for neutral decays in emulsion was estimated from the ratio of e^+e^- pairs (associated with neutrino interactions) found by volume scanning, to the total number of e^+e^- pairs expected from conversions in the emulsion from π^0 decay ($\sim 2\pi^0/\nu$-interaction). The volume scanning efficiency for finding e^+e^- pairs in the vertical emulsion was found to have a spatial dependence of the form:

$$\varepsilon(Z) = 0.60(1 - 0.05\ Z\ (\mathrm{mm}))$$

The volume scanning efficiency for finding e^+e^- pairs in emulsion is an upper limit on efficiency for finding decays of neutral charmed particles, as the track from an e^+e^- pair is 2 x minimum ionizing, whereas the tracks from the decay of a neutral charmed particle are only minimum ionizing.

Charged Decay Scanback Efficiency

The charged decay scanback efficiency was determined from knowledge of the number of tridents N with k reconstructed decay tracks, and the efficiency for finding a spectrometer track on the changeable sheet and following it into the emulsion. The scanning efficiency for finding a track on the changeable sheet is

$$\varepsilon_{cs} = 142/148 = 96 \pm 2\%$$

The charged scanback efficiency is given by the following:

$$\varepsilon_{sb}^{ch} = \frac{1}{N} \sum_k n_k (1-(1-\varepsilon_{cs})^k), \quad N = \sum_k n_k \quad .$$

Where n_k is the number of tridents with k reconstructed decay tracks.

The charged scanback efficiency was found to be significantly different for parent momenta above and below 10 GeV/c, as shown below. The average charged scanback efficiency (integrated over parent momentum spectrum) was obtained using all charged multi-prong decays.

k	$n_k(P_c<10GeV/c)$	$n_k(P_c>10GeV/c)$	n_k(Avg.)
0	4	0	4
1	7	1	8
2	4	1	5
3	0	6	6

Thus, the charged scanback efficiency is

$$\varepsilon_{sb}^{<ch} = 71 \pm 13\% \ (P_c < 10 \text{ GeV/c})$$

$$\varepsilon_{sb}^{>ch} = 100 \pm 13\% \ (P_c > 10 \text{ GeV/c})$$

$$\varepsilon_{sb}^{ch} = 81 \pm 9\% \ (\text{Average})$$

Neutral Scanback Efficiency

The neutral scanback efficiency was determined in a similar manner as for charged decays;

$$\varepsilon_{sb}^{N} = \frac{1}{N} \sum_k n_k (1-(1-\varepsilon_{cs})^k)$$

2-Prongs		4-Prongs		6-Prongs	
k	n_k	k	n_k	k	n_k
0	1	0	0	0	0
1	6	1	1	1	0
2	4	2	3	2	0
		3	1	3	0
		4	3	4	0
				5	2
				6	0

Thus the neutral scanback efficiency is $\varepsilon^{N}_{sb} = 94 \pm 5\%$. The momentum spectrum for neutral charmed particle decay candidates is significantly harder than for the charged charm decay candidates, having no low momentum event, except 635-4949. The charged scanback efficiency is lower than the neutral scanback efficiency, primarily due to the charmed baryon decays which have lower parent momenta, and thus lower daughter momenta; the daughter tracks are emitted at correspondingly larger angles in the laboratory. As a result, the track reconstruction efficency will therefore be lower for tracks from the decays of charmed baryons. See Fig.38.

Charged and Neutral Decay Scanning Efficiencies

The total scanning efficiencies for charged and neutral decays (shown in Fig.42) were obtained by joining together the scanning efficiencies in each region, weighted by the number of ν-events found by the horizontal and vertical emulsion groups. The events found by the Ottawa and Korean groups were classified with the vertical emulsion for the first 30 μm from the primary vertex, and with the horizontal emulsion for distances greater than this, because of the absence of scanback information for these two groups. For the vertical emulsion, the scanback of spectrometer tracks extended all the way up to the primary vertex, hence the vertical scanning efficiency included the track following (volume scanning) efficiency in each region and the charged (neutral) scanback efficiency for charged (neutral) decays, respectively.

The numerical values of the charged and neutral scanning efficiencies are summarized in Tables 3 and 4.

A summary of the event finding statistics appears in Table 5.

TABLE 3

CHARGED DECAY SCANNING SFFICIENCY

RANGE (μm)	ε^{ch} (%)	
0-2	0±8	
2-5	18±8	
5-10	50±6	
10-30	76±4	
30-3000	95±5	
3000-6000	85±6	
6000-60000	42±13	(P_c < 10 GeV/c)
6000-60000	59±13	(P_c > 10 GeV/c)
6000-60000	47±11	(Average)

TABLE 4

NEUTRAL DECAY SCANNING EFFICIENCY

RANGE (μm)	ε^{N} (%)
0-2	0±8
2-5	14±7
5-10	32±6
10-30	68±5
30-400	81±15
400-1000	71±11
1000-60000	55±5

DISCUSSION OF EVENT FINDING AND CHARM SEARCH

The flight lengths of charm decay candidates are shown in Fig.42 for charged and neutral charmed particles. The distribution of found events in Z indicates the unbiased nature of the scanning methods used in this experiment. The flight length distribution drops (nearly) to zero (with the exception of one event out of 49 total) at 20 μm, well before any significant drop in the scanning efficiency (See Figs.37, 38 and 39). Similarly, the event distribution drops to zero well before the downstream end of the target is reached (5 cm), while the scanning efficiency is still high in this region.

A significant number of charm decays would not have been observed without the use of the scanback technique, in that 5 out of 18 D^0, 2 charged decays and one neutral baryon candidate were found by this method. One event (665-4023) out of the 45 multi-prong charm decay candidates decayed in the changeable sheet (not in the fiducial volume) after travelling 6820 ± 100 μm and is therefore not included final event sample.

A plot of the production angles of charmed particles is shown in Fig.43. The angular distribution is observed to fall to zero well before the limits set by scanning criteria. The track following efficiency is high (95 ± 5%) for tracks with $\theta < 200$ mrad and follow length less than 6 mm The volume scanning efficiency for neutral decays falls of as 1 - 0.05L (mm), where L is the distance from the primary vertex. The volume scanning efficiency is thus only weakly θ-dependent. The θ-dependence of the scanback efficiency is a primarily a function of the track reconstruction efficiency angular dependence, which is in excess of (85 ± 5%) for $\theta < 200$ mrad.

A plot of the number of charm decays vs. Z is shown in Fig.35. The relative charm neutrino event finding efficiency (normalized to unity) is also shown in this figure. The effects of the overall event reconstruction efficiency were removed in the same manner as that for neutrino events in general (Fig.34.) As can be seen from the figure, the efficiency for finding charm is not flat in Z. Statistically, the ratio of the number of events found in the downstream half of the target to that for the upstream half of the target is 1.7 ± 0.5.

$$\langle P^{tot}_{0\text{-odd}} \rangle = 3.0 \pm 0.5\% \text{ (charged)}$$

$$\langle P^{tot}_{0\text{-even}} \rangle = 4.7 \pm 0.6\% \text{ (neutral)}$$

The probability $P_{P > P_{cut}}$ of the incident hadron having a momentum greater than a specified momentum cut P_{cut} is given by:

Charged Hadrons

$$P_{P_{proton} \geq P_{cut}} = \mathrm{Exp}(-0.77 P_{proton}) \text{ for protons}$$

$$P_{P_{\pi} \geq P_{cut}} = \mathrm{Exp}(-0.40 P_{\pi}) \text{ for pions}$$

(Spectra obtained from TOF identification.)

Neutral Hadrons

$$P_{P_{neutron} \geq P_{cut}} \simeq \mathrm{Exp}(-0.77 P_{neutron}) \text{ for neutrons}$$

(From isospin invariance.)

$$P_{P_{K^0} \geq P_{cut}} = b P_{K^0}^{-b+1},\ b = 2.32 \pm 0.44 \text{ for } K^0 \text{ [131]}$$

Since the ability to observe a nuclear interaction is not flat over all distances from the primary vertex, the interaction probability over a given scanning region $\mathrm{Pint}(Z_i)$ must be weighted by the scanning efficiency $\varepsilon(z_i)$ over that region.

$$\mathrm{Pint}(Z_i) = (\exp(-Z^L/\lambda_{int}) - \exp(-Z^H/\lambda_{int})); \qquad Z_i^L \leq Z_i \leq Z_i^H$$

The total probability of interacting in the emulsion and being detected is therefore $\sum_i \varepsilon_i(Z_i)\mathrm{Pint}(Z_i)$.

The charged and neutral scanning efficiencies (Fig.42) are summarized in Tables 3 and 4. Charged tracks are followed 6.0 mm on average. Scanback of charged tracks takes over after this point. Since not all primary tracks

Thus $\sum_i \varepsilon_i^{chgd}(Z_i)\mathrm{Pint}(Z_i) = 2.4\%$ for charged hadron interactions.

Neutral decays are volume scanned for 1.0 mm, along with scanback of charged tracks from neutral decays where needed. The last region must be weighted by the fraction of tracks that are scanned back.

Thus $\sum_i \varepsilon_i^{neut}(Z_i)\mathrm{Pint}(Z_i) = 1.0\%$ for neutral hadron interactions.

The number of events from hadronic interactions in charged current neutrino interactions mimicking charmed particle decays is obtained from the product of the factors discussed above.

<u>Number of Charged Hadronic Background Events:</u>

$$N_{int}^{proton} = 0.46 \ (0.02)$$

$$N_{int}^{\pi\pm K\pm} = 2.80 \ (0.57)$$

$$N_{int}^{chgd} = 3.26 \ (0.59)$$

<u>Number of Neutral Hadronic Background Events</u>

$$N_{int}^{neutron} = 0.23 \ (0.01)$$

$$N_{int}^{K^0} = 0.05 \ (0.01)$$

$$N_{int}^{\Lambda^0} = 0.02 \ (0.00)$$

$$N_{int}^{neutral} = 0.30 \ (0.02)$$

$$N_{INT}^{TOT} = 3.55 \ (0.60)$$

The first number is the total number of such background interactions over all incident particle momenta, and the numbers in parentheses are the number of events with incident hadron momenta above P_{cut} = 4.0 GeV/c.

Note that these numbers agree with the number of nuclear interactions mimicking charm decays as determined from the total number of observed charged (neutral) nuclear interactions (see Table 5), and the fractional NH = 0, NS = odd (even) prong rates.

The numbers given above are in fact upper limits to hadron induced backgrounds, as spectrometer/emulsion information on particle identity may be used in conjunction with known conservation laws (e.g. flavor and baryon number conservation) to eliminate (or confirm) nuclear interaction hypotheses. (See for example, event 635-4949.) Most nuclear interactions will not yield acceptable 3-C kinematic fits as charm decays.

TABLE 5

SUMMARY of EMULSION SCANNING RESULTS (August,1981)

	VERTICAL NAGOYA	VERTICAL OTTAWA	HORIZONTAL	TOTAL
EVENT FINDING				
# computer predictions	944	179	977	2100
# in fiducial volume	822	146	861	1829
# found	726	133	383	1242
(vol. scan)	0	78	314	392
(followback)	726	55	69	850
# failed	96	13	341	450
event finding efficiency (%)	93	90	53	68
<NH>	3.6	4.0	6.5	4.0
<NS>	5.8	6.0	6.2	6.0
CHARM SEARCH				
CHARGED DECAYS:				
# events searched	617	101	383	1101
# tracks followed	3027	509	1969	5505
# tracks followed/event	4.9	5.1	5.1	5.0
total track length followed (m)	16.4	5.7	12.7	34.8
length followed/track (mm)	5.4	11.1	6.4	6.3
# nucl int (multi-prong)	42	9	38	89
# kinks (non-charm)	22	5	21	48
# chgd charm cand	18	2	8	28
# kinks	3	0	2	5
# tridents	14	2	6	22
# double charged	1	0	0	1
NEUTRAL DECAYS:				
# events searched	617	116	383	1116
total volume scanned (mm^3)	174.5	43.3	175.0	392.8
# nucl. int.	1	0	0	1
# e^+e^- pairs (v.s.+ s.b.)	138	23	33	194
# vees (non-charm)	2	1	1	4
# neut charm cand	18	0	3	21
# vees *	11	0	1	12
# 4-prong	6	0	1	7
# 6-prong	1	0	1	2
# charm candidates (multi-prong)	33	2	9	44
# charm candidates (total)	36	2	9	49
# Identified Charm Candidates:				
D^+	4	0	1	5
D^0 *	17	0	2	19
F^+	2	0	1	3
Λ_c^+	4	2	2	8
Neutral Charm Baryon	1	0	0	1
# Ambiguous Charm Candidates:				
D^+/F^+	2	0	0	2
$D^+/F^+/\Lambda_c^+$	6	0	4	10

* Two of the D^0 (vee) candidates come from a single event (i.e.charm pair-production).

CHARM PARTICLE DECAY EVENT RECONSTRUCTION

For each neutrino event with a charmed particle decay found in the emulsion, a "standard" analysis procedure was adopted for reconstruction of not only the decay, but the entire neutrino interaction. This procedure was used in the reconstruction of all charm decay candidates. The average amount of time spent on reconstruction of each charm decay event was in excess of one man-month.

EVENT RECONSTRUCTION ALGORITHM:

1. Receive emulsion event information (e.g. NH, NS, X', Y', event vertex location, etc.)

2. Check with logbook for unusual data taking conditions (e.g. magnet off).

3. Dump visual display of event using "Analyzer" program, get X, U, V displays of hits in drift chambers, over-all event display, blow-ups of drift chamber hits, hits in TOF II, PbG array, and display of the calorimeter energy flow (paddle by paddle). Reconstruct charged tracks by hand using ruler and pencil, in all three views. Check for "out-of-time" tracks in drift chambers.

4. "Refit" event using MJG ν event track refitting program.

5. Account for all observed emulsion tracks. Compare NRS, TSY, MJG reconstruction programs for consistency, and consistency with visual information. Compare reconstruction programs and visual information with emulsion information. Request emulsion exit angles, $P\beta$ and ionization measurements for unreconstructed primary and charm decay tracks. Check again when requested emulsion information is received. Use weighted average of up-only and $P\beta$ measurements for momenta of up-only tracks. Account for all kinks, nuclear interactions, etc. in event; find associated shower tracks in drift chambers. Check for pion, kaon decay.

6. Look for extra tracks in drift chambers. (up-to-down, upstream only and downstream only tracks). Scanback these tracks.

7. Look for V^0-decay in drift chambers (both upstream and downstream). Reconstruct decay vertex. If in emulsion, scanback these tracks. Use available TOF information to determine if meson or baryon decay. Check $L/\gamma\beta c\tau$ for neutral decay particle hypotheses (e.g. K^0, Λ^0 etc.) Test coplanarity for two-body decay hypothesis, and whether neutral particle came from primary or secondary vertex. If coplanarity test results poor, look for additional neutral particles, e.g gammas and pi-zeros, for hypotheses for $K_L{}^0$, Σ^0 and Ξ^0 decay. Kinematic 1-C, 2-C and 3-C fits for V^0 decays to K^0_S, Λ^0, K^0_L, Σ^0, Ξ^0 decays

8. Check consistency of TOF II hits with tracks in downstream drift chambers. Check Y-positions of drift chamber tracks and TOF II predictions. Beware of backsplash from the lead glass array. Check timing of hits in TOF II counters. Obtain TOF I.D. for reconstructed up-to-down tracks. Check start time.

9. Project downstream drift chamber tracks into PbG array. Check consistency of hits in PbG with downstream drift chamber tracks and TOF information. Look for evidence of electrons (i.e. energy in region of entry of charged track E(PbG) > P(trk). Check TOF for consistency. Check whether electron comes from primary or secondary vertex, if track does not originate from either, perform scanback for e^+e^- pairs or decay vertex. Check for presence of opposite sign track with similar slopes. Check for effects of bremmstrahlung in appropriate PbG blocks. Check calorimeter row behind PbG blocks for consistency with electron hypothesis. (Interacting hadrons in PbG can mimick electrons, see Fig.25.)

10. Obtain "gamma candidates". Remove M.I. hits and electron energy, bremmstrahlung from blocks in lead glass array. "gamma candidates" are defined as the found e^+e^- pairs, plus the residual energy left over in each of the lead glass blocks. The slopes for each PbG gamma candidate are calculated using the centers of each block. Use "gamma" program to calculate two-gamma invariant masses, parent slopes, and momentum for all possible gamma candidate combinations. Adjacent two-block combinations for gamma candidates were processed in a similar manner, for one-block two-block and two-block two-block combinations.

11. Pi-zero (eta) candidates are defined as $M_{\pi^0(\eta)} = M_{\gamma\gamma} \pm 2.0$ S.D. or $E_{blk} > 4.0$ (16.3) GeV (Coalesced gamma's). Search for evidence of $K^0_s \rightarrow \pi^0\pi^0$ decay in π^0-π^0 mass combinations. Perform 1-C fits to pi-zero, eta and K^0_s candidates.

12. Project downstream drift chamber tracks into calorimeter. Check E(cal) for consistency with E(inc) row by row. Check shower development structure row by row. Look for excess E(cal) due to neutral hadrons. Check muon track, charm decay tracks and other tracks for consistency as muons and/or hadrons.

13. Project downstream drift chamber tracks into muon steel. Account for hits in muon counters. Check muon candidates for punchthrough.

14. Kinematic fits to charm decay candidates. Fit events with various kinematic fitting programs, utilizing all the available information on the event. Try various decay hypotheses to determine particle identity if the particle type is not obvious (see below). le Calculate decay time $\tau = (m/P)(\ell/c)$.

15. Look for evidence of resonant daughter states with two and three body mass combinations (e.g. $\rho^{\pm,0}$'s, K*'s, Δ's Σ*'s, etc.)

16. Look for evidence of resonant charm states with two and three body mass combinations of charm particle with charged particle from primary vertex, and/or gamma and pi-zero candidates.

17. Check for strange particle production in charm events, especially for F^+ meson and charmed-strange baryon decay candidates.

18. Calculate kinematical variables associated with event, e.g. E_{had}, E_ν, Q^2, ν, W, X, Y, Z, $\phi_{\mu ch}$.

MOMENTUM MEASUREMENT and PARTICLE IDENTIFICATION in EMULSION

Pβ Multiple Scattering Measurements in the Emulsion

Much more information concerning the decays of charmed particles could be obtained from measurements made in the emulsion than just information of a geometrical nature. The downstream spectrometer apparatus was not 100% efficient at reconstructing all decay tracks, particularly low momentum wide-angle tracks. For these tracks momentum information could be obtained from Pβ multiple scattering measurements in the emulsion. Pβ measurements for a particular track are obtained using a "stiff" track from the same event as a reference track, (usually the muon, for a charged current event), and measuring the deviations of the slow track relative to the reference track at various points along the particle's track [122,134,135]. In this way, the effects from microscope stage noise and distortion in the emulsion were eliminated to first order. The measurement of Pβ in the emulsion was more accurate than for drift chamber measurements of up-only tracks below 700 MeV/c. The weighted average of emulsion and counter measurements of the particle's momentum was used in the kinematic fits for such decay tracks.

Specific Ionization Measurements in Emulsion

Particle identification in emulsion was also possible from ionization measurements in the emulsion, provided the particle momentum was also known. The number of silver grains per unit length N/100 μm in the emulsion are counted along a track length, with a statistical resolution proportional to $\sqrt{N}$. The ionization I for a given track is then normalized to the ionization I_0 of the reference track (i.e. the muon or a fast hadron in the same event) to eliminate the effects of track fading and local grain density variations in the emulsion. Two corrections, both angular in nature were made to I/I_0. The first merely corrected for the true track length (as only the Z-distance is measured in the emulsion). The other correction (applied only for events found in the vertical emulsion) accounted for grain obscuration effects for steep tracks (small θ). Fig.44 shows a calculation for I/I_0 vs Pβ for e,μ,π,K,p in emulsion [134,135]. Pions are capable of being distinguished from kaons up to 800 MeV/c, kaons from protons up to 1.5 GeV/c. Electrons were identified in the emulsion from observation of trident (or pseudo-trident) production and/or shower production in the emulsion.

Range-Energy Measurements in Emulsion

For very slow tracks not exiting the emulsion, the (kinetic) energy of the particle could be determined from energy loss in the emulsion; the range-energy relationship is of the form [134,135]:

$$E_m = bM^{1-n} R_m^n \text{ (MeV)}$$

Where $b = 0.251$, $M_k = m_k/m_p$, m_p = proton mass

R_m = range (cm), $n = 0.581$

This measurement technique was used for only for one charmed decay track in the entire data sample (Event 549-4068).

KINEMATIC FITS to CHARMED PARTICLE DECAYS

Each charm decay candidate was kinematically fit with as high a constrained fit as possible. The kinematic fitting programs used in the data analysis were variations of a standard fitting program [217] which used the method of linearized least squares in conjunction with Lagrange multipliers. 0, 1, 2 and 3-C fits were made for the decays of charmed particles;

1. 0-C fits for decays with an (unobserved) missing neutral. Parent mass assumed, the parent momentum and missing neutral momentum and slopes are calculated.

2. 1-C fits for short decays (unmeasurable parent slopes). Parent mass assumed, parent momentum and slopes are fitted. There were no charged decay candidates in this category, and only one neutral decay candidate (654-3711).

3. 2-C fits, measured parent X and Y slopes, fitted parent mass and momentum.

4. 3-C fits, measured parent slopes, parent mass assumed, fitted parent momentum.

5. Kinematical fits to decays of daughter particles. 1-C fits to pi-zeroes; 1, 2 and 3-C fits to K_s^0 and Λ^0.

6. 2-C and 3-C fits to nuclear and neutrino interactions.

CHARM DECAY FITTING ALGORITHM:

The following procedure was used for fitting charm decays:

1. Check parent slopes and decay slopes for geometrical evidence of missing neutrals. If neutral two-body decay, test coplanarity. (e.g. K^0_S, neutral hyperon background.)

2. 1-C, 2-C, 3-C fits: The initial fit hypothesis consisted only of charged decay tracks. TOF, emulsion I.D. information used to limit number of hypotheses.

3. If $P_\perp$ balance poor (i.e. C.L.(2-C) 1.0%), try all decay hypotheses consistent with $\Delta C = -\Delta S$ rule, for a single observed and reconstructed neutral particle, with $P_\perp$ in required quadrant. If there are no observed neutrals, or if the event is a semi-leptonic decay, perform -1C fit with accompanying 0-C missing neutral fit to assumed charmed particle. Input solutions of 0-C fit to primary vertex fit of entire event to determine correct 0-C solution, if feasible.

4. For 2-C and 3-C fits, if $P_\perp$ balance still poor and/or 2-C mass below charm particle mass, try all decay hypotheses consistent with $\Delta C =- \Delta S$, with multiple neutral daughters. For situations where the inclusion of a pi-zero in the decay hypothesis has several pi-zero candidates, all of which may yield acceptable 2-C and 3-C fits, the pi-zero which simultaneously has the greatest 1-C pi-zero C.L., and 2-C and 3-C charm decay fit C.L. is assumed to be the most likely candidate. If the event is unreconstructable, 0-C fits to assumed charmed particles. (Input solutions of 0-C fit to primary vertex fit of entire event to determine correct 0-C solution, where possible.)

5. For 1-C and 3-C fits, the values used for the masses of the charmed particles were [160]:

$$M_{D^+} = 1868.3 \text{ MeV}/c^2$$

$$M_{D^0} = 1863.1 \text{ MeV}/c^2$$

$$M_{F^+} = 2030.0 \text{ MeV}/c^2$$

$$M_{\Lambda_c^+} = 2285.0 \text{ MeV}/c^2$$

6. 1, 2 and 3-C fits of decay as hadron-induced nuclear interaction. Use decay hypotheses consistent with nuclear interactions. Test hypotheses for pion, kaon, and nucleon-induced reactions. (All events were tested in this manner and failed as nuclear interactions, i.e. 2-C and 3-C C.L.< 1%).

7. Identify decay particle from χ^2, C.L., TOF and emulsion I.D. information. For fitted events, only those decay hypotheses with 1-C, 2-C or 3-C confidence levels greater than 1% are kept.

8. Calculate decay-times and decay-time errors using fitted 3-C momentum.

CALCULATION OF PARTICLE MEAN LIFETIMES

The mean lifetime for each charmed particle species was determined by the method of maximum likelihood. For an unstable particle obeying an exponential decay distribution with a mean lifetime τ, the probability of decaying at the time t_i in the time interval dt is given by:

$$dP(t_i,\tau) = P(t_i,\tau)dt = 1/\tau \exp(-t/\tau)dt$$

$$\text{with } \int_0^\infty P(t_i,\tau)dt = 1$$

As the scanning efficiency for observing decays is biased against observing extremely short and also long decay times, the analytic form of the decay distribution must be modified to reflect this bias, and is given by:

$$dP(t_i,\tau) = \varepsilon(\ell_i)\frac{1}{\tau} e^{-t_i/\tau} /A_i(\tau)dt$$

Where $\varepsilon(\ell_i)$ is the scanning efficiency in the i-th region, and ℓ_i is the distance from the primary vertex.

$$t_i = \frac{m}{P_i}\frac{\ell_i}{c}$$

$$A_i(\tau) = \int_0^\infty \frac{1}{\tau}\varepsilon(\ell_i \frac{t}{t_i})e^{-t/\tau}dt = \frac{m}{P_i c}\int_0^\infty \frac{1}{\tau}\varepsilon(Z)e^{-mZ/P_i c\tau}dZ$$

$$t = \frac{m}{P_i}\frac{Z}{c}$$

$$p_i c = m\ell_i/t_i = mz/t$$

$$t = \frac{Z}{\ell_i} t_i \text{ or } z = \frac{t}{t_i}\ell_i$$

For a set of N independent decays which have the decay probability distribution given above, the likelihood function $\mathscr{L}(\tau)$ is defined as:

$$\mathscr{L}(\tau) = \prod_{i=1}^{N} P(t_i,\tau) = \prod_{i=1}^{N} \varepsilon(\ell_i)\frac{1}{\tau}\frac{e^{-t_i/\tau}}{A_i(\tau)}$$

The most likely value of the mean lifetime τ is that value of τ which maximizes the likelihood function $\mathscr{L}(\tau)$, or more conveniently $\ln(\mathscr{L}(\tau))$:

$$\partial \ln(\mathscr{L}(\tau))/\partial\tau = 0$$

The one and two S.D. limits (68.3% C.L., 95.4% C.L., respectively) on the lifetime are determined from the values of τ where $\ln(\mathscr{L}(\tau))$ is reduced by 0.5 and 2.0 respectively, i.e.

$$\text{1 S.D. LIMITS: } \ln\mathscr{L}(\tau) - 0.5$$

$$\text{2 S.D. LIMITS: } \ln\mathscr{L}(\tau) - 2.0$$

A more detailed discussion of the method of maximum likelihood appears in Refs.[123,136].

CHARM DECAY CANDIDATE EVENT SAMPLE

From the charged charm candidate event sample of 23 multi-prong and 5 single-prong events, 5 events were unambiguously reconstructed as the decays of D^+ mesons, 3 events were unambiguously reconstructed as the decays of F^+ mesons, and 8 events were reconstructed as the decays of Λ_c^+ charmed baryons. The remaining 12 charm decay candidates were also reconstructed, but with varying degrees of uncertainty and ambiguity as to parent identity, due to specific difficulties associated with each event. (e.g. complicated event, magnet off, secondary nuclear interactions of daughter tracks in emulsion, etc.)

A brief discussion of each charged charmed particle decay candidate is given in the Appendices. The raw counter and emulsion data for each event are contained in data summary sheets in Table 23. A description of the format and how to read the summary sheets is given in Appendix B.

The decay times, parent masses and momenta as obtained from the results of the kinematic fits for each event are summarized in Tables 6 and 8 for the D^+ and F^+ mesons, Table 10 for the Λ_c^+ baryons, and Table 12 for the ambiguous events. The charge sign of the muon from the primary vertex is included for each event entry in these tables, to indicate neutrino or anti-neutrino induced production of charm. In one event (597-1851) no muon was observed, although it was not possible to positively <u>exclude</u> the presence of a muon from the primary vertex, due to the inability to identify <u>all</u> particles in this event.

For each of the charmed particle decay candidates, daughter particles emitted in the decay of the parent which have been identified with > 90% C.L. by TOF (or emulsion) methods are underscored with a _ (~) respectively.

For all events listed with a neutral particle as one of the decay products, the charged-tracks-only 2-C fit indicated the presence of one or more neutral particles in the decay with > 99% C.L. Neutral particles emitted in the decay which are unobserved in the spectrometer are enclosed in parentheses, e.g. (π^0). Neutral particles not enclosed in parentheses are observed either in the emulsion and/or the spectrometer, and are underscored if identified in a similar manner to that for charged tracks, e.g. $\Lambda^0 \rightarrow p\pi^-$, or from kinematic analysis (i.e. a unique interpretation).

The individual χ^2, C.L. results for the kinematic fits to charm decays are summarized in Tables 7, 9, 11, 13 for the D^+, F^+, Λ_c^+ and ambiguous charm events, respectively. The results for both 2-C and 3-C fits are given, as they collectively determine, on an event-by-event basis, the consistency of the event sample with a given particle state, and test for systematic effects on the likelihood of additional missing neutrals, offsets in energy and momentum calibrations, etc.

The number of iterations the kinematic fitting program takes to converge (i.e. to conserve energy and momentum) is included in the tables, as it is an important indicator of the validity, or "goodness of fit" for each event. It was observed during the course of event fitting that incorrect or incomplete decay hypotheses would, apart from having poor χ^2 and C.L.'s, also take many iterations to converge. Events with the number of iterations > 5 were almost always unacceptable for the above reasons, and also because of kinematic fits with too large input errors.

The collective χ^2, C.L. distributions, along with the ΔPx and ΔPy for charm decays are shown in Fig.45. The constrained charmed particle masses from 2-C fits are shown in Fig.48. An investigation of the possiblity of systematic "pulls" in the kinematic 2-C and 3-C fits found no evidence for significant shifts in any of the measured vs. fitted variables. The results of this investigation are summarized in Tables 21 and 22.

1-C fits of π^0's used in the reconstruction of charmed particles are summarized in Table 19. 1-C fits of K_S^0 and Λ^0 used in the reconstruction of charm decays are summarized in Table 20. The 3-C decay times of the unambiguous charmed particle decays for each particle species were used in the determination of the mean lifetime for that particle type.

DETERMINATION OF THE D^+ LIFETIME

The mean lifetime for the D^+ was determined from the reconstructed decays of 5 unambiguously identified D^+ mesons, summarized below in Tables 6 and 7. The D^+ lifetime is:

$$\tau_{D^+} = 10.3 \begin{smallmatrix} +10.3 \\ -4.2 \end{smallmatrix} \times 10^{-13} \text{ sec}$$

A plot of $\ln \mathscr{L}(\tau)$ vs. τ for the D^+ is shown in Fig.50.

The averaged parent momentum was used to determine the mean decay time for one event (580-4508) which had a missing neutral (and thus two momentum solutions, 600 MeV/c apart). The other two events with 0-C fits had unique solutions (see Appendix A.). (Equal weights are assigned to the two momentum solutions, in the absence of an (independently measured) charmed particle momentum spectrum.)

The charged scanning efficiency with the scanback efficiency for P > 10 GeV/c was used in the lifetime calculation, corresponding to the observed D^+ momentum spectrum. A one S.D. change in the overall charged decay scanning efficiency shifts the fitted D^+ lifetime by 8%. The sensitivity of the D^+ lifetime on the scanback efficiency is 5.0% (2.5%) for the worst case (average) charged scanback efficiencies. (Worst case = scanback efficiency for charm decays with $P_{c^-} < 10$ GeV/c.) Choosing the high or low solution in the unconstrained 0-C fit displaces the lifetime by ± 2.1%.

The (weighted) mass for the D^+ is 1851 ± 20 MeV/c^2 . (The value obtained for the D^0 is 1856 ± 15 MeV/c^2 [123].)

TABLE 6

SUMMARY OF D^+ DECAY CANDIDATES

EVENT NUMBER	MUON	DECAY MODE HYPOTHESIS	D.L. (μm)	P_c (GeV/c)	MASS (MeV/c^2)	DECAY TIME ($x10^{-13}$ sec)
512-5761	-	$D^+ \to K^- \pi^+ \underline{\pi}^+ \pi^0$	457±5	10.4±0.1	1829±35	2.77±0.05
		$F^+ \to K^- K^+ \underline{\pi}^+ \pi^0$		10.3±0.1	2011±33	3.00±0.05
546-1339	-	$D^+ \to K^- \pi^+ \underline{\mu}^+ (\nu_\mu)$	2150±50	16.6±0.2	0-C	8.06±0.22
		$F^+ \to \pi^- \pi^+ \underline{\mu}^+ (\mu_\nu)$		13.3±0.2	0-C	10.94±0.16
				36.8±0.2		2.95±0.02
580-4508	+	$D^- \to \pi^+ \underline{K} e^- (\bar{\nu}_e)$	2307±50	9.46±0.15	0-C	15.20±0.40
				10.01±0.13		14.37±0.36
598-1759	-	$D^+ \to K^- K^+ \underline{\pi}^+ \underline{\pi}^0$	1802±15	17.4±0.3	1862±25	6.44±0.13
663-7758	-	$D^+ \to K^- \pi^+ e^+ (\nu_e)$	13000±50	114.3±7.6	0-C	7.08±0.44
		$F^+ \to \pi^- \pi^+ \underline{e}^+ (\nu_e)$		96.8±7.6	0-C	8.36±0.47

TABLE 7

SUMMARY OF D^+ DECAY KINEMATIC FITS

EVENT NUMBER	2-C FITS χ^2	2-C FITS C.L.	2-C FITS ITER	3-C FITS χ^2	3-C FITS C.L.	3-C FITS ITER	ΔP_x (MeV/c)	ΔP_y
512-5761	5.98	0.05	3	7.07	0.07	2	-114±16	87±52
	5.98	0.05	3	6.26	0.10	2	-114±16	87±52
598-1759	2.23	0.33	2	2.27	0.52	2	-44±79	-85±67

F^+ and Λ_c^+ Background in D^+ Decays

The F^+ background associated with the above sample of semi-leptonic D^+ decays occurs from the processes shown by the Feynman diagrams in Fig.49. The number of contaminant F^+ decays within the D^+ sample is the combined sum of the probabilities for each individual D^+ event to be from the decay of an F^+, rather than a D^+ meson. Each individual F^+ probability is the product of the probability of producing an F^+ (relative to a D^+) in a neutrino interaction, and the specific decay background probability for that event. Assuming equal production ratios for D^+ and F^+ mesons (as an upper limit), along with the assumption that $Br(F^+ \to \pi^+\pi^-\ell^+\nu_\ell) < 5\%$, based on theoretical calculations of the rates associated with the diagrams in Fig.49, and the measured F^+ lifetime (see Appendix A for further details). Thus, the maximum F^+ contamination, or F^+ background in the D^+ decay candidates is:

$$N^{F^+}_{BKGND} < 0.5(0.20 + 0.05 + 0.00 + 0.20 + 0.05) = 0.25 \text{ Events}$$

The individual F^+ contributions from event 512-5761 and event 598-1759 are due to π/K ambiguity associated with one of the daughter tracks (favored to be a π^+ at the 80% C.L.) and a unobserved π^0, respectively. See Appendix A for further details.

Since the F^+ lifetime is observed to be shorter than the D^+ (see below), the most conservative method of estimating the F^+ background is to cast out the event with the shortest decay time (Event 512-5761). The average decay time is thus increased by 16%, a small effect in comparison to the statistical error on the mean lifetime.

The Λ_c^+ contamination in the D^+ sample, obtained by postulating a missing neutron or assuming the untagged positive hadrons in the decays are protons, is negligibly small, as the minimum mass possible is more than 3 S.D. above the Λ_c^+ mass in all cases except event 598-1759 where the 3-C C.L. = 0.035 for $\Lambda_c^+ \to K^-p\pi^+\pi^0$

Determination of the Ratio of D^+, D^0 Lifetimes

The lifetime of the D^+ is measured to be a factor of three longer (by 1.7 S.D.) than the lifetime of the of the D^0 meson using all 18 reconstructed D^0 decays:

$$\tau_{D^0} = 3.2 \begin{smallmatrix} +1.0 \\ -0.7 \end{smallmatrix} \times 10^{-13} \text{ sec}$$

However, it was noticed that within the D^0 sample, there are indications of distinct lifetime populations, in that:

$$\tau(D^0 \rightarrow \text{S.L.}) = 8.5 \begin{smallmatrix} +9.2 \\ -3.6 \end{smallmatrix} \times 10^{-13} \text{ sec (3 Events)}$$

$$\tau(D^0 \rightarrow \text{N.L.}) = 2.3 \begin{smallmatrix} +0.8 \\ -0.5 \end{smallmatrix} \times 10^{-13} \text{ sec (15 Events)}$$

The semi-leptonic D^0 decays appear to be longer-lived than the non-leptonic decays. The identity of the 15 non-leptonic decays is more certain, as 11 are fully-constrained 3-C fits; of the other 4, three are 0-C fits (all of which have a single solution; 1 at minimum mass, 2 have D*'s) and one is a 1-C fit (6.5 μm decay length). All of the semi-leptonic D^0 decays have two momentum solutions, with significant separation. (The same averaging technique was applied for the parent momenta of semi-leptonic D^0 decays as for 0-C fits of charged charmed particles.) The probability that all three semi-leptonic decays have the longest decay times in the D^0 sample with the same mean lifetime as that of the other D^0 decays is less than 1.5%, based on binomial statistics. These two "lifetimes" for the neutral D^0 meson represent a 2.0 S.D. effect. It is interesting to note that several visible (semi-leptonic) neutral decay candidates have been observed in bubble chamber neutrino experiments [97-100]. The exact nature of the origin of this phenomenon is difficult to determine at this time. Possible sources are D^0-$\bar{D}^0$ mixing, statistical fluctuations, or perhaps a particle state distinct from the D^0. See Ref.[123] for further discussion.

In determining the ratio of D^+ to D^0 lifetimes, the D^0 lifetime as determined from the non-leptonic D^0 decays is used. Several methods may be used to determine the ratio of D^+ to D^0 lifetimes. A naive method is to simply take the ratio of the two lifetimes, and attempt to estimate (asymmetric) errors. This method yields

$$\tau^+/\tau^0 = 4.5 \begin{smallmatrix} +4.8 \\ -2.1 \end{smallmatrix}$$

A more sophisticated method is to observe that the likelihood functions for the D^+ and D^0 are approximately log-normal,

$$\mathscr{L}(\tau) \sim \exp[-(\ln \tau/\tau_{MAX})^2/2\sigma^2)]$$

Thus, via Monte Carlo techniques [123], ratios of the D^+ to D^0 lifetimes are generated from log-gaussian distributions of the lifetimes. The results are histogrammed and the errors on the ratio of lifetimes obtained from the points where 68.3% of the distribution is contained within the high and low 1 S.D. limit points, the remaining 31.7% divided into two equal parts (15.8%) above and below the 1 S.D. limit points. The ratio of lifetimes as computed via this method is:

$$\tau^+/\tau^0 = 4.5 \begin{smallmatrix} +4.4 \\ -2.3 \end{smallmatrix} \text{ (Monte Carlo calculation)}$$

This ratio differs by more than 2.5 standard deviations from unity. The probability of the D^+ and D^0 having equal lifetimes (with a mean lifetime of 4.8×10^{-13} sec) and obtaining the measured D^+, D^0 lifetimes as given above is less than 1.0%.

A third method used to determine the lifetime ratio was to define a a two-parameter likelihood function $\mathscr{L}(\tau^+,\tau^0;R)$; i.e. the product of the single-parameter likelihood functions for the D^+ and D^0 samples:

$$\mathscr{L}(\tau^+,\tau^0;R) = \mathscr{L}(\tau^+) \times \mathscr{L}(\tau^0) \quad \text{Where } R = \tau^+/\tau^0$$

$$= \prod_i^{N^+} \varepsilon^+(\ell_i) \frac{1}{\tau^+} \frac{e^{-t_i^+/\tau^+}}{A_i^+(\tau^+)} \prod_j^{N^0} \varepsilon^0(\ell_j) \frac{1}{\tau^0} \frac{e^{-t_j^0/\tau^0}}{A_j^+(\tau^0)}$$

The one and two S.D. limits (or contours in the $\tau^+ - \tau^0$ plane) are shown in Fig.51 for the log of the likelihood function $\ln\mathscr{L}(\tau^+,\tau^0;R)$ The log of the likelihood function $\ln\mathscr{L}(\tau^+,\tau^0;R)$ is multi-valued for a fixed value of R, and has a global maximum at the arithmetic ratio of the lifetimes.

For a given value R of the ratio of lifetimes, there exists a maximum value for $\ln \mathscr{L}(\tau^+,\tau^0;R)$ which we denote as $\ln \xi(R)$, which is the most probable value of the D^+, D^0 lifetimes for this R-value. If R is allowed to vary i.e. $0 < R < \infty$ then the resulting curve for $\ln\xi(R)$ is the envelope of most probable values of the D^+, D^0 lifetimes at each value of R, as shown in Fig.52. The ratio of the D^+ to D^0 lifetimes, as obtained from $\ln\xi(R)$ is:

$$\tau^+/\tau^0 = 4.5 \begin{smallmatrix} +5.0 \\ -2.0 \end{smallmatrix} \text{ (Max. Likelihood Method)}$$

This ratio differs by more than 2.6 standard deviations from unity. The three methods of determination of the D^+, D^0 lifetime ratio yield similar results.

The ratio of D^+, D^0 lifetimes is also subject to uncertainties which are systematic in origin, in that the true decay times of the events in the ambiguous charged charm decay sample may have significant impact on the D^+ lifetime, and thus on the lifetime ratio. (See the discussion below for these events, and for their impact on the D^+, F^+ and Λ_c^+ lifetimes.)

An additional word of caution is necessary here, as it must be pointed out that if the preliminary indications (using all 18 D^0 events) for distinct lifetime populations within the D^0 sample turn out to in fact be true (e.g. there exists a D_L^0 and a D_S^0), then the D^+, D^0 ratio as presently measured must be understood as an <u>average</u> of lifetimes between the D^0 populations. The ratio of D^+, D^0 lifetmes for this situation is (for all 18 D^0 events):

$$\tau^+/\tau^0 = 3.2 \begin{smallmatrix} +3.0 \\ -1.5 \end{smallmatrix}$$

The probability of the D^+ and D^0 mesons having equal lifetimes and obtaining this ratio of R is less than 2.2%, for this sample of D^0 events.

DETERMINATION OF THE F^+ LIFETIME

Three charm candidates in the charged event sample were found to be inconsistent with D^+ meson (Λ_c^+ baryon) decays, in that the reconstructed masses were well above (below) the D^+ (Λ_c^+) mass in each event. Furthermore, the observed decay modes for these three events are not consistent with Cabibbo-favored decays of D^+ mesons, but are consistent with the (Cabibbo-favored) decays expected of F^+ mesons, (and Cabibbo-unfavored decays of D^+ mesons).

A discussion of each F^+ charmed candidate event is given in Appendix A. The tables below summarize the relevant kinematical information.

The mean lifetime for the F^+ as determined from this sample of events using the method of maximum likelihood is:

$$\tau_{F^+} = 2.0 \begin{smallmatrix} +1.8 \\ -0.8 \end{smallmatrix} \times 10^{-13} \text{ sec}$$

A plot of $\ln \mathscr{L}(\tau)$ vs. τ for the F^+ is shown in Fig.50.

The charged scanning efficiency with the averaged scanback efficiency was used in the lifetime calculation, corresponding to the observed F^+ momentum spectrum.

A 1 S.D. change in the scanning efficiency has little effect on the F^+ lifetime; the F^+ lifetime is sensitive to the scanback efficiency at the 0.5% level i.e. use of the value for the scanback efficiency above and below 10 GeV/c changes the F^+ lifetime by this amount.

The (weighted) F^+ mass is 2042 ± 33 MeV/c^2 .

TABLE 8

SUMMARY OF F^+ DECAY CANDIDATES

EVENT NUMBER	MUON	DECAY MODE HYPOTHESIS	D.L. (μm)	P_c (GeV/c)	MASS (MeV/c^2)	DECAY TIME ($x10^{-13}$ sec)
527-3682	_	$F^+ \rightarrow \pi^+\pi^-\pi^-\pi^0$	670.0±4.0	12.2±0.3	2026±56	3.70±0.08
597-1851	*	$F^+ \rightarrow K^-\pi^+\pi^+K^0_L$	130.0±1.0	9.3±0.4	2057±110	0.97±0.09
638-9417	-	$F^+ \rightarrow K^+K^-\pi^+\pi^0$	153.0±8.0	6.0±0.1	2050±45	1.72±0.09

* No muon observed, see Appendix A. for details.

TABLE 9

SUMMARY OF F^+ DECAY KINEMATIC FITS

EVENT NUMBER	2-C FITS χ^2	2-C FITS C.L.	2-C FITS ITER	3-C FITS χ^2	3-C FITS C.L.	3-C FITS ITER	ΔP_x (MeV/c)	ΔP_y (MeV/c)
527-3682	2.27	0.32	2	2.30	0.51	1	-141±120	63±76
597-1851	1.43	0.49	3	1.50	0.68	2	9±583	-153±128
638-9417	1.35	0.51	2	2.03	0.57	3	16±73	300±97

D^+ and Λ_c^+ Background in F^+ Decays

The D^+ background in each of the 3 F^+ events is purely kinematic in origin; i.e. the 3-C confidence level for a Cabibbo-unfavored decay of a D^+ with mass 1868.3 MeV/c^2 compared to that for for a F^+ meson with mass 2030.0 MeV/c^2. The D^+ decay background in the F^+ candidates is thus:

$$N_{BKGND}^{D^+} < 0.50(0.013 + 0.030 + 0.000) = 0.022 \text{ Events}$$

Equal production rates for D^+ and F^+ were assumed. For smaller F^+/D^+ production ratios, e.g. 0.3, the D^+ background will scale (i.e. increase) accordingly. If the TOF information is ignored, the D^+ decay background for decay hypotheses where the K^+ is taken to be a π^+ is less than 0.009 events. The Λ_c^+ decay background in the F^+ sample is negligible, as all of the positive hadrons from the F^+ decays are identified by TOF as kaons or pions, in excess of 3.5 S.D. from a proton in all cases. The 3-C confidence levels for Λ_c^+ decay hypotheses are negligible (0.00%) for such decays, in any case. Therefore, identification of these charm decay candidates as particles other than D^+ mesons or Λ_c^+ baryons does <u>not</u> depend upon TOF information.

Thus, it can be seen from the above that this experiment has obtained strong, clear, and unambiguous evidence for the existence of the F^+ meson, in that the F^+ lifetime, mass, and observed decay modes are distinct from those of the D^+ meson and Λ_c^+ baryon, also because of the low (1%) D^+ and Λ_c^+ background in the F^+ sample.

DETERMINATION OF THE Λ_c^+ LIFETIME

The mean lifetime for the Λ_c^+ was determined from the decays of 8 identified Λ_c^+ baryons (summarized in the tables below) using the method of maximum likelihood.

$$\tau_{\Lambda_c^+} = 2.3 \begin{smallmatrix}+1.1\\-0.7\end{smallmatrix} \times 10^{-13} \text{ sec}$$

A plot of $\ln \mathscr{L}(\tau)$ vs. τ for the Λ_c^+ is shown in Fig.50.

For the Λ_c^+ decay candidates with 0-C fits, the average value of the decay times was used in the lifetime determination. Choosing all high (or low) 0-C solutions shifts the fitted lifetime by less than 3%. A 1 S.D. change in the scanning efficiency affects the Λ_c^+ lifetime at the 5% level. The Λ_c^+ lifetime is not sensitive to the scanback efficiency at the 0.1% level.

The weighted mass of the Λ_c^+ is 2265 ± 30 MeV/c^2 . The currently accepted value for the Λ_c^+ mass is 2285 ± 5 MeV/c^2 [85,91].

D^+ and F^+ Background in Λ_c^+ Decays

Nuclear Interaction Background in Λ_c^+ Decays

The D^+ and F^+ background is negligible for Λ_c^+ decay, as the daughter protons in four of the eight Λ_c^+ decays are identified from TOF by more than 3.5 S.D. in all cases, and the presence of the Λ^0 in each of the four other Λ^0 events is necessary to balance momentum at the decay vertex. As the momentum spectrum of the Λ_c^+ charmed baryons is lower than that for the other charmed particles, the probability of nuclear interaction background within the event sample is highest for the Λ_c^+, due to this fact, and also due to the presence of a identified baryon in the final state. Thus, the probability of nuclear background interaction as the source of each event was calculated, using the method described above. The total number of nuclear interaction background events in the Λ_c^+ sample of eight events is calculated to be less than 2.3×10^{-2} events. (See Appendix A for further details and a event-by-event summary of the nuclear interaction background for charmed baryons.)

TABLE 10

SUMMARY OF Λ_c^+ DECAY CANDIDATES

EVENT NUMBER	MUON	DECAY MODE HYPOTHESIS	D.L. (μm)	P_c (GeV/c)	MASS (MeV/c^2)	DECAY TIME ($\times 10^{-13}$ sec)
476-4449	-	$\Lambda_c^+ \to p\pi^+\pi^+(K_L^0)$	27.2±1.0	2.7±0.1 4.8±0.1	0-C	0.79±0.04 0.44±0.04
498-4985	-	$\Lambda_c^+ \to \Lambda^0\pi^+\pi^-\pi^+$	180.0±5.0	8.4±0.1	2274±41	1.63±0.05
499-4713	-	$\Lambda_c^+ \to \Sigma^0\pi^+$	366.0±6.0	4.2±0.1	2269±17	6.60±0.14
549-4068	-	$\Lambda_c^+ \to pK^-\pi^+(\pi^0)$	20.6±2.0	1.9±0.1 2.5±0.1	0-C	0.77±0.07 0.63±0.07
567-2596	-	$\Lambda_c^+ \to p\ K_L^0$	175.0±5.0	5.8±0.1	2204±207	2.30±0.08
602-2032	-	$\Lambda_c^+ \to p\pi^+\pi^-(K_S^0)$	282.5±5.0	6.3±0.1	0-C	3.40±0.10
610-4088	-	$\Lambda_c^+ \to \Lambda^0\pi^+\pi^-\pi^+$	221.0±4.0	4.7±0.2	2374±62	3.60±0.19
650-6003	-	$\Lambda_c^+ \to \Lambda^0\pi^+\pi^-\pi^+$	40.6±2.0	5.7±0.1	2131±63	0.54±0.03

TABLE 11

SUMMARY OF Λ_c^+ DECAY KINEMATIC FITS

EVENT NUMBER	2-C FITS χ^2	2-C FITS C.L.	2-C FITS ITER	3-C FITS χ^2	3-C FITS C.L.	3-C FITS ITER	ΔP_x (MeV/c)	ΔP_y (MeV/c)
498-4985	2.83	0.24	2	2.90	0.41	2	251±157	-55±89
567-2596	0.15	0.93	4	0.28	0.97	3	-137±169	-89±620
610-4088	5.48	0.06	6	8.08	0.04	5	114±90	213±156
650-6003	0.14	0.93	2	3.89	0.27	4	27±86	-44±89

AMBIGUOUS CHARM DECAY CANDIDATES

Nine charged multi-prong and three single-prong (kink) charm decay candidates were found in the emulsion, which, for various reasons it was not possible to obtain satisfactory kinematical fits. Hence, it was not possible to determine parent identity and/or decay times with a high degree of certainty in these events. For example, event 502-354 occurred when the magnet was off; consequently no momentum information from the spectrometer was available to aid in event reconstruction. In event 665-4023, the decay occurred in the lucite base of the changeable sheet (outside the fiducial volume).

Only two of the remaining seven events have acceptable constrained 2-C and 3-C fits. The quality of track information for the other five events was such that no acceptable 2-C and 3-C kinematic fits were obtained. In each of these events, the presence of a neutral particle is required to balance momentum at the decay vertex, for which evidence was observed in the spectrometer, but not in such a way as to uniquely determine the parent identity. Thus, unfortunately, it was not possible to include these events in the determination of charmed particle lifetimes.

To first order, the predominant effect of non-inclusion of these events in the lifetime data sample is to merely degrade the statistical error on the mean lifetime and increase the statistical fluctutations of the measured lifetime about the true lifetime for the particular charmed particle species to which they belong.

The determination of the mean lifetime for a given particle species may be affected from biases other than those due to purely geometrical scanning inefficiencies. One such bias, that of a momentum dependence for scanback of spectrometer track, has already been discussed above in some detail. Another possible source of bias associated with 0-C fits is discussed below. Biases associated with the geometrical acceptance of the spectrometer have been shown to be small.

The kinematical fit results for each event are summarized in the tables below. for the constrained and unconstrained charged charm decay candidates.

Ambiguous Charm Decay Candidates (Constrained Events)

The first of the two ambiguous constrained events has a rather long decay time. Inclusion of this event in the lifetime determination for the D^+ has little impact on the D^+ lifetime:

$$\tau_{D^+} = 10.9 \begin{smallmatrix} +9.0 \\ -4.1 \end{smallmatrix} \times 10^{-13} \text{ sec}$$

i.e. a change of approximately 6% in the D^+ lifetime. However if this event is included in the F^+ or Λ_c^+ lifetime determination, the F^+ and Λ_c^+ lifetimes are shifted by factors of 2.4 and 1.6 respectively, i.e. approximately a 1.5 S.D. change in the F^+ and Λ_c^+ lifetimes:

$$\tau_{F^+} = 4.7 \begin{smallmatrix} +3.6 \\ -1.8 \end{smallmatrix} \times 10^{-13} \text{ sec}$$

$$\tau_{\Lambda_c^+} = 3.4 \begin{smallmatrix} +1.6 \\ -0.9 \end{smallmatrix} \times 10^{-13} \text{ sec}$$

The second event has no obvious kinematical preference among the three charged charmed particle types. Inclusion of this event with the 5 D^+ unambiguous decays has a 20% effect on the D^+ lifetime:

$$\tau_{D^+} = 8.4 \begin{smallmatrix} +6.8 \\ -3.1 \end{smallmatrix} \times 10^{-13} \text{ sec}$$

Inclusion of this event with the F^+ sample has a 10% effect on the F^+ lifetime:

$$\tau_{F^+} = 1.8 \begin{smallmatrix} +1.3 \\ -0.7 \end{smallmatrix} \times 10^{-13} \text{ sec}$$

Inclusion of this event with the Λ_c^+ sample has little effect;

$$\tau_{\Lambda_c^+} = 2.2 \begin{smallmatrix} +0.9 \\ -0.6 \end{smallmatrix} \times 10^{-13} \text{ sec}$$

TABLE 12

SUMMARY OF AMBIGUOUS CHARM DECAY CANDIDATES
(Constrained Events)

EVENT NUMBER	MUON	DECAY MODE HYPOTHESIS	D.L. (μm)	P_c (GeV/c)	MASS (MeV/c^2)	DECAY TIME (x10^{-13}sec)
493-1235	-	$D^+ \to \pi^+\pi^+\pi^-K_L^0$	2203±10	11.9±1.3	2061±156	11.5±1.2
		$F^+ \to \pi^+\pi^+K^-K_L^0$		11.7±0.7	2246±166	12.7±0.8
		$\Lambda_c^+ \to \pi^+\pi^+K^-n$		13.3±2.0	2330±123	12.6±1.9
656-2631	-	$D^+ \to \pi^+K^-\pi^+\pi^0$	570.0±11.0	32.6±1.2	1933±73	1.09±0.05
		$F^+ \to K^+K^-\pi^+\pi^0$		32.4±1.1	2099±73	1.19±0.05
		$\Lambda_c^+ \to pK^-\pi^+$		31.7±1.2	2317±76	1.36±0.06

TABLE 13

SUMMARY OF KINEMATIC FITS OF AMBIGUOUS CHARM DECAYS
(Constrained Events)

EVENT NUMBER	2-C FITS χ^2	2-C FITS C.L.	2-C FITS ITER	3-C FITS χ^2	3-C FITS C.L.	3-C FITS ITER	ΔP_x (MeV/c)	ΔP_y
493-1235	1.85	0.40	4	4.32	0.23	10	-454±482	-205±867
	1.85	0.40	4	4.57	0.21	10	-454±482	-205±867
	1.85	0.40	4	2.00	0.57	5	-454±482	-205±867
656-2631	0.38	0.83	3	1.29	0.73	2	-42±89	-20±157
	0.38	0.83	3	1.42	0.70	2	-42±89	-20±157
	2.66	0.27	3	2.85	0.42	2	-105±87	-50±143

Ambiguous Charm Decay Candidates (Unconstrained Events)

The unconstrained ambiguous charm decay candidates are summarized in the table below. For the events listed in the table which have only one decay hypothesis, uncertainties associated with the event reconstruction (e.g. magnet off, interaction of the daughter tracks in the emulsion) prevent their elevation from the ambiguous to unambiguous category of charm candidates, and hence their use in the determination of charmed particle lifetimes. See Appendix A for further details.

Several of the unconstrained events have relatively long decay times (events 522-2107, 563-5269, 665-4023, 671-2642), These events, if construed as the decays of D^+ mesons shift the D^+ lifetime by a factor of approximately 2 x longer than is obtained with the unambiguous D^+ decays:

$$\tau_{D^+} = 24.5 \; {}^{+20.7}_{-9.2} \times 10^{-13} \text{ sec}$$

Note that this is approximately 1.5 S.D. from the D^+ lifetime as determined with the five unambiguous D^+ decays. If these events are taken to be the decays of F^+ mesons or Λ_c^+ baryons, then they can cause a significant change in their lifetimes, i.e.

$$\tau_{F^+} = 24.9 \; {}^{+24.5}_{-9.6} \times 10^{-13} \text{ sec}$$

$$\tau_{\Lambda_c^+} = 20.9 \; {}^{+9.5}_{-5.6} \times 10^{-13} \text{ sec}$$

These values for the F^+ and Λ_c^+ lifetimes are more than four S.D. from the lifetimes as obtained using the unambiguous F^+ and Λ_c^+ decays. It must be pointed out that one of the consequences of (improper) reconstruction of decays with more than a single missing neutral particle is to systematically under-estimate the parent momentum, thereby over-estimating the individual decay times for such events. However, the presence of additional missing neutrals in unreconstructed decays of charmed particles will result in only a 20% decrease in the observed decay time (on average), based on the momentum spectrum of the daughter particles emitted in the reconstructed charmed particle decays.

It is kinematically possible for the missing neutral(s) emitted in these decays to carry off a significant fraction of the parent momentum, thereby reducing the decay times.

Several of the unconstrained events have relatively short decay times (events 502-354 (baryon), 529-271, 547-3192, 665-2113 and 670-12 (baryon)). The three events

which have meson decay hypotheses can have a significant impact on the D^+ lifetime:

$$\tau_{D^+} = 6.3 \begin{smallmatrix} +3.6 \\ -2.1 \end{smallmatrix} \times 10^{-13} \text{ sec}$$

This value for the D^+ lifetime is 60% shorter than that obtained using the 5 unambiguous D^+ decays, but is still within one standard deviation of this lifetime. The effect of these events on the F^+ lifetime is less than that for the D^+:

$$\tau_{F^+} = 2.0 \begin{smallmatrix} +1.2 \\ -0.6 \end{smallmatrix} \times 10^{-13} \text{ sec}$$

Use of events 502-354, 665-2113 and 670-12 in the Λ_c^+ lifetime determination also has a small effect:

$$\tau_{\Lambda_c^+} = 1.9 \begin{smallmatrix} +0.7 \\ -0.5 \end{smallmatrix} \times 10^{-13} \text{ sec}$$

There are several distinctions between charmed mesons and charmed baryons which may be used to aid in identification of the charmed particles that have ambiguous constrained or unconstrained fits. The momentum spectrum of charmed baryons tends to be lower than that for charmed mesons, as shown in Fig.62. The production angle of charmed mesons, particularly that of D^+ and D^0 mesons tends to be in the forward direction, while that for the Λ_c^+ is larger, as shown in Fig.43. Furthermore, the Feynman-X distribution for the charmed particles (essentially the θ_{cm}^* (angular) distribution in the hadronic center of mass W), indicates that the D^+, D^0 mesons are produced in the current fragmentation region ($X_F > 0$) while the Λ_c^+ baryons tend to be produced in the target fragmentation region ($X_F < 0$) [120]. The F^+ mesons appear to be intermediate between the charmed D^+, D^0 mesons and Λ_c^+ baryons in all of the above situations. Note that these three items, i.e. the charm momentum spectrum, angular distribution in the lab and Feynman-X distribution are not independent quantities, but are related to each other via energy and momentum conservation, and the Lorentz transformation from the laboratory into the hadron center of mass. Therefore, from this standpoint, it is unlikely that events 522-2107 and 665-4023 are Λ_c^+ baryons, as they appear to have D^+ (and D^0) meson-like characteristics. Conversely, it is unlikely that events 665-2113 and 671-2642 are D^+ mesons, as the appear to have Λ_c^+ baryon-like characteristics, i.e. low momentum, and (large) negative Feynman-X For events 563-5269 and 671-2642, which have long decay lengths and thus long decay times, we wish to point out that the nuclear interaction background is also Λ_c^+ baryon-like in its characteristics, i.e. peaked at low momentum and in the target-fragmentation region. The

situation is more difficult to discern for the F^+ meson, which appears to hold the middle ground between the D^+ meson and Λ_c^+ baryon.

Another perspective on the unfitted decay candidates is from the following. We note that the ratio of fully-reconstructed $D^+ : F^+ : \Lambda_c^+$ decays is 5.0 : 3.0 : 8.0 (5.0 : 3.0 : 6.0 for multi-prong decays). If the events summarized in the table below are weighted equally, according to their parent ambiguity for D^+, F^+ and Λ_c^+ (e.g. for $D^+ F^+ \Lambda_c^+$ ambiguous events the weights are 1/3, 1/3, 1/3.), then the $D^+ : F^+ : \Lambda_c^+$ ratio for the unfitted events is approximately 2.2 : 3.5 : 3.3 by this method (2.0 : 2.0 : 2.6 for multi-prong decays), in reasonable agreement with the unambiguous $D^+ : F^+ : \Lambda_c^+$ ratio. However, the ratio of "preferred" decay hypotheses for these events (as discussed in Appendix A) is $D^+ : F^+ : \Lambda_c^+$ = 6.0 : 1.5 : 2.5. If the kinks are removed from this sample of events, then the $D^+ : F^+ : \Lambda_c^+$ = 3.0 : 1.5 : 2.5, in reasonable agreement with the unambiguous multi-prong ratio of 5.0 : 3.0 : 6.0. If the single-prong events are included, then the fraction of unfitted D^+ decays appears to be higher than for the F^+ or Λ_c^+ decay candidates. This may indeed be true, as the momentum spectrum of the D^+, D^0 mesons appears to be harder than that of the F^+ and Λ_c^+ baryon (see Fig.61); such decays are less likely to be successful in obtaining a unique determination of parent identity.

Thus, the existence of ambiguous decay candidates within the sample of charm events has the potential for significant changes in the D^+, F^+ and Λ_c^+ lifetimes, however from their overall characteristics, their momentum distributions, their preferred solutions, etc., their impact on the Λ_c^+ lifetime appears to be small. The impact of these events on the on the D^+, F^+ lifetimes is much more uncertain.

TABLE 14

SUMMARY OF AMBIGUOUS CHARM DECAY CANDIDATES

(Unconstrained 0-C Events)

EVENT NUMBER	MUON	DECAY MODE HYPOTHESIS	D.L. (μm)	P_c (GeV/c)	MASS (MeV/c^2)	DECAY TIME ($\times 10^{-13}$sec)
502-354	-	$Y^{++} \to \underline{\Lambda}^0 \pi^+ h^+ (\pi^0)$	66±6	?	?	?
		$\Sigma_c^{++} \to \Lambda_c^+ \pi^+$			strong decay	
		$\Lambda_c^+ \to \underline{\Lambda}^0 \pi^+ \pi^0 (\pi^0)$		6.3±0.3	0-C	0.80±0.05
				8.3±0.3	0-C	0.60±0.04
522-2107	-	$D^+ \to \pi^+ \underline{\pi}^- K^- (\pi^0)$	13600±100	23.5±1.3	0-C	36.0±1.8
				31.7±1.3		26.7±1.3
		$F^+ \to K^+ \underline{\pi}^+ K^- (\pi^0)$		22.5±1.3	0-C	40.9±1.9
				32.7±1.3		28.1±1.1
		$\Lambda_c^+ \to p \underline{\pi}^+ K^- (\pi^0)$		22.5±1.3	0-C	46.0±2.5
				31.5±1.3		32.9±1.3
529-271	-	$F^+ \to K^+ (K_L^0)$	2547±30	43.1±0.2	0-C	4.0±0.1
		$D^+ \to \pi^+ \pi^0 (K_L^0)$		55.4±0.5	0-C	2.9±0.1
		$F^+ \to K^+ \pi^0 (K_L^0)$		38.4±0.5	0-C	4.5±0.1 *
533-7152	-	$F^+ \to K^+ (K_L^0)$	5246±50	34.8±0.2	0-C	10.2±0.1
		$D^+ \to \pi^+ \pi^0 (K_L^0)$		40.1±0.4	0-C	8.1±0.1 *
547-3192	-	$F^+ \to \pi^+ \pi^- \pi^+ (\pi^0)$	185±10	9.6±1.2	0-C	1.3±0.2
563-5269	-	$D^+ \to \pi^+ (K_L^0)$	6600±50	25.9±0.3	0-C	15.8±0.1 *
		$F^+ \to K^+ (K_L^0)$		10.9±0.3	0-C	40.6±0.1
		$\Lambda_c^+ \to p (K_L^0)$		4.9±0.3	0-C	100.5±0.1

TABLE 14 (CONTINUED)

665-2113	-	$D^+ \to \pi^+\pi^-\pi^+(K^0)$	33±5	2.7±0.04	0-C	0.76±0.05
		$F^+ \to \pi^+\pi^-\pi^+(\pi^0)$		2.7±0.04	0-C	0.83±0.05
		$\Lambda_c^+ \to \pi^+\pi^-\pi^+(\Lambda^0)$		3.6±0.04	0-C	0.70±0.04
665-4023	-	$D^+ \to K^-K^+\pi^+(\pi^0)$	6820±100	15.3±0.4	0-C	25.7±0.7
		$D^+ \to K^-\pi^+\pi^+(\pi^0)$		15.2±0.4	0-C	27.9±0.7
		$F^+ \to K^{-+}(\pi^0)$		15.2±0.4	0-C	28.0±0.7
		$\Lambda_c^+ \to K^-p\pi^+(\pi^0)$		15.2±0.4	0-C	31.5±0.7
		$D^+ \to \pi^-\pi^+\pi^+(\bar{K}^0)$		16.8±0.4	0-C	25.3±0.6
		$F^+ \to \pi^-K^+\pi^+(\bar{K}^0)$		16.7±0.4	0-C	27.6±0.6
		$F^+ \to K^-\pi^+\pi^+(\bar{K}^0)$		16.8±0.4	0-C	27.5±0.7
		$\Lambda_c^+ \to \pi^-p\pi^+(\bar{K}^0)$		16.8±0.4	0-C	30.9±0.7
670-12	-	$\Lambda_c^+ \to K^+p\pi^-(\pi^0)$	56±10	2.4±0.2	0-C	1.8±0.1
671-2642	-	$D^+ \to \pi^+\pi^-\pi^+(\bar{K}^0)$	2345±10	2.1±0.1	0-C	69.5±3.0
		$D^+ \to \pi^+\pi^-\pi^+\pi^0(\bar{K}^0)$		3.0±0.1	0-C	48.7±1.6
		$F^+ \to \pi^+\pi^-K^+(\bar{K}^0)$		2.35±0.05	0-C	67.5±1.5
				4.05±0.05		39.2±0.5
		$\Lambda_c^+ \to \pi^+\pi^-\pi^+(\Lambda^0)$		2.50±0.05	0-C	71.4±1.5
		$\Lambda_c^+ \to \pi^+\pi^-\pi^+\pi^0(\Lambda^0)$		4.00±0.10	0-C	44.7±1.1
		$A^+ \to \pi^+\pi^-\pi^+(\Lambda^0)$		2.25±0.05	0-C	85.4±2.0
		$A^+ \to \pi^+\pi^-\pi^+\pi^0(\Lambda^0)$		3.50±0.10	0-C	54.7±1.5

* physically favored solution, see Appendix A.

Kink Events

Fifty-three "kink" or single-prong events were found in the emulsion, the majority of which are from conventional sources, such as π and K decay, hyperon decay (one event, 603-6143, is a candidate for neutrino production and decay of a $\Omega^- \rightarrow \Lambda^0 K^-$!), in addition to single-prong elastic scatters and local shear and distortion effects in the emulsion. Approximately 10 kink decays of charged charmed particles are expected, based on measurements of the D^+ single-prong branching fraction (45.3 ± 4.9% [131-144,160]) and estimates of the single-prong branching fraction for the F^+ and Λ_c^+ (~35% for each) [184]. Within the sample of kink events, only five are consistent with the decays of charmed particles, as determined from transverse momentum and flight length distributions for the multi-prong charm decays. As the mean scanning efficiency for kinks is lower than that for multi-prongs (~50%) [120,233], it is perhaps no suprise that fewer than expected charmed candidate kink events are observed. Reconstruction of these events is also more difficult due to the decreased "signal to noise ratio" in these events, and also that more than one neutral particle may have been emitted in the decay. Two out of the five single-prong charm decay candidates (499-4713 and 567-2596) were successfully reconstructed as kinematically unambiguous Λ_c^+ decays. The other three events (529-271, 6533-7152 and 563-5269) are D^+/F^+ ambiguous on the basis of mass. (The last event also supports a Λ_c^+ decay hypothesis, but it is not favored on the basis of energy contained in the calorimeter. See Appendix A for details.)

The reduced ability to observe and reconstruct single-prong decays of charmed particles (relative to the multi-prong decays) has no first-order effect on the determination of particle lifetimes (other than to reduce the statistics of the sample), as no known correlation exists between decay mode/multiplicity and lifetime for charged particles. (Note that this is not true for neutral particles, e.g. the K_L^0 and K_S^0 [160].)

CHAPTER III

LONG-LIVED NEUTRAL CHARMED BARYON CANDIDATE

EVENT 635-4949 $\quad NB \rightarrow \underline{p}\ \pi/K^- K^0_S$

Several events were found in the emulsion which, for various reasons (specific to each event) do not "fit in" with the present, or conventional understanding of weak interaction phenonomena. The event discussed below is one of these events, for which the quality of spectrometer and emulsion information was such that an excellent experimental understanding was obtained.

Event Topology and Associated Kinematics

Event 635-4949 is a neutrino-induced (NH = 1, NS = 6) C.C. interaction in which a second vertex (with NH = 0, NS = 2) was found 4386 ± 40 μm downstream of the primary vertex, by scanback of a track identified by TOF as a proton (3 S.D. from a K^+). (Thus, the second vertex was "in-time" with the rest of the event.) The X-Z projection of this event is shown in Fig.57. No black tracks, recoil stub or elongated grains are observed at the secondary vertex. The other track from the secondary vertex is momentum analyzed by the fringe field of the magnet, and is measured to be negatively charged. I/I_0 measurements identify this track as either a pion or a kaon (but 2 S.D. from a proton).

From geometrical considerations alone, it is not possible for the two tracks from the secondary vertex to originate from the (two-body) decay of a neutral hyperon produced at the primary vertex, as the parent X slope (from primary-to-secondary vertex) is not contained within the daughter X slopes. Transverse momentum imbalance is $\Delta Px = -652 \pm 114$ MeV/c, $\Delta Py = -124 \pm 98$ MeV/c at the secondary vertex with only the two charged tracks. The minimum of the -1C $p\pi^-$ mass curve (Fig.58) occurs at 1135 ± 1.8 MeV/c^2, 11 S.D. above the Λ^0 mass. (The two-body invariant mass is 1350 ± 130 MeV/c^2 using the measured momenta from both tracks.) This decay hypothesis is consistent, however, with $\Xi^0 \rightarrow p\pi^-$ (for a decay at 1/220 proper Ξ^0 lifetimes); a 1-C fit to the Ξ^0 mass has a $\chi^2 = 0.10$, C.L. = 75%. However, the experimental limit on the branching ratio for $\Xi^0 \rightarrow p\pi^-$ is less than 10^{-5} [160].

A volume search for NH = 0, NS = 0 type stars was performed in the region between the primary and secondary vertices. Several such stars were found, however none of them are consistent as a nuclear interaction from a incident neutral particle produced at the primary vertex.

The minimum mass for a particle produced at the primary vertex which decays to $p-\pi^-$ and a (massless) unobserved neutral particle at the secondary vertex is 2175 ± 295 MeV/c^2, and a missing neutral momentum of $\sim$2 GeV/c.

No $\pi^{0's}$, $\gamma's$, or electrons are observed in the lead glass. No excess energy is observed in the calorimeter. A V^0 is observed to decay with large X', Y' in the drift space between the emulsion and the drift chambers, 0.60 ± 0.17 cm (3.0 S.D.) upstream of TOF I. The tracks from this decay are unable to be momentum analyzed reliably in the fringe field of the magnet. The reconstructed decay tracks miss intersection of each other by less than 500 μm. The V^2 decay plane misses the secondary vertex by 1.0 ± 1.5 mm.

If the V^0 is emitted from the decay of a neutral baryon at the secondary vertex, momentum imbalance in both transverse directions is simultaneously minimized to within $\Delta Px = 29 \pm 77$ MeV/c, $\Delta Py = 11 \pm 57$ MeV/c only when the V^0 mass is at the K^0_s mass as shown in Fig.59. Independent kinematic analysis of the V^0 as a $K^0_s \rightarrow \pi^+\pi^-$ is in excellent agreement with these results. The ratio of flight length L to the $\gamma\beta c\tau$ for the K^0_s is 1.4 The decay is also "symmetric", a characteristic feature of $K^0_s \rightarrow \pi^+\pi^-$ decay. As all three momenta are unknown for the K^0_s decay, a 0-C fit does not yield a unique solution (the Jacobian is singular; the pion momenta scale with the K^0_s momentum.) A 1-C fit to $K^0_s \rightarrow \pi^+\pi^-$ is unique; the results of this fit are input to a 2-C fit for the decay hypothesis of $NB \rightarrow p\pi^-/K^- K^0_s$, with the results as summarized in the following table.

TABLE 15

SUMMARY OF KINEMATIC FITS FOR EVENT 635-4949

Decay Mode	Mass(MeV/c^2)	P(GeV/c)	τ(x10^{-13}sec)	χ^2	C.L.
NB $\rightarrow$ p $\pi^- K^0_S$	2450±15	4.64±0.51	77.2±0.9	0.13	0.94
NB $\rightarrow$ p $K^- K^0_S$	2647±11	4.64±0.51	83.4±0.9	0.13	0.94

Ignoring the TOF information on track V-1, the kinematic fits for meson hypotheses are:

NM $\rightarrow$ $\pi^+\pi^- K^0_S$	2107±15	4.64±0.51	66.4±0.7	0.13	0.94
NM $\rightarrow$ $K^+\pi^- K^0_S$	2203±15	4.64±0.51	69.4±0.7	0.13	0.94
NM $\rightarrow$ $K^+K^- K^0_S$	2331±13	4.64±0.51	80.4±0.8	0.13	0.94

We wish to emphasize the "goodness of kinematic fit" for this event, as indicated by the 2-C χ^2, C.L. and number of iterations (ITER = 2). This event was measured in the emulsion three times, each time with improved resolution and refined technique. The final grain-to-grain measurements were performed on the Nikon machine at Nagoya University, with spatial resolution of 0.1 μm in X and Y (via a laser interferometer) and 0.5 μm in Z (along the optical axis, via a position encoder) for each measured grain coordinate. The track slopes and decay lengths from the three measurements are in excellent agreement with each other, within one to two mrad for track slopes and few tens of microns for flight lengths. Because of the repeated measurements and high resolution with which they were obtained, all tracks have extremely small slope errors. The neutral parent direction is also extremely well known, due to the long flight length and the high resolution. Thus, the χ^2, C.L. and number of iterations are indicative of the necessity of the K^0_S as a crucial part of this event, and also of the reliability and correctness of the reconstruction of this event, for the above (baryon) decay hypotheses.

The fitted errors on the mass, momentum and lifetime appear to be unreasonably small. These errors are in fact correct, as the geometrical aspects of the decay (as shown by Fig.60) are such that large changes and/or uncertainties in the momenta of the three decay particles have only small effects on the parent mass, momentum and lifetime (The shape of the χ^2 surface for this event is a deep well with very steep sides, the directional derivative being very large) This effect was verified kinematically by deliberately shifting the starting momentum of either track V_2 or the V^0 (but not both) by factors of two. The resulting fitted masses were within 15 MeV/c^2 of each other in all instances. The 2-C chi-squared is also at a minimum for the observed values of decay parameters, for the fit. The momentum of the neutral parent particle is also consistent with the observed momenta of charmed baryons (see Fig.61). The transverse momenta of the three decay particles with respect to the parent direction are quite large, even larger than for the majority of charm decays.

$$P_\perp(\text{proton}) = 427 \pm 6 \quad \text{GeV/c}$$

$$P_\perp(\pi^-/K^-) = 426 \pm 179 \quad \text{GeV/c}$$

$$P_\perp(K^0_S) = 650 \pm 31 \quad \text{GeV/c}$$

The mean transverse momentum for a particle from a three-body decay of a 2450 MeV/c^2 baryon is $\langle P_\perp \rangle \approx 450$ MeV/c.

From the geometry of the event, it is not possible to substantially reduce the observed decay time by postulating a neutral baryon decay to all-neutral secondaries, one of which then decays to $p\,\pi^-$. (The decay of the neutral particle to $p\,\pi^-$ cannot be from Λ^0 decay, as explained above, and so the only other possibility is $\Xi^0 \rightarrow p\pi^-$, which is also unlikely.) As the decay length is made shorter, the momentum imbalance at the parent and daughter $p\,\pi^-$ and "K^0_S" vertices are simultaneously made worse, until it is no longer possible for the decay to occur without the emission of another unseen neutral particle (e.g. a π^0) purely due to geometrical momentum balancing constraints. This point occurs for decay lengths shorter than 850 μm; hence no short-lived neutral baryon hypotheses are acceptable without additional unobserved neutral particles emitted in the decay. As momentum is conserved well within errors at the $p\,\pi^-$ vertex, this can also be taken as an indication of the level at which there are missing neutrals, and also as an independent indication that the $p\,\pi^-$ vertex is indeed the true decay point of the parent neutral baryon.

Discussion of Background for Event 635-4949

The most probable background for an event with this topology comes from the interaction of incident K^0 with a single neutron in a nucleus in the emulsion. Conservation of baryon number rules out the possibility of an incident neutron or neutral hyperon. (Only one baryon is observed in the final state; momentum balance at the V_1-V_2 vertex is excellent, indicating that the emission of additional neutral particles (e.g. a neutron) is less than 5%). Strangeness conservation (and also isospin conservation) in the strong interactions allows an incident K^0 only for a single strange particle (the K^0_S) in the final state.

One immediate problem associated with a nuclear interaction hypothesis for this event is that the major elements of which (Fuji ET-7B) nuclear emulsion is composed have nuclei whose isotopes (less one neutron) are all unstable, most with half-lives of less than one hour. Table 16 summarizes this data (see Ref.[148] for further information on nuclear decay modes). α, β and γ decay modes are readily observable in emulsion from nuclear decay tracks, or from nuclear recoil (elongated grains). The emulsion was not processed for several weeks after the event occurred.

TABLE 16

Nuclear Activity of Fuji ET-7B Emulsion

ELEMENT	%WEIGHT	INITIAL STATE	%ABUN-DANCE	FINAL STATE	$T_{1/2}$	DECAY MODES
Hydrogen	0.9					
Carbon	7.4	$^{6}C_{12}$	98.9	$^{6}C_{12}$	20.3m	β^{+} EC
Nitrogen	2.7	$^{7}N_{14}$	99.6	$^{7}N_{13}$	10.0m	β^{+}
Oxygen	4.3	$^{8}O_{16}$	99.8	$^{8}O_{15}$	124s	β^{+}
Sulfur	0.4	$^{16}S_{32}$	95.0	$^{16}S_{32}$	2.7s	β^{+}
Bromine	33.7	$^{35}Br_{79}$	50.7	$^{35}Br_{79}$	6.4m	β^{+} EC
		$^{35}Br_{81}$	49.3	$^{35}Br_{80}$	17.6m	$\beta^{+}\beta^{-}$EC
Silver	46.5	$^{47}Ag_{107}$	51.8	$^{47}Ag_{106}$	24.0m	β^{+} EC
		$^{47}Ag_{109}$	48.2	$^{47}Br_{109}$	2.4m	β^{+}ECβ^{-}
Iodine	1.3	$^{53}I_{127}$	100.0	$^{53}I_{126}$	13d	β^{+}ECβ^{-}

No kinematically allowed solutions exist for a nuclear interaction hypothesis, even with the inclusion of Fermi motion effects within the target nucleus. Imaginary solutions exist for the incident hadron and/or target mass for all regions of nuclear phase space. Only for a small region of phase space where the target neutron has the maximum allowed Fermi momentum ($\sim$ 260 MeV/c for a nucleus such as silver [161]), and is oriented along the direction of the incident K^0 does the simultaneous solution of the four energy-momentum equations come near to having real solutions. (They miss being satisfied by approximately 1 S.D. for this case.) This may offer an explanation why NH = 0 at the secondary vertex, if indeed this event is a hadronic interaction.

There are five factors which need to be taken in to consideration to calculate the hadronic background probability for this event:

1.) Expected K^0 Flux:

The K^0 production rate in charged-current ν-N interactions is 15 ± 1% [133]. However, it must be pointed out that this measurement of the K^0 production rate is "colored" by ν-production of charm. Not only will this rate be affected, but also the K^0 momentum spectrum and angular distribution. The existence of charm increases the strange particle production rate and broadens both the longitudinal and transverse strange particle momentum distributions. Hence, use of such measurements will serve as an upper limit. Thus, for 1241 found (C.C. plus N.C.) neutrino interactions, we expect $N_{K^0} = 133 \pm 11$.

2.) Probability of Incident K^0 With $P^{\parallel}_{K^0} > P^{\parallel}_{OBS}$, $P^{\perp}_{K^0} > P^{\perp}_{OBS}$:

The measured longitudinal K^0 momentum dependence [131] is of the form:

$$dN/dP_{\parallel} = N^0 P_{\parallel}^{-b} \text{ where } b = 2.32 \pm 0.44$$

Thus, the probability of producing a K^0 with momentum greater than 4.6 GeV/c is:

$$P_{P^{\parallel}_{K^0} > P^{\parallel}_{OBS}} = 10.1 \begin{smallmatrix} +19.6 \\ -6.2 \end{smallmatrix} \%$$

The measured K^0 transverse momentum dependence [132] is of the form:

$$dN/dP_{\perp} = N \exp(-bP_{\perp}^2)$$

Where:

$$b = 4.31 \pm 0.35 \quad (\bar{\nu}N \text{ data}) \quad [132]$$
$$= 4.59 \pm 0.11 \quad (\pi p \text{ data}) \quad "$$
$$= 5.80 \pm 1.10 \quad (\nu\text{-}p \text{ data}) \quad "$$

Using the smallest value of b ($\bar{\nu}N$ data) to maintain an upper limit on the background calculation for this event, the probability of producing a K^0 with transverse momentum of $P_\perp > 0.9$ GeV/c is [149]:

$$P_{P^\perp_{K^0} > P^\perp_{OBS}} = 5.3 \begin{smallmatrix} +2.2 \\ -1.4 \end{smallmatrix} \times 10^{-3}$$

The joint probability of the longitudinal and transverse momentum probabilities should be taken, except for the fact that there exist correlations between the two (i.e. the "seagull effect"); hence we use only the transverse momentum constraint, to maintain our calculation as an upper limit.

3.) Probability of a K^0 Interacting in the Emulsion:

The probability of a K^0 interacting within the last 1.0 cm of emulsion is

$$P_{INT} = 3.8 \begin{smallmatrix} +0.7 \\ -0.4 \end{smallmatrix} \%$$

for a measured interaction length in emulsion of

$$\lambda_{INT} = 26.0 \begin{smallmatrix} +3.2 \\ -4.2 \end{smallmatrix} \text{ cm}$$

Note that the probability of a K^0 interacting within the last 1.0 cm of emulsion and being detected (observed) is 0.44%.

4.) Probability of a NH = 0, NS = 2 Interaction:

The probability of an NH = 0, NS = 2 interaction (linearly extrapolated to 4.6 GeV/c) is [137]:

$$P_{\substack{NH=0 \\ NS=2}} = 2.9 \pm 0.5\%$$

5.) Probability of a Q = 0 Interaction:

The probability of (apparent) charge conservation in nuclear interactions in emulsion is not unity. From Ref.[137], this probability is estimated to be less than 40 ± 8%.

Thus, the net probability for this event to be due to a K^0 interaction with a nucleus is the product of the above probabilities:

$$P_{INT}^{TOT} = \prod_i P_i$$

$$P_{INT}^{TOT} < (133\pm11)(0.53\ ^{+0.22}_{-0.14}\%)(3.8\ ^{+0.7}_{-0.4}\%)(2.9\pm0.5\%)(40\pm8\%)$$

$$P_{INT}^{TOT} < 3.1\ ^{+1.6}_{-1.3} \times 10^{-4} \text{ events}$$

This number should be compared with the background calculations for the entire charged current event sample (as discussed above) and also with similar background calculations for the Λ_c^+ charmed baryon candidates, done on a per-event basis (summarized below in Table 18).

We emphasize that the above calculation is a very conservative upper limit to the background for this event. Other factors, such as the probability that the reaction $K^0 n \rightarrow K^* p$ have the observed transverse momenta for the secondaries from the V^1-V^2 vertex have not been included (estimated to be a further factor of x (5 $\pm$ 10%) using the measured t-distributions for low-energy K^- - p and K^0- n reactions [162-169].)

This event has several important similarities to the neutrino events in which Λ_c^+(cud) charmed baryons are produced. The parent momentum of the neutral baryon candidate (4.6 GeV/c) is low, in accord with the Λ_c^+ charmed baryon momentum spectrum, as shown in Fig.61. The lab production angle is quite large, θ_{ch}^L = 198 ± 2 mrad, as is shown in Fig.43. The Λ_c^+ charmed baryons tend to be produced with larger θ_{ch}^L than for the mesons. The angle θ_{ch}^* of the neutral baryon candidate with respect to the total hadron momentum vector in the hadronic center of mass (with invariant mass W) is large negative, as is the case for many of the observed Λ_c^+'s, (See Ref.[120].) The neutral baryon momentum vector in this system is also large negative. Thus, the Feynman-X of this event is also large negative, as is the case for many of the Λ_c^+'s.

The muon from the primary vertex in this event is measured to have a momentum of $P\mu = -212\ ^{+\infty}_{-115}$ GeV/c.

Calculation of the standard kinematical variables (e.g. X, Y, Q , W, etc.) give unphysical values unless the muon momentum is reduced to approximately $P\mu$ = -60 GeV/c, in agreement with the observed systematic offset in Q = 1/P of ΔQ = 0.005 (which reduces the momentum of negative tracks, and increases the momentum of positive tracks). The standard kinematic variables have been calculated for this event and are summarized in the table below. See Ref.[160] for definitions of these variables.

TABLE 17

KINEMATIC VARIABLES FOR EVENT 635-4949

$E_\nu = 89.3 \pm 8.6$	$E_{HAD} = 28.7 \pm 2.8$	$P_\mu = -60.6^{+\infty}_{-18.4}$
$Q^2 = 13.9 \pm 3.5$	$W = 6.24 \pm 0.49$	$X_F = -.88 \pm 0.34$
$X_B = 0.27 \pm 0.06$	$Y_B = 0.31 \pm 0.03$	$Z_P = 0.18 \pm 0.02$
$P = 4.61 \pm 0.51$	$P^*_c = -2.37 \pm 1.00$	$P_c = 0.48 \pm 0.07$
$\phi_{\mu ch} = 155 \pm 3$	$\theta^L_c = 0.20 \pm 0.00$	$\theta^*_c = -0.20 \pm 0.05$

The probability for observing an event with a mean lifetime equal to that of the Λ_c^+ at > 80.0 x 10^{-13} sec is exp(-80). The probability for observing an event with a mean lifetime comparable to the D^+ lifetime is exp(-8) = 10^{-4}. It must also be pointed out that the observed spread in decay times within our own data sample for a given species spans over three orders of magnitude in some cases (e.g. the D^0; see Ref.[123]).

To obtain an estimate of the range allowed for the mean lifetime, we use the method of maximum likelyhood to obtain 1 and 2 S.D. limits. From one-event statistics, the "lifetime" is

$$\tau_{NB} = 77.3^{+264.4}_{-47.0}\ ^{+\infty}_{-63.5} \times 10^{-13} \text{ sec} \quad (p\ \pi^- K^0_s)$$

$$\tau_{NB} = 83.4^{+286.6}_{-50.9}\ ^{+\infty}_{-68.7} \times 10^{-13} \text{ sec} \quad (p\ K^- K^0_s)$$

1 S.D.(2 S.D.) limits

Discussion of Event 635-4949 in the Context of Existing Theory

In the framework of SU(4), there are three particle states in the $J^P = 1/2^+$ 20m (mixed-symmetric) multiplet for which 635-4949 could be a candidate (see Fig.1). The Σ^0(cdd), (expected to decay strongly to Λ_c^+ via π^- emission), the A^0(csd) and the T^0(css) states. The expected masses for these states are 2450 (25 MeV/c^2 above pion threshold), 2495 MeV/c^2 and 2760 MeV/c^2 respectively [170]. For the Σ_c^0, the possibility exists that higher order QCD effects could drop the mass below pion threshold, and thus this state would become stable against strong decays [227].

The decay mode of $p\pi^- K_s^0$ is consistent with the Cabibbo-favored decay of the Σ_c^0, and the Cabibbo-unfavored decay of the A^0. The $p K^- K_s^0$ decay mode is consistent with the Cabibbo-favored decay of the A^0, and the Cabibbo-unfavored decay of the T^0. The predicted lifetimes for the A^0 and T^0 are 5.35×10^{-14} sec, 5.44×10^{-14} sec respectively [175]. Of the three expected neutral charmed baryon states, this event appears to favor the Cabibbo-unfavored decay of the A^0, although there is clearly a large disparity between the measured and predicted lifetimes.

The (phenomenological) $\Delta n_t = 0$ rule (quark number conservation) [41,228-230,225] predicts the lifetime of the T^0(css) state to be longer than for other charmed particles, as the Cabibbo-favored decays of the T^0 violate this rule. (The number of quarks in the final state is not equal to that of the initial state; $q\bar{q}$ pairs of the same flavor are not counted in the final state.) The Cabibbo-favored decays of the A^0(csd) do not violate the $\Delta n_t = 0$ rule, however, its isodoublet partner the A^+(csu) does. Note further that the Cabibbo-favored decays of charm-strange baryons may have conflicts with the exclusion principle, due to the presence of multiple strange quarks in the final state (e.g 3 for the T^0). As baryons are color singlets, such a problem is perhaps not expected to occur; however the presence of gluons within the initial and final baryon state may in principle, generate a problem of this nature.

For the A^0(csd) baryon, things are more complicated. Strong mixing effects are expected between the antisymmetric A^+(csu) - A^0(csd) isodoublet and their symmetric S^+(csu) - S^0(csd) counterparts [226,227]. It is possible that one of the effects of such mixing between the A^0 and S^0 states could reduce the hadronic matrix elements for one of the physical particle states, resulting in a longer lifetime. The other physical state (having enhanced

hadronic matrix elements), would decay rapidly. If it was heavier than the long-lived state, it would decay radiatively to the lighter (longer-lived) state. Thus, only one stable particle state would be observed in this case [226].

Another (bizzare) possibility, provided the Σ_c^0(cdd) state is stable against strong decays is the occurrence of (weak) mixing between the Σ_c^0(cdd) and A^0(csd) states, since their expected masses are roughly equal.

Is it mere coincidence that the decay time for this event is a factor of roughly twenty times longer than the mean lifetime of the Λ_c^+, and that the viable decay modes of the A^0 and T^0 baryons for this event are also Cabibbo-unfavored? The observed decay time is in good agreement for Cabibbo-unfavored-only decays of such baryons, were the Cabibbo-favored decays to be forbidden by some (unknown and/or not presently understood) selection rule.

One other possible explanation for the anomalously long lifetime exists in the "longevity" diagram (to coin a phrase) as shown in Fig.62 for decays of charm-strange baryons (A^+(csu), A^0(csd) and T^0(css). The charmed quark and strange quarks c and s exchange a W^+ boson, transmuting themselves into each other. Thus, for each W^+ exchange, an "old" charmed quark decays, and a "new" one is created. The process is twice Cabibbo-favored, i.e. a factor of Ucs occurs at each vertex. The particle does not physically decay of course, rather, <u>the particle literally "decays" into itself.</u> This process continues until the charmed quark decays via the Cabibbo-supressed c - d transition, which occurs with the factor Ucd, i.e. a factor of roughly 1 in 20 (in transition rate). To understand the relevance of this diagram for the lifetime of this particle, one must not think in terms of <u>decay</u> rates, but rather, return to the basic principles of quantum mechanics and think in terms of a quantum system in one quantum state making <u>transitions</u> to another quantum state, which for this diagram, happens to be identical to the initial state, with <u>different</u> constituents in the final state than in the initial state. Then the effects of this diagram on the <u>decay</u> rate can be understood more clearly. It can be seen that if this mechanism were to dominate the weak interactions taking place within charmed-strange baryons, the A^0(csd), A^+(csu), T^0(css) and X^+(ccs), then not only would the lifetimes of charm-strange baryons be correspondingly longer, but their decays would also be predominantly Cabibbo-supressed non-leptonic decays. Note that no such supression mechanism is available to mesons, nor to any of the hyperons. If this phenomenon exists, then it should re-appear for top-bottom (or

truth-beauty) baryons, i.e. tbq q = u,d,s,c,t,b states. The neutron lifetime may also, in part, reflect this phenomena.

There are several difficulties associated with such a diagram, in that the spatial part of the c and s quark wave functions must have appreciable overlap (at the origin) for the W^+ exchange to occur [222]. It is not clear however, that this is unlikely, as the wave functions of quarks within baryons in general are not well understood, and for the $A^+ - A^0$ $S^+ - S^0$ system, where mixing effects between these states are expected to occur, the situation becomes even more complicated. Another source of difficulty with such a diagram is that the A^0(csd) baryon can exchange a W^+ between the c and d quarks, (with Cabibbo-favored transitions at the c-s and d-u vertices), thus decaying conventionally (with a short lifetime) [225], unless the same mechanism required for the large spatial overlap of the c and s quark wave functions simultaneously has a small overlap between the c and d quarks. Recently, several theoretical calculations have explored such dynamical pairing effects [151,152] and have found possible indications within presently existing data for such phenomena for light (u,d,s) baryon states, although the level at which the pairing occurs is less than is required for explanation of the long lifetime of this event. Whether or not similar pairing effects occur for charmed baryons and the level at which it occurs remains to be seen, both theoretically and experimentally. On a more fundamental level, it is possible that such dynamical pairing effects may have their origins in supersymmetry, with quark-quark (i.e. di-quark) couplings to elementary color-bearing scalar particles in the 15-40 GeV/c^2 mass range [155-157].

From the experimental measurement of the Λ_c^+ lifetime as obtained in E-531, the fact that the Λ_c^+ lifetime is shorter than that of the D^+ (or the theoretical free charmed quark lifetime, for that matter) indicates that non-spectator processes are involved in the decay of the Λ_c^+. This statement is further strengthened by the possibility that 2 out of 8 observed Λ_c^+ decay via $\Lambda_c^+ \to \Delta^{++} K^{*-}$, which can only occur via W^+ exchange between the c and d quarks within the Λ_c^+(cud). This then may be taken as evidence for the occurrence of dynamical pairing within the cud quark system for the Λ_c^+. Hence, similar effects could occur within other charmed baryons, such as the A^0(csd) and A^+(csu) baryons.

Note further that the observed masses for the decay hypotheses $A^0(csd) \to p\,\pi^- K_s^0$ and $T^0(css) \to p\,K^- K_s^0$ are approximately 45 MeV/c^2 and 115 MeV/c^2 below the predicted A^0, T^0 masses, respectively. This may, perhaps, be an

indication of larger-than-expected binding energies between the quarks within this baryon state, which in turn may be evidence for such pairing effects as discussed above. A shift in the A^0 mass is expected due to the effects of mixing with the S^0, however no such effect is expected for the T^0.

Another possible explanation for the long lifetime is that the particle exchanged between the c and s quark in the longevity diagram could be a light (2-4 GeV/c^2) charged Higgs scalar, i.e. one of the light axions, P^+ (predicted to exist in some of the extended technicolor theories [153,154], and some electro-weak theories with non-minimal Higgs structure [158,159].) The restriction on wave function overlap for the c, s quarks is relaxed somewhat due to the relatively light mass of the axion. Furthermore, the coupling of the axion is semi-weak and also mass-dependent, i.e.

$$g_a \sim M_Q\sqrt{(G_F\sqrt{2})}$$

the axion - Qq coupling increases with the mass of the heavy quark Q (the rate is proportional to the square of the mass). Therefore, the axion P^+ (if it exists) will couple preferentially to heavy quarks (and leptons). Thus, as the coupling is semi-weak, this diagram could dominate the "decay" rate for charmed-strange baryons (and for truth-beauty baryons). The existence of a light charged Higgs scalar also has ramifications for the lifetimes of beauty particles, as well as for other charmed particles (in particular, the F^+ meson lifetime) along with effects on the semi-leptonic decay rates. Thus a delicate "balance" between "old" and "new" physics is required to incorporate such a particle (theoretically) into the existing framework of physics.

Another distinct possibility is that this event may not be the decay of a neutral charmed baryon, but rather the decay of a fundamentally new type of baryon, carrying a hitherto unknown quantum number. Such a possibility exists within the theoretical framework of supersymmetry [155,156], in that many new particle states are predicted to exist (e.g. "R-hadrons": "R-mesons" and "R-baryons"), particularly in this mass region (1.5-2.5 GeV), with predicted lifetimes ranging from 10^{-12} to 10^{-15} sec.

If this event is taken at face value, then it is a very high energy neutrino (?) interaction, with a stiff muon and non-trivial amount of missing transverse momentum at the primary vertex. Were the neutral baryon to be indeed carrying a new type of quantum number then it is plausible that it was pair produced, the other particle escaping

detection in the spectrometer apparatus (e.g. a goldstino or photino).

Yet another possibility, as pointed out by H.J.Lipkin [223], is that this event may be an example of a five quark $\bar{c}sqqq$ (exotic) anti-charmed strange state, such as a bound state of a D^- with a proton (i.e. $D^-p = (\bar{c}d)(uud)$) [179,see also 180-183]. The hypothesis of a D^- meson implies an anti-neutrino interaction. From the above discussion on production kinematics, this possibility appears to be unlikely, as the sign of the muon (which is essentially unknown for momenta above 80 GeV) favors the negative charge. This event is also favored as a neutrino-induced charged-current event, based on the observed $\bar{\nu}_\mu/\nu_\mu$ ratio of 7.5 ± 2.0%. Applying charge conservation (and ignoring the single black (evaporation) track at the primary vertex), track 4 must be positive for the interaction to occur off of a neutron target. If the muon were from an anti-neutrino interaction, then track 4 must be negative to balance charge, but then the kinematical variables computed for the event are unphysical, and applying the Q-shift makes matters worse. For the interaction to occur off of a proton target, it is not possible to conserve charge for any combination of either charge sign of muon with track 4, as there are an even number of charged prongs in this event. Hence, a neutrino interaction is the most likely source of this event Therefore, it is unlikely that this event is an anti-charmed state.

More plausible exotic baryon interpretations for this event are that of a bound state of a D^0 with a neutron i.e. $D^0n = (c\bar{u})(udd)$, or a $\Lambda_c^+ - K^-$ bound state, $(cud)(s\bar{u})$, or a $\Sigma_c^+ - K^-$ $(cud)(s\bar{u})$ or $\Sigma_c^0 - K^0$ $(cud)(s\bar{d})$ bound state [224]. The decay of the exotic $D^0n(2450)$ state to $p\,\pi^-K_s^0$ is Cabibbo-favored, while the decay of the exotic $\Lambda_c^+ - K^-(2650)$, $\Sigma_c^+ - K^-(2650)$ and $\Sigma_c^0 - K^-(2650)$ states to $pK^-K_s^0$ are also Cabibbo-favored. The observed lifetime may result from possible restrictions on phase space available in the decay of an exotic five-quark state [223].

It should be noted that long-lived charged and neutral events are not without experimental precedent, although the identities of these particles are not known with any degree of certainty (see Refs. [63,98-100]).

Is this truely a stable high-mass neutral baryon? The kinematical and physical evidence indicates this to be so, although the observed decay time is not consistent with the measured lifetimes of known charmed particles, nor with (conventional) theoretical expectations for neutral charmed baryons. No matter how compelling the physical evidence may be, this event still has only the statistical weight of one. Whether or not this event is the first observation of a long-lived neutral baryon, and more specifically that of a neutral charmed baryon will hopefully be resolved in the (not-too-distant) future (both experimentally and theoretically).

CHAPTER IV

SUMMARY OF EXPERIMENTAL RESULTS

The mean lifetimes of charmed particles as determined from the reconstructed decays of 5 D^+, 15 D^0, 3 F^+ mesons and 8 Λ_c^+ baryons observed in this experiment are:

$$\tau_{D^+} = 10.3^{+10.3}_{-4.2} \times 10^{-13} \text{ sec}$$
$$\tau_{D^0} = 2.3^{+0.8}_{-0.5} \times 10^{-13} \text{ sec}$$
$$\tau_{F^+} = 2.0^{+1.8}_{-0.8} \times 10^{-13} \text{ sec}$$
$$\tau_{\Lambda_c^+} = 2.3^{+1.0}_{-0.6} \times 10^{-13} \text{ sec}$$

The lifetimes of the D^0, F^0 and Λ_c^+ are measured to be shorter than the D^+ meson, by approximately 2.3, 2.5 and 2.2 standard deviations, respectively. The lifetimes of the D^0, F^+ and Λ_c^+ are within one standard deviation of each other.

The ratio of D^+ to D^0 lifetimes, as measured in this experiment is

$$\tau^+/\tau^0 = 4.5^{+3.4}_{-1.4}$$

This ratio differs by more than 3.1 standard deviations from unity. The probability that the D^+ and D^0 have the same mean lifetime and are measured to have the observed lifetimes is less than 1.0%.

The masses of the charmed D^+, D^0, F^+ mesons and Λ_c^+ baryons measured in this experiment are:

$$M_{D^+} = 1851 \pm 20 \text{ MeV/c}^2$$
$$M_{D^0} = 1856 \pm 15 \text{ MeV/c}^2$$
$$M_{F^+} = 2042 \pm 33 \text{ MeV/c}^2$$
$$M_{\Lambda_c^+} = 2265 \pm 30 \text{ MeV/c}^2$$

This experiment has obtained clear evidence for the existence of the $F^+(c\bar{s})$ meson, not only from its mass, but also from its observed decay modes, lifetime and small (1%) D^+ and Λ_c^+ background.

This experiment has observed one candidate event for the production and decay of a long-lived neutral baryon, with the decay mode, mass and decay time of:

Decay Mode	Mass (MeV/c^2)	Decay Time ($\times 10^{-13}$sec)
$NB \rightarrow p\ \pi^- K_s^0$	2450 ± 14	77.2 ± 0.9
	or	
$NB \rightarrow p\ K^- K_s^0$	2647 ± 11	83.4 ± 0.9

The probability of this event originating from background nuclear interactions within the (entire) data sample is less than 3.1×10^{-4} events.

DISCUSSION OF EXPERIMENTAL RESULTS

Comparison of Results With Theory

It is seen that to first order, the predicted theoretical lifetime for charm is correct to within an order of magnitude:

$$T_{CH}\ (\text{thy}) \simeq 5\text{-}6 \times 10^{-13}\ \text{sec}$$

$$T_{CH}\ (\text{exp}) \simeq 3.5 \times 10^{-13}\ \text{sec}$$

However, the "naive" free quark model, which predicts the lifetimes of charmed particles to be the same, is in poor agreement with the experimental data, although differences in the D^+, D^0 and F^+ lifetimes were expected on theoretical grounds [21,35-37,41-44], due to the interplay of the strong interactions with the weak for non-leptonic decays; the strong interactions renormalizing the strength of the weak interactions in such a way as to enhance charm-changing (pure) $\Delta I = 1/2$ non-leptonic transitions over those of (mixed) $\Delta I = 1/2$, $3/2$ non-leptonic transition i.e. "20-plet dominance" [21,42,185,186,199,203-205]. (The (two-body) Cabibbo-favored decays of D^0 and F^+ mesons to two pseudoscalar mesons may proceed through the pure $\Delta I = 1/2$ transition, while the D^+ may proceed only by the mixed $\Delta I = 1/2$, $3/2$ transition.) The modification of the weak decays of charmed particles by the strong interactions may also be understood as being due to QCD radiative corrections (i.e. diagrams involving hard gluon emission and absorbtion) [192-199].

Several other mechanisms are predicted to enhance the decay rates of charmed particles, such as non-spectator interactions, i.e. W^+ annihilation and W^+ exchange between quarks (accompanied with gluon bremmstrahlung in meson decays, thus removing the helicity supression effects associated with spin-0 mesons) [176,212-215]. The predicted enhancement of the D^+ relative to the D^0 is 1:20 due to the Cabibbo-unfavored nature of this decay mode for the D^+.

As an example, the predicted Λ_c^+ lifetime, taking into account such non-spectator interactions (the W^+ exchange diagram), scaled to the experimentally measured D^+ lifetime (taken to be the theoretical lifetime of the free charmed quark) is [176]:

$$\tau_{\Lambda_c^+} = 2.0 \pm 0.2 \times 10^{-13}\ \text{sec} \quad (\text{theory})$$

in good agreement with the measured Λ_c^+ lifetime (i.e. within 0.5 S.D.).

In addition to the enhancement processes, other phenomena are predicted to supress the D^+ decay rate relative to that of the free charmed quark, such as strong color-clustering/interference effects associated with the (color-connected) W-radiation decay diagram(s) for the D^+ meson, Pauli exclusion principle supression effects due to the two d anti-quarks in the D^+ final state, violation of the $\Delta n_t = 0$ rule for Cabibbo-favored decays of the D^+ meson, to mention only a few [216,see also 231;41,225,228-230].

The penquin diagram, which is believed to play an important role in the decays of strange particles [185,186,205] is not expected to contribute significantly to the decays of charmed particles [186,205,218-220].

The Feynman diagrams associated with such processes are shown in Fig.62 for charmed mesons and baryons.

It is hoped that with the improved statistics on charm decays expected from the second run of E-531 (already concluded; analysis is in progress), the necessary data with which to perform critical tests of theoretical predictions for the differences in charmed pariticle lifetimes will be obtained.

Comparison of Results With Other Experimental Data

Many experiments previous to and since E-531 have observed visible decays of charmed particles [45,47-52,59-70,96-100,109,114,232]. However, with few exceptions, very few of these events were fully reconstructable, to the extent that the parent identity was unambiguously known, and that the mass and momentum of the parent were also known, within small (5%) errors.

Several experiments have obtained a measurement of the average charmed particle lifetime, i.e. averaged over particle type (as the identity of the parent in each event was not known). However comparison of the average lifetime obtained from this experiment (neutrino production of charm), cannot be directly compared with data from the hadro-production and photo-production of charm, without taking into account relative production rates of D^+, D^0, F^+ and Λ_c^+ (i.e. their cross-sections, along with the energy dependence of the charm cross-sections) which are at present not experimentally known.

On an individual particle species level it is only meaningful to compare the results of this experiment with the fully reconstructed and unambiguously identified decays of charmed particles observed in other experiments. No such candidates for D^+ decay from experiments other than E-531 have been reported to date.

Several fully reconstructed D^0 candidates have been observed, in the Ω-spectrometer and the LEBC experiments at CERN, with decay times of 0.23,0.86 x 10^{-13} sec [67,68] and 2.1,5.9 x 10^{-13} sec [232] respectively. Even here, it is difficult for a quantitative inter-comparison of experimental data (i.e. to use all events in a single maximum likelihood fit) due to the differences in scanning biases (i.e. scanning efficiencies) except to say that the experimental results are consistent with each other.

Two fully reconstructed candidates for the decay of a Λ_c^+ have been observed in experiments other than E-531. A $\Lambda_c^+ \rightarrow p\, K^- \pi^+$ decay was observed in the WA-17 (BEBC) experiment a with a measured decay time of 7.3 x 10^{-13} sec [65], somewhat longer than the measured Λ_c^+ lifetime as obtained in our experiment. A $\Lambda_c^+ \rightarrow \Lambda^0 \pi^+$ decay was observed in the CERN Ω-Spectrometer/emulsion experiment, with a measured decay time of 0.6 x 10^{-13} sec [68].

FNAL experiment E-564, which ran simultaneously with E-531 (and E-553) in the neutrino beam has reported on the neutrino production and decay of an $F^+ \to \pi^+\pi^-\pi^+\pi^0$, with a flight length of 50 ± 2 μm, a momentum of 2.42 ± 0.30 GeV/c, mass of 2017 ± 25 MeV/c^2 and decay time of 1.40 ± 0.05 x 10^{-13}sec [114].

The scanning biases for finding (short decay length) charged charmed decays are not so dissimilar between the two experiments, that it is not unreasonable to include this event in a maximum likelihood fit for four F^+ events. (This, however, is not the case for inclusion of the Λ_c^+ events from the CERN experiments, due to radically different charged decay scanning efficiencies than for this experiment.) Thus, for four F^+ events:

$$\tau_{F^+} = 1.8 \begin{smallmatrix}+1.3\\-0.7\end{smallmatrix} \times 10^{-13} \text{ sec}$$

The (weighted) $F^\pm$ mass, using all four events is 2026 ± 20 MeV/c^2 .

Comparison of D^+, D^0 Lifetime Ratios

The ratio of the D^+ to D^0 lifetimes as determined in this experiment is in reasonable agreement with the D^+ D^0 lifetime ratios obtained by e^+e^- experiments at SPEAR (Mk.II and DELCO) from measurements of the semi-leptonic branching ratios of the D^+ and D^0 at the ψ'' resonance [139-144]:

$$Br(D^+ \to X^0e^+\nu_e) = 16.8 \pm 6.4\% \qquad \text{Mk.II}$$

$$= 22.0 \begin{smallmatrix}+4.4\\-2.2\end{smallmatrix}\% \qquad \text{DELCO}$$

$$Br(D^0 \to X^-e^+\nu_e) = 5.5 \pm 3.7\% \qquad \text{Mk.II}$$

$$< 4.0\% \ (95\% \text{ C.L.}) \qquad \text{DELCO}$$

The ratios of the lifetimes of the D^+ to D^0 as determined by these two experiments are:

$$\tau^+/\tau^0 = 3.1 \begin{smallmatrix}+4.2\\-1.4\end{smallmatrix} \qquad \text{Mk.II}$$

$$> 4.3 \ (95\% \text{ C.L.}) \qquad \text{DELCO}$$

Both Mk.II and DELCO experiments have characterized the D^+, D^0 lifetime ratio R in terms of the function $\ln\xi(R)$ [142-144,145], as shown in Fig.53. The statistical significance of the difference in D^+, D^0 lifetimes is strengthened by combining the results from the three experiments.

Adding together the $\ln\xi(R)$ curves for E-531 and Mk.II (Fig.54), the ratio of D^+, D^0 lifetimes is

$$\tau^+/\tau^0 = 4.2\ ^{+2.5}_{-1.7}\ \text{(E-531 and Mk.II)}$$

This ratio of the lifetimes differs by more than 3.3 standard deviations from unity.

The "World Average" of the ratio of lifetimes may be obtained by combining the results of E-531, Mk.II and DELCO (Fig.54), however, since the DELCO result is a lower limit on the lifetime ratio, the combined result of the three experminents may only be interpreted likewise. The "world average" of the D^+, D^0 lifetime ratio thus differs by more than 4.2 standard deviations from unity.

The (experimentally determined) semi - electronic partial width for $D^+ \to X^0 e^+ \nu_e$ may be obtained from the product of the semi-electronic branching ratio and the D^+ lifetime. Averaging the semi-electronic branching ratios for the D^+ as measured by the two e^+e^- experiments:

$$Br(D^+ \to X^0 e^+ \nu_e) = 20.5\ ^{+3.6}_{-2.1}\%$$

$$\Gamma(D^+ \to X^0 e^+ \nu_e) = 2.0\ ^{+2.0}_{-0.9} \times 10^{11}\ \text{sec}^{-1}$$

in reasonable agreement with theoretical calculations of the semi-leptonic width for free charmed quark decay [21,193-196]:

$$\Gamma(c \to s\ell^+\nu_\ell) = 1.6 \pm 0.3 \times 10^{11}\ \text{sec}^{-1}$$

and also with:

$$\Gamma(D \to X\ell^+\nu_\ell) = 2.2 \pm 0.4 \times 10^{11}\ \text{sec}^{-1}$$

(This number is the sum of the semi-leptonic widths for D decays to K an K*.[201])

Assuming that the annihilation diagram for the D^+ contributes negligibly to the total D^+ rate (due to the $U_{c\bar{d}} = \sin\theta_1\cos\theta_2$ factor at the $c\bar{d}$ vertex), the semi-electronic partial widths will be the same (to first order) for the D^+ and D^0. (The hadrons in the final states of semi-leptonic ($\Delta I = 0$) decays of D^+, D^0 mesons have total isospin $I = 1/2$, and are related to each other by isospin rotations [125].) Thus using the measured D^0 lifetime, the semi-electronic branching ratio for the D^0 is:

$$Br(D^0 \to X^- e^+ \nu_e) = 4.7\ ^{+4.0}_{-3.1}\% \qquad \text{(E-531)}$$

The semi-leptonic branching ratio as obtained above for the D^0 is in good agreement with the measurements obtained at SPEAR. It can be argued that the semi-leptonic width for the Λ_c^+ should be approximately the same as that for the D^+ and D^0, since only the W^+-radiation diagram can contribute to the semi-leptonic decay of the Λ_c^+. Hence to first order, the D^0 and Λ_c^+ should have the same semi-leptonic branching ratios, for the same lifetimes. An experimental lower limit on the F^+ semi-leptonic branching ratio is obtained by the same methods:

$$BR(F^+ \to X^0 e^+ \nu_e) > 4.0 \begin{smallmatrix}+4.6\\-3.6\end{smallmatrix}\%$$

Note that the contribution to the semi-leptonic decay rate from the W^+ annihilation diagram is expected to be less than 5% for the F+.

$F^+ \to \tau\nu_\tau$ Leptonic Branching Ratio:

An estimate of the leptonic $F^+ \to \tau\nu_\tau$ branching ratio may be obtained from:

$$Br(F^+ \to \tau\nu_\tau) = \Gamma(F^+ \to \tau\nu_\tau)\ \tau_{F^+}$$

Where the theoretical partial leptonic width for $F^+ \to \tau\nu_\tau$ is [209-211]:

$$\Gamma(F^+ \to \tau^+\nu_\tau) = \frac{G_F^2}{8\pi} M_F^5 \frac{f_F^2}{M_F^2} |U_{CS}||U_{\tau\nu_\tau}| \frac{M_\tau^2}{M_F^2}\left(1 - \frac{M_\tau^2}{M_F^2}\right)^2$$

Where $G_f = 1.66 \times 10^{-5}$ GeV
$M_f = 2.030$ GeV/c^2 $\quad M_t = 1.784$ GeV/c^2
$f_F = 170$ MeV [205] $\quad U_{cs} = 0.95 \quad U_{\tau\nu_\tau} = 1.00$

(See Refs.[188-192] for a determination of the central values of the K-M matrix, and Refs.[205-208] for estimates of the values of the decay constants for pseudoscalar mesons.)

$$\Gamma(F^+ \to \tau^+\nu_\tau) = 7.2 \begin{smallmatrix}+21.6\\-5.4\end{smallmatrix} \times 10^{10}\ sec^{-1}$$

The uncertainty in the theoretical width calculation is due to the factor-of-two uncertainty in the F^+ decay constant f_F. The "central value" of several theoretical calculations has been used. Using the F^+ lifetime as measured in this experiment, the $F^+ \to \tau\nu_\tau$ branching ratio is

$$Br(F^+ \to \tau\nu_\tau) = 1.4\% \begin{pmatrix}+1.3\\-0.6\end{pmatrix}\%^{exp} \oplus \begin{pmatrix}+4.3\\-1.1\end{pmatrix}\%^{thy}$$

$$Br(F^+ \to \tau\nu_\tau) = 1.4 \begin{smallmatrix}+4.4\\-1.1\end{smallmatrix}\%$$

CHAPTER V

CONCLUSIONS

A single experiment has obtained measurements of the individual lifetimes for four types of charmed particles, the D^+, D^0 and F^+ mesons, and the Λ_c^+ charmed baryon, finding evidence for differences in the lifetimes of the observed charmed particles.

The experimental results are in reasonable agreement with theory, although additional work is required both theoretically, to determine which mechanisms (and to what level such mechanisms) are responsible for the differences in charmed particle lifetimes, and experimentally, to reduce the statistical errors associated with the each of the individual lifetimes, and to determine whether or not new phenomena are extant within the D^0 sample, such that critical comparison can be made.

The (meaningful) results obtained from other experiments are in agreement with the data obtained from this experiment. In this respect, the results obtained from e^+e^- experiments at SPEAR for the D^+, D^0 lifetime ratio provide the strongest comparison at this time.

With regard to the neutral baryon candidate, no "natural" theoretical explanation for the long lifetime exists at the present time. Whether or not this one event truely is the decay of a stable neutral baryon is not known with absolute certainty, although strong experimental evidence exists to support this hypothesis.

It is sincerely hoped that the answers to this and many other tantalizing questions will be answered experimentally from the second run of E-531 (and other experiments), and that theoreticians will extend their efforts toward improving and expanding the theoretical framework of charm. There is much physics left to be done, much physics left to be discovered, and much physics left to be understood!

APPENDIXES

APPENDIX A

CHARM CANDIDATE EVENTS

This section consists of a brief discussion of each event, and is limited to salient features and specific problems associated with the event reconstruction, and their effect on determination of the lifetimes. Several events are discussed in greater detail to elucidate the methods employed in event fitting. The data is organized into four groups, charged D^+ mesons, F^+ mesons, charmed Λ_c^+ baryons and ambiguous charm decay candidates.

A systematic search for interesting and relevant submass combinations of daughter particles was made (for particle states such as K^*, ρ, ϕ, Δ, Σ, etc.), along with a similar search for resonant charm states (such as D^*, F^*, Σ_c, Σ_c^*, etc.). In order to limit the amount of information presented, only those mass combinations relevant to the above particle states are presented. All others are supressed. If no specific mention is made of a particular mass combination for a given event, it is because no candidates exist within 2 S.D. of the particle state in question.

D^+ DECAY CANDIDATES

EVENT 512-5761 $D^+ \rightarrow K^-\pi^+\underline{\pi}^+\pi^0$

One of the positive tracks from the decay vertex is identified by TOF as a π^+. This event is D^+/F^+ ambiguous on the basis of mass, however the other positive track from the decay vertex is identified by TOF as a π^+ at the 80% C.L.; thus the D^+ hypothesis is preferred. The net F^+ background for this event is therefore 10%, assuming equal neutrino production rates for D^+ and F + mesons.

EVENT 546-1339 $D^+ \rightarrow K^-\pi^+\underline{\mu}^+(\nu_\mu)$

A photo-micrograph of this event is shown in Fig.46. One of the decay tracks (5-2) is identified as a 4.64 GeV/c μ^+ from penetration through both planes of muon counters. The probability of $\pi^+ \rightarrow \mu^+\nu_\mu$ decay using the observed momentum for this track is 1.6%. Tracks 5-1 and 5-3 are not identified by TOF, however the invariant mass of these two tracks for the above decay hypothesis is $M_{K\pi} = 928 \pm 12$ MeV/c^2 consistent with a $K^{*0}(892)$. As the missing neutral is assumed to be a neutrino, no constrained (> 0-C) fit is possible. The minimum mass of the 1-C curve (shown in Fig.47) for the decay hypothesis $D^+ \rightarrow K^-\pi^+\mu^+(\nu_\mu)$. Thus, hypotheses with additional missing neutrals (e.g. π^0's) are not allowed for D^+ decay. No solution exists for the decay hypothesis $F^+ \rightarrow K^-K^+\mu^+(\nu_\mu)$, as the minimum mass is 2244 ± 30 MeV/c^2. 0-C solutions exist for the decay hypothesis $F^+ \rightarrow \pi^+\pi^-\mu^+(\nu_\mu)$, which can occur via three possible decay mechanisms, as shown in Fig.49. The relevance of these diagrams for $F^+ \rightarrow \pi^+\pi^-e^+\nu_e$ decay, as a background in D^+ decays is discussed at the end of this section on D^+ decays. The maximum F^+ background for this event (see below) is 2.5% for equal production rates of D^+ and F^+ mesons.

2.44 ± 0.23 GeV of excess energy is observed in one isolated lead glass block (# 40). The invariant D^+-γ mass is

$$M_{D^\pm\gamma_+} = 2002 \pm 13 \text{ MeV}/c^2$$

consistent with the D^{*+}. No other mass combinations of the D^+ with any of the other particles in this event have masses within 4 S.D. of the D^{*+} mass. No F^{*+} candidates exist for either solution of the $F^+ \rightarrow \pi^+\pi^-\mu^+(\nu_\mu)$ decay hypothesis within 4 S.D. of the expected F^{*+} mass ($M_{F^*} = 2140 \pm 35$ MeV/c^2 [160]).

EVENT 580-4508 $D^- \rightarrow \pi^- \underline{K}^+ \underline{e}^- (\bar{\nu}_e)$

This event is an anti-neutrino induced charged-current interaction, in which the μ^+ from the primary vertex identified by penetration through both muon counter planes. One of the charged particles from the primary vertex decays after 2307 ± 50 μm. Decay track 1-1 passes through an isolated lead glass block, in which 6.7 ± 0.4 GeV of energy was observed. The momentum of track 1-1 is measured to be 4.24 ± 0.09 GeV/c. The difference $E_{pbg} - P_{trk} = 2.5 \pm 0.4$ GeV is consistent with electron bremmstrahlung in the emulsion, as the decay tracks must traverse 2.7 cm of emulsion (1 radiation length) before exiting the emulsion module. As the momentum is greater than 3.0 GeV/c, the electron and bremmstrahlung enter the same lead glass block.

Track 1-3 is identified from TOF as a K^+. The invariant mass of track 1-3 and 1-2 is 894 ± 132 MeV/c^2, consistent with the $K^{*0}(892)$. The two 0-C solutions for the above decay hypothesis are less than 600 MeV/c apart (see Fig.47); the fractional difference in the decay times is less than 6% (a difference of 2 S.D.). No solutions exist for the decay hypotheses

$$F^- \rightarrow K^- K^+ e^- (\nu_e)$$

$$F^- \rightarrow K^- \pi^+ e^- (\bar{\nu}_e)(K^0)$$

Solutions do exist for the decay hypothesis

$$F^- \rightarrow \pi^- \pi^+ e^- (\bar{\nu}_e)$$

However, track 1-2 is identified by TOF as a K^+. Hence, this event is not consistent with F^- decay, therefore the F-background associated with this event is effectively zero. No D^{*-} or F^{*-} candidates exist for this event, as there are no gamma candidates in the lead glass.

EVENT 598-1759 $D^+ \rightarrow K^+K^-\underline{\pi}^+\underline{\pi}^0$

This event, from kinematic analysis, was determined to be consistent only with the Cabibbo-unfavored decay of a D^+, as the 2-C masses are such that the 3-C fits are unacceptable for the decay hypotheses:

Decay Mode	3-C C.L.
$D^+ \rightarrow K^+\pi^-\underline{\pi}^+\underline{\pi}^0$	0.000
$F^+ \rightarrow K^+\pi^-\underline{\pi}^+\underline{\pi}^0$	0.000
$\Lambda_c^+ \rightarrow p\ K^-\underline{\pi}^+\underline{\pi}^0$	0.035

0-C hypotheses exist for:

$$D^+ \rightarrow K^+\pi^-\underline{\pi}^+\underline{\pi}^0(\pi^0)$$

$$F^+ \rightarrow K^+K^-\underline{\pi}^+\underline{\pi}^0(\pi^0)$$

However, no evidence for the additional π^0 is observed in the apparatus. The probability of such a π^0 avoiding detection is 20%, thus the maximum F^+ background for this event is 10%.

The decay occurs within the (70 μm thick) plastic base of one of the emulsion plates, 10μm from the downstream edge of the plastic base. No black tracks are observed to emerge from the decay region. Typical ranges of black tracks from nuclear break-up in emulsion are 100μm Thus, a range of 2.5 x this is expected in plastic, on the basis of the ratio of energy losses in plastic and emulsion [160]. The probability of non-observation of black tracks from a nuclear interaction is therefore small, ($\lesssim$ 4.0%).

There are no K^*, ρ or φ candidates. The three body mass combinations are:

$$M_{K^+K^-\pi^+} = 1663 \pm 22\ \mathrm{MeV/c^2}$$

$$M_{K^+K^-\pi^0} = 1381 \pm 28\ \mathrm{MeV/c^2}$$

$$M_{K^-\pi^+\pi^0} = 1157 \pm 21\ \mathrm{MeV/c^2}$$

The last two three body combinations are consistent with Q(1400) and Q(1280) mesons, respectively.

No higher resonant charmed states are observed.

EVENT 663-7758 $D^+ \rightarrow K^-\pi^+\underline{e}^+(\nu_e)$

The energy of the incident neutrino in this event is $E_\nu = 280 \pm 60$ GeV. 90% of the available hadron energy is carried away by a single charged particle, observed to decay 13000 ± 50 μm from the primary vertex. As the momenta of the decay tracks are high, no particle identification from TOF is possible.

The three decay tracks 1-1, 1-2 and 1-3 all pass through the same lead glass block (along with the muon). The energy deposited in this block is $E_{PBG} = 19.9 \pm 0.7$ GeV, with 4.0 ± 0.5 GeV/c in two neighboring blocks. The energy deposition and track locations in the lead glass are consistent only with the hypothesis of track 1-3 ($P_{1-3} = 15.5 \pm 2.0$GeV/c) as an electron. The excess lead glass energy is consistent with bremmstrahlung from 1-3 as it traverses 2.24 cm (one radiation length) of emulsion before exiting the emulsion module.

The 0-C solution for $D^+ \rightarrow K^-\pi^+e^+(\nu_e)$ occurs at the minimum of the 1-C curve. Acceptable F^+ decay solutions exist only for $F^+ \rightarrow \pi^+\pi^-e^+(\nu_e)$. The high solution is excluded by maximum beam energy constraints (350 GEV).

It should be noted that in the above listed semi-leptonic D^+ decays, (indeed, for all of the observed semi-leptonic decays in the data sample, including the D^0 decays), a muon from the primary vertex is identified in every event. Thus the semi-leptonic decays are unlikely to be due to decays of objects other than charmed particles (e.g. heavy charged and/or neutral leptons), unless the production mechanism for such objects is similar to that for charm.

F^+ and Λ_c^+ Background in D^+ Decays

The F^+ background associated with the above sample of semi-leptonic D^+ decays occurs from the processes shown by the Feynman diagrams in Fig.49.

1. $c\bar{s}$ W^+-Annihilation/Gluon Bremmstrahlung.
   The branching ratio for this diagram is estimated to be 2.5%, using the rates calculated in Refs.[212-215] (assuming that the gluon(s) fragment with unit probability into a $\pi^+\pi^-$ pair and the virtual W^+ decays to a $\ell^+\nu_\ell$ pair), along with the measured F^+ lifetime. (The actual number calculated for this diagram is 1.5%.)

2. W^+-Radiation/OZI-Supressed $s\bar{s}$ Annihilation.
   An estimate of the branching ratio for this process can be obtained from the following [222].

   The branching ratio for the OZI-allowed process $\phi \to K\bar{K}$ is $Br(\phi \to K\bar{K}) = 83.8 \pm 1.7\%$ [160]. The branching ratio for the OZI-supressed process $\phi \to \pi^+\pi^-\pi^0$ (including $\rho\pi$) is

   $$Br(\phi \to \pi^+\pi^-\pi^0) = 14.7 \pm 0.7\% \text{ [160]}.$$

   Assuming that the quark content of the ϕ is entirely $s\bar{s}$ as an upper limit, (the ϕ wave function contains $u\bar{u}$ and $d\bar{d}$ components due to mixing with other neutral vector mesons, i.e. $\psi_\phi = 1/\sqrt{3}(u\bar{u}+d\bar{d}+s\bar{s})$; correcting for phase space (where both of the above ϕ decay modes vary as Q^3, $Q(\phi \to \rho\pi) = 183$ MeV/c, $Q(\phi \to K\bar{K}) = 119$ MeV/c); and assuming as an upper limit that the 3 π decay mode of the ϕ meson is all from $\phi \to \rho\pi$, then an estimate for the $F^+ \to \pi^+\pi^-\ell^+\nu_\ell$ branching ratio via OZI-supressed $s\bar{s}$ annihilation is [234]:

   $$Br(F^+ \to \pi^+\pi^-\ell^+\nu_\ell) \simeq Br(c \to s\,\ell^+\nu_\ell) \times R^F(\text{OZI/Strong})$$

   Where $Br(c \to s\,\ell^+\nu_\ell) = 20\%$ (free quark model)

   $$R^F(\text{OZI/Strong}) \simeq R^\phi(\text{OZI/Strong})$$

   $$R^\phi(\text{OZI/Strong}) = \frac{Br(\phi \to \rho\pi)\; Q^3(\phi \to K\bar{K})}{Br(\phi \to K\bar{K})\; Q^3(\phi \to \rho\pi)}$$

   $$Br(F^+ \to \pi^+\pi^-\ell^+\nu_\ell) \simeq (.20)(4.8\%) = 1.0\%$$

3. <u>Second Order Weak Processes.</u>
The contributions from these diagrams are expected to be $(G_F/\sqrt{2})$ smaller than leading first-order processes, i.e. miniscule. Hence they are neglected.

The number of F^+ decays in the above sample of D^+ decays is the sum of the probabilities of F^+ decay for each individual event. Each probability is the product of the probability of producing an F^+ (relative to a D^+) and the specific decay background probability for that event. Assuming equal production ratios for D^+ and F^+ mesons as an upper limit, along with the assumption that $Br(F^+ \rightarrow \pi^+\pi^-\ell^+\nu_\ell) < 5\%$, the maximum F^+ contamination, or F^+ background in the D^+ decay candidates is:

$$N^F_{BKGND} < 0.5(0.20 + 0.05 + 0.00 + 0.20 + 0.05) = 0.025 \text{ Events}$$

The Λ_c^+ contamination in the D^+ sample, obtained by postulating a missing neutron or assuming the untagged positive hadrons in the decays are protons, is negligibly small, as the minimum mass possible is more than 3 S.D. above the Λ_c^+ mass in all cases except 598-1759 where the 3-C C.L. = 0.035.

F^+ DECAY CANDIDATES

Three charm candidates were found, which upon reconstruction were determined to be inconsistent with D^+ meson decays, in that the measured masses were well above the D^+ mass; the observed decay modes for each of the events are also Cabibbo-unfavored decays for D^+ mesons. The events are consistent with decays of F^+ mesons, both in the observed masses and observed decay modes.

EVENT 527-3682 $\quad F^- \rightarrow \underline{\pi}^+\underline{\pi}^-\pi^-\underline{\pi}^0$

A photo-micrograph of this event is shown in Fig.46. The background fog grains have been removed to improve contrast. This event is an anti-neutrino induced charged-current event, as the muon from the primary vertex has positive charge. No charged strange particles are observed in this event, although a total of 11 GeV of excess energy is observed in three out of four calorimeter rows, where no charged particles are incident. Two of the charged tracks from the decay are identified as pions by TOF. Transverse momentum does not balance at the decay vertex (with C.L. > 99%.) A π^0 is observed in the lead glass which balances transverse momentum (within errors) at the decay vertex. The 2-C mass for an all-pion decay hypothesis is 2026 ± 56 MeV/c. The 3-C C.L. for a Cabibbo-unfavored D^- decay is 1.3%, and smaller still for the Cabibbo-favored D^- decay. (Not allowed by TOF, in any case.) The two and three-body neutral mass combinations of the decay particles are listed below:

$$M_{12} = 611 \pm 27 \text{ MeV/c}^2$$

$$M_{23} = 780 \pm 17 \text{ MeV/c}^2$$

$$M_{124} = 1296 \pm 59 \text{ MeV/c}^2$$

$$M_{234} = 1338 \pm 41 \text{ MeV/c}^2$$

Note that the branching ratio of the $\omega(783)$ to $\pi^+\pi^-$ is 1.4% [160].

No F* candidates exist within 3 S.D. of the F*(2140) mass.

EVENT 597-1851 $F^+ \rightarrow \underline{K}^+\underline{\pi}^+\underline{\pi}^- K_L^0$

No muon from the primary vertex is identified (by penetration through the muon steel) in this event. The shower tracks from the primary vertex, other than the track which decays all have large X and/or Y slopes; thus a muon cannot be excluded in this event.

All of the charged tracks from the decay are identified by TOF. Transverse momentum does not balance at the decay vertex (> 99% C.L.). Excess energy is observed in the calorimeter, and a small amount of energy is deposited in a lead glass block where no charged track is incident. The observed calorimeter energy and location from the lead glass are in excellent agreement with predictions from a 0-C fit to $F^+ \rightarrow \underline{K}^+\underline{\pi}^+\underline{\pi}^- K_L^0$:

	0-C fit values	Observed Values
$P_{K_L^0}$:	3.5 ± 0.5 GeV/c	3.1 ± 1.9 GeV/c
$X_{K_L^0}$:	-0.280 ± 0.018	-0.303 ± 0.015
$Y_{K_L^0}$:	-0.045 ± 0.013	-0.009 ± 0.015

The 3-C C.L. for the Cabibbo-unfavored decay of a D^+ is C.L. < 3.0%.

The (doubly Cabibbo-unfavored) decay hypothesis $\Lambda_c^+ \rightarrow K^+\pi^+\pi^- n$ has a C.L. 0.01%.

The two body $K_L^0 - \pi^+$ mass is $M_{K\pi} = 867 \pm 55$ MeV/c^2 .

The invariant mass of the K^+ and π^- is $M_{K\pi} = 752 \pm 5$ MeV/c^2 .

No other strange particles are identified in this event.

EVENT 638-9417 $F^+ \rightarrow \underline{K}^+K^-\pi^+\underline{\pi}^0$

The K^+ is identified by TOF, 3.5 S.D. from a proton. The K^- is 2 S.D. from either K^- or antiproton, i.e. ambiguous between the two negative particle types. The event occurs in the upstream portion of the target. The π^0 is identified by conversion of both γ's in the emulsion. This event has much electromagnetic shower activity as a result of the vertex location. The tracks from the shower are confined to the upstream drift chambers, for the most part. The pulse height in TOF I is correspondingly larger for this event. A further consequence of this is that the fitted TOF start is pulled early, resulting in a slower observed transit time for the tracks which penetrate to TOF II, which in turn shifts TOF identification towards heavier particles.

The 2-C fitted mass for the decay hypothesis $F^+ \rightarrow K^+K^-\pi^+\pi^0$ is $M_{F+} = 2050 \pm 45$ MeV/c^2.

The K^+-K^- invariant mass is $M_{KK} = 1000 \pm 3$ MeV/c^2,

consistent with the S*(980) and/or δ(980) mesons.

The invariant π^+-π^0 mass is $M_{\pi\pi} = 572 \pm 37$ MeV/c^2, not consistent with a ρ^+.

A 220 MeV/c photon is observed in an isolated block of the lead glass array. The invariant $F^+ - \gamma$ mass is $M_{F\gamma} = 2135 \pm 45$ MeV/c^2, consistent with a F^{*+} (2140).

No other strange particles are identified in this event. The 3-C C.L.'s are negligibly small (i.e. $\lesssim 0.01\%$) for the Cabibbo-unfavored decay of a D^+, and for $\Lambda_c^+ \rightarrow p\,K^-\pi^+\pi^0$ (not allowed by TOF).

Λ_c^+ DECAY CANDIDATES

EVENT 476-4449 $\Lambda_c^+ \rightarrow p\pi^+\pi^-(\bar{K}^0)$

This event has an unusually high charge multiplicity (NH = 20, NS = 12) at the primary vertex. The event is an unambiguous charmed baryon decay candidate, as one of the decay tracks is identified by TOF as a proton (3.0 S.D. from a kaon). The pions from the decay were identified by emulsion $P\beta$ and I/I_0 measurements. Over 11,000 individual grains of silver were counted along each of the tracks, thus obtaining a I/I_0 measurement accurate to 1%. (This event was our first charm decay candidate to be found in the emulsion, by the Ottawa group.) A missing neutral is required to balance transverse momentum. The $1-C_c$ curve (shown in Fig.47) for the decay hypothesis $\Lambda_c^+ \rightarrow p\pi^+\pi^-(\bar{K}^0)$ has two solutions for the K^0 momentum.
No K_S^0 is observed to decay in the drift chambers. The high momentum solution is the physically favored solution, as 10 GeV of excess energy is observed in the calorimeter in the region where a 2.5 GeV K_L^0 is expected (although other neutral hadrons are likely to be present in the calorimeter, with the charge multiplicity as high as it is in this event). Furthermore, the Feynman-X ($X_F \equiv P^*_{11}/P^*_{MAX,B}$) for this event
preferentially selects out the high momentum solution, as the low momentum solution has $X_F < -1$ by more than three standard deviations which is unphysical ($\sigma(X_F) = 0.1$). For the high momentum solution, $X_F < -1$ by only a fraction of a standard deviation.

The invariant submass combinations have

$$M_{p\pi^+} = 1212 \pm 19 \text{ MeV/c}^2 \quad (\Delta^{++}(1236))$$

$$M_{K^0\pi^-} = 896 \pm 20 \text{ MeV/c}^2 \quad (K^{*-}(892))$$

(High solution only)

Combination of either momentum solution for the Λ_c^+ decay with track 7 (π^+) have the invariant masses:

$$M_{\Lambda_c^+\pi^+} = 2485 \pm 3 \text{ MeV/c}^2 \quad \text{(low solution)}$$

$$M_{\Lambda_c^+\pi^+} = 2440 \pm 3 \text{ MeV/c}^2 \quad \text{(high solution)}$$

(The order of high and low $\Lambda_c^+ - \pi^+$ solutions is correct). The mass of the Σ_c^{++} has been measured to be 2450 ± 10 MeV/c². [160].

EVENT 498-4985 $\Lambda_c^+ \to \underline{\Lambda}^0 \underline{\pi}^+ \underline{\pi}^- \underline{\pi}^+$

All the decay products in this event are identified. The Λ^0 is observed to decay to p-π. The invariant $\Sigma^0 - \pi^0$ mass is

$$M_{\Lambda^0\pi^-} = 1406 \pm 5 \text{ MeV/c}^2$$

consistent with the $\Sigma^-(1385)$. The $\Lambda_c^+ - \pi^+$ invariant mass for tracks 1 and 3 with the $\Lambda_c^+ - \pi^+$ are

$$M_{\Lambda_c^+\pi^+} = 2463 \pm 5 \text{ MeV/c}^2$$

$$M_{\Lambda_c^+\pi^+} = 2443 \pm 4 \text{ MeV/c}^2$$

No other mass combinations below 2650 MeV/c of the Λ_c^+ with other primary tracks exist.

EVENT 499-4713 $\Lambda_c^+ \to \underline{\Sigma}^0 \pi^+$, $\Sigma^0 \to \underline{\Lambda}^0(\gamma)$.

Track 2 is observed to kink 366 ± 6μm from the primary vertex, with kink angle $\theta_K = 0.255$ rad and $\Delta P_K = 680 \pm 12$ MeV/c. Track 2-1 favors identification as a π^+ over a K^+ by 1.4 S.D. (i.e. 85% C.L.) from TOF information. No π^0 or γ are observed in the lead glass array. A Λ^0 is observed to decay in the drift chambers, with the proton identified by TOF.

The 3-C fit to $\Lambda_c^+ \to \underline{\Lambda}^0\pi^+$ has an unacceptable fit, as the 3-C C.L. < 0.01%, due to the fact that the 2-C mass is 2175 ± 17 MeV/c^2, with 2-C C.L. = 90.6%, $\Delta P_x = -7 \pm 28$ MeV/c, $\Delta P_y = -16 \pm 38$ MeV/c.

A 0-C fit to $\Lambda_c^+ \to \Lambda^0\pi^+\pi^0$ has a minimum mass of 2331 ± 16 MeV/c , more than 2.8 S.D. above the Λ_c^+ mass. Separate 0-C fits to $\Lambda_c^+ \to (\Sigma^0)\pi^+, \Sigma^0 \to \Lambda^0(\gamma)$ have a unique solution for the γ momentum in the decay of the $\Sigma^0 \to \Lambda^0\gamma$ such that the effective 1-C fit to the decay chain:

$$\Lambda_c^+ \to \Sigma^0\pi^+,\ \Sigma^0 \to \Lambda^0(\gamma),\ \Lambda^0 \to p\pi^-$$

(involving 12 equations and 11 unknowns) has masses of

$$M_{\Lambda_c^+} = 2269 \pm 17 \text{ MeV/c}^2 \qquad M_{\Sigma^0} = 1189 \pm 11 \text{ MeV/c}^2$$

$$M_{\Lambda^0} = 1124 \pm 5 \text{ MeV/c}^2$$

The direction of the emitted gamma from Σ^0 decay is such that it does not pass though the aperture of the magnet.

The invariant $\Lambda_c^+ \to \pi^+$ mass of the Λ_c^+ with track 3 (π^+) is consistent with the expected Σ_c^{*++} mass, 2500 MeV/c [170].

EVENT 549-4068 $\Lambda_c^+ \rightarrow K^- p \pi^+ (\pi^0)$

This event is poorly reconstructed in the spectrometer as the momenta of the charged hadrons from the decay are all low. Track 2-2 is measured as a positive-charged particle, momentum analyzed by the fringe field of the magnet. Emulsion measurements for 2-2 identify it as a proton (3.0 S.D. from a kaon.) The momenta of tracks 2-1 and 2-3 are measured in the emulsion; track 2-1 is consistent with either a proton or a kaon, as the errors in the I/I_0 measurement are large because of the small θ for this track. Decay track 2-3 is emitted backward in the laboratory system, and is identified as a 47.4 ± 0.7 MeV/c π^+ by range measurments from the observed decay chain

$$\pi^+ \rightarrow \mu^+ \nu_\mu; \quad \mu^+ \rightarrow e^+ \nu_e \bar{\nu}_\mu$$

as the π^+, μ^+ and e^+ all stop in the emulsion.

A missing neutral is required to balance momentum at the decay vertex. The lead glass has no π^0 or γ candidates. The -1C curve for $\Lambda_c^+ \rightarrow pK^-\pi^+(\pi^0)$ for an unobserved π^0 in the spectrom has two solutions for the π^0 momentum, as shown in Fig.47. The high momentum solution is favored, as the Feynman-X for this event exceeds -1.0 by more than 1.5 S.D. for the low momentum solution. The invariant submass combinations are

$$M_{p\pi^+} = 1157 \pm 5 \text{ MeV/c}^2$$

$$M_{K^-\pi^0} = 915 \pm 26 \text{ MeV/c}^2$$

(High solution only.)

The fractional difference in the decay times for the high and low momentum solutions is less than 25% (0.63 vs. 0.77 x 10^{-13} sec). Thus, the 0-C ambiguity (two solutions) will have only a small effect on the mean lifetime for the Λ_c^+.

EVENT 567-2596 $\Lambda_c^+ \rightarrow \underline{p}\ K_L^0$

One of the tracks from the primary vertex (track 3) is observed to kink after 175 ± 10μm with kink angle θ_K =0.409 ± 0.002 rad. Track 3-1 is identified as a proton by TOF, 4.5 S.D. from a K^+. The decaying baryon cannot be a hyperon, since ΔP_K = 605 ± 15 MeV/c.

No $V^{0's}$ are observed to decay in the drift chambers; no excess electromagnetic energy is observed in the lead glass. 3.1 GeV of excess energy is observed in row 3 of the calorimeter. The magnitude and location of the energy excess in the calorimeter is in good agreement with the high solution to a 0-C fit of $\Lambda_c^+ \rightarrow p\ K_L^0$.

	0-C Fit Values	Measured Values
$P_{K_L^0}$	: 4.0 GeV/c	3.1±1.8 GeV/c
$X'_{K_L^0}$	: -0.065 rad	-0.034±0.050 rad
$Y'_{K_L^0}$	: -0.025 rad	-0.000±0.200 rad

The two-body invariant mass of the Λ_c^+ with track 4(π^-) has a mass

$$M_{\Lambda_c^+\pi^-} = 2468 \pm 3\ \mathrm{MeV/c^2}$$

This event is unambiguously not consistent with F^+ decay via $c\bar{s}$ annihilation to $p\bar{n}$ [146], using the observed excess calorimeter energy.

EVENT 602-2032 $\Lambda_c^+ \rightarrow \underline{p}\pi^+\pi^-(K_S^0)$

Track 2-1 from the decay undergoes an elastic scatter i.e. kinks) after 2.7 cm in the emulsion, with kink angle θ_K = 0.084 rad and ΔP_K = 160 MeV/c. TOF information identifies track 2-1-1 as a proton. The likelihood of a charged pion or kaon scattering off of a nucleus, producing only a proton in the final state is quite small (1%). Thus track 2-1 is most likely to be due to the elastic scattering of a proton. Hence this event is most likely a Λ_c^+. Tracks 2-2 and 2-3 are identified as π^+ and π^- respectively from I/I_0 measurments in emulsion. The high momentum solution to $\Lambda_c^+ \rightarrow p\pi^+\pi^-(K_L^0)$ is favored, as a track observed in the drift chambers (and not in the emulsion) is identified as a π^+ by TOF and misses the primary vertex in the transverse direction by more than 3.0 cm (the up-only track for the π^- is not reconstructed in the spectrometer, due to its large negative Y-slope and many hits in the upstream drift chambers.)

The invariant submass combinations for the daughter particles are:

$$M_{p\pi^+} = 1124 \pm 7 \text{ MeV/c}^2$$

$$M_{p\pi^-} = 1160 \pm 6 \text{ MeV/c}^2$$

$$M_{K\pi^+} = 771 \pm 35 \text{ MeV/c}^2$$

$$M_{K\pi^-} = 845 \pm 25 \text{ MeV/c}^2$$

Only poor K* or Δ^{++} (correlated) mass combinations exist for this decay candidate.

EVENT 610-4088 $\Lambda_c^+ \rightarrow \underline{\Lambda}^0 \underline{\pi}^+ \underset{\sim}{\pi}^- \underset{\sim}{\pi}^+$

The Λ^0 in this event is poorly reconstructed as it decays in the last few upstream drift chambers. Although the momenta of the proton and pion from the Λ^0 decay are reconstructed by hand, the calculated flight times are in excellent agreement with TOF measurements for their assumed identity, and inconsistent with K_S^0, K_L^0 or Ξ^0 decay. The three charged decay tracks are identified as pions from TOF and emulsion information. No π^0's, γ's or other charged tracks are observed in the downstream spectrometer. The invariant Λ^0-π^- mass is
$M_{\Lambda^0\pi^-} = 1401 \pm 33$ MeV/c^2, consistent with the $\Sigma^-(1385)$.

EVENT 650-6003 $\Lambda_c^+ \rightarrow \underline{\Lambda}^0 \underline{\pi}^+ \pi^- \underset{\sim}{\pi}^+$

Two of the three charged decay tracks are identified in this event. The Λ^0 is observed to decay to p-π^- and balances transverse momentum at the decay vertex. The invariant mass of the Λ^0 with the π^- is
$M_{\Lambda^0\pi^-} = 1401 \pm 95$ MeV/c^2, consistent with the $\Sigma^-(1385)$.
The invariant mass of the Λ_c^+ with track 4 (π^+) is
$M_{\Lambda_c^+} = 2447 \pm 11$ MeV/c^2, consistent with the $\Sigma_c^{++}(2450)$.

Discussion of Λ_c^+ Decays

The two-body $\Lambda_c^+ - \pi^{\pm,0}$ mass combinations for Λ_c^+ decay are shown in Fig.55. Evidence exists, although somewhat limited by the statistics for the resonant $\Sigma^-(1385)$ state, as indicated by the clustering of negative charge near this mass, and is consistent with theoretical expectations [170-174,178].

The decay mode $\Lambda_c^+ \to \Delta^{++}K^{*-}$ can only occur via the W^+-exchange diagram. For the $(p-\pi)(K-\pi)$ (correlated) mass combinations, evidence exists (although weak, due to lack of statistics) for $\Lambda_c^+ \to \Delta^{++} K^{*-}$ decay from events 476-4449 and 549-4068. (i.e. the high solutions are chosen in both cases, which are the physically favored solutions for each event).

$\Lambda_c^+-\pi^{\pm}$'s mass combinations with pions from the primary vertex also show evidence of higher mass resonant charmed baryon states, near 2450 MeV/c^2, consistent with that observed for the Σ_c^{++} [73,82,83,160]. (See Fig.56.)

Calculation of Nuclear Interaction Backgrounds for Charmed Baryons Produced in Neutrino Interactions

As the nuclear interaction background is highest for the charmed baryons (due to the presence of a baryon in the final state, and lower parent momentum), the nuclear interaction background for the charmed baryons is calculated below on a per-event basis, using the methods from the section above on calculation of nuclear interaction backgrounds (for the whole charged current event sample), along with the necessary information from each charm decay candidate such as decay length, momentum, charge multiplicity, etc.

TABLE 18

NUCLEAR INTERACTION BACKGROUNDS FOR CHARMED BARYONS

EVENT NUMBER	INCIDENT HADRON	BACKGROUND PROBABILITY
476-4449	π^+, K^+	3.8×10^{-4}
498-4985	π^+, K^+	1.2×10^{-3}*
499-4713	π^+, K^+	1.0×10^{-2}*
549-4069	π^+, K^+, p	9.0×10^{-4}
567-2596	K, p	4.5×10^{-5}
602-2032	π^+, K^+	4.2×10^{-3}
610-4088	π^+, K^+	5.0×10^{-3}*
650-6003	π^+, K^+	4.6×10^{-4}*
635-4949	K^0	5.6×10^{-3}

The total number of background events for the Λ_c^+ sample (8 events) is less than 2.3×10^{-2} background events. Note that for the events with $\Lambda_c^+ \rightarrow \Lambda^0\pi^+\pi^-\pi^+$ decays (*), the nuclear interaction hypotheses are "exotic", in that the wrong sign of strangess occurs for a final state with net positive charge for an incident K^+. (This aspect was not included in the above calculation.) It is emphasized that these calculations are to be taken as <u>upper limits</u> to the nuclear interaction background, as the initial assumptions used in the calculations are all extremely conservative.

The nuclear interaction background probabilities for the Λ_c^+ and neutral baryon event as calculated here should be compared with the calculation done (in a slightly different manner) for event 635-4949:

$$N = 3.1 \begin{smallmatrix} +1.6 \\ -1.3 \end{smallmatrix} \times 10^{-4} \text{ events (see above)}$$

AMBIGUOUS CHARM DECAY CANDIDATES

EVENT 493-1235 $D^+ \rightarrow \pi^+\underline{\pi}^+\pi^-K_L^0$,

$F^+ \rightarrow \pi^+\pi^+K^-K_L^0$, $\Lambda_c^+ \rightarrow \pi^+\pi^+K^-n$

The ambiguity in this event is two-fold in that the identity of track 3-3 is not certain, and the identity of the neutral particle is ambiguous between a K_L^0 and a neutron. Excess energy is observed in the hadron calorimeter in the region predicted from 0-C fit information. The 2-C and 3-C kinematic fits are poor due to the large errors associated with the neutral hadron and track 3-1, which interacts in the emulsion (with NH = 19, NS = 0).

EVENT 502-354 Y^{++} "Double Charged" Event

$Y^{++} \rightarrow \underline{\Lambda}^0\pi^+h^+\pi^0(\pi^0)$; $\Sigma_c^{++} \rightarrow \Lambda_c^+\pi^+$, $\Lambda_c^+ \rightarrow \underline{\Lambda}^0\pi^+\pi^0(\pi^0)$

Unfortunately, the magnet was off in this run due to a power supply failure. Thus, most momentum information is obtained from emulsion measurements, except for the lambda, which was reconstructed and identified from TOF information (!). This event is most likely a neutrino, as opposed to an anti-neutrino interaction, due to the ratio of anti-neutrinos to neutrinos in the beam.

The grain density of the parent track is significantly higher than minimum ionizing tracks in this event. The magnitude of the charge of the parent particle is

$$|Q| = 2.05 \begin{smallmatrix} +1.61 \\ -0.91 \end{smallmatrix}$$

as obtained from densitometry measurements. If this event is truely a doubly-charged particle, e.g. a stable doubly-charged charmed baryon, or possibly a 5-quark exotic state, or perhaps a super-fragment, then it has no impact on the lifetimes of the more common types of charmed particles. However, an alternate interpretation of this event is $\Sigma_c^{++} \rightarrow \Lambda_c^+\pi^+$, with $\Lambda_c^+ \rightarrow \pi^0\pi^+\pi^0(\pi^0)$. The 0-C solutions for this decay hypothesis are quite compatible with the measured Λ_c^+ lifetime.

EVENT 522-2107 $D^+ \to \pi^+\pi^-K^-(\pi^0)$,

$F^+ \to K^+\pi^+K^-(\pi^0)$, $\Lambda_c^+ \to p\pi^+K^-(\pi^0)$

The neutral particle in the charm decay of this event, most likely a π^0, is not fully reconstructed in the spectrometer, due to the large y-slope of the parent. There are several π^0 candidates, however none of them balance momentum at the decay vertex. The 2-C and 3-C confidence levels reflect this fact. A 0-C fit to the above decay hypotheses has acceptable solutions for D^+, F^+ and Λ_c^+ decays, however, one or both of the gammas from the π^0 decay are not detected by the lead glass, hence the resulting ambiguity in parent identity. The high momentum solution for the π^0 is favored, as a gamma candidate is observed in the region near the top of the lead glass array, in the area expected for the fast π^0. As the observed decay time is quite long, this event is most compatible with a D^+ meson decay hypothesis.

EVENT 529-271 $D^+ \to \pi^+(K_L^0)$, $F^+ \to K^+(K_L^0)$,

$\Lambda_c^+ \to p(K_L^0)$, $D^+ \to \pi^+\pi^0\ (K_L^0)$, $F^+ \to K^+\pi^0(K_L^0)$

Track 2 is observed to kink 2547 ± 30 μm from the primary vertex with kink angle $\theta_k = 0.085$ rad, $\Delta P_K = 518 \pm 17$ MeV/c. Acceptable 0-C solutions exist for the following decay hypotheses:

Decay Mode	$(E_{cal}-E_{K_L^0})/\sigma(E_{cal})$
$D^+ \to \pi^+(K_L^0)$	3.8
$F^+ \to K^+(K_L^0)$	2.0
$\Lambda_c^+ \to p(K_L^0)$	1.8
$D^+ \to \pi^+\pi^0(K_L^0)$	2.0
$F^+ \to K^+\pi^0(K_L^0)$	0.6

In each case, the high solution is favored by the observed excess energy in the calorimeter $E_{cal} = 27 \pm 5$ GeV. The difference (in S.D.) of the excess calorimeter energy and the energy of the missing neutral is given for each hypothesis. The last decay hypothesis is in closest agreement with the observed calorimeter energy.

EVENT 533-7152 $D^+ \rightarrow \pi^+(K_L^0)$, $F^+ \rightarrow K^+(K_L^0)$, $D^+ \rightarrow \pi^+\pi^0(K_L^0)$, $F^+ \rightarrow K^+\pi^0(K_L^0)$

One of the charged tracks (track 1) is observed to kink 5246 ± 40 μm from the primary vertex with kink angle θ_k = 0.103 rad, and ΔP_k = 550 ± 16 MeV/c. Acceptable 0-C solutions exist for the following decay hypotheses:

Decay Mode	$(E_{cal}-E_{K_L^0})/\sigma(E_{cal})$
$D^+ \rightarrow \pi^+(K_L^0)$	3.4
$F^+ \rightarrow K^+(K_L^0)$	0.0
$D^+ \rightarrow \pi^+\pi^0(K_L^0)$	0.0
$F^+ \rightarrow K^+\pi^0(K_L^0)$	2.2

In each case, the high solution is favored by the observed excess energy in the calorimeter E_{cal} = 28 ± 5 GeV. The π^0 is reconstructed from the (double) e^+e^- shower of one of the γ's, the other γ is observed in the lead glass. No Vees are observed to decay in the drift chambers, thus no 0-C decay hypotheses for D^+, F^+ or Λ_c^+ decay with K_s^0 or Λ^0 are allowed. No K* solutions exist for the above allowed D^+ solutions, as the Pmax = 456 MeV/c associated with such decays is less than the observed ΔP_k. K* solutions are allowed for F^+ decay, as Pmax = 726 MeV/c. As the decay time is quite long, this event is most consistent with D^+ decay.

EVENT 547-3192 $F^+ \rightarrow \pi^+\pi^-\pi^+(\pi^0)$

Unfortunately, two out of the three decay tracks interact in the emulsion before exiting the module. Kinematical analysis of this event, from the information available from the emulsion and spectrometer allow only an all-pion decay hypothesis for a F^+ meson decay. The minimum masses for Cabibbo-favored decays of D^+ mesons, Λ_c^+ baryons are well over two standard deviations above their respective masses. Note that the decay time for the F^+ decay hypothesis is compatible with the mean F^+ lifetime. Although only one acceptable decay hypothesis exists for this event, the uncertainty associated with the assumptions used in the reconstruction of the two decay tracks which interact in the emulsion prohibits elevation of this event to the unambiguous charm candidate category.

EVENT 563-5269 $D^+ \to \pi^+(K_L^0)$, $F^+ \to K^+(K_L^0)$, $\Lambda_c^+ \to p(K_L^0)$

Track 2 is observed to kink 6600 ± 50 μm from the primary vertex, with kink angle $\theta_k = 0.353$ rad, $\Delta P_k = 318 \pm 100$ MeV/c. Excess energy is observed in the calorimeter, $E_{cal} = 35 \pm 6$ GeV with evidence for two separate showers, from the structure of the energy deposition in the 5 calorimeter planes in rows 2 and 3. 0-C solutions exist for the following decay hypotheses. The difference between observed and predicted excess energy in the calorimeter (in S.D.) due to the presence of a K_S^0 is also given.

Decay Mode	$(E_{cal}-E_{K_L^0})/\sigma(E_{cal})$
$D^+ \to \pi^+(K_L^0)$	1.7
$F^+ \to K^+(K_L^0)$	4.2
$\Lambda_c^+ \to p(K_L^0)$	5.2

The D^+ decay hypothesis is the physically favored solution. The D^+ decay hypothesis is also the favored solution on the basis of decay time. Alternate decay modes with more than one missing neutral K_L^0 meson (or neutron) cannot be excluded. No π^0 or vees are observed in the spectrometer. Although this event strongly favors a D^+ hypothesis, it is not a unique interpretation of this event. The majority of the energy of the decay is carried away by a neutral particle, and is observed only in the calorimeter. Furthermore, the nuclear interaction background for this event is non-neglible (i.e. ~0.5 events), as the decay length is long, and the p-perp is within the domain of nuclear interactions. Hence, conservatism prevents its use in the lifetime determination.

EVENT 656-2631 $D^+ \to \pi^+K^-\pi^+\pi^0$, $F^+ \to K^+K^-\pi^+\pi^0$, $\Lambda_c^+ \to pK^-\pi^+$

This ambiguity in this event revolves solely around the identity of track 3-1, which is too fast for TOF identification, at 11.4 GeV/c. All of the hits in the lead glass are accounted for, in that three π^0 and a single remnant gamma are reconstructed, such that no ambiguity exists in the gamma-gamma mass combinations for the π^0's.

The invariant mass combinations of the charmed particle with the single gamma and π^0 are:

$$M_{D^+\gamma} = 1978 \pm 28 \text{ MeV/c}^2$$

$$M_{D^+\pi^0} = 2070 \pm 33 \text{ MeV/c}^2$$

$$M_{F^+\gamma} = 2135 \pm 27 \text{ MeV/c}^2$$

$$M_{\Lambda_c^+\gamma} = 2383 \pm 24 \text{ MeV/c}^2$$

$$M_{\Lambda_c^+\pi^0} = 2494 \pm 28 \text{ MeV/c}^2$$

As the observed decay time is short, and the parent momentum is high, this event is most compatible with the decay of an F^+ meson, further strengthened by the F^+ candidate. If this event is included in the F^+ sample, the mean lifetime is (for four events):

$$\tau_{F^+} = 1.8 \begin{smallmatrix}+1.3\\-0.6\end{smallmatrix} \times 10^{-13}\text{sec}$$

The weighted F^+ mass is 2052 ± 30 MeV/c^2 . If the E-564 F^+ event is included, the F^+ lifetime is (for five F^+ events):

$$\tau_{F^+} = 1.7 \begin{smallmatrix}+1.0\\-0.6\end{smallmatrix} \times 10^{-13}\text{sec}$$

The weighted F^+ mass is 2031 ± 19 MeV/c^2 . The weighted F^{*+} mass using the two F^+ events with F* candidates is 2135 ± 23 MeV/c^2.

EVENT 665-2113 $D^+ \rightarrow \underline{\pi}^+\underset{\sim}{\pi}^-\underset{\sim}{\pi}^+(\bar{K}^0)$,

$F^+ \rightarrow \underline{\pi}^+\underset{\sim}{\pi}^-\underset{\sim}{\pi}^+(\pi^0)$, $\Lambda_c^+ \rightarrow \underline{\pi}^+\underset{\sim}{\pi}^-\underset{\sim}{\pi}^+(\Lambda^0)$

The charged tracks in this event are all identified as pions, however the identity of the parent is totally ambiguous, as acceptable 0-C fits exist for D^+, F^+ and Λ_c^+ decays. The high momentum solution is excluded in all the decay hypotheses for this event, as no high momentum (8-12 GeV) neutral hadron is observed in the spectrometer. The decay times for each hypothesis are quite short. Therefore this event could have a significant effect on the D^+ lifetime, but little effect on the F^+ or Λ_c^+ lifetimes.

EVENT 665-4023

The decay occurs in the 800 μm thick lucite base of the changeable sheet (outside the fiducial volume for the emulsion target). Thus, as the decay vertex is not observed, the possiblity of a nuclear interaction cannot be ruled out, although the probability of a nuclear interaction is small due to the (reasonably high) parent momentum (> 15 GeV/c). No black tracks are observed to originate from the decay region. In (unfortunate) addition to this, the event is highly D^+, F^+, Λ_c^+ ambiguous due to the lack of TOF identification for any of the charged decay tracks, and the presence of an unobserved neutral particle in the decay. The charged tracks are all known to be hadrons, due to lead glass information. The high momentum 0-C solution is excluded in each case, as no evidence for a high momentum neutral hadron is observed in the spectrometer.

The decay times for each decay hypothesis are quite long in this event, thus, if this event were a F^+ or a Λ_c^+, their lifetimes would be significantly affected. However the probability of observing the decays of an F^+ or Λ_c^+ with the decay times listed in the table, with mean lifetimes as measured with the unambiguous decay candidates is less than 10^{-5} in both cases. The decay time for this event is long relative to the unambiguous D^+ decays, therfore this event can also have a significant impact on the D^+ lifetime.

EVENT 670-12 $\Lambda_c^+ \rightarrow K^+p\pi^-(\pi^0)$

One of the decay tracks from this event is identified as a proton from emulsion measurements. The other positive track is ambiguous between a K^+ and a proton. (Thus this event may be a nuclear interaction, particularly when a Λ^0 to decay in the drift chambers.) If it is assumed that this event is the (doubly-Cabibbo-unfavored) decay of a Λ_c^+, the observed decay time is compatible with the mean Λ_c^+ lifetime as obtained with the unambiguous Λ_c^+ decays. Therefore this event has little impact on the Λ_c^+ lifetime.

EVENT 671-2642

This event has many kinematically acceptable decay hypotheses for D^+, F^+ and Λ_c^+ decay (see Table 14). Note that the decay time for this event is extremely long ($\sim 60 \times 10^{-13}$sec), using the observed charged momenta. The transverse momentum of the daughter tracks with respect to the parent direction are small. Thus, due to this fact and the long path length, the probability of this event originating from a nuclear interaction is non-negligible (~0.5 events). However, it is possible that this event may be the decay of a long-lived charged charmed particle, perhaps related to 635-4949, since the lifetimes are comparable. (e.g. the isodoublet partner to the A^0(csd), the A^+(csu) which is predicted to have a mass of $M_{A^+} = 2500$ MeV/c^2 [170].) If this is indeed true, then the event has no impact on the D^+, F^+ and Λ_c^+ lifetimes. Due to the long observed decay time, this event can have a significant impact on the F^+ and Λ_c^+ lifetimes. The impact on the D^+ lifetime is also significant, although the D^+ lifetime is affected to a lesser extent than for the F^+ or Λ_c^+. (Note that this event is not consistent with the decay of a K^+.)

No excess energy is observed in the calorimeter, and no high momentum vees are observed in the drift chambers. Thus the high momentum solutions in most of the 0-C fits to D^+, F^+ and Λ_c^+ decay hypotheses are excluded.

APPENDIX B.

CHARMED CANDIDATE EVENT SUMMARY SHEETS

The raw data information for the charged charmed decay candidates and the neutral charmed baryon candidate are listed in Table 23. These data summary sheets represent the contents of a disk file generated by the event re-analysis program and subsequently modified by hand as was deemed necessary. The listings follow a fixed format readable by a FORTRAN program. Since this is a printed listing, the first character is a carriage control and thus does not appear. The formats given below are those used to read the disk file and thus contain room for these control characters.

HEADER INFORMATION

1. Run and Record: 4X,I5,7X,I7 format.

2. Institution and Scan Number, NH, NS:
   1X,A3,I5,3X,I3,3X,I3 format.

3. Last Revision Date, Yr., Mo., Day:
   15X,I2,1X,I2,1X,I2 format.

VERTEX INFORMATION

Vertices are classified into two types.
Type 1 vertices are those determined by the computer event reconstruction programs and are measured in inches.
Type 2 vertices are from decays of charmed particles, nuclear interactions, etc. as observed and measured in the emulsion; distances relative to the primary vertex are listed in microns.

1. Number of Vertices: 1X,I3 format.

2. Description Line: 1X format.

3. Vertex Number, Vertex Type, Vertex Position in X, Y, and Z
   Type 1: 1X,I4,I6,1X,3F8.3 format.
   Type 2: 1X,I4,I6,1X,3F8.1 format.

ENERGY INFORMATION

1. Total Calorimeter Energy: 28X,F7.2 format.

2. Calorimeter Energy in Columns 1,2,3,4: 1x,4F7.2 format.

3. Total Lead Glass Energy: 27X,F7.2 format.

EMULSION INFORMATION

The emulsion information section contains information on tracks observed in the emulsion and/or deduced from decays or interactions in the spectrometer. The organization is as follows:

1. Number of "Emulsion" Tracks: 1X,I3 format.

2. Header Line 1: 1X format.

3. Header Line 2: 1X format.

For each track the following information is given:

1. Track identifier, track slopes in X and Y, emulsion exit slopes, specific ionization, $1/P\beta$ as measured in the emulsion, vertex at which the track ends. 1X,A7,4F7.3,F7.2,F9.3,I3 format.

2. The second line contains the error associated with each parameter above it in the same format. 1X,7X,4F7.3,F7.2,F9.3,I3 format.

The track identifier obeys the following conventions (m and n are integers):

1. nTrack n from the primary vertex.

2. n-m Charged decay track m from track n.

3. 0V Neutral Decaying Particle.

4. V-m Charged track m from neutral decay.

5. In-m Charged track m from interaction of track n.

6. 0I Neutral Interacting Particle.

7. U-m Unmatched track m.

8. En-m Electron m from pair conversion n.

9. G-m Gamma m from lead glass block.

10. L-m Lambda decay track m.

11. K^-m Kaon decay track m.

SPECTROMETER INFORMATION

1. Total Number of Tracks: 1X,I2 format.

2. Header Line: 1X format.

For each track the following information is given in:

1X,A7,3F7.3,3I3,F6.3,1x,O6,F6.2,F6.3,I2,2F6.3,I2 format.

TRACK	Track identifier.
DX/DZ	X slope.
DY/DZ	Y slope.
1/P	1/momentum as measured by the spectrometer or 1/momentum as fitted by decay fitting program for daughter particles or 1/block energy for gammas.
Q	Particle charge.
UP	Number of upstream drift chamber hits used
DN	Number of downstream drift chamber hits used or associated lead glass block for gammas.
CHISQ	Chi-squared for fitted track or Chi-squared of 3-C fit for decaying tracks.
ID	Octal formatted binary code for possible particle types. Assignments are:

1.	000001	Gamma
2.	000002	Electron
3.	000004	Muon
4.	000010	Pion
5.	000020	Kaon
6.	000040	Eta
7.	000100	Proton
8.	000200	Lambda
9.	000400	Sigma
10.	010000	D

11. 020000 F^+

12. 040000 Lambda-c

EPBG	Lead glass energy associated with track
BETA	1-β from TOF
V	Vertex at which track begins
XMISS	Amount by which track misses vertex 1 in X
YMISS	Amount by which track misses vertex 1 in Y
F	Fit flag = 1/0 if track is used to fit decay vertex

AUXILLIARY INFORMATION

No present use at this time. Reserved for future information.

COMMENTS

General comments on event.

APPENDIX C.

SUMMARY OF KINEMATIC FITS OF π^0 OBSERVED IN CHARMED PARTICLE DECAYS

The results of 1-C kinematic fits to π^0 decays for π^0 observed in the decays of charmed particles, and for associated π^0's produced in neutrino interactions in which charmed particles were produced are summarized in the following table:

TABLE 19

SUMMARY OF π^0 KINEMATIC FITS

EVENT NUMBER	MASS MEV/C	1-C FITS χ^2	C.L.	ITER
512-5761	129±21	0.08	0.77	2
513-8010	126±21	0.17	0.68	2
518-4935	215±75	1.16	0.28	2
527-3682	141±49	0.02	0.89	1
533-7152	147±6	0.03	0.85	1
547-2197	166±24	1.94	0.16	2
556-152	185±47	1.31	0.25	3
598-1759	122±19	0.42	0.52	2
638-5640	122±27	0.20	0.65	3
638-9417	134±24	0.02	0.96	2
656-2631	125±22	0.17	0.68	2
661-2729	80±22	4.62	0.03	4
Other (clean) π^0:				
512-5761	178±29	2.66	0.10	3
521-5901	111±11	4.16	0.04	2
546-1339	130±27	0.03	0.86	2
556-152	151±24	0.49	0.49	2
638-5640	131±22	0.04	0.85	2
638-5640	135±17	0.01	0.98	1
638-9417	134±30	0.00	0.97	1
656-2631	117±40	0.20	0.66	2
656-2631	147 29	0.18	0.67	2

The mean value for π^0 mass is obtained in a similar manner as that for charmed particles, the mean χ^2 and C.L. are:

$$\langle M_{\pi^0}\rangle = 134.6 \pm 7.3 \text{ MeV/c}^2$$
$$\langle \chi^2\rangle = 1.05 \pm 1.42$$
$$\langle \text{C.L.}\rangle = 0.52 \pm 0.34$$

Inclusion of the clean π^0 not used in the charm decay, but observed in the event has little effect:

$$\langle M_{\pi^0}\rangle = 134.8 \pm 5.9 \text{ MeV/c}^2$$
$$\langle \chi^2\rangle = 0.75 \pm 1.23$$
$$\langle \text{C.L.}\rangle = 0.60 \pm 0.32$$

APPENDIX D.

SUMMARY OF Λ^0 and K^0_S FITS OBSERVED IN CHARMED EVENTS

The results of 1-C kinematic fits to Λ^0 and K^0_S observed in the decays of charmed particles, or observed in neutrino interactions where a charmed particle is produced is summarized in the table below.

TABLE 20

SUMMARY OF Λ^0 AND K^0_S FITS

EVENT NUMBER	MASS MEV/C	1-C FITS χ^2	C.L.	ITER
K^0_S's:				
661-2729	504±7	0.69	0.41	2
Λ^0's:				
498-4985	1116±37	0.00	0.99	1
502-354	1094±10	0.19	0.67	2
610-4088	1191±27	0.39	0.53	2
650-6003	1187±55	5.57	0.02	4
670-12	1119±4	0.82	0.37	2

The (weighted) value for the Λ^0 mass is:

$$M_{\Lambda^0} = 1116.9 \pm 3.5 \text{ MeV/c}^2$$

MEASUREMENT OF THE LIFETIMES OF D^+, F^+ + Λ_c^+

PH.D. THESIS: STEVE ERREDE.

ERRATA

Please make the following corrections:

Page			
31	$7_\nu \rightarrow 7_\nu$		$\left(\int_0^{350} \sigma(E_\nu) 7_\nu(E_\nu) \delta E_\nu \right.$
73	$\prod_i^{N^0} \epsilon^0 \rightarrow \prod_j^{N^0} \epsilon^0$		(switch $i \rightarrow j$ in second Π)

94 TABLE 16 should be:

FINAL STATE

$^{6}C_{11}$ ←
$^{7}N_{13}$ ←
$^{8}O_{15}$ ←
$^{16}S_{31}$ ←
$^{35}Br_{78}$ ←
$^{47}Ag_{106}$ ←
$^{47}Ag_{108}$ ←
$^{53}I_{126}$ ←

ALL ONE less than for INITIAL STATES

111	$\Gamma(c \rightarrow s\ell^+\nu_\ell) = 1.6 \pm 0.3 \times 10^{11} sec^{-1}$ (ν_ℓ, NOT ν_e)
112	$Br(F^+ \rightarrow \tau\nu_\tau) = 1.4\% \left(^{+1.3}_{-0.6}\right)\%_{exp} \oplus \left(^{+4.3}_{-1.1}\right)\%_{thy}$ (i.e. add in parentheses)
119	$R^F(OZI/STRONG) \simeq R^\phi(OZI/STRONG)$ (i.e. $\simeq$, NOT $=$)
145	MONTE CARLO RESULTS....
146	LAST GROUP OF ΔQ, $\Delta X'$, $\Delta Y'$ is UP-DOWN TRACKS.
213	TOP FIGURE IS (MKII), NOT (E-531).

APPENDIX E.

INVESTIGATION of SYSTEMATIC SHIFTS IN KINEMATIC FITS OF CHARMED PARTICLE DECAYS

An investigation of possible systematic shifts in the measured variables used in the kinematic fitting of charm decays, such as X', Y' and Q (=1/P), was performed to determine whether or not "pulls", or offsets of any statistical significance were present. No such effects were found; the results are summarized in the table(s) below. For each measured varible variable X, ΔX is the average difference in the values and after the kinematic fit, σx is the S.D. on the distribution for ΔX, for 24 events (except for χ^2, C.L. and ITER, which are the average values for the 24 events). The first six variables (χ^2, C.L., ITER, ΔP_x, ΔP_y, ΔP, the transverse momentum balance about the parent direction) in Table 22 are in good agreement with the values obtained from a Monte Carlo program (see Table 21), which mimicked the decays of charmed particles (using the resolution of the experimental apparatus); charmed particle decays were then fit with the same kinematic fitting programs, histogramming the results. For each of the measured variables, the Monte Carlo program had a mean of zero for ΔX and a S.D. consistent with the experimental resolution. Monte Carlo methods were also used to check out the fitting program using dummy decays (for comparison with known results), and to check the error analysis subroutines. In the tables below, the units for ΔP_x, ΔP_y, ΔP are GeV,

the units for ΔQ are 1/(GeV/c); for $\Delta X'$, $\Delta Y'$, the units are mrad.

TABLE 21

MONTE-CARLO RESULTS OF KINEMATIC FITS TO CHARMED PARTICLE DECAYS

ITEM	X_{2C}	σx_{2C}	X_{3C}	σx_{3C}
χ^2	2.00	2.00	3.00	2.46
C.L.	0.50	0.29	0.50	0.29
ITER	2.3	0.6	2.0	0.5
ΔP_x	0	120	0	120
ΔP_y	0	120	0	120
ΔP	137	74	138	74

TABLE 22

INVESTIGATION of SYSTEMATIC SHIFTS IN KINEMATIC FITS

OF CHARMED PARTICLE DECAYS

(24 EVENTS)

	ITEM	X_{2C}	σx_{2C}	X_{3C}	σx_{3C}
	χ^2	2.04	2.25	2.69	2.72
	C.L.	0.53	0.34	0.57	0.32
	ITER.	2.9	1.1	2.5	1.4
	ΔP_x	-13	110	-13	111
	ΔP_y	-28	119	-28	119
	ΔP	137	91	138	92
CHARM SLOPES	$\Delta X'$	1.0	10.7	0.6	11.1
	$\Delta Y'$	0.29	4.40	-0.07	8.10
ALL DECAY TRACKS	ΔQ	-0.003	0.124	0.003	0.135
	$\Delta X'$	-0.28	2.50	-0.06	2.70
	$\Delta Y'$	-0.47	3.20	-0.35	3.40
UP-ONLY TRACKS	ΔQ	0.06	0.20	-0.00	0.27
	$\Delta X'$	0.20	0.51	0.10	0.45
	$\Delta Y'$	0.00	0.01	-0.20	0.40
π^0's IN DECAYS	ΔQ	-0.009	0.017	-0.010	0.023
	$\Delta X'$	-1.2	5.3	-1.3	5.6
	$\Delta Y'$	-0.4	3.4	-0.3	4.9
EMULSION TRACKS	ΔQ	0.0001	0.0006	0.0001	0.0010
	$\Delta X'$	-0.2	1.0	-0.2	1.0
	$\Delta Y'$	-0.0	0.5	-0.0	0.5
UP-DOWN TRACKS	ΔQ	-0.01	0.35	0.09	0.35
	$\Delta X'$	-0.00	0.46	-0.00	0.46
	$\Delta Y'$	0.00	0.26	0.00	0.26

LIST OF REFERENCES

1. C.H.Llewellyn-Smith, "Topics in Quantum Chromodynamics", in Quantum Flavordynamics, Quantum Chromodynamics and Unified Theories, edited by K.T.Mahanthappa and James Randa, Nato Advanced Study Institutes Series, (Series B Physics) p.59,60,76-86, 1980.
   and
   O.W.Greenberg, C.A.Nelson, Physics Reports, 32C , (1977), 93-94.
   and
   J.S.Bell, R.Jackiw, Nuovo Cimento 61 , (1969), 47.
   and
   S.l.Adler, Phys.Rev. 177 , (1969), 2426.
   and
   S.M.Bilenky, "Introduction to Feynman Diagrams", (Oxford, Pergammon Press, 1974), P.163-166.

2. R.L.Glasser, N.Seeman, and B.Stiller, Phys.Rev. 123 (1961), 1014.

3. H.Schwe, F.M.Smith, and W.H.Barkas, Phys.Rev. 136 (1964), 1839.

4. M.Gell-Mann and A.Pais, Phys.Rev. 97 (1955), 1387.

5. K.Lande, E.T.Booth, J.Impeduglia, L.M.Lederman and W.Chinowsky, Phys.Rev. 103 (1956), 1901.
   ibid., Phys.Rev. 105 (1957), 1925.

6. T.D.Lee and C.N.Yang, Phys.Rev. 104 , (1956), 254.

7. C.S.Wu, E.Ambler, R.W.Hayward, D.D.Hoppes and R.P.Hudson, Phys.Rev. 105 , (1957), 1413.

8. J.H.Christenson, J.W.Cronin, V.L.Fitch, and R.Turlay, Phys.Rev.Lett. 13 , (1964) 138.

9. A.Abashian, R.J.Abrams, D.W.Carpenter, G.P.Fisher, B.M.K.Nefkens, J.H.Smith, Phys.Rev.Lett. 13 , (1964), 243.

10. A.Pais and O.Piccioni, Phys.Rev. 100 , (1955) 1487.

11. N.Cabibbo, Phys.Rev.Lett. 10 , (1963), 531.

12. B.Pontecorvo, JETP 33 , (1957), 549.

13. Z.Maki, M.Nakagawa and S.Sakata, Prog.Theor.Phys. 28 (1962), 247.

14. B.Pontecorvo, JETP 53 , (1967), 1717.

15. B.Pontecorvo, JETP 26 , (1968), 984.

16. V.Gribov and B.Pontecorvo, Phys.Lett. 28B , (1969), 493.

17. G.Feinberg, M.Goldhaber and B.Steigman, Phys.Rev. D18 , (1979), 1602.

18. R.E.Marshak and R.N.Mohapatra, Phys.Lett. 91B , (1980), 222.

19. R.E.Marshak and R.N.Mohapatra, Phys.Rev.Lett. 44 , (1980), 1316.

20. J.D.Bjorken and S.L.Glashow, Phys.Lett. 11 , (1964), 255.

21. M.K.Gaillard, B.W.Lee and J.L.Rosner, Rev.Mod.Phys. 47 , (1975), 277.

22. S.L.Glashow, Nucl.Phys. 22 , (1964), 579.

23. S.Weinberg, Phys.Rev.Lett. 19 (1967), 1264.

24. A.Salam, in "Elementary Particle Theory: Relativistic Groups and Analyticity (Nobel Symposium no.8), edited by N.Svartholm, (Almquist and Wiksell, Stockholm, 1968), 367.

25. S.L.Glashow, J.Iliopoulos, L.Maiani, Phys.Rev. D2 (1970), 1285.

26. S.H.Aronson et al., Phys.Rev.Lett. 25 (1970), 1057.

27. W.C.Carithers et al., Phys.Rev.Lett. 30 , (1973), 1336.
ibid., 31 , (1973), 1025.

28. Y.Fukushima et al., Phys.Rev.Lett. 36 , (1976), 348.

29. G.D.Cable, R.H.Hildebrand, C.Y.Pang and R.Steining, Phys.Rev. D8 , (1973), 3807.

30. H.I.Vainhstein, I.B.Kriplovich, JETP 18 (1973), 141.

31. E.Ma, Phys.Rev. D9 , (1974), 1303.

32. A.Gavrielides, Ph.D.Thesis, University of Minnesota, 1974, (unpublished).

33. S.Adler, 1974 (unpublished).

34. S.Joglekar, 1974.

35. M.K.Gaillard, B.W.Lee, Phys.Rev. D10 , (1974), 897.

36. G.Altarelli, N.Cabibbo and L.Maiani, Phys.Rev.Lett. 35 , (1975), 635.

37. M.Einhorn, Academic Lecture Series, FNAL 75/1, (1975).

38. J.L.Rosner, Institute For Advanced Study, Princeton Preprint C00-2220-102, (1977), 26.
and
Orbis Scientiae, Deeper Pathways in High Energy Physics, edited by A.Perlmutter and L.F.Scott, (Plenum, New York, 1977), P.489.

39. J.L.Rosner, Bartol Conference, University of Delaware, (1978), 297.

40. N.Cabibbo and L.Maiani, Phys.Rev.Lett. 35 , (1978), 109.

41. T.Hayashi, M.Nakagawa, H.Nitto and S.Ogawa, Prog.Theor.Phys. 49 , (1973), 350.
ibid., 52 , (1974), 636.

T.Hayashi et al., Prog.Theor.Phys. 55 , (1976), 968.

42. M.Einhorn, C.Quigg, Phys.Rev. D12 , (1975), 2015.

43. G.Altarelli, N.Cabibbo and L.Maiani, Nucl.Phys. B88 (1975), 285

44. R.L.Kingsley, S.B.Tremain, F.Wilczek and A.Zee, Phys.Rev. D11 , (1975), 1919.

45. K.Niu, E.Mikumo, Y.Maeda, Prog.Theor.Phys. 46 , (1971), 1644.

46. T.Hayashi et al., Prog.Theor.Phys. 47 , (1972), 280.

47. K.Hoshino et al., in "Proceedings of the Fourteenth International Conference on Cosmic Rays, Munich, W.Germany, 1975. (Max Planck Institute fur Extraterestrische Physik,Garching, W.Germany, 7 (1975), p.2442.

48. K.Niu, in "Proceedings of the Nineteenth International Conference on High Energy Physics", Tokyo, Japan, 1978. (Physical Society of Japan, Tokyo, (1979), 447.)

49. M.Kaplon, B.Peters and D.Ritson, Phys.Rev. 85 , (1952), 900.

50. K.Nishikawa, Jour.Phys.Soc.Japan, 14 , (1959), 880.

51. Kuramata et al., in "Proceedings of Thirteenth International Cosmic Ray Conference", Denver, 3 , (1973), 2239.

52. S.Kuramata, in "Compilation of X-Particles (Short-Lived Particles Observed by Emulsion Techniques)", Summer Study on Weak Interactions, Aichi University of Education, Japan, Sept. 1977, (unpublished).

53. J.J.Aubert et al., Phys.Rev.Lett. 33 , (1974), 1404.

54. J-E.Augustin et al., Phys.Rev.Lett. 33 , (1974), 1046.

55. G.Goldhaber et al., Phys.Rev.Lett. 37 , (1976), 225.

56. I.Peruzzi et al., Phys.Rev.Lett., 37 , (1976), 569.

57. J.E.Wiss et al., Phys.Rev.Lett., 37 , (1976), 1531.

58. G.Feldman et al., Phys.Rev.Lett., 38 , (1977), 1313.

59. E.H.S.Burhop et al., Phys.Lett. 65B , (1976), 299.

60. A.A.Komer et al., JETP Lett. 28 , (1978), 453.

61. N.Ushida et al., Lett.Nuovo Cimento, 23 , (1978), L 577.

62. H.Fuchi et al., Phys.Lett. 85B , (1979), 135.

63. H.Fuchi et al., Nagoya University Preprint DPNU-42-80, (1980), (Submitted to Lett.Nuovo Cimento).

64. C.Angelini et al., Phys.Lett. 80B , (1979), 428.

65. C Angelini et al., Phys.Lett. 84B , (1979), 150.

66. D Allasia et al., Phys.Lett. 87B , (1979), 287.

67. M.I.Adamovich et al., Phys.Lett. 89B , (1980), 427.

68. M.I.Adamovich et al., Phys.Lett. 99B , (1981), 271.

69. A.Conti et al., Contributed paper to "International Symposium on Lepton-Photon Interactions at High Energies, (Fermilab, Illinois, 1979.)

70. M.I.Adamovich et al., in "Proceedings of the Twentieth International Conference on High Energy Physics", (Madison, Wisconsin, 1980.)

71. H.Deden et al., Phys.Lett., 58B , (1975), 361.

72. J.Blietschau et al., Phys.Lett., 60B , (1976), 207.

73. E.G.Cazzoli et al., Phys.Rev.Lett., 34 , (1975), 1125.

74. W.Braunschweig et al., Phys.Lett. 63B , (1976), 471.

75. J.von Krogh et al., Phys.Rev.Lett. 36 , (1976), 710.

76. H.Deden et al., Phys.Lett., 67B , (1977), 474.

77. P.Bosetti et al., Phys.Rev.Lett., 38 , (1977), 1248.

78. P.Bosetti et al., Phys.Lett., 73B , (1978), 380.

79. C.Baltay et al., Phys.Rev.Lett., 38 , (1977), 1248.

80. C.Baltay et al., Phys.Rev.Lett., 39 , (1977), 62.

81. C.Baltay et al., Phys.Rev.Lett., 41 , (1978), 73.

82. C.Baltay et al., Phys.Rev.Lett., 42 , (1979), 1721.

83. A.M.Cnops et al., Phys.Rev.Lett., 42 , (1979), 197.

84. J.Blietschau et al., Phys.Lett., 86B , (1979), 108.
ibid., 99B , (1981), 159.

85. G.S.Abrams et al., Phys.Rev.Lett., 44 , (1980), 10.

86. B.Knapp et al., Phys.Rev.Lett. 37 , (1976), 882.

87. M.S.Atiya et al., Phys.Rev.Lett. 43 , (1979), 414.

88. M.C.Goodman et al., Phys.Rev. D22 , (1980), 537.

89. P.Avery et al., Phys.Rev.Lett., 44 , (1980), 1309.
and
P.Avery, Ph.D. thesis, University of Illinois, 1980, (unpublished).

J.J.Russell et al., Phys.Rev.Lett., 46 , (1981), 799.
and
J.J.Russell, Ph.D. thesis, University of Illinois, 1981, (unpublished).

90. D.Aston et al., Phys.Lett. 94B , (1980), 113.
ibid., 100B , (1981), 91.
and
D.Aston et al., CERN preprint EP/81-41, (1981), submitted to Nucl.Phys.B.

91. R.Brandelik et al., Phys.Lett. 70B , (1977), 132.
ibid., 80B , (1979), 412.

92. K.Giboni et al., Phys.Lett. 85B , (1979), 437.

93. W.Lockman et al., Phys.Lett. 85B , (1979), 443.

94. D.Drijard et al., Phys.Lett., 85B , (1979), 452.

95. A.Kernan, in the "1979 International Symposium on Lepton Photon Interactions at High Energies", (Fermilab, Illinois, 1979), p.535.

96. J.Sandweiss et al., Phys.Rev.Lett., 44 , (1980), 1104.

97. D.S.Baranov et al., Phys.Lett., 70B , (1977), 269.

98. H.C.Ballagh et al., LBL-Fermilab-Hawaii-Washington-Wisconsin Collaboration Preprint UH-511-351-79 (1979), (unpublished).

99. D.D.Reeder, in the "Proceedings of the 1979 International Symposium On Lepton and Photon Interactions at High Energies" (Fermilab, Illinois, 1979), p.553.

100. A.M.Cnops et al., Brookhaven-Columbia-Collaboration preprint BNL-26309 (1979), (unpublished).

101. A.Benvenuti et al., Phys.Rev.Lett. 34 , (1975), 419.

102. A.Benvenuti et al., Phys.Rev.Lett. 35 , (1975), 1199.

103. A.Benvenuti et al., Phys.Rev.Lett. 35 , (1975), 1203.
ibid., 35 , (1975), 1249.

104. B.C.Barish et al., Phys.Rev.Lett. 36 , (1976), 939.

105. B.C.Barish et al., Phys.Rev.Lett. 39 , (1977), 981.

106. A.Benvenuti et al., Phys.Rev.Lett. 41 , (1978), 1204.

107. P.C.Bosetti et al., Phys.Lett. 73B , (1978), 380.

108.O.Erriquez et al., Phys.Lett. 77B , (1979), 227.

109.L.Voyvodic, in "Proceedings of the 1979 International Symposium on Lepton-Photon Interactions at High Energies", Fermilab, Illinois, 1979.

110.N.W.Reay, in "Proceedings of the Twentieth International Cosmic Ray Conference", Kyoto, Japan, 1979, (unpublished).
and
N.W.Reay, in "Particles and Fields - 1979", AIP Conference Proceedings 59 , (Am.Inst.Phys., New York, 1980), p.77.

111.J.D.Prentice, in the "Proceedings of the International Symposium on Lepton and Photon Interactions", (Fermilab, Illinois, 1979), p.563.

112.J.D.Prentice, in the "Proceedings of Baryon Spectroscopy Conference", (Toronto, Ontario, Canada, 1980).

113.K.Niu, in the "Proceedings of the Twentieth International Conference on High Energy Physics, (Madison, Wisconsin, 1980).

114.R.Ammar et al., Phys.Lett. 94B , (1980), 118.

115.N.Ushida et al., Phys.Rev.Lett. 45 , (1980), 1049.

116.N.Ushida et al., Phys.Rev.Lett. 45 , (1980), 1053.

117.F.Nezrick, FNAL TM-555, (1975).

118.S.Mori, FNAL TM-888, (1979).
and
J.Grimson and S.Mori, FNAL TM-824, (1978).

119.J.Hanlon, private communication. We are grateful to him for kindly providing us with data from E-545 concerning the neutrino event rate at the 15' B.C. for the 350 GeV horn-focussed wide-band neutrino beam.

120.D.Bailey, Ph.D. Thesis, McGill University, 1982, (unpublished).

121.D.Pitman, Ph.D. Thesis, University of Toronto, 1982, (unpublished).
and
D.Pitman, M.Sc. Thesis, University of Toronto, 1979, (unpublished).

122.T.Hara,Ph.D Thesis,Kobe University,1982,(unpublished).

123.M.Gutzwiller, Ph.D.Thesis, The Ohio State University, 1981, (unpublished).

124.R.M.Egloff, Ph.D.Thesis, University of Toronto, 1979, (unpublished).

125.M.Peshkin, J.L.Rosner, Nucl.Phys. B122 , (1977), 144.

126.A.Bodek, in the "Proceedings of the Calorimeter Workshop, (Fermilab, May, 1975, edited by M.Atac, 1975) p.229.

127.A.Grant, NIM 131 , (1975), 167.

128.C.Baltay, in "Particles and Fields - 1979", (APS/DPF Montreal, edited by B.Margolis and D.G.stairs, AIP Conference Proceedings 59 (American Institute of Physics, New York, 1980), p.25.

129.W.Sippach, "Nevis Drift Chamber TDC System", 1977, (unpublished),
and
W.Sippach, "8-Channel Time Recorder Module for Drift Chamber Readout System", 1977, (unpublished).

130.L.Pape et al., Contributed Paper to the Topical Conference on Neutrino Physics, Oxford, July, 1978
and
Cern preprint EP Phys.78-25.

131.J.W.Chapman et al., Phys.Rev. D14 , (1976), 5.

132.J.P.Berge et al., Phys.Rev. D18 , (1978), 1359.
and
J.P.Berge et al., FNAL.PUB.79/51 (1979).
and
P.H.Stuntebeck et al., Phys.Rev. D9 , (1974), 608.

133.J.P.Berge et al., FNAL.PUB.80/44 (1980).

134.C.F.Powell, P.H.Fowler, D.H.Perkins, The study of Elementary Particles by the Photographic Method" Pergammon Press, 1959.

135.W.H.Barkas, "Nuclear Research Emulsions", Academic Press, New York, London, 1963, p.263-463.

136.W.T.Eadie et al., "Statistical Methods in Experimental Physics", North Holland Publishing Company, New York, p.155.

137.H.Winzeler, Nucl.Phys. 69 , (1965), 661.
and
H.Winzeler et al., Nuovo Cimento 17 , (1960), 8.

138.P.L.Jain et al., Nucl.Phys. 67 , (1965), 641.

139.V.Luth, in the "Proceedings of the 1979 International Symposium on Lepton and Photon Interactions at High Energies", (Fermilab, Illinois, 1979), p.78.

140.J.Kirkby, in the "Proceedings of the 1979 International Symposium on Lepton and Photon Interactions at High Energies", (Fermilab, Illinois, 1979), p.107.

141.J.Dorfan, in "Particles and Fields - 1979", edited by B.Margolis and D.G.Stairs, (AIP, New York, 1980), p.159.

142.R.H.Schindler, Ph.D.Thesis, Stanford University, 1979.

143.R.H.Schindler et al., SLAC-pub-2507, LBL-10905, (1981), submitted to Phys.Rev.D.

144.W.Bacino et al., Phys.Rev.Lett. 45 , (1980), 329.

145.G.Donaldson, private communication. We are grateful to him for kindly providing us with the likelyhood function for the D , D lifetime ratio as obtained from the DELCO data.

146.X.Y.Pham, Phys.Rev.Lett. 45 , (1980), 1663.

147.I.I.Bigi, Institute fur Theoretische Phyisk der RWTH, Aachen, Frankfurt,Germany preprint, 1981.

148.C.R.C. Handbook of Chemistry and Physics, 52 Ed. C.R.C., (1972), B-245, and references therein.

149.M.Abramowitz, I.A.Stegun, Handbook of Mathematical Functions, NBS Applied Mathematics Series 55, (1970), 295.

150.S.J.Barish et al., Phys.Lett. 66B , (1977), 291.
and
W.Lerche et al., Nucl.Phys. B142 , (1978), 65.
and
J.Hanlon et al., Phys.Rev.Lett. 45 , (1980), 1817.
and
N.Armenise et al., Phys.Lett. 102B , (1981), 374.

151. H.J.Lipkin, ANL preprint ANL-HEP-PR-81-11, (1981).
and
J.Franklin, D.B.Lichtenberg, W.Namgung and D.Carydas, Indiana University preprint IUHET-64, (1981).

152. D.P.Stanley and D.Robson, Phys.Rev.Lett. 45 , (1980), 235.
and
X.Yicheng, Institute fur Theoretische Physic, University of Heidelberg, W.Germany preprint HD-THEP-81-12, (1981).
and
I.Bediaga, E.Predazzi and A.F.S. Santoro, CERN preprint REF.TH.3104-CERN, (1981).

153. J.Ellis, M.K.Gaillard, D.V.Nanopoulos and P.Sikivie, CERN preprint TH-2938, (1980).

154. E.Farhi and L.Susskind, CERN preprint TH-2975, (1980).

155. G.R.Farrar, DoE Research and Development Report CalTech 68-681, (1978).
and
P.Fayet, DoE Research and Development Report CalTech 68-692, (1978).
and
P.Fayet, Paris LPTENS preprint 81/9, (1981).

156. N.Cabibbo, G.R.Farrar and L.Maiani, Univ.Rome preprint RU-81-33, (1981).

157. S.Dimopoulos, S.Raby, F.Wilczek, Santa Barbara preprint NSF-ITP-81-31, (1981).
and
E.Golowich and E.Hagg, NSF-ITP Santa Barbara preprint NSF-ITP-81-39, (1981).

158. D.A.Ross and M.Veltman, Nucl.Phys. B45 135, (1975).

159. D.R.T.Jones, G.L.Kane and J.P.Leveille, University of Michigan preprint UM-HE-81-45, (1981).
and
A.I.Vainshtein, V.I.Zakharov and M.A.Shifman, Sov.Phys.Usp. 23(8) , (1980), 429.

160. Particle Data Group, Rev.Mod.Physics 52 , (1980).

161. E.J.Moniz et al., Phys.Rev.Lett. 26 , (1971), 445.

162. A.Firestone et al., Phys.Rev.Lett. 16 , (1966), 556.

163. A.D.Brody et al., Phys.Rev.Lett. 26 , (1971), 1050.

164.G.W.Brandenburg et al., Phys.Rev. D9 , (1974), 1939.

165.G.W.Brandenburg et al., Nucl.Phys. B45 , (1972), 397.

166.G.W.Brandenburg et al., Phys.Rev.Lett. 28 , (1972), 932.

167.J.N.Carney et al., Nucl.Phys. B107 , (1976), 381.

168.N.A.McCubbin and L.Lyons, Nucl.Phys. B86 , (1975), 13.

169.S.L.Baker et al., Nucl.Phys. B99 , (1975), 211.

170.B.W.Lee, C.Quigg, J.L.Rosner, Phys.Rev. D15 , (1977), 157.

171.A.DeRujula, H.Georgi, S.L.Glashow, Phys.Rev. D12 , (1975), 147.

172.L.A.Copley, N.Isgur and G.Karl, Phys.Rev. D20 , (1979), 768.

173.K.Maltman and N.Isgur, Phys.Rev. D22 , (1980), 1701.

174.C.Avilez, T.Kobayashi, J.G.Korner, Phys.Rev. D17 , (1978), 709.

175.J.G.Korner, G.Kramer, J.Willrodt, Z.Phys.C, Part. and Fields, (1979), 117.

176.V.Barger, J.P.Leveille,P.M.Stevenson, Phys.Rev.Lett. 44 , (1980), 226.

177.J.G.Korner, G.Kramer, J.Willrodt, Phys.Lett. 78B , (1978), 492.
ibid., (erratum), 81B , (1979), 419.

178.R.L.Kingsley, S.B.Treiman, F.A.Wilczek and A.Zee, Phys.Rev. D12 , (1975), 106.

179.H.J.Lipkin, in the "Proceedings of Baryon Spectroscopy Conference" (Toronto, Ontario, 1980), p.10.

180.H.J.Lipkin, Phys.Lett. 70B , (1977), 113.

181.H.J.Lipkin, ANL preprint CP-80-71, (1980),

182.N.Isgur and H.J.Lipkin, Phys.Lett. 99B , (1981), 151.

183.Berthold Stech, Phys.Rev.Lett. 38 , (1977), 304.

184.C.Quigg and J.L.Rosner, Phys.Rev. D17 , (1978), 239.

185.M.K.Gaillard, and B.W.Lee, Phys.Rev.Lett. 33 , (1974), 108.

186.M.K.Gaillard, in the "Proceedings of the 1979 International Symposium on Lepton and Photon Interactions at High Energies", (Fermilab, Illinois, 1979), p.397.
and
M.K.Gaillard, "Weak Decays of Heavy Quarks" FNAL pub. 78/64 Thy, (1978) (See also 1978 SLAC Summer School Notes).

187.M.Kobayashi, K.Maskawa, Prog.Theor.Phys. 49 , (1973), 652.

188.R.E.Schrock and L.L.Wang, Phys.Rev.Lett. 41 , (1978), 1692.

189.R.E.Schrock, S.B.Treiman and L.L.Wang, Phys.Rev. D19 , (1979), 2148.

and
R.E.Schrock, M.B.Voloshin, Phys.Lett. 87B , (1979), 375.
and
V.Barger, W.F.Long and S.Pakvasa, Phys.Rev.Lett. 42 , (1979), 1585.
and
R.E.Schrock, S.B.Treiman and L.L.Wang, Phys.Rev.Lett. 42 , (1979), 1589.

190.V.Barger and S.Pakvasa, Phys.Rev.Lett. 43 , (1979), 812.
and
M.Suzuki, Phys.Rev.Lett. 43 , (1979), 818.
and
M.Suzuki, Phys.Lett. 85B , (1979), 91.

191.L.L.Wang, BNL preprint 28280 (1980).

192.S.Pakvasa, S.F.Tuan, J.J.Sakurai, Phys.Rev. D23 , (1981), 2799.

193.N.Cabibbo and L.Maiani, Phys.Lett. 79B , (1978), 109.

194.N.Cabibbo, G.Corbo and L.Maiani, Nucl.Phys. B155 , (1979), 93.

195.M.Suzuki, Nucl.Phys. B145 , (1978), 420.

196.G.Altarelli, N.Cabibbo and L.Maiani, Nucl.Phys. B88 , (1975), 285.

197.B.Guberina, R.D.Peccei, R.Ruckl, Max Planck Institute fur Physik und Astrophysik, Munich Preprint MPI-PAE/PTH 56/79 (1979),
and
ibid., Preprint MPI-PAE/PTH 56/79 (1979).

198.G.Altarelli, G.Curci, G.Martinelli and S.Petrarcha, Phys.Lett. 99B , (1981), 141.

199.J.Ellis, M.K.Gaillard and D.V.Nanopoulos, Nucl.Phys. B100 , (1975), 313.

200.R.L.Kingsley, S.B.Treiman, F.Wilczek and A.Zee, Phys.Rev. D11 , (1975), 1919.

201.D.Fakirov and B.Stech, Nucl Phys. B133 , (1978), 315.

202.C.Quigg, Z.Phys.C, Particles and Fields, 4 , (1980), 55.

203.J.C.Pati and C.H.Woo, Phys.Rev. D3 , (1971), 2920.

204.S.Wolfram, Caltech preprint CALT-68-790, (1980).

205.J.Ellis, M.K.Gaillard, D.V.Nanopoulos and S.Rudaz, Nucl.Phys. B131 , (1977), 285.

206.M.Suzuki, Univ. of Calif., Berkeley, preprint UCB-PTH-80/4, (1980).

207.G.Ebel Nucl.Phys. B33 , (1971), 317.

208.R.E.Marshak, Riazuddin and C.P.Ryan, "Theory of Weak Interactions in Particle Physics", First ed. Wiley Interscience, New York, (1969), p.446.

209.H.Pietschmann, "Formulae and Results in Weak Interactions", Springer-Verlag, Wien, (1974), p.36.

210.C.Quigg, "Lectures on Charmed Particles", FNAL-78/37, p.47.

211.R.E.Schrock, Institute for Theoretical Physics, State Univ. of New York at Stony Brook preprint ITP-SB-80-56.

212.M.Bander, D.Silverman and A.Soni, Phys.Rev.Lett. 44 (1980), 7.
ibid. (erratum), 44 , (1980), 962.

213. H.Fritzsch and P.Minkowski, Univ. of Bern preprint (1979).

214. V.Barger, J.P.Leveille and P.M.Stevenson, Phys.Rev. D22 , (1980), 693.

215. V.Barger, R.N.Cahn, Y.Kang, J.P.Leveille S.Pakvasa and M.Suzuki, (1979), unpublished.

216. B.Guberina, S.Nussinov, R.D.Peccei and R.Ruckl, Phys.Lett. 89B , (1979), 111.

217. Cern Summer School (Yellow Report), Herceg Novi, (1964), p.92-99.

218. A.I.Vainstein, V.I.Zakharov, M.A.Shifman, JETP Lett. 22 , (1975), 55.

219. M.B.Wise, E.Witten, Phys.Rev. D20 , (1980), 1216.

220. L.F.Abbot, P.Sikivie and M.B.Wise, Phys.Rev. D21 , (1980), 768.

221. N.Ushida et al., "Upper Limits to $\nu_\mu - \nu_\tau$ Oscillation and $\nu_\mu - \tau$ Coupling", submitted to Phys.Rev.Lett., August, 1981.

222. C.Quigg, private communication. We are indebted to him for much help and encouragement given during the preparation of this thesis.

223. H.J.Lipkin, private communication.

224. J.L.Rosner, private communication.

225. S.Ogawa, private communication.

226. S.Sawada, private communication.

227. S.Sawada, Prog.Theor.Phys. 63 , (1980), 572-579. ibid., 55 , (1976), 818-831.

228. M.Matsuda, M.Nakagawa, S.Ogawa, Prog.Theor.Phys. 63 , (1980), 351.
and
M.Matsuda, M.Nakagawa, S.Ogawa, "Quark Number Conservation and New Particle Decays", Meijo University Preprint MCU-DP-042, (1981).

229. I.I.Bigi, L.Stodolsky, SLAC Pub 2410, (1979).

230. E.Ma, S.Pakvasa and W.Simmons, University of Hawaii Preprint UH-511-369-79, (1979).

231. D.G.Hitlin, "Weak Decays of Strange and Heavy Quarks", 1980 SLAC Summer School, (1980), P.67-140.

232. B.Adeva et al., CERN preprint CERN/EP 81-28, submitted to Phys.Lett.B., (1981).

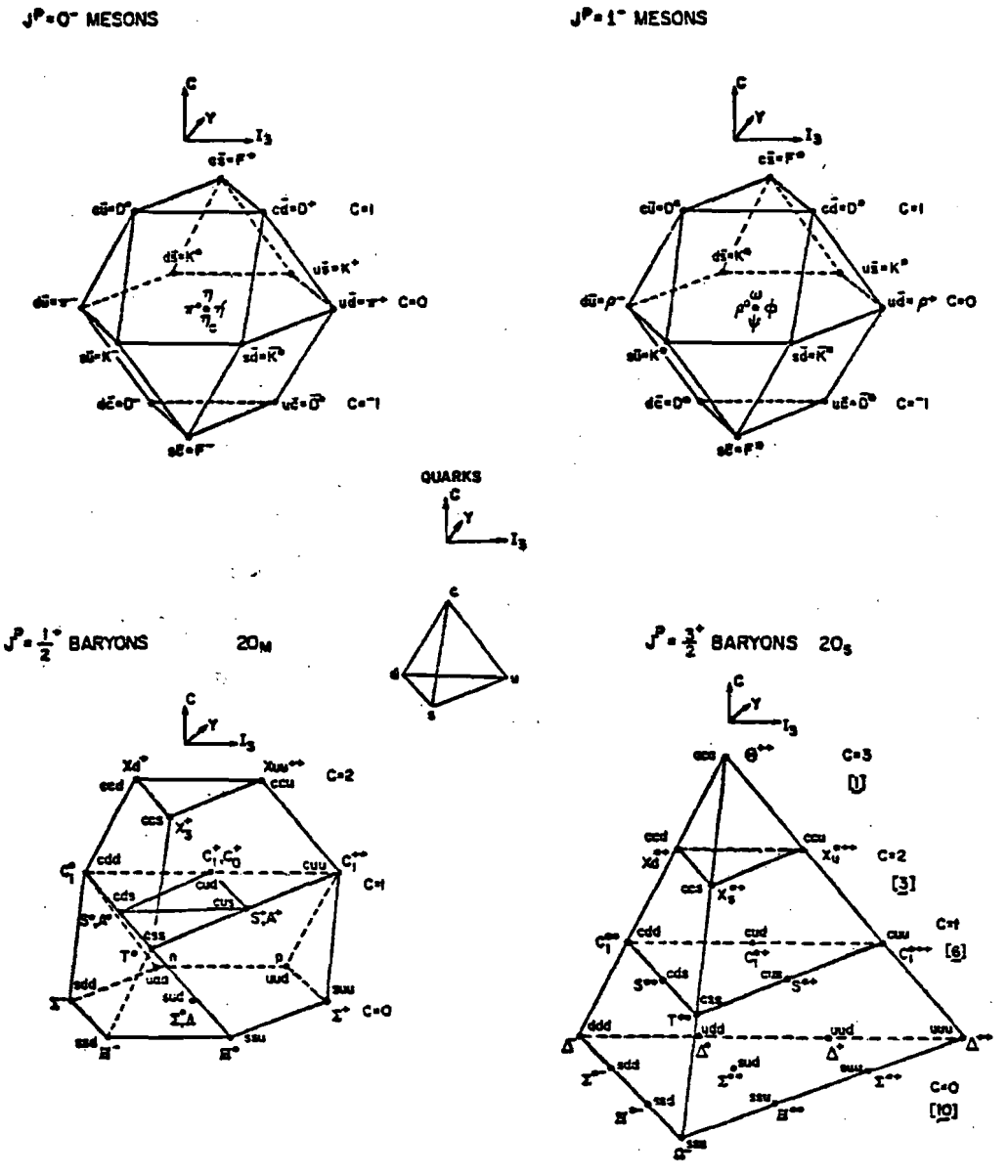

Figure 1. Meson and Baryon SU(4) Multiplets

CHARM PRODUCTION DIAGRAMS

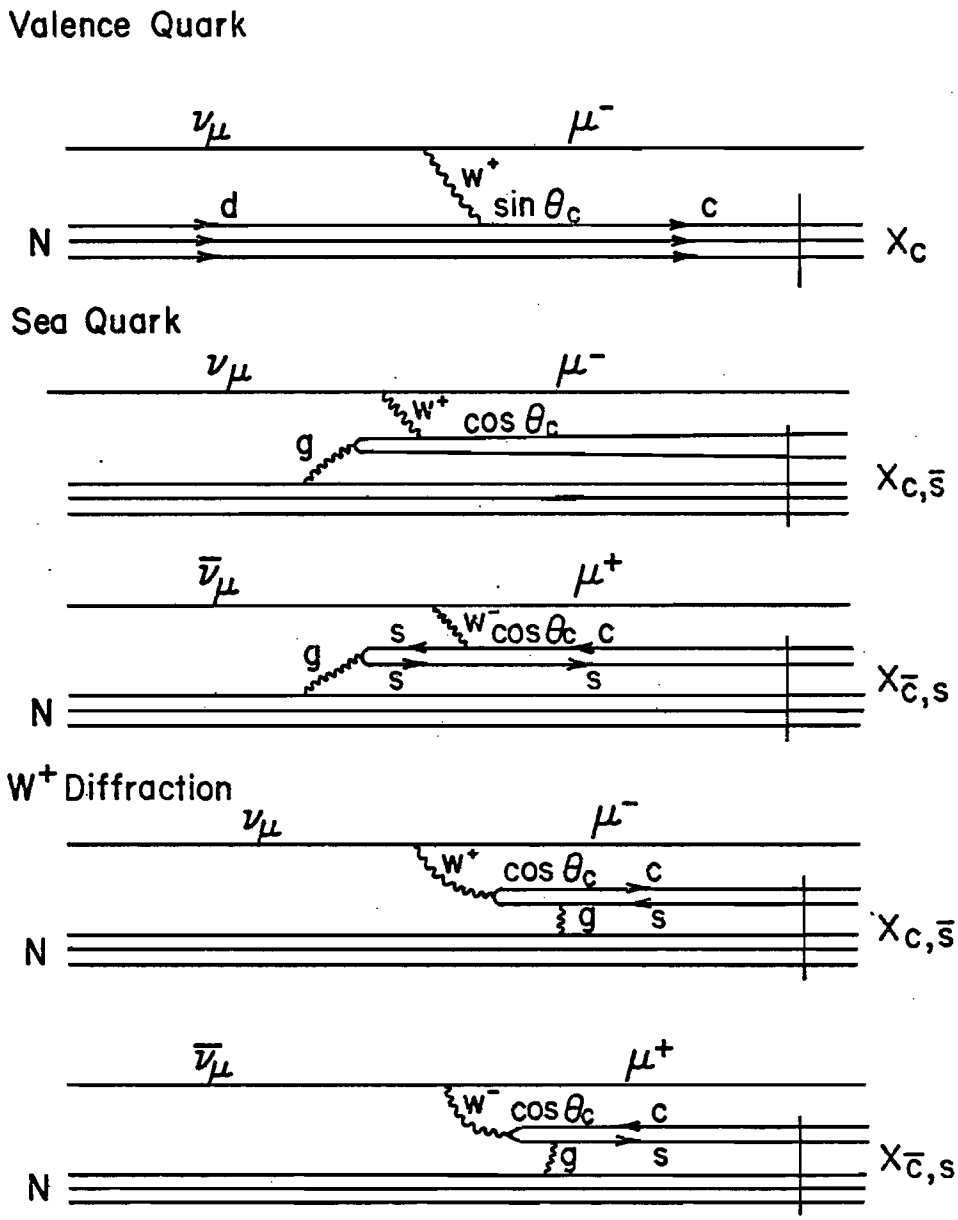

Figure 2. Neutrino Production of Charm

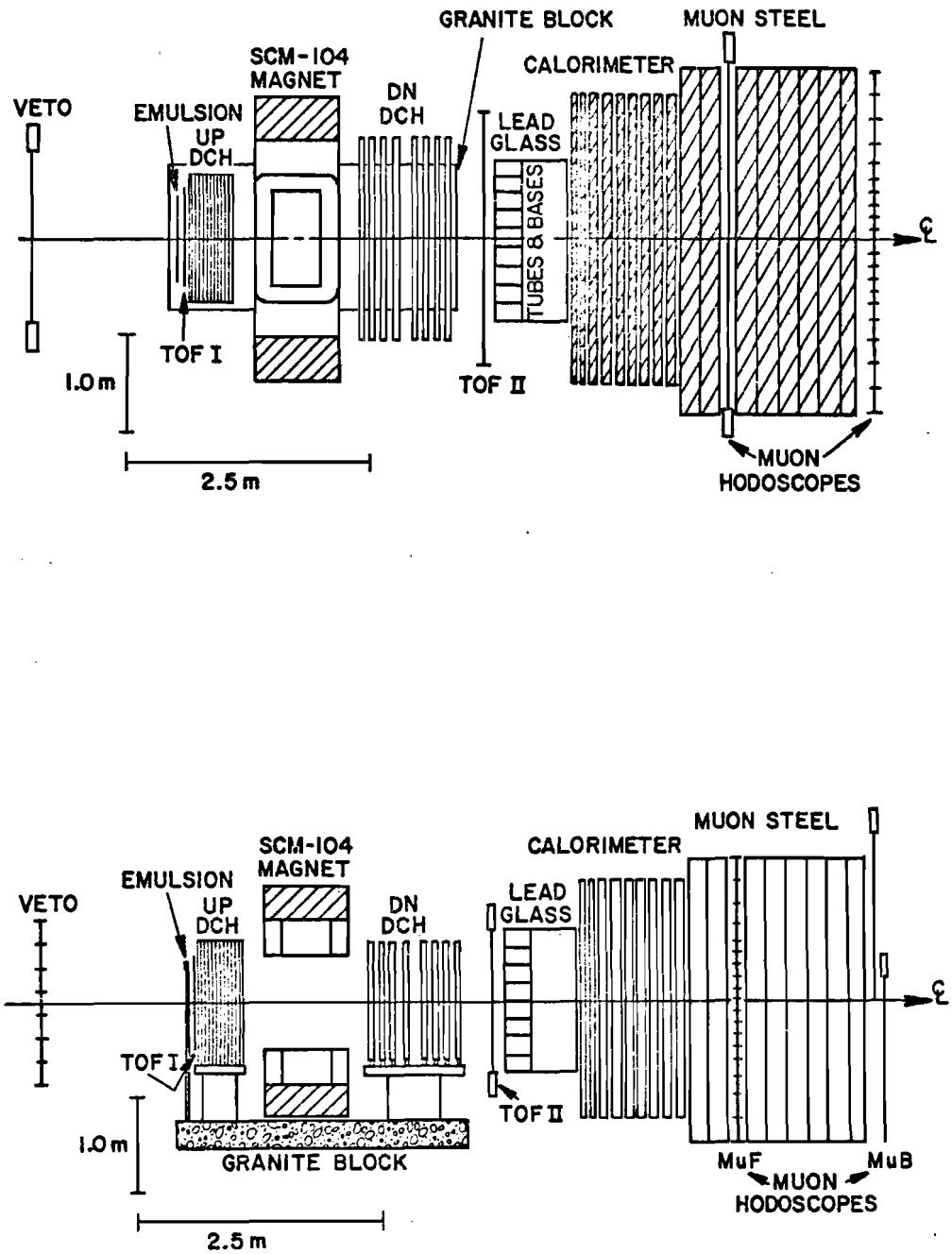

Figure 3. Plan and Elevation View of E-531

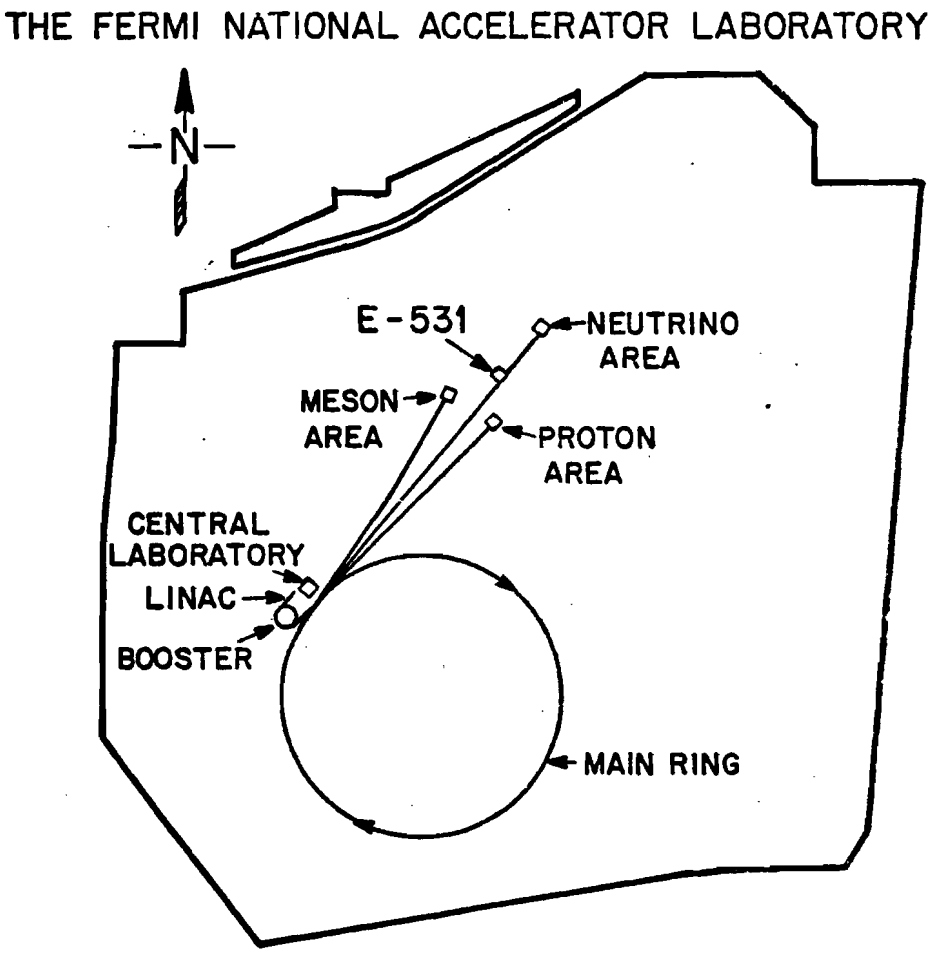

Figure 4. The Fermi National Accelerator

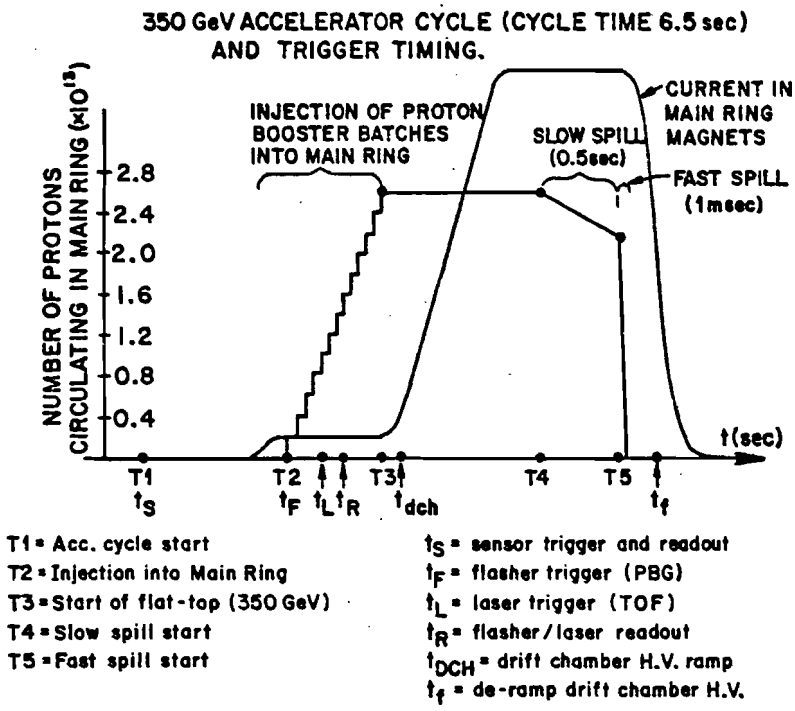

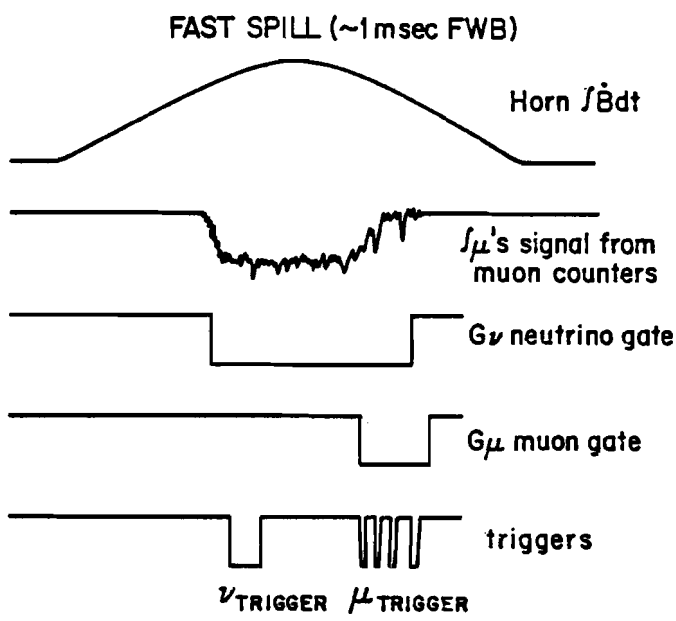

Figure 5. 350 GeV Accelerator Cycle and Trigger Timing

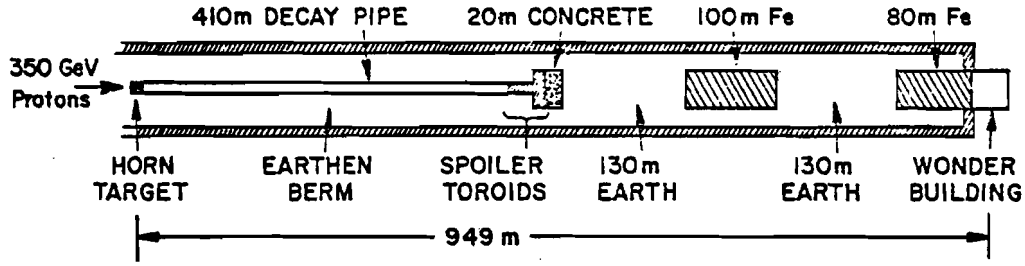

Single Horn Neutrino Target

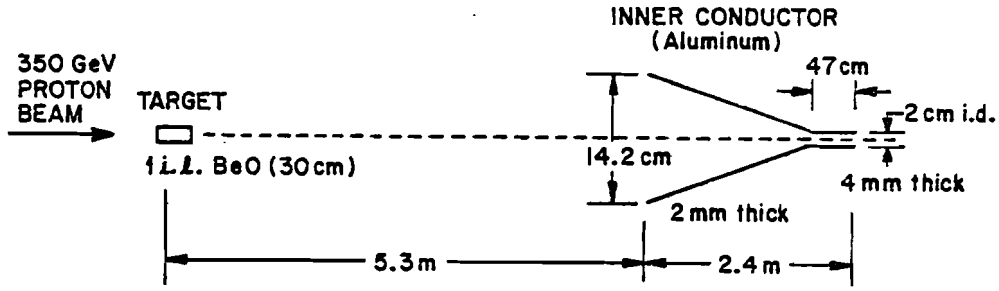

Operating Conditions:

$I = 80$ kA

$\Delta p_T = 0.17$ GeV/c

Figure 6.

The 350 GeV Wide-Band Single Horn Neutrino Beam

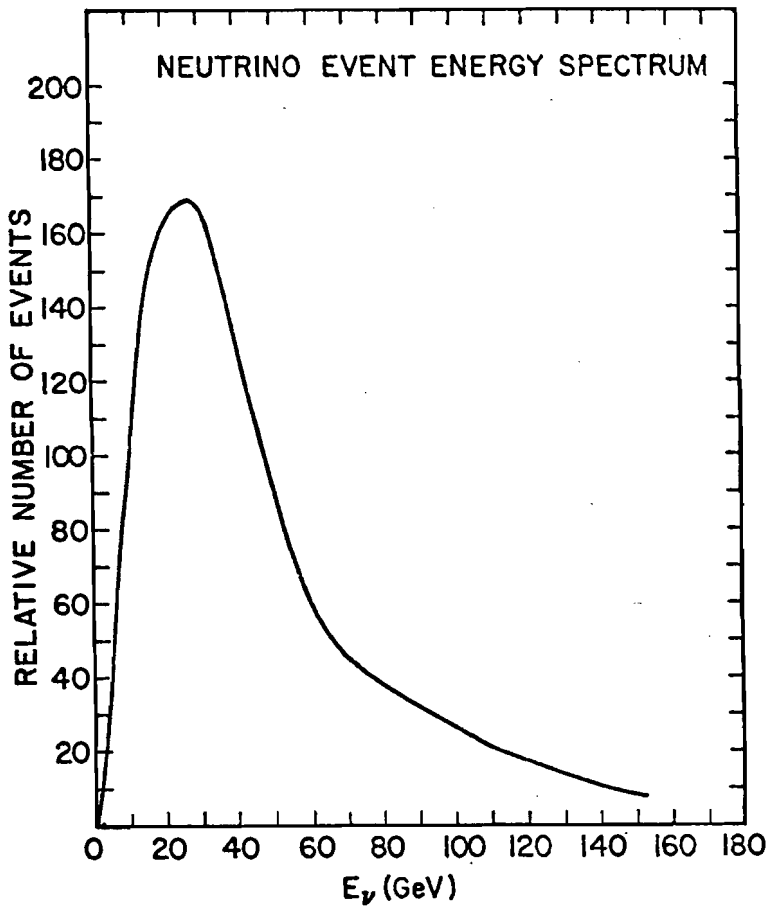

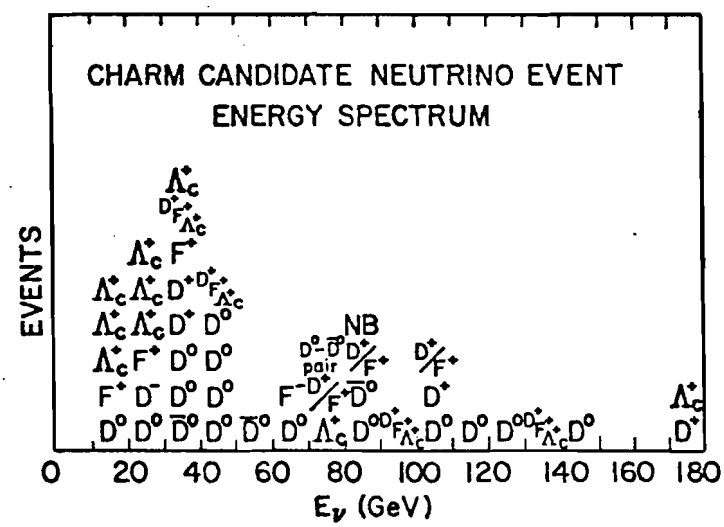

Figure 7. Neutrino Event Spectrum,

Charm Candidate Event Distribution

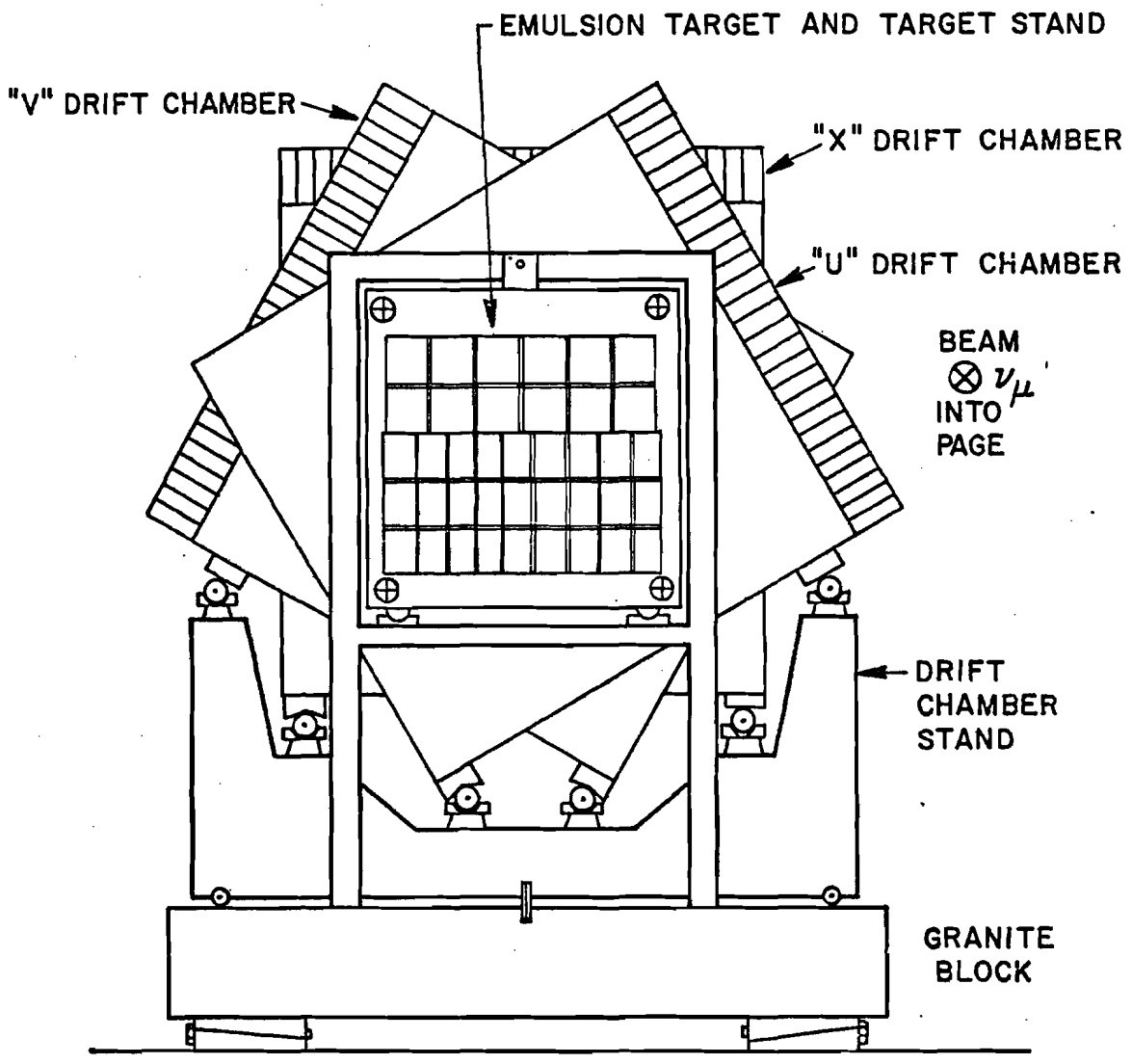

Figure 8. Detail of Emulsion Target and Upstream Drift Chambers (Beam View)

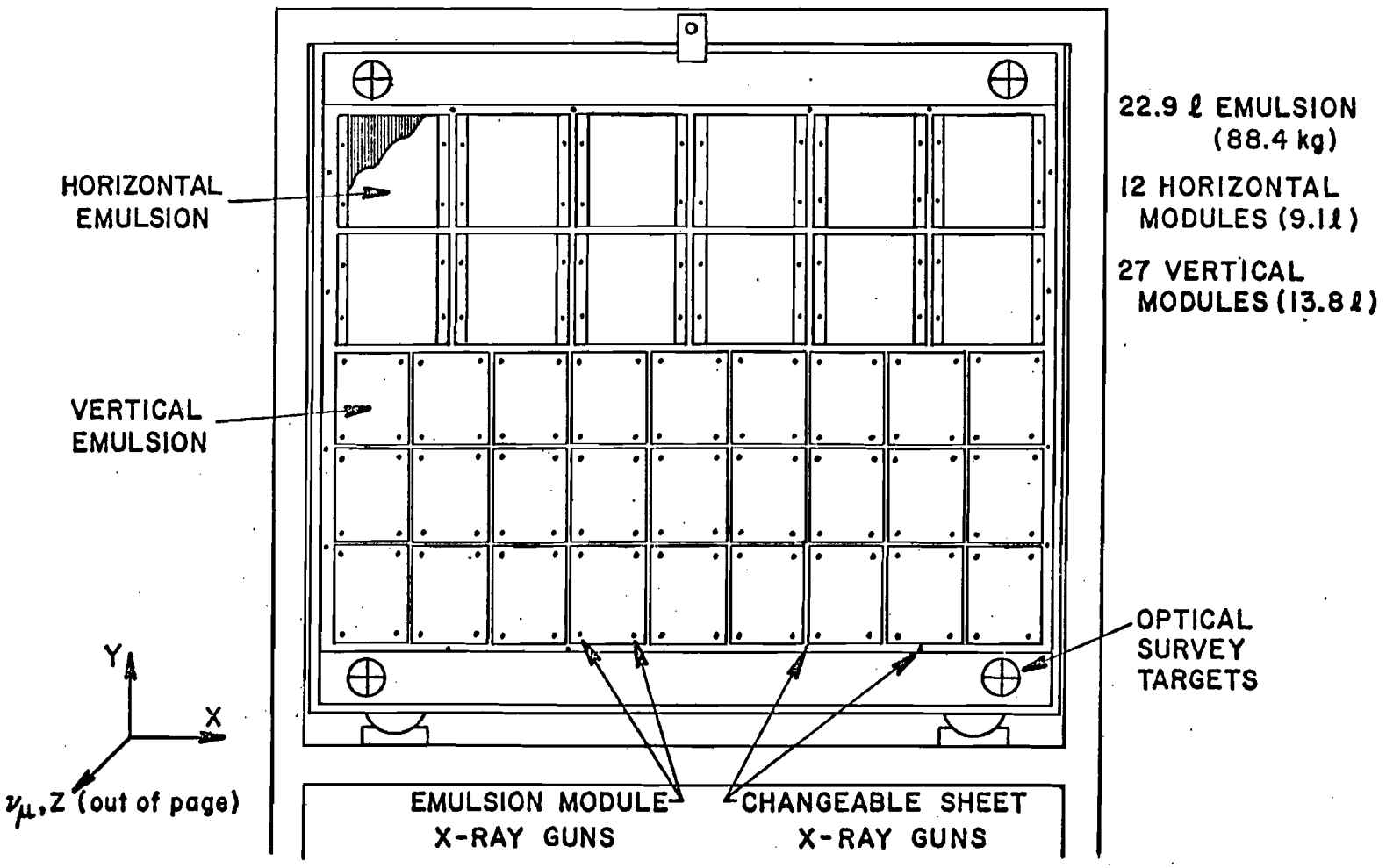

Figure 9. Detail of Emulsion Target and Emulsion Modules

(Downstream View)

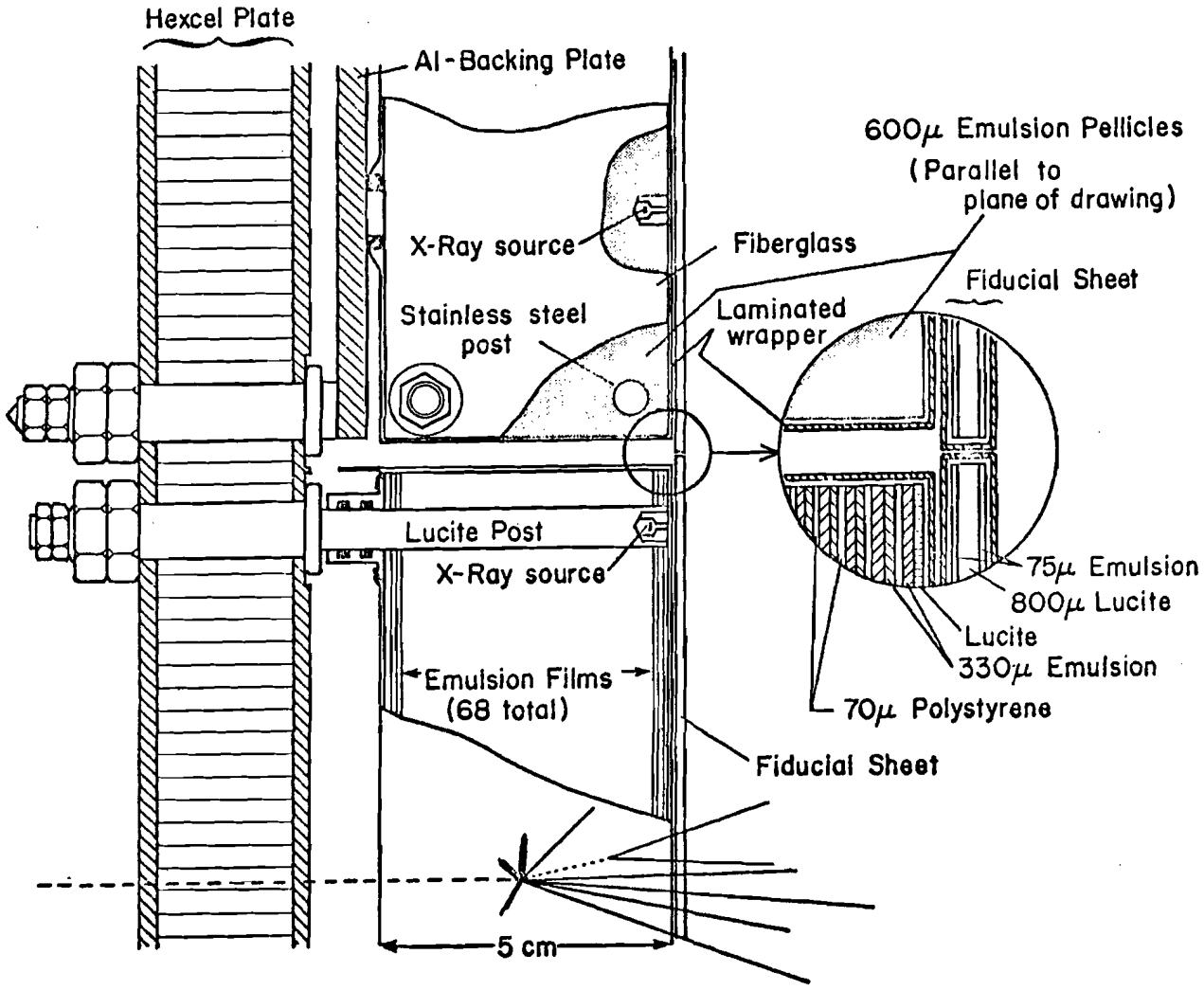

Figure 10. Elevation View of Emulsion Target

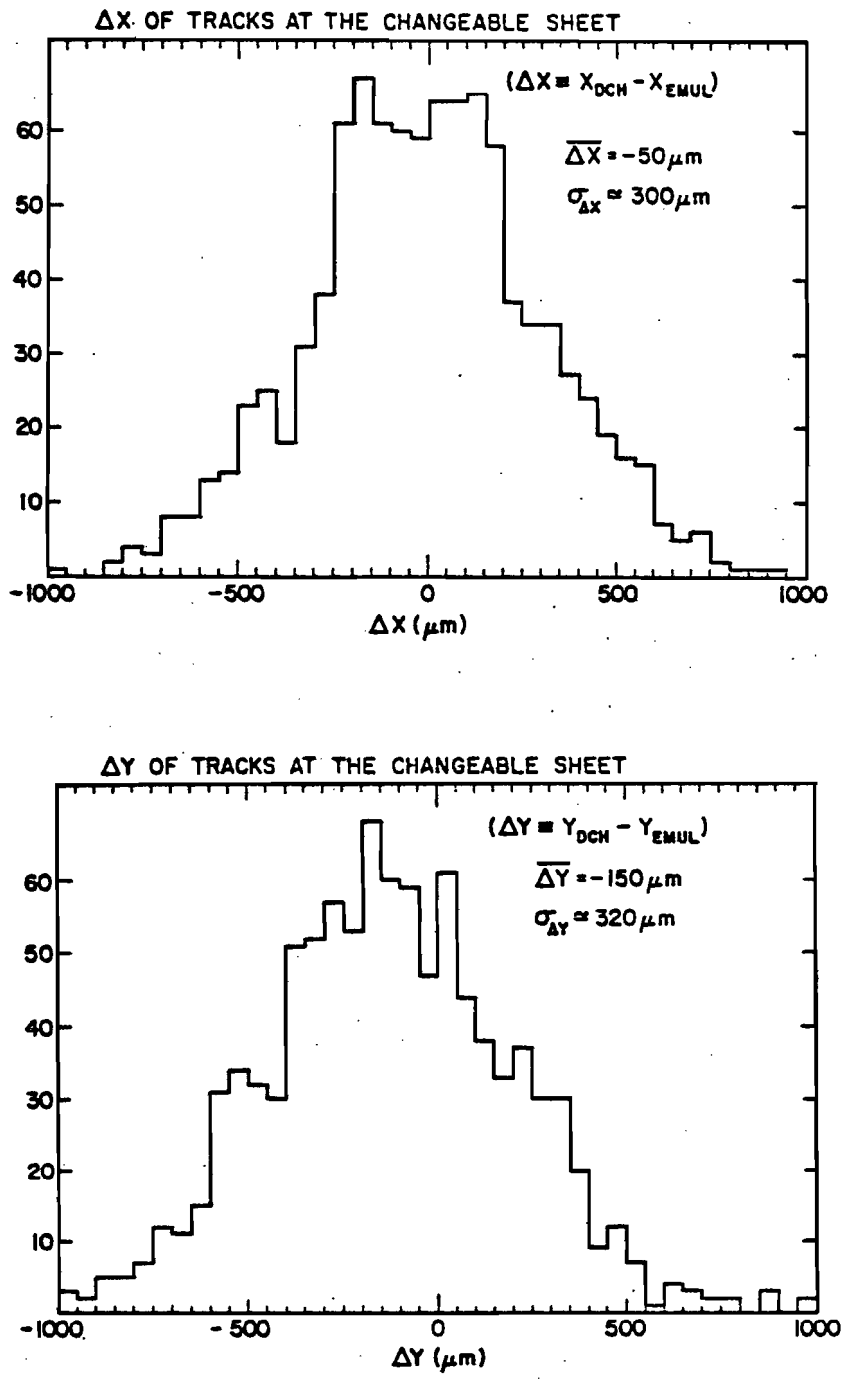

Figure 11. ΔX, ΔY of Tracks at the Changeable Sheet

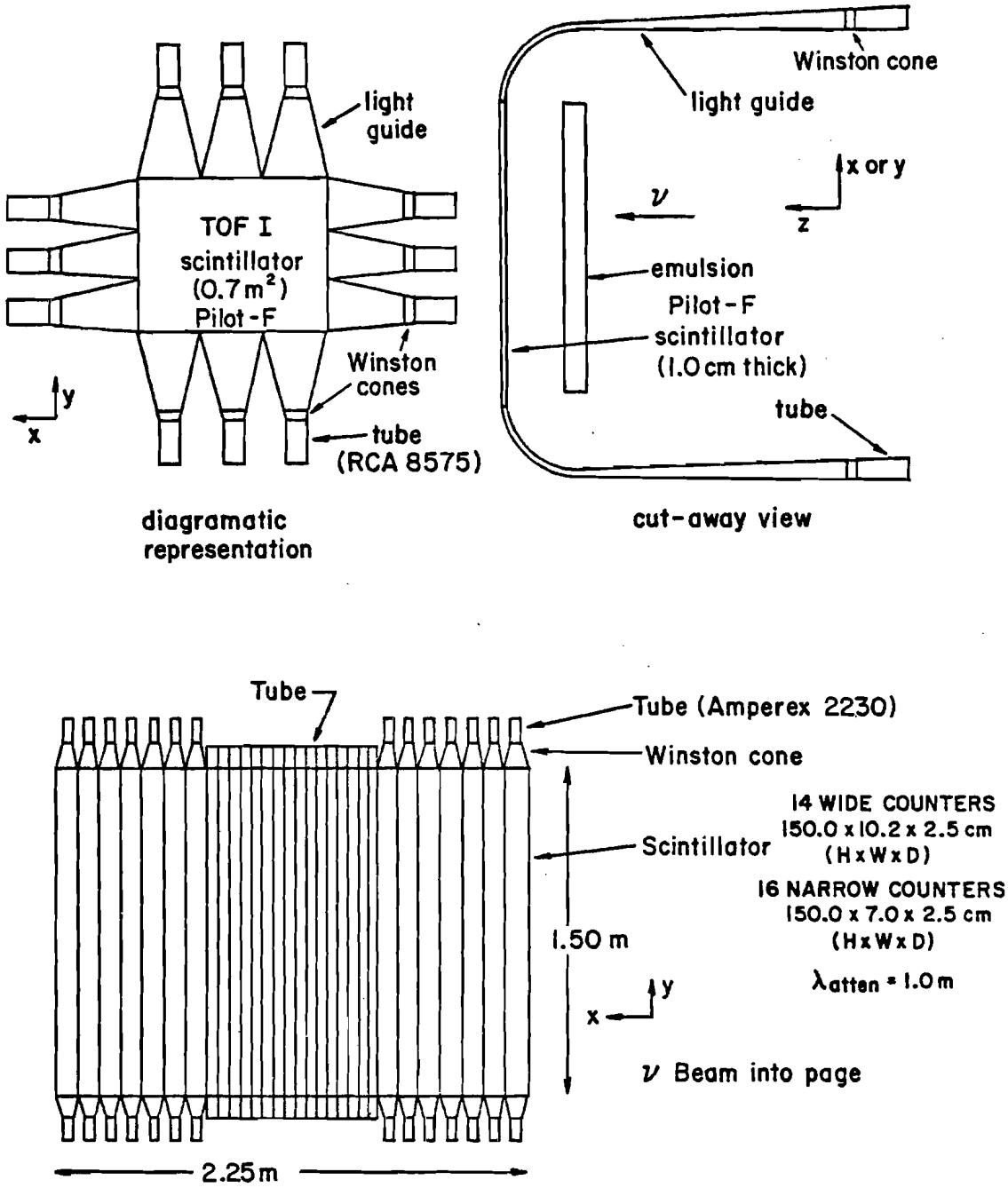

Figure 12. The TOF Counters

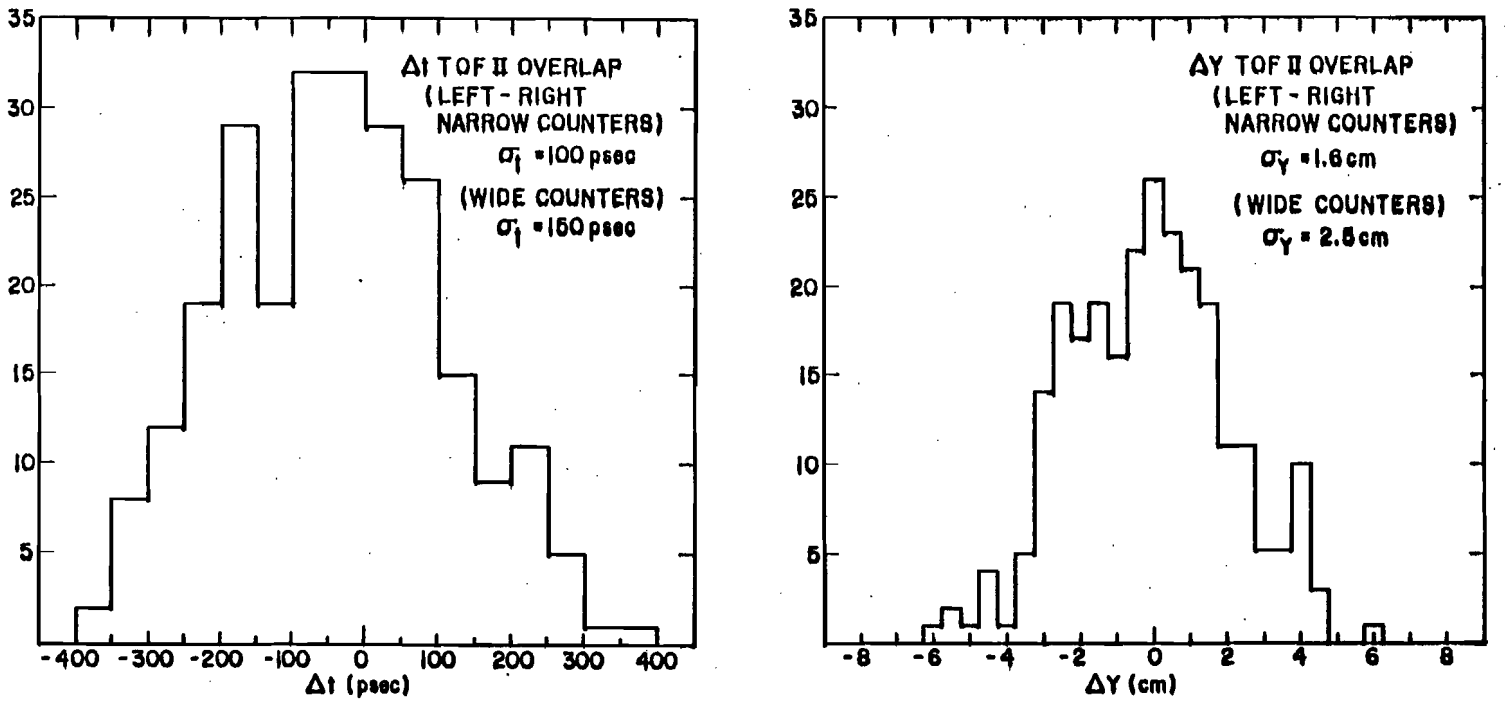

Figure 13. TOF II Δt and ΔY for Muon Overlap Events

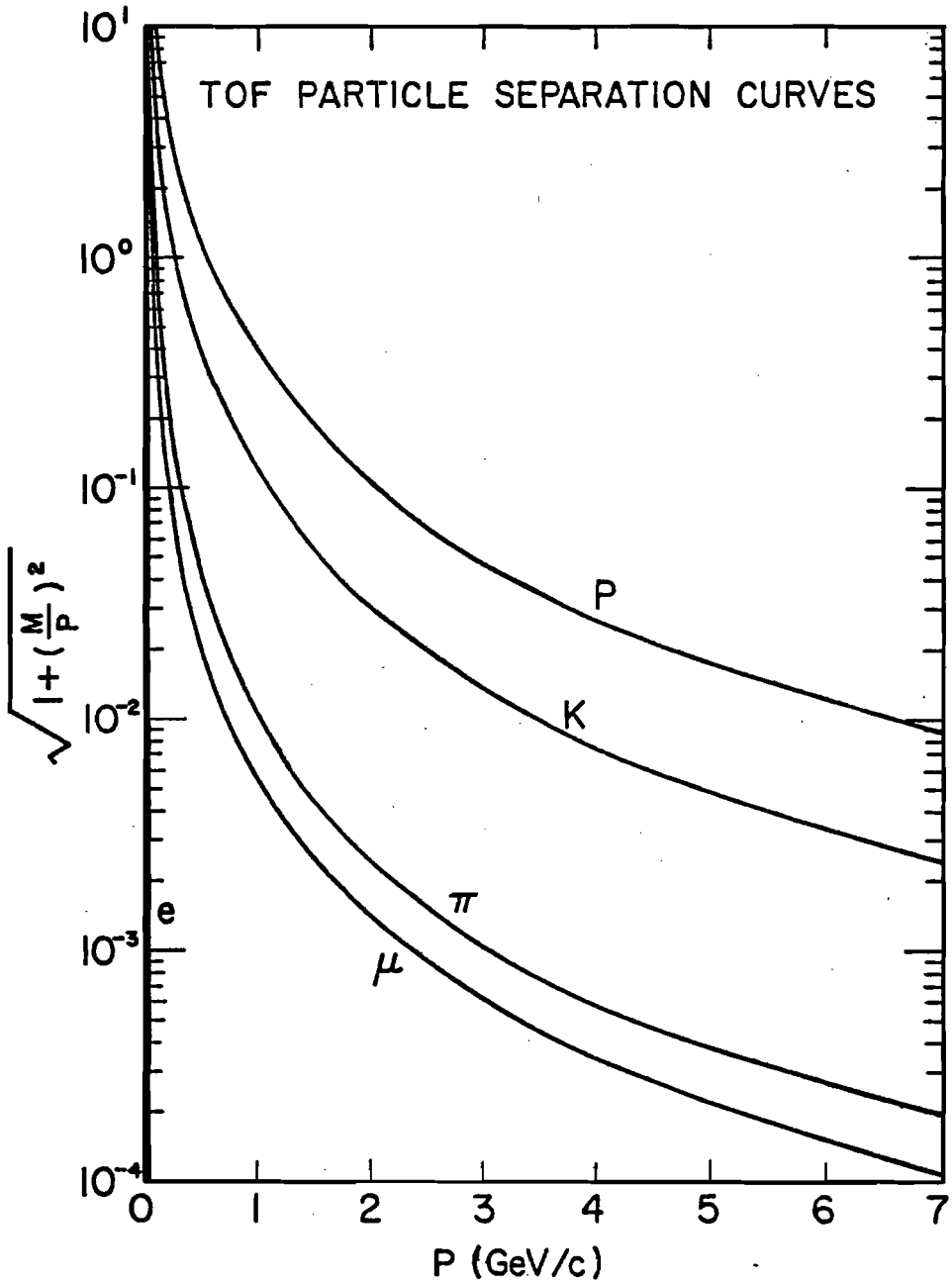

Figure 14. TOF Particle Identification:

$1+(m/p)^2$ vs. Momentum P

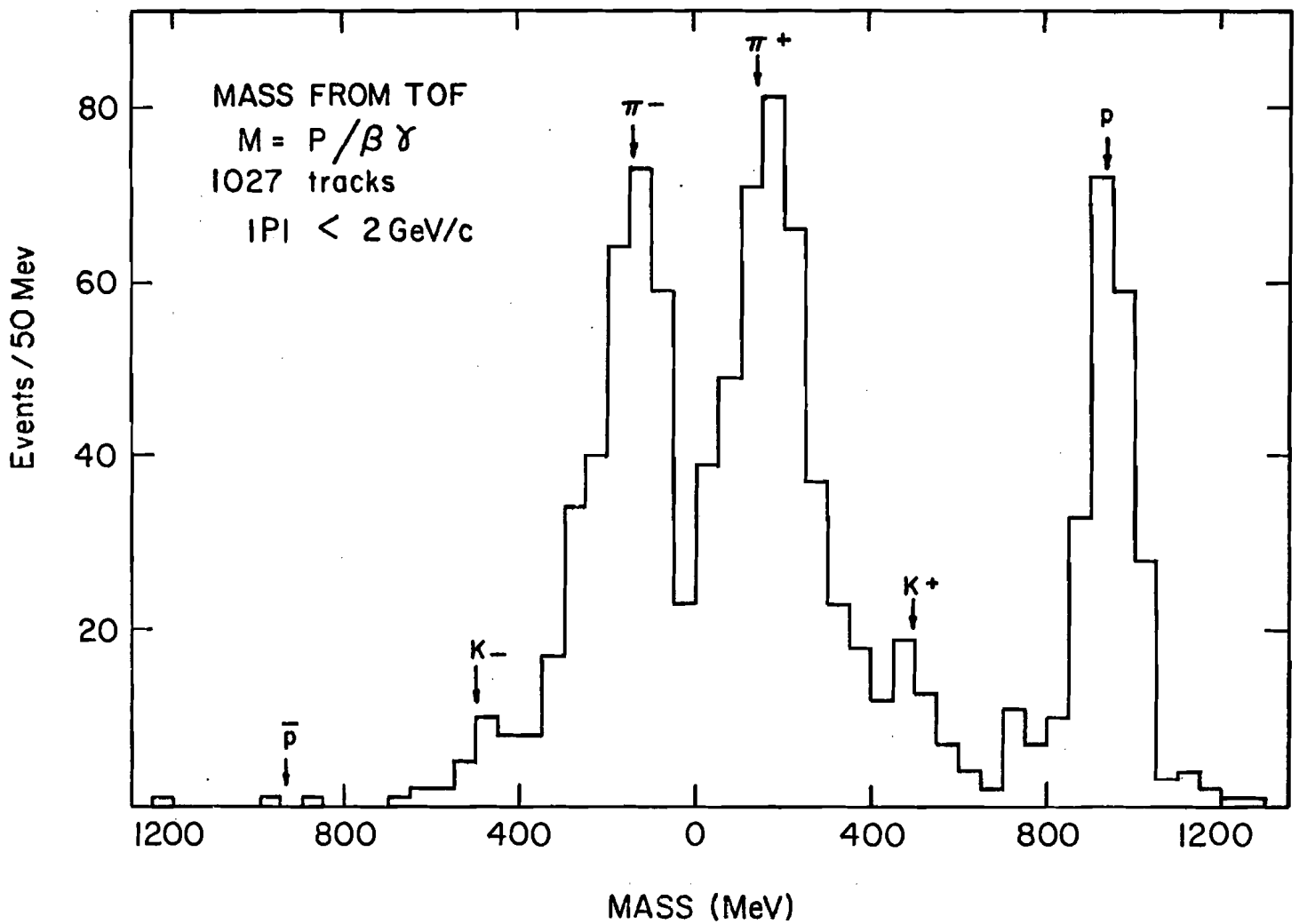

Figure 15. Particle Mass from TOF

CELL CONFIGURATION AND
EQUIPOTENTIALS FOR UPSTREAM DRIFT CHAMBERS

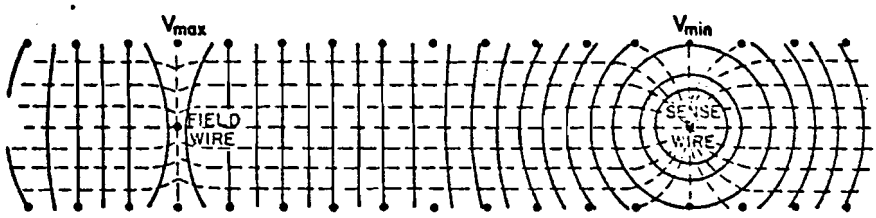

Sense wire: 20μm dia. Au-W wire
Field wire & cathode plane wires: 75μm dia. Cu-Be wire
Cell size = 4.0 cm
2.0 mm cathode wire spacing
7.0 mm cathode plane spacing
V_{max} = 3.1 kV
V_{min} = 1.7 kV
E = 700 V/cm

Figure 16. Upstream Drift Chamber Cell Configuration

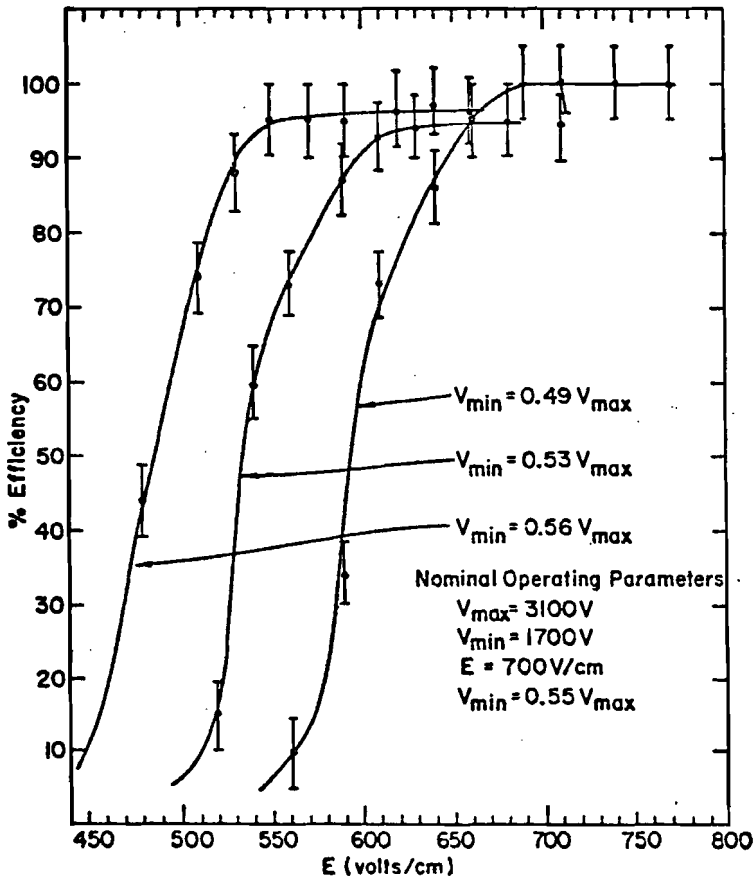

Figure 17. Upstream Drift Chambers:

Efficiency vs. E-Field

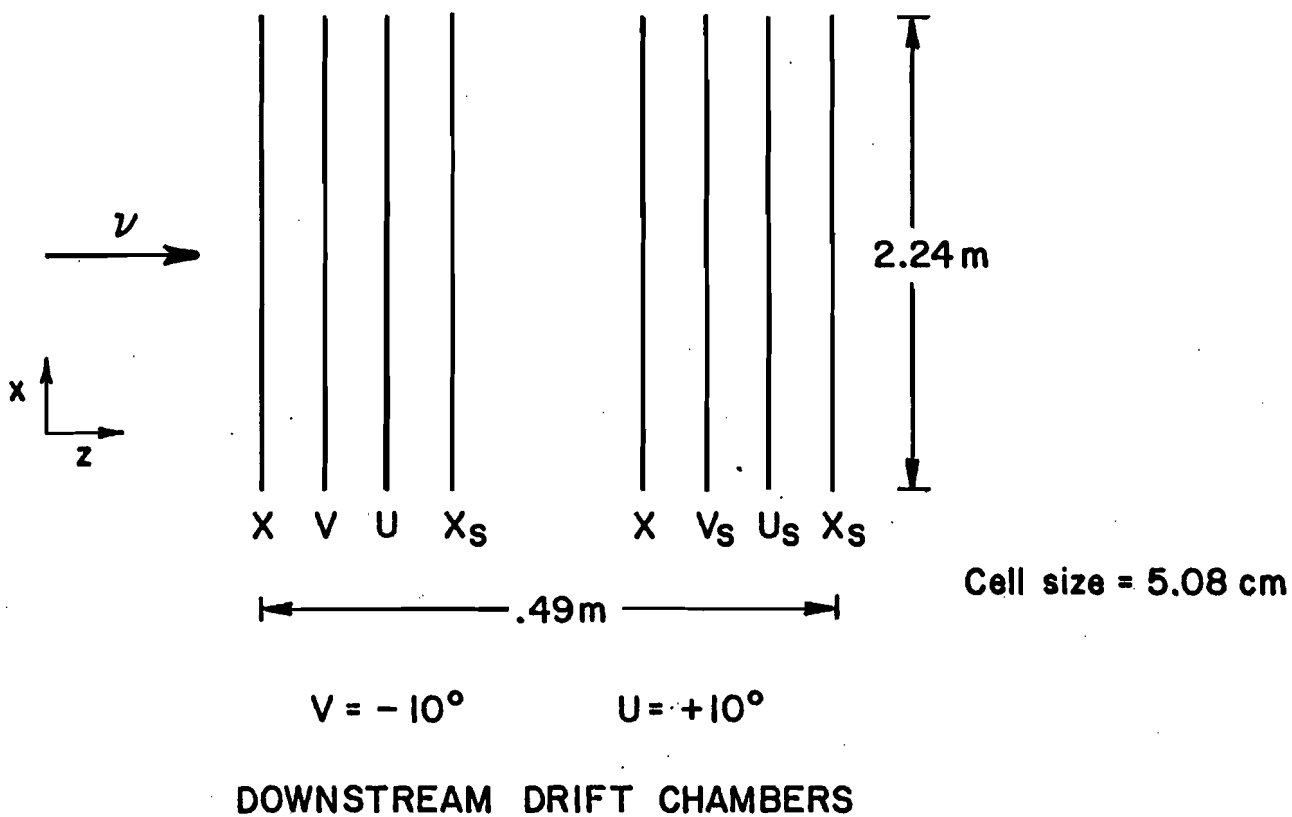

Figure 18. The Downstream Drift Chambers

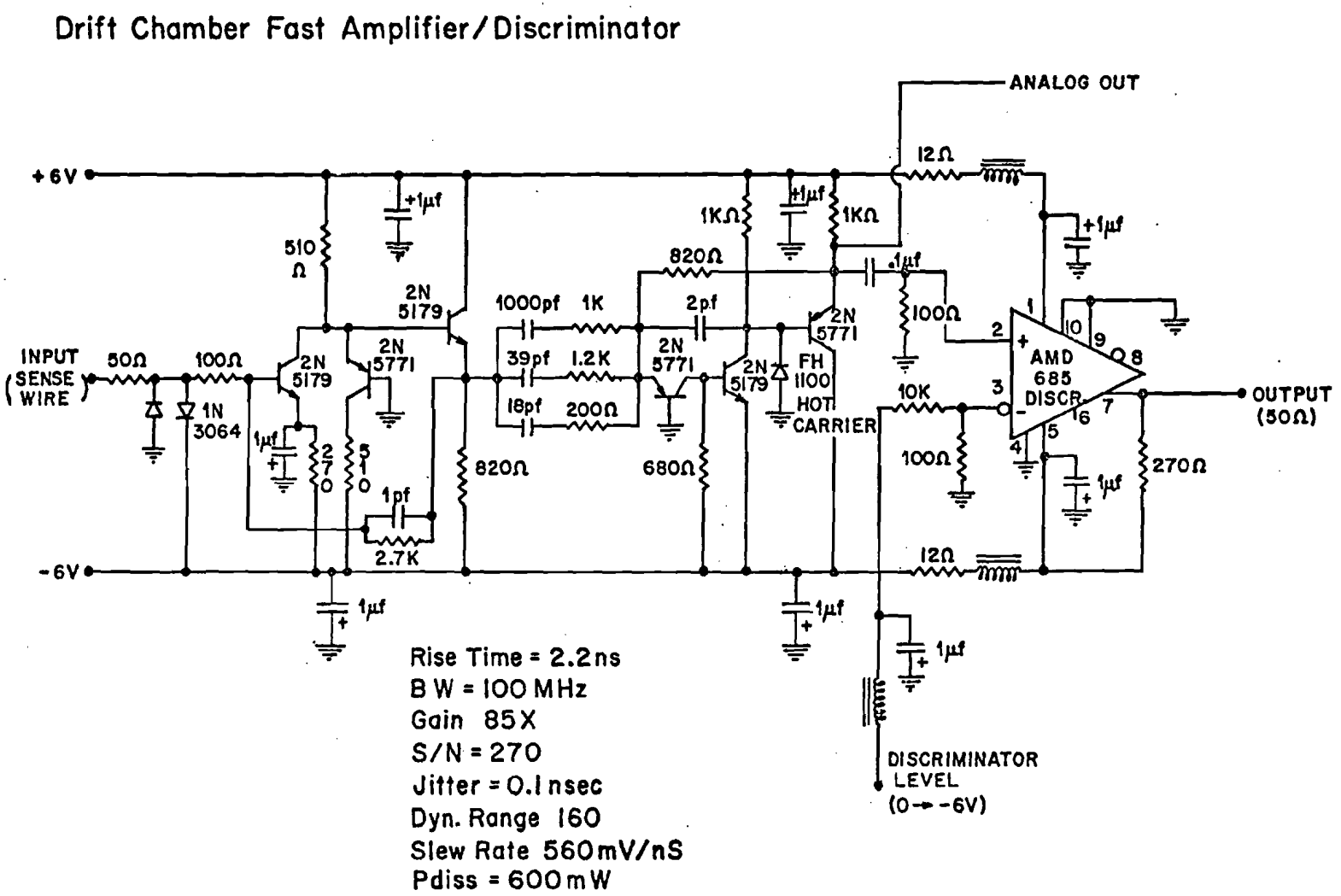

Figure 19. Drift Chamber Fast Amplifier/Discriminator

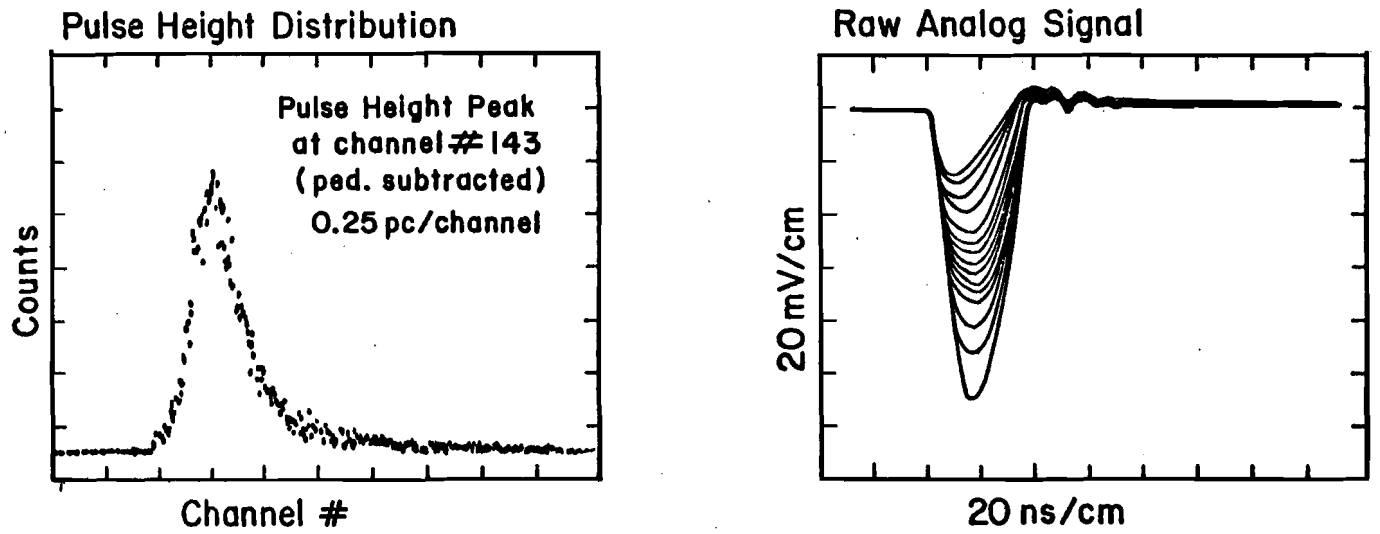

PH 100 mV @ Input to discriminator
Magnet on
V_{max} = 3100V
V_{min} = 1700V
DL = 15 mV

Figure 20. Drift Chamber Pulse Height Spectrum - Minimum Ionizing Muons

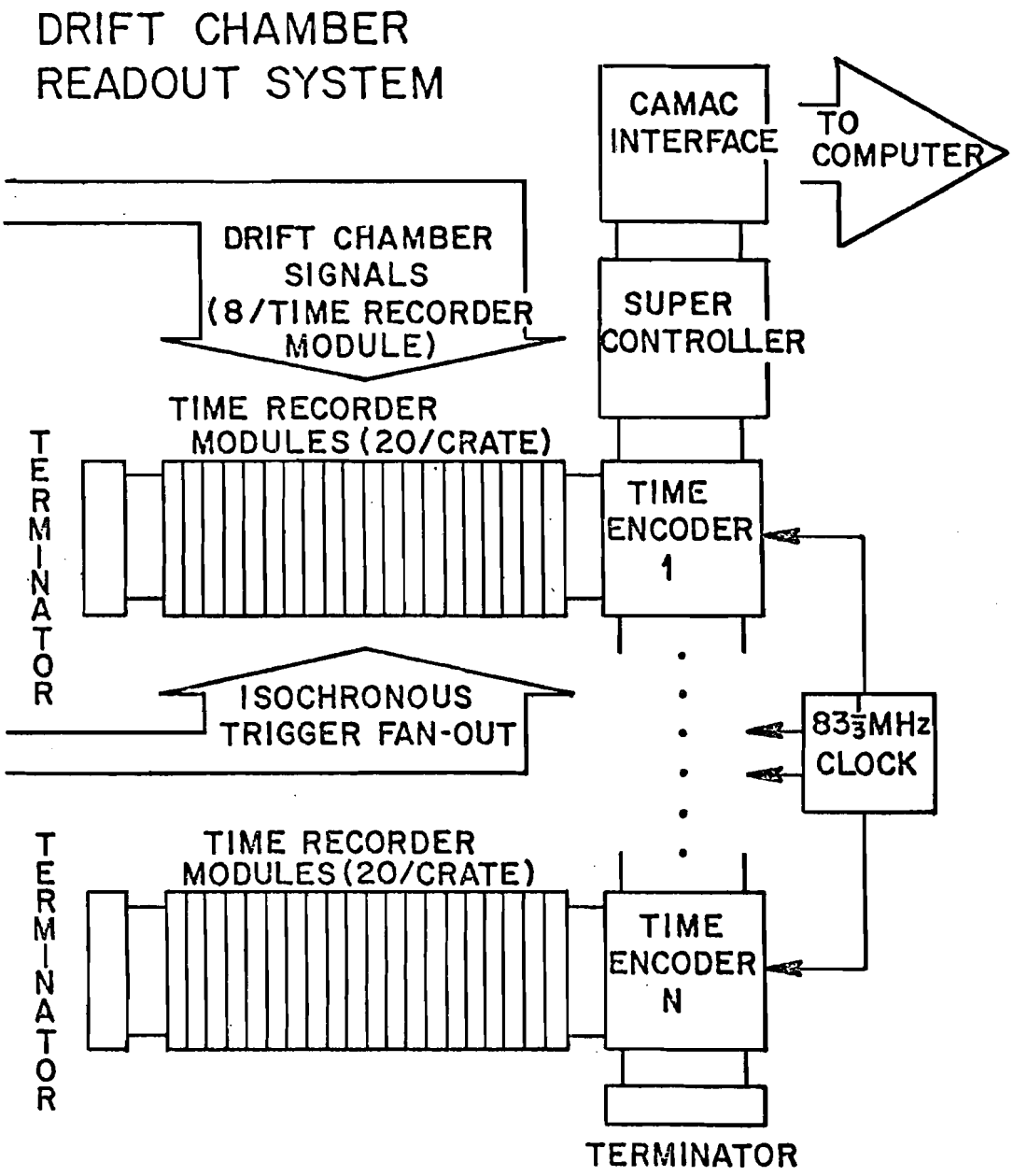

Figure 21. Drift Chamber Readout System Electronics

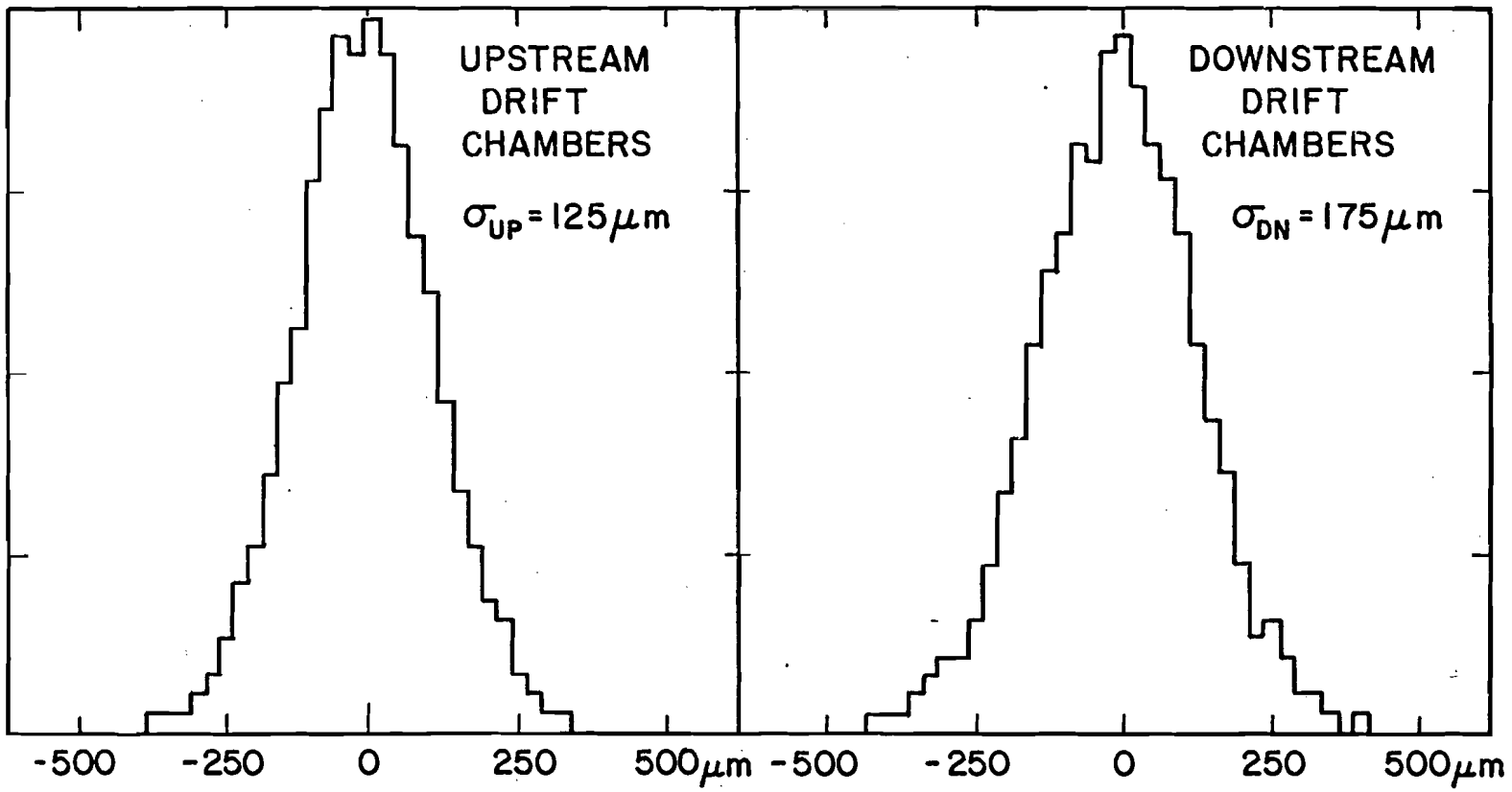

Figure 22. Drift Chamber Resolution

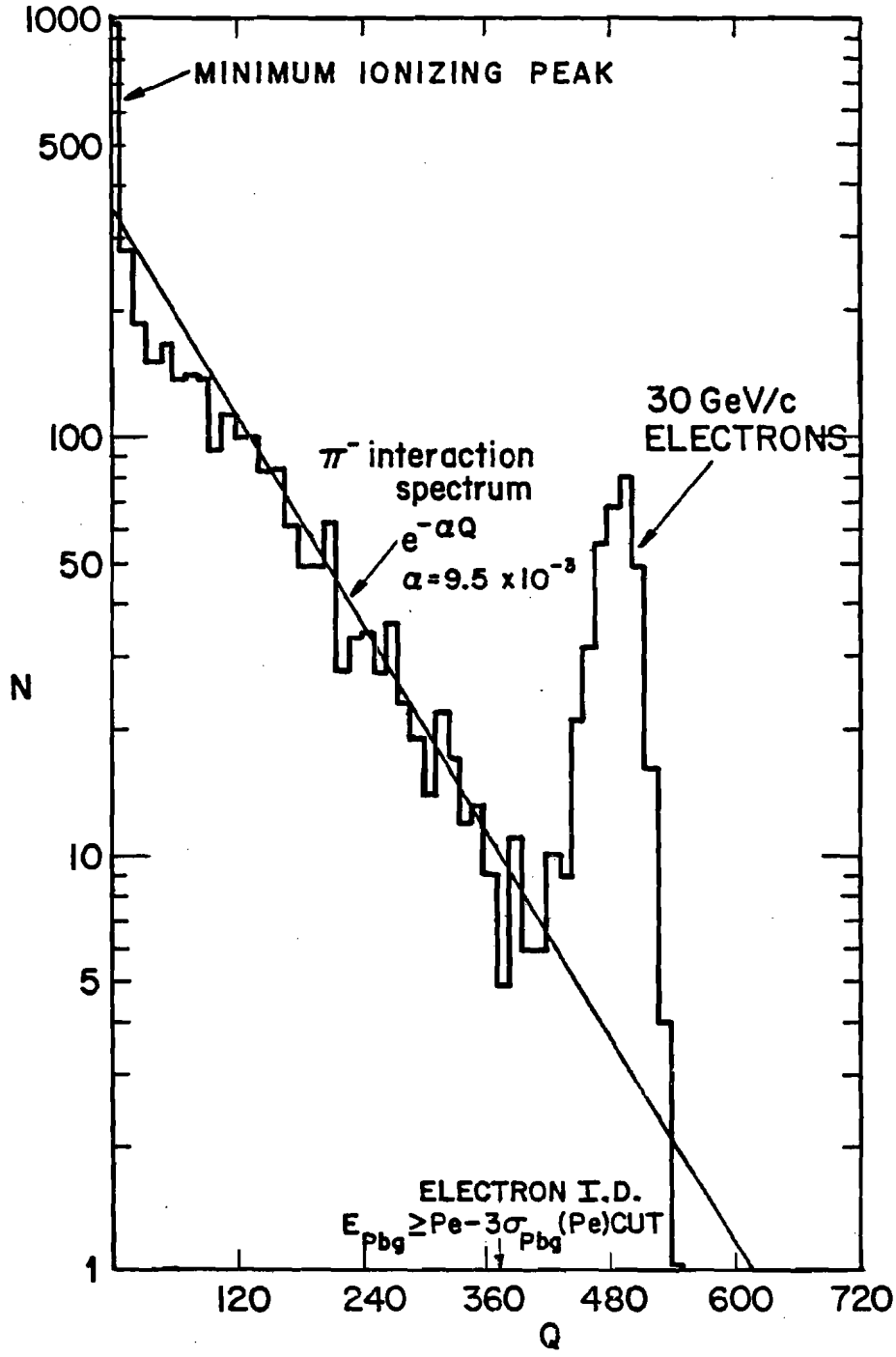

Figure 25. Lead Glass Pulse Height Spectrum,

M-5 Tests, 30 GeV/c Negatives

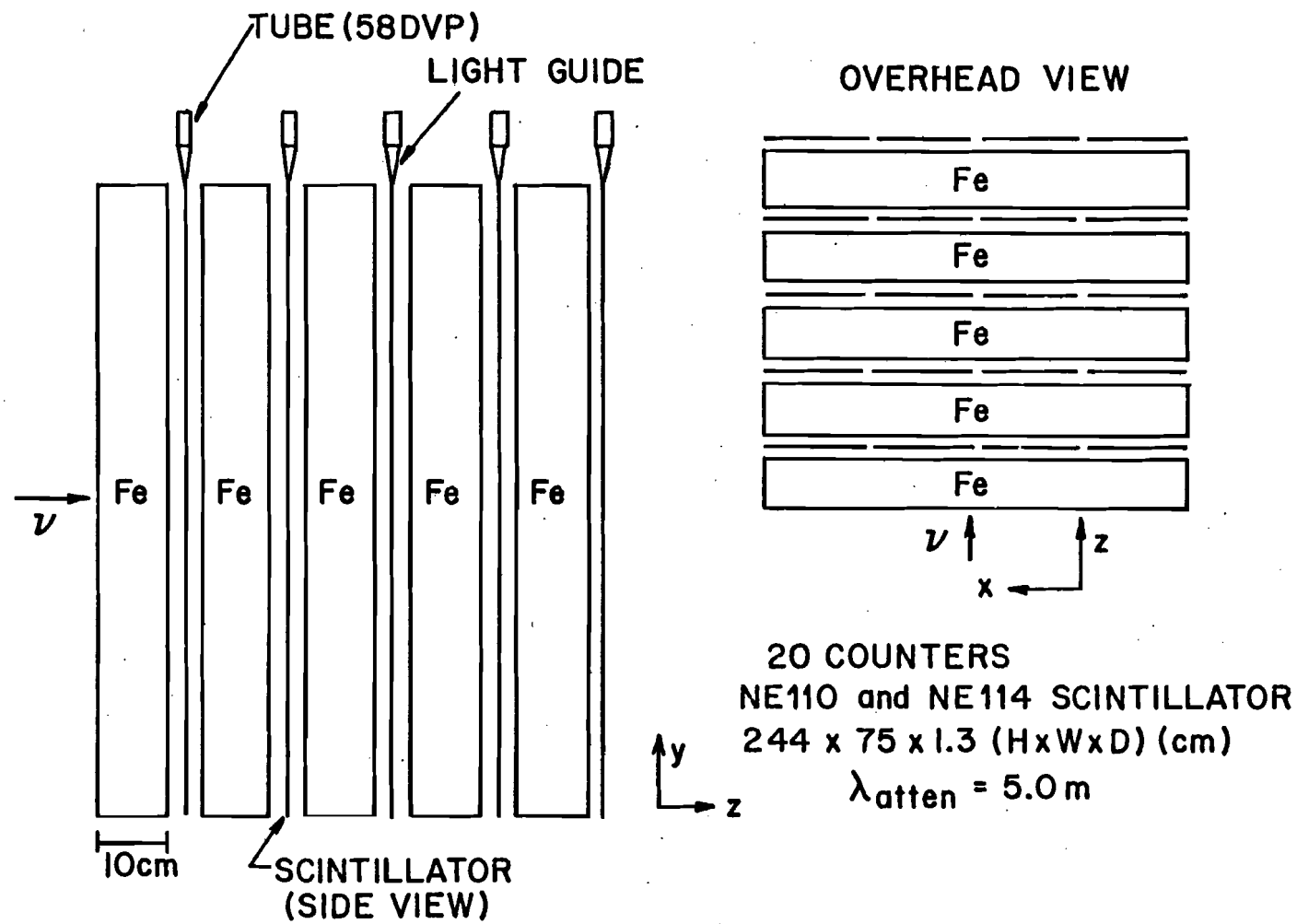

Figure 26. The Hadron Calorimeter

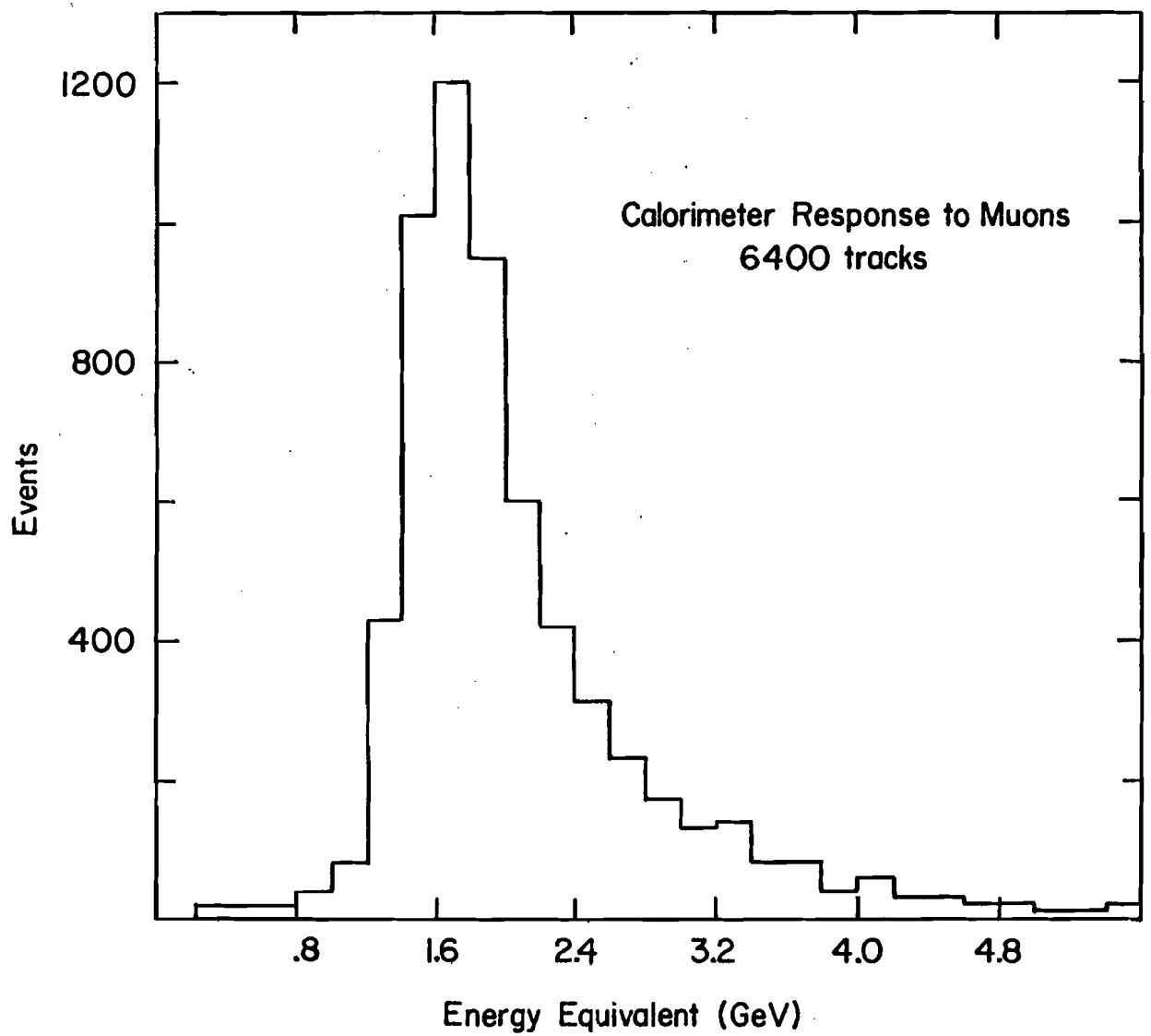

Figure 27. Hadron Calorimeter Response to Minimum Ionizing Muons

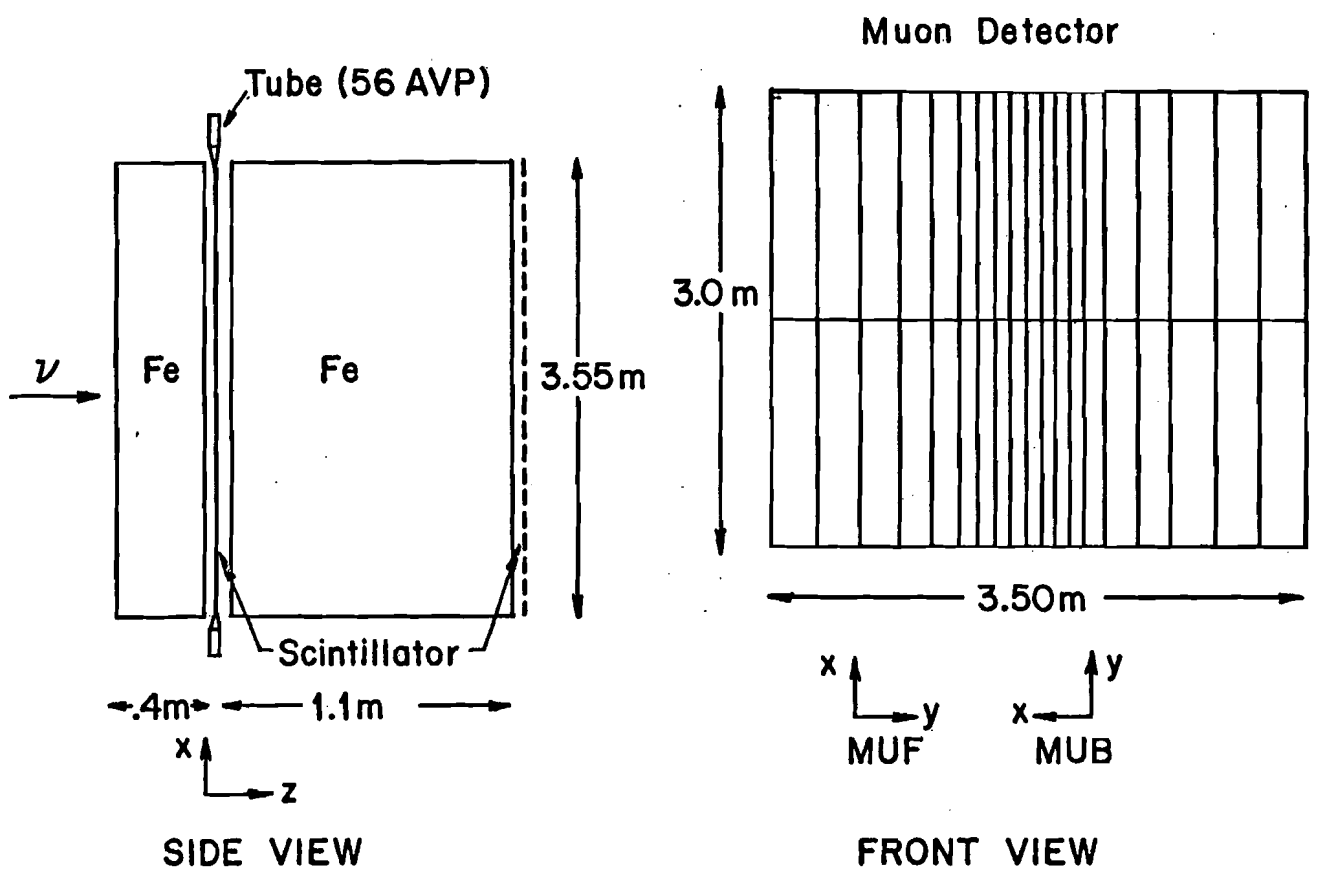

Figure 28. The Muon Detection Array

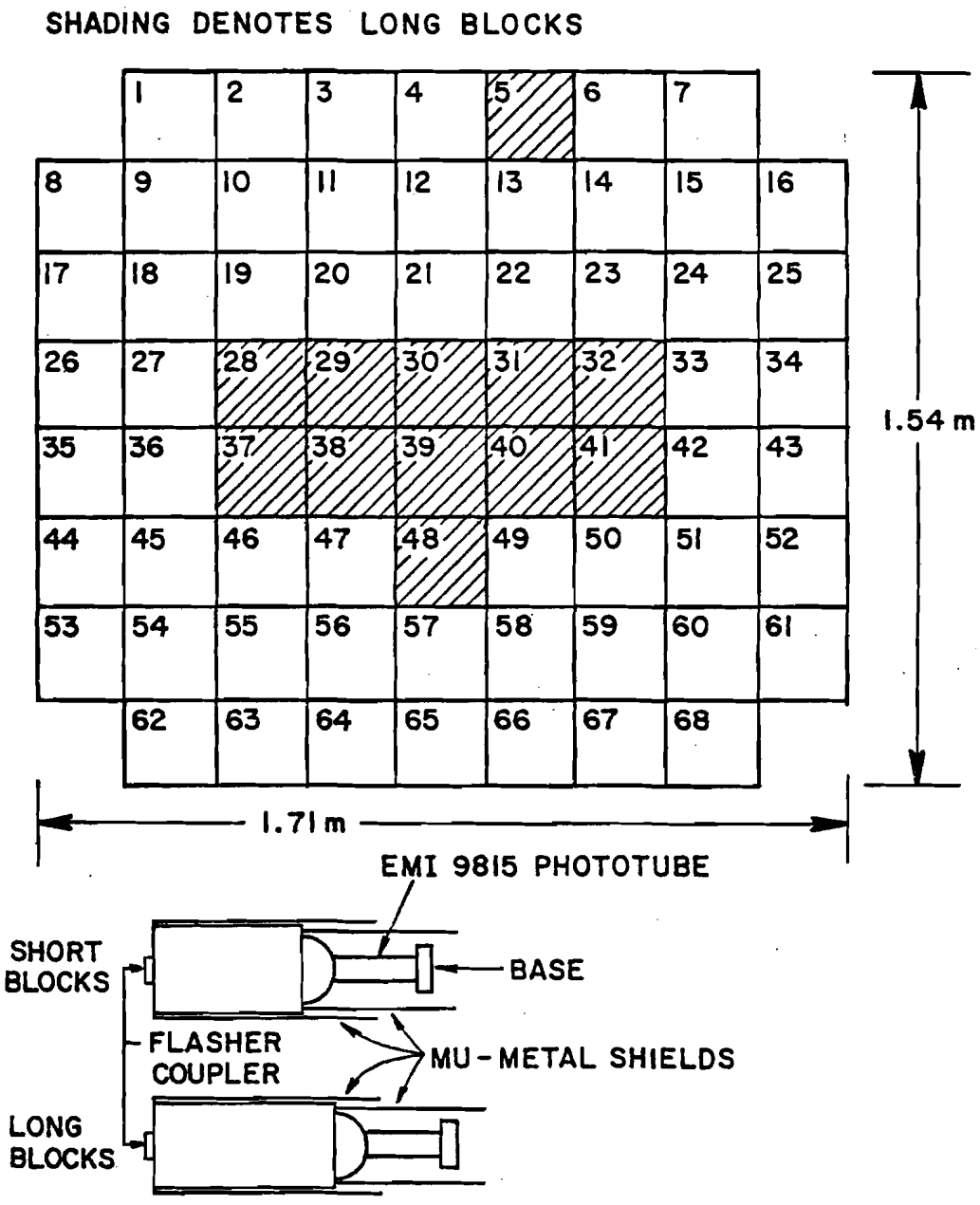

Figure 23. Lead Glass Array

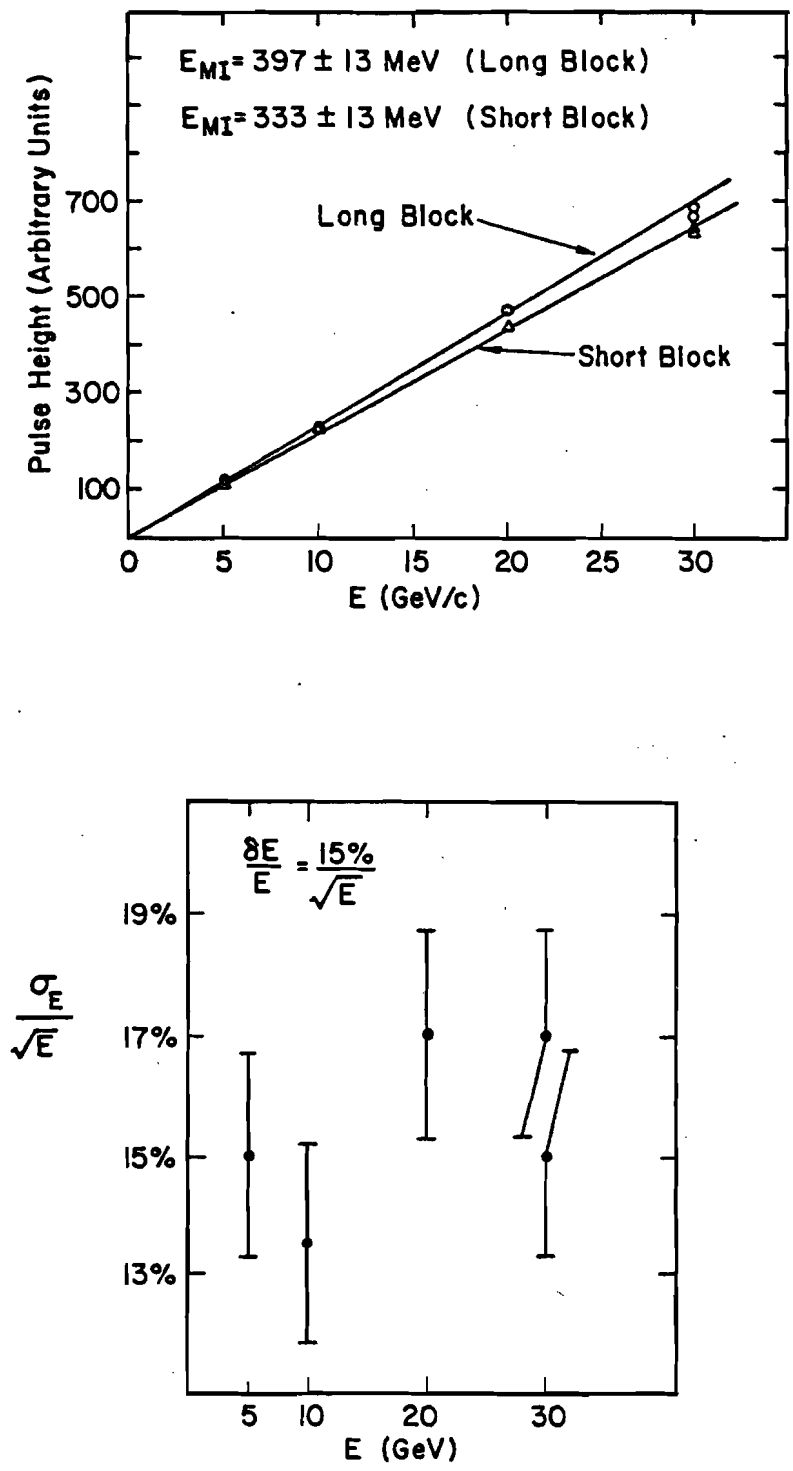

Figure 24. Lead Glass Energy Response and Resolution

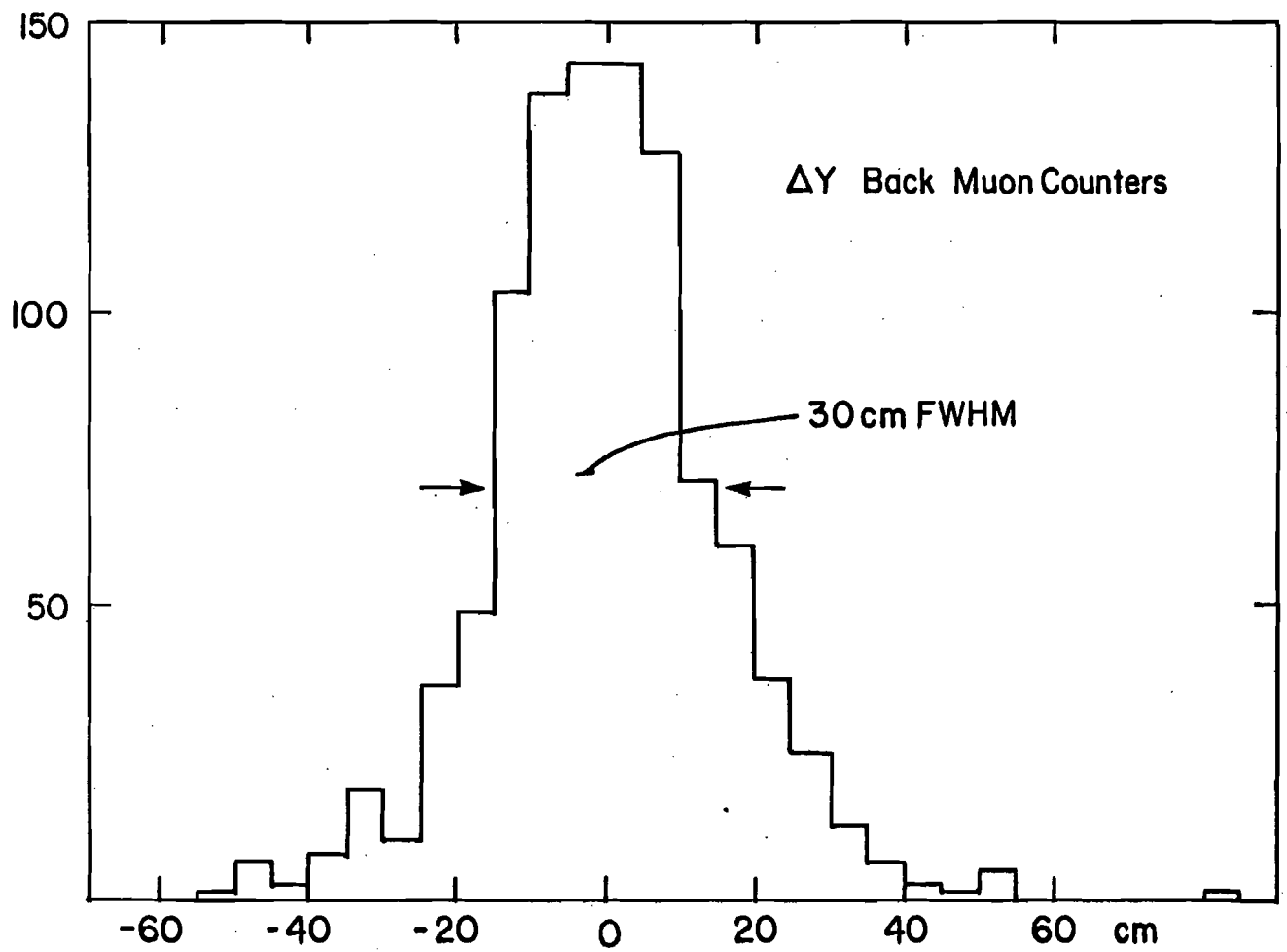

Figure 29. ΔY of Back Muon Counters

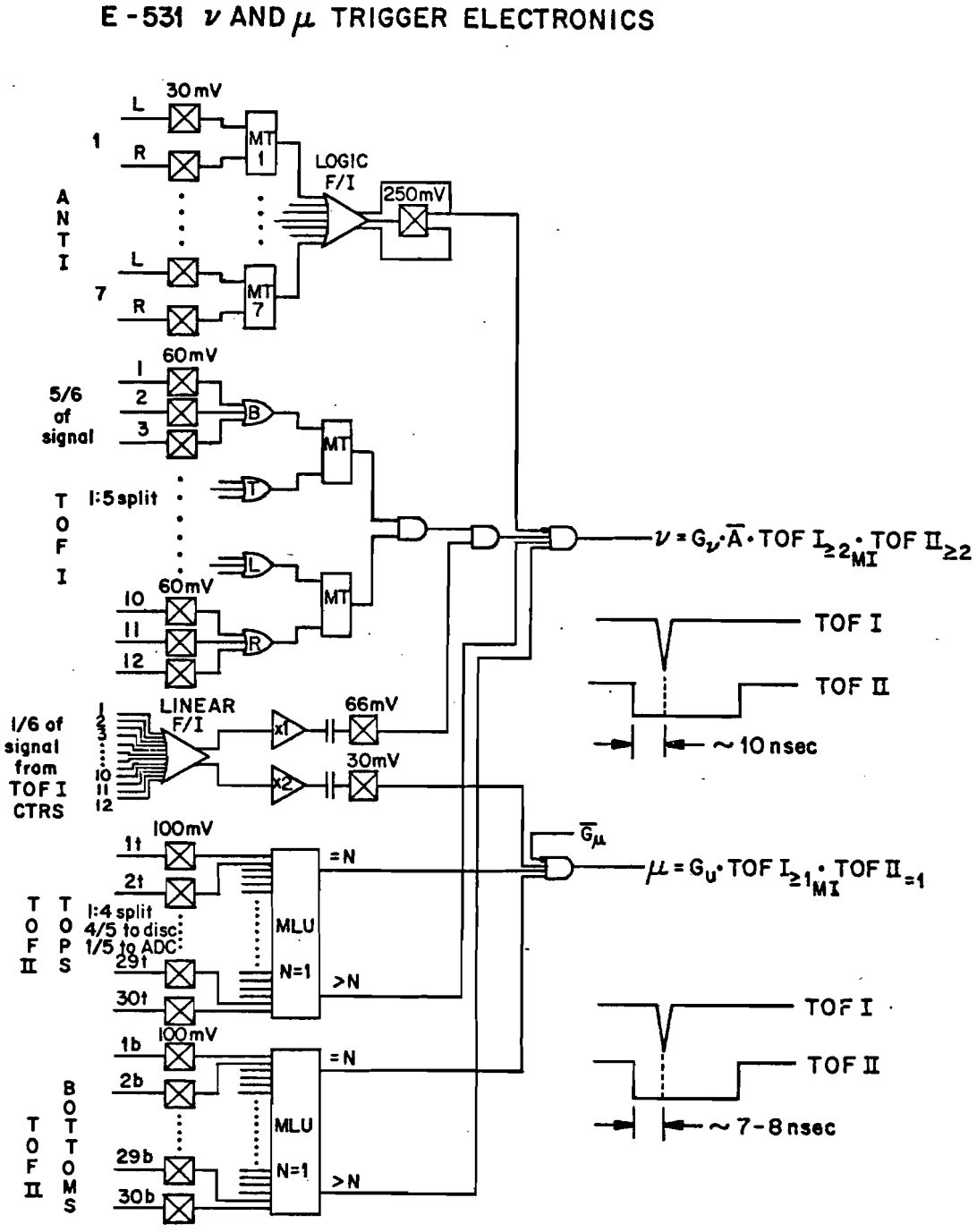

Figure 30. Neutrino and Muon Trigger Electronics

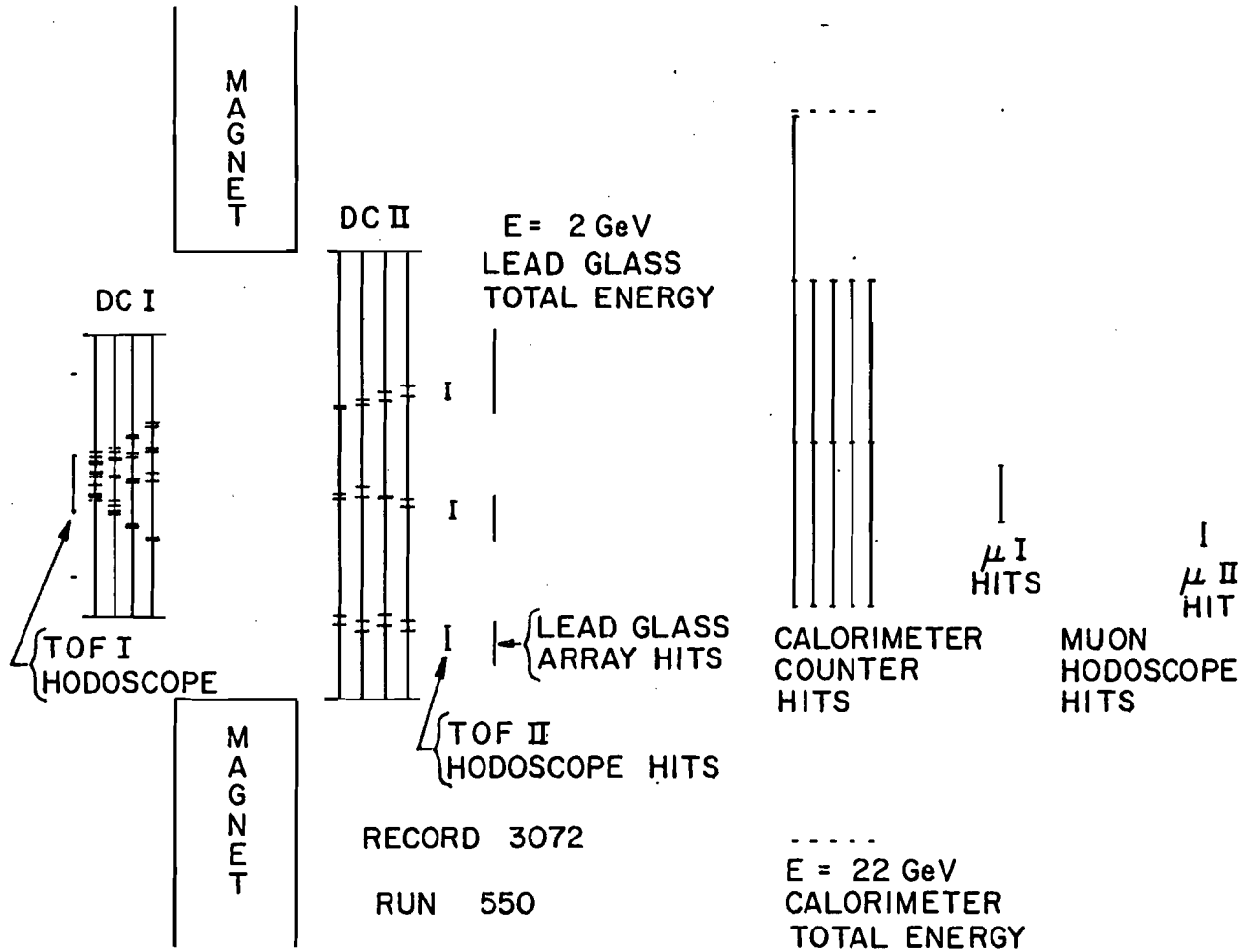

Figure 31. Example of On-Line Display of a Neutrino Interaction

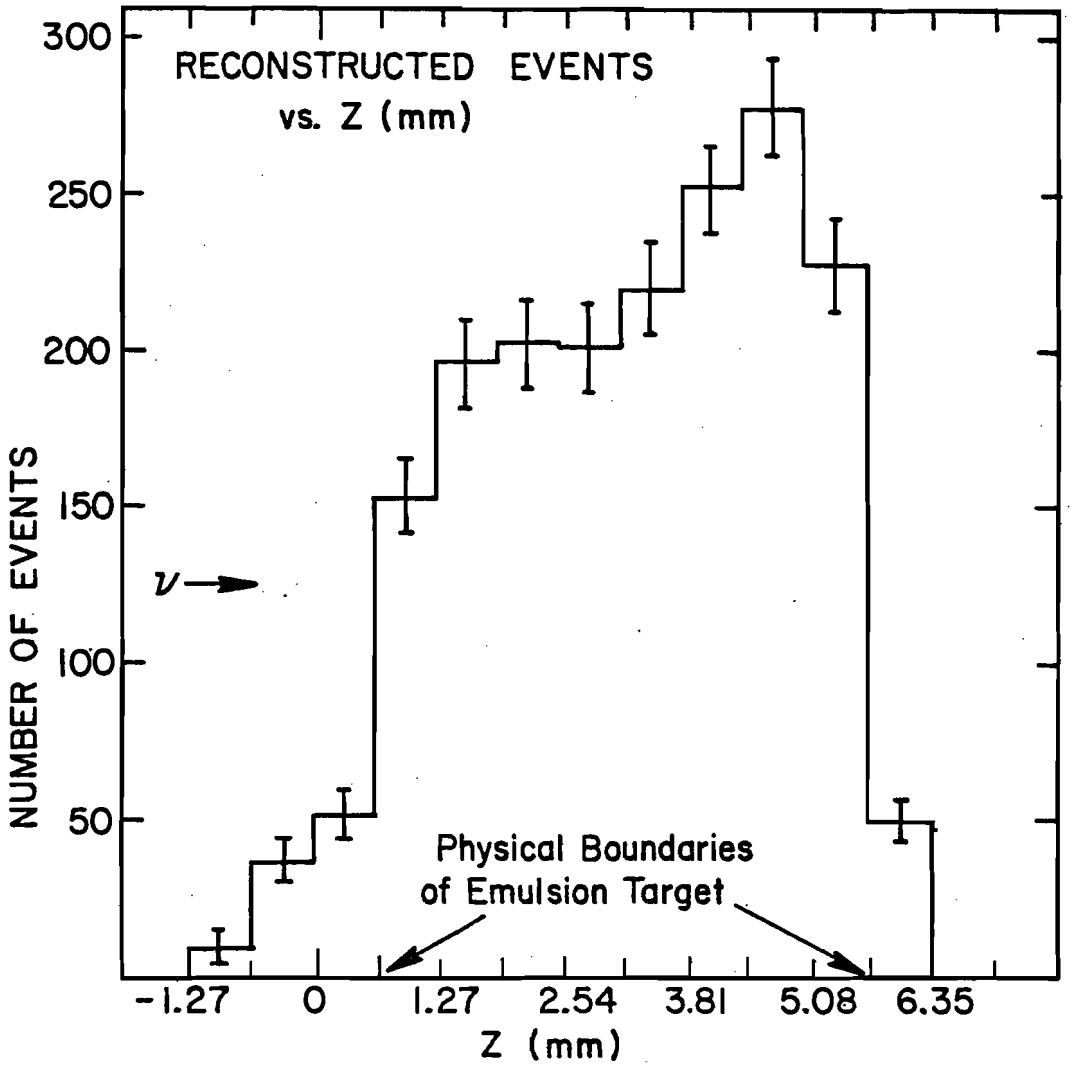

Figure 32. Reconstructed Events vs. Z

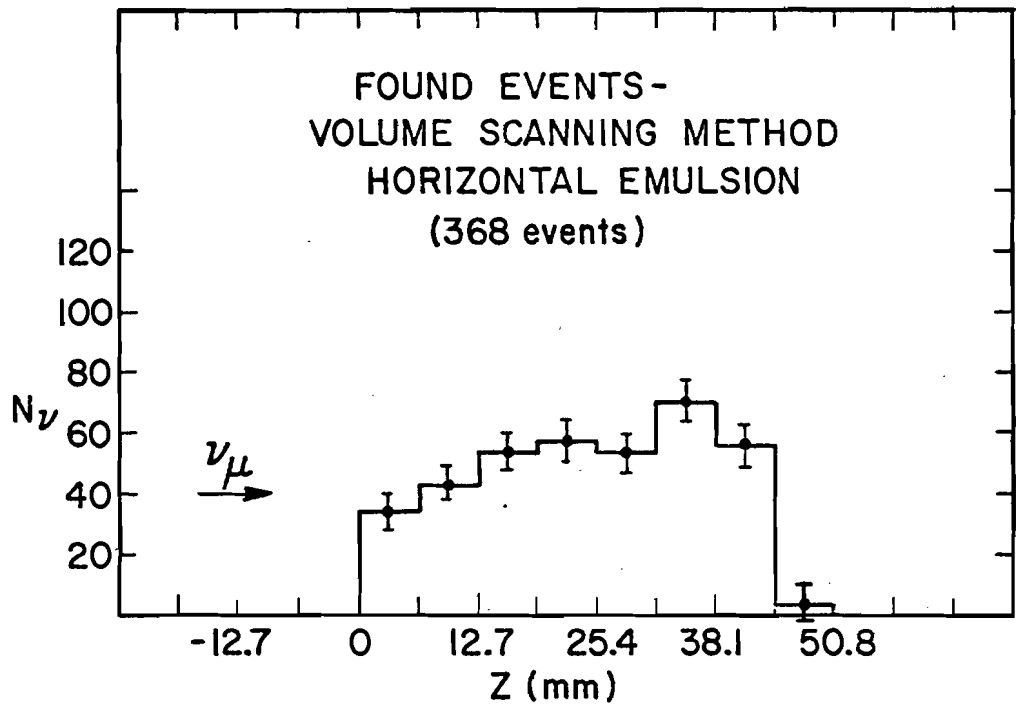

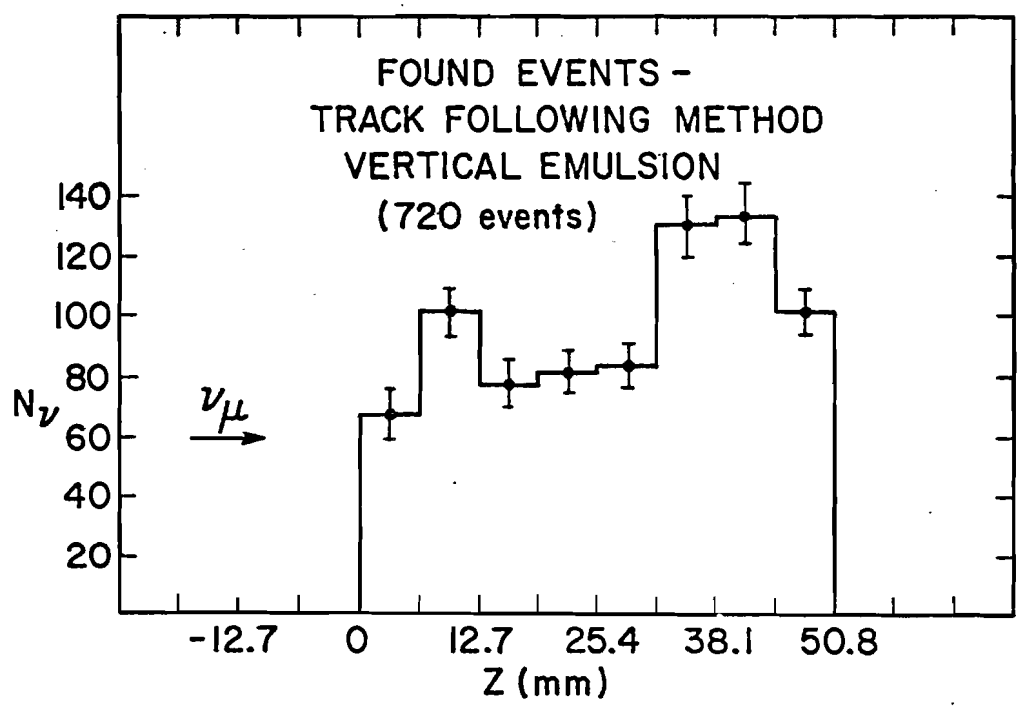

Figure 33. Found Neutrino Events vs. Z

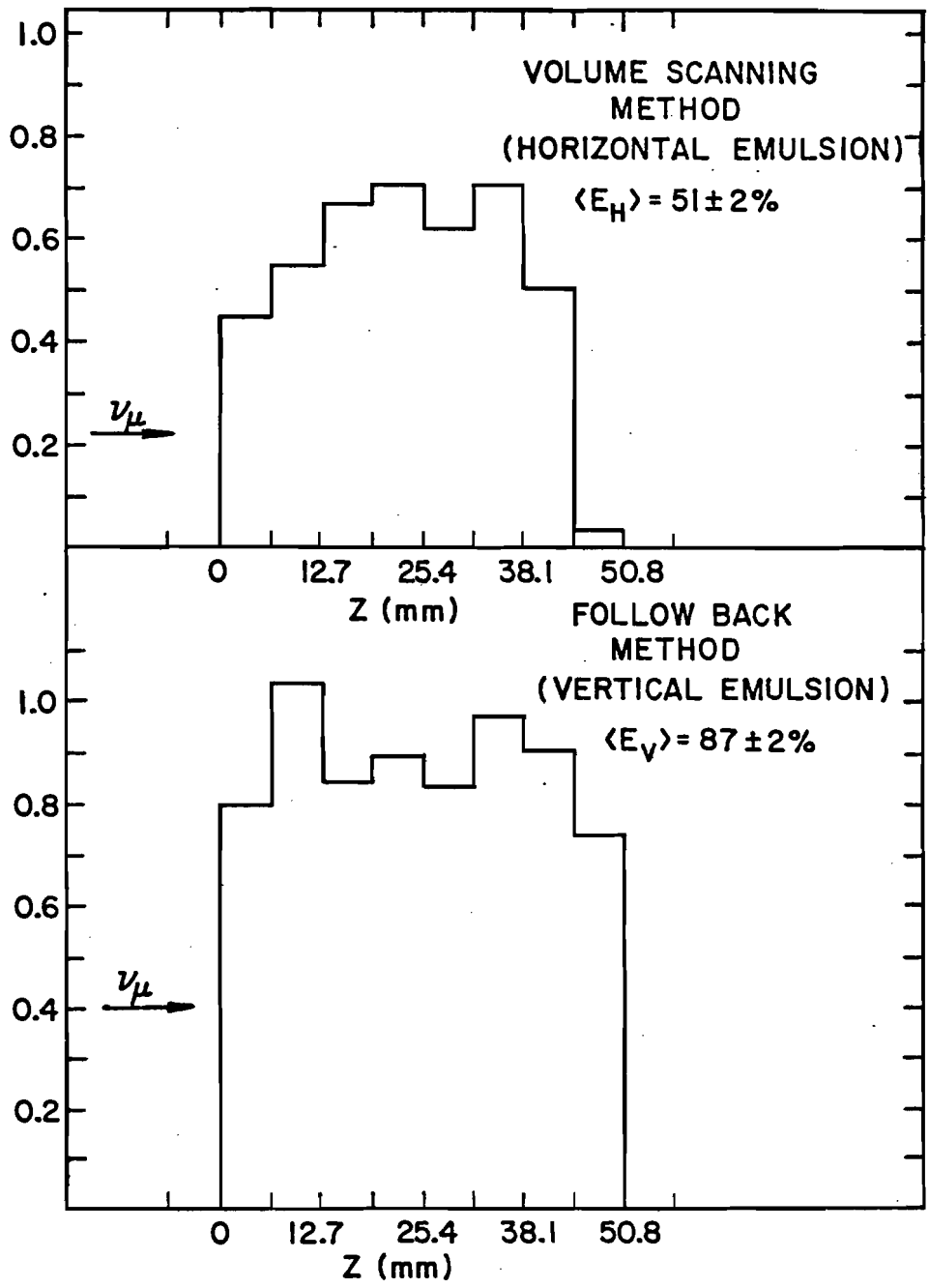

Figure 34. Event Finding Efficiency vs. Z

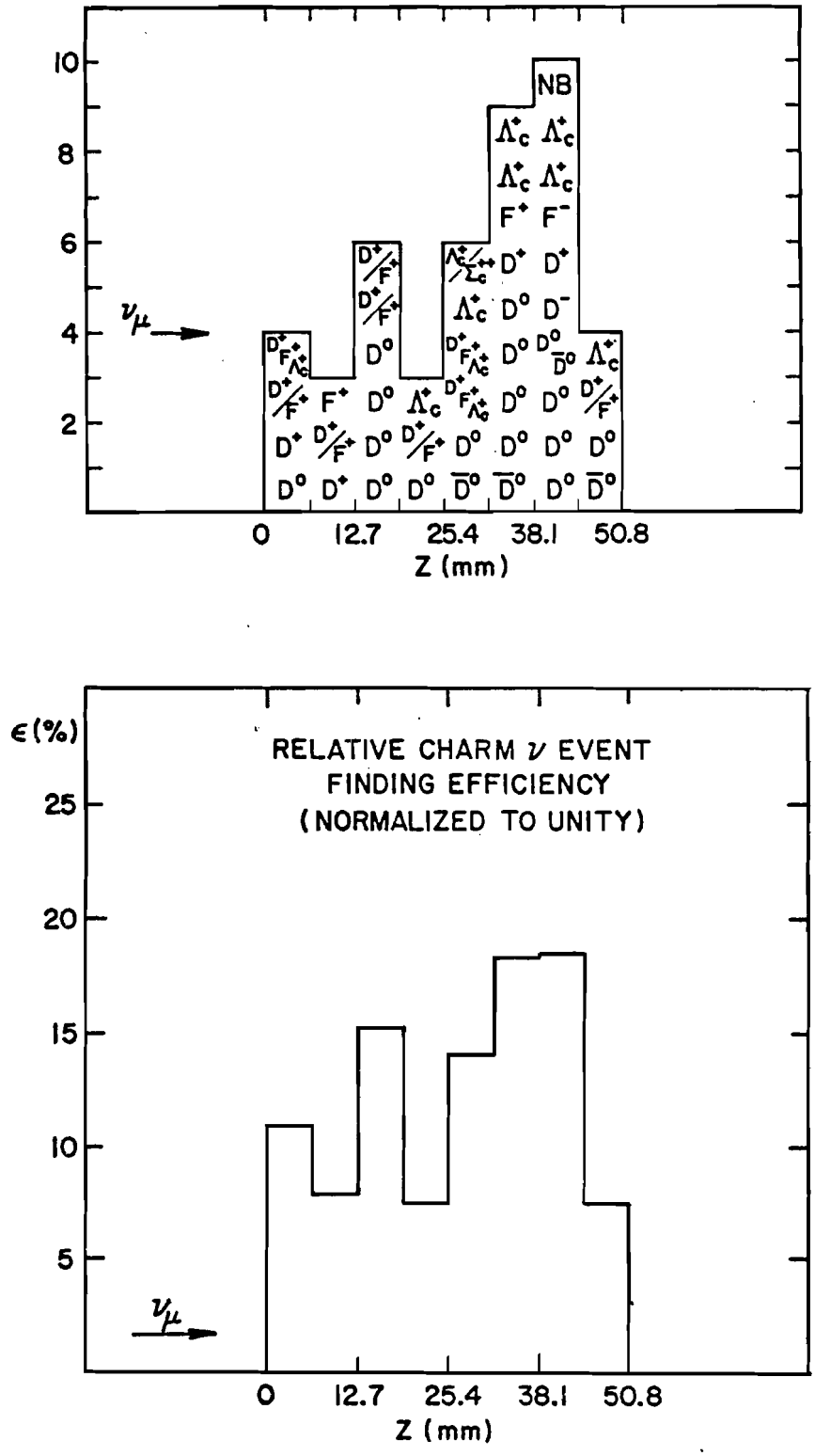

Figure 35. Charm Candidate ν-Event Distribution and Relative Charm ν-Event Finding Efficiency

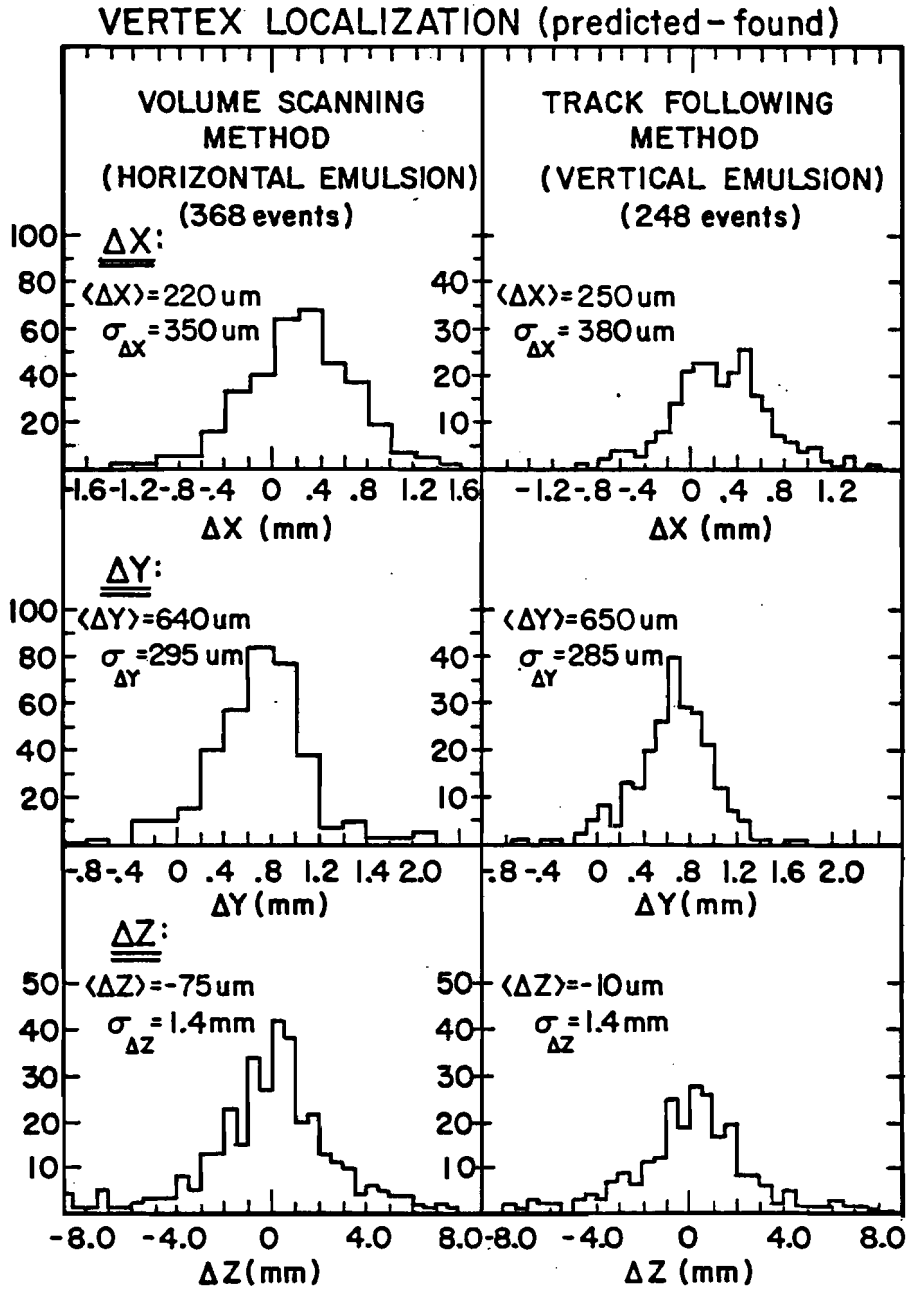

Figure 36. Predicted vs. Found Events:

Vertex Localizations

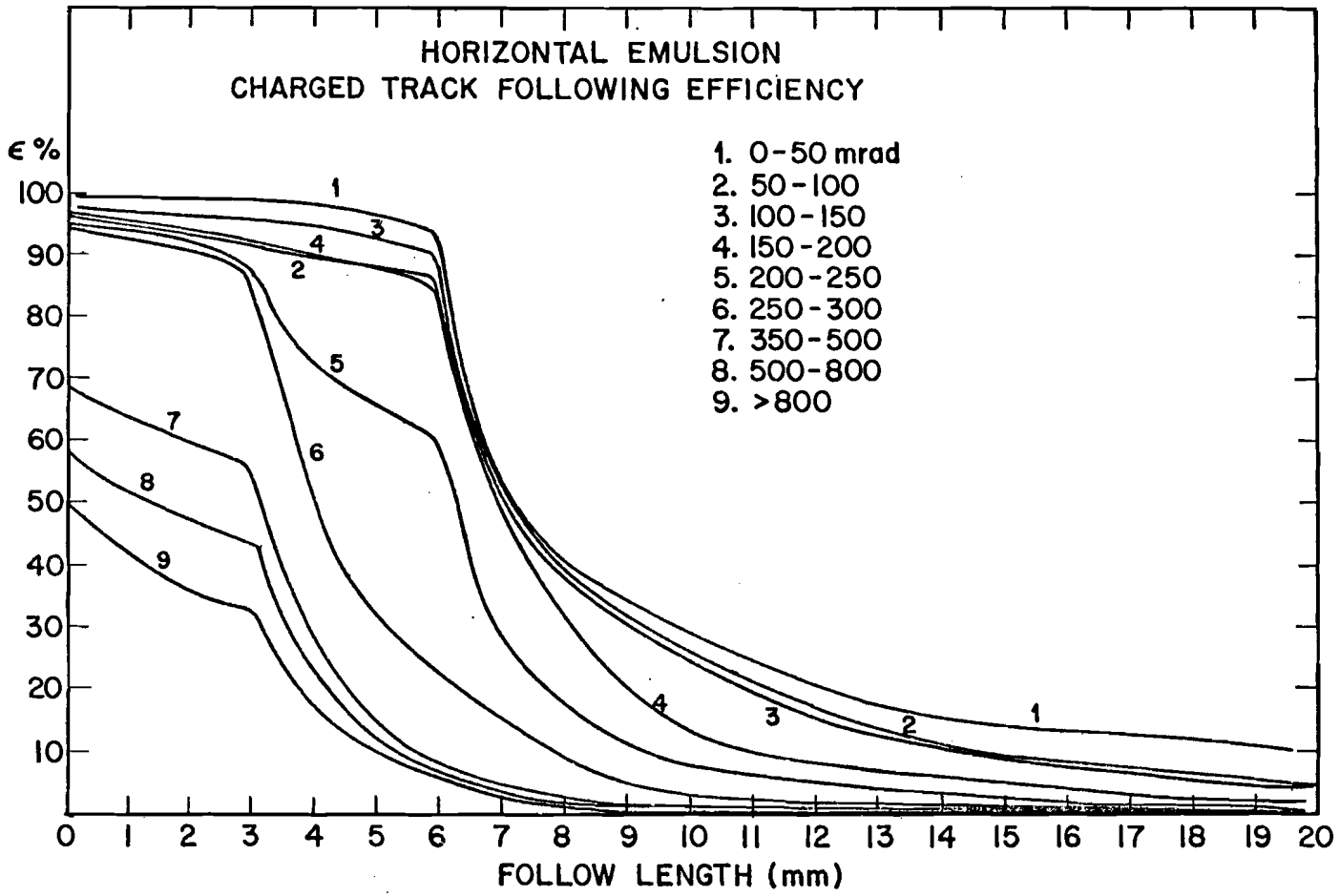

Figure 37. Charged Track Following Efficiency (Horizontal Emulsion)

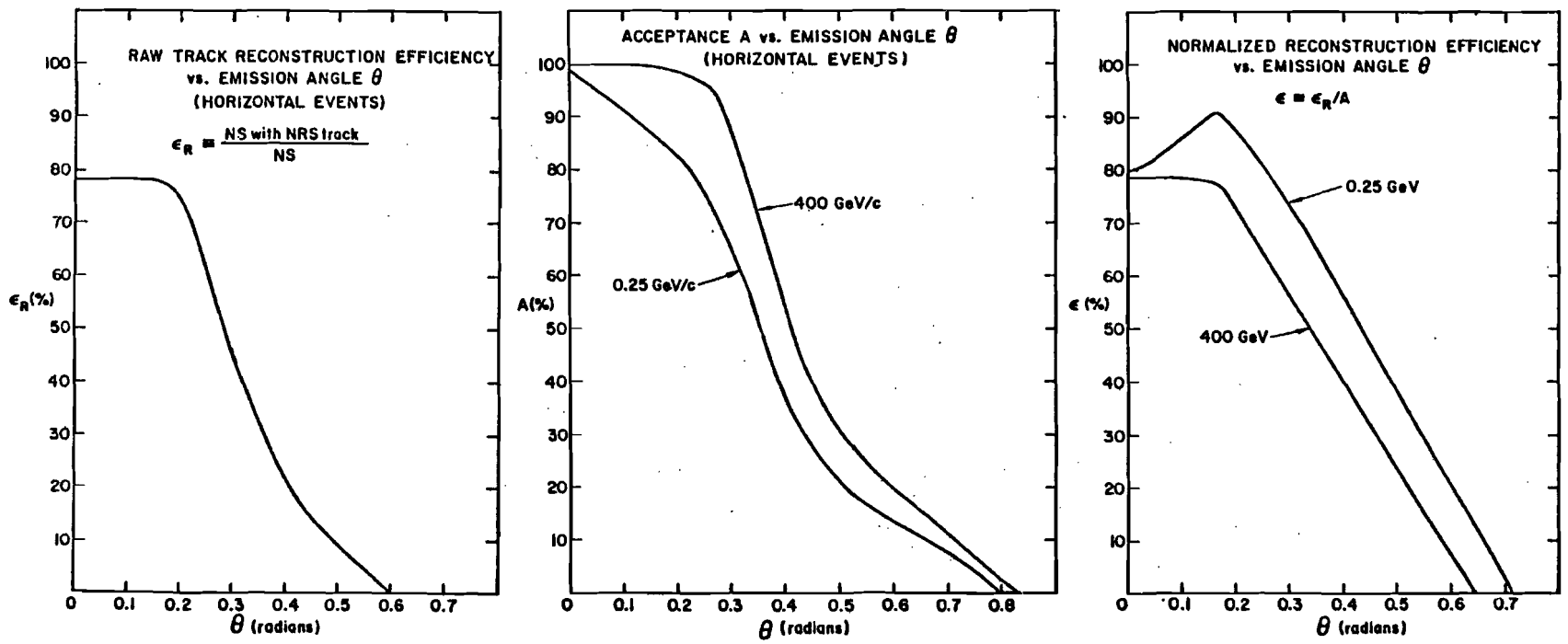

Figure 38. Track Reconstruction Efficiency vs. Emission Angle

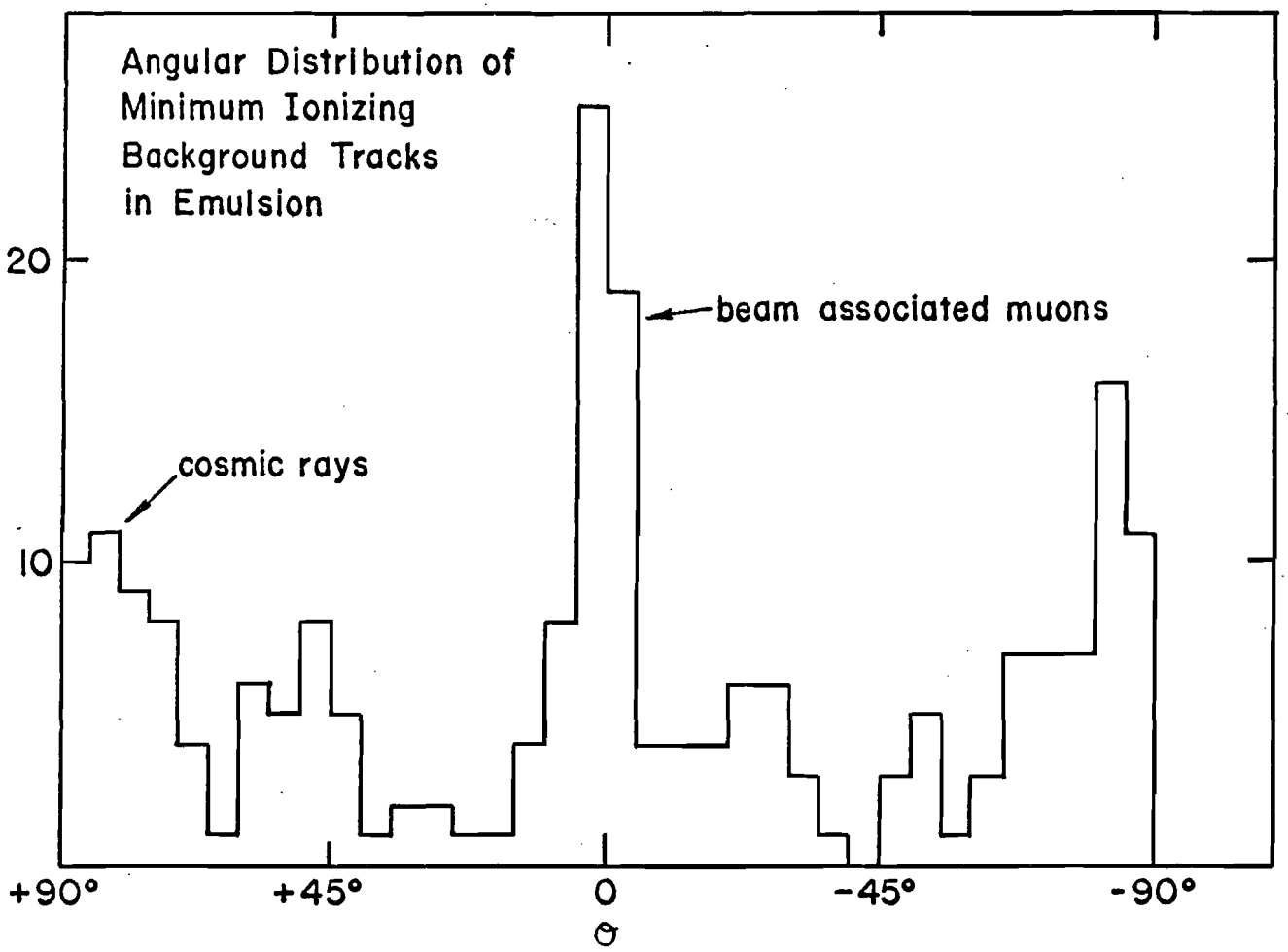

Figure 39.

Angular Distribution of Minimum Ionizing Background Tracks in Emulsion

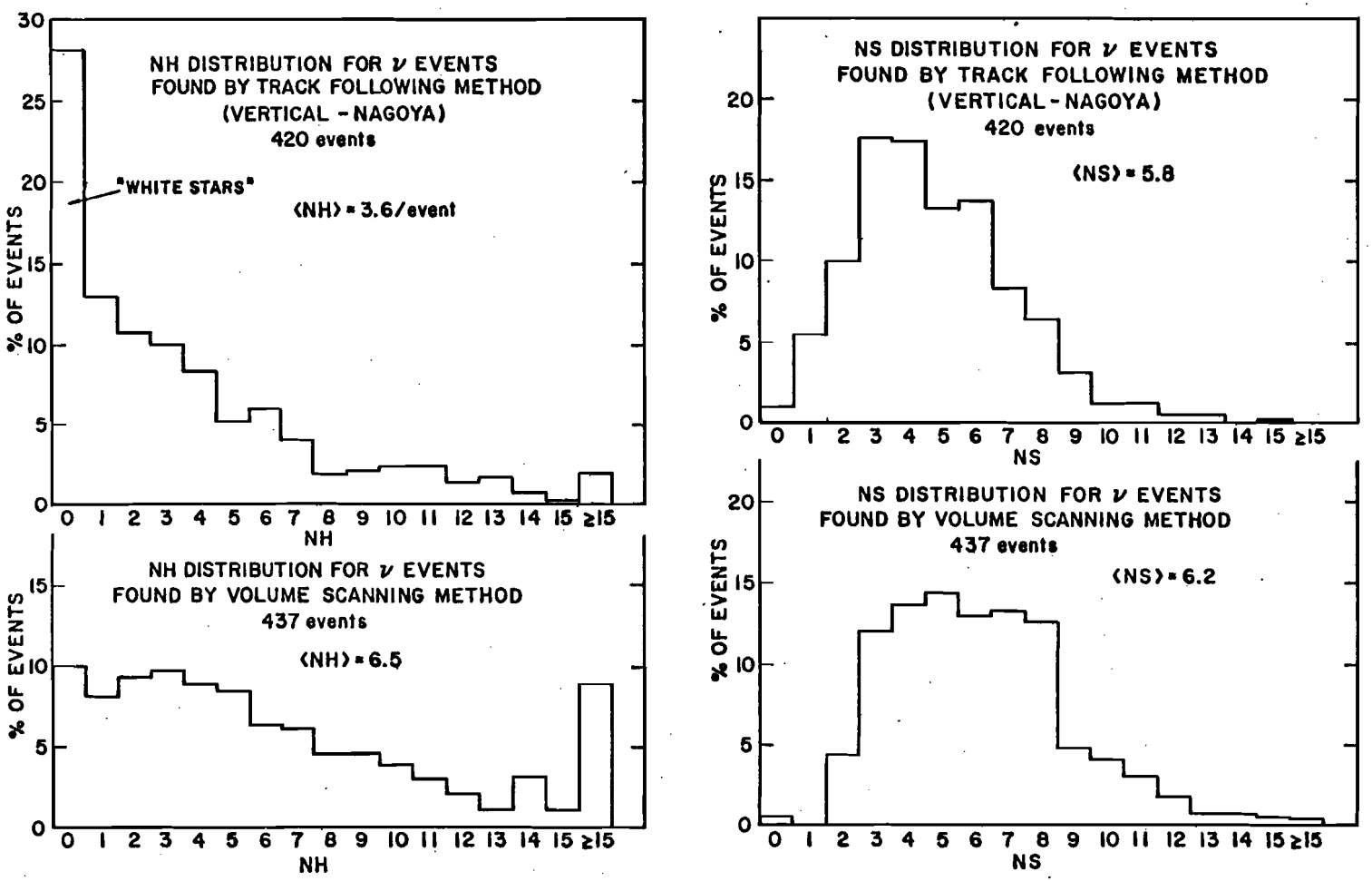

Figure 40. NH and NS Distributions for Neutrino Events

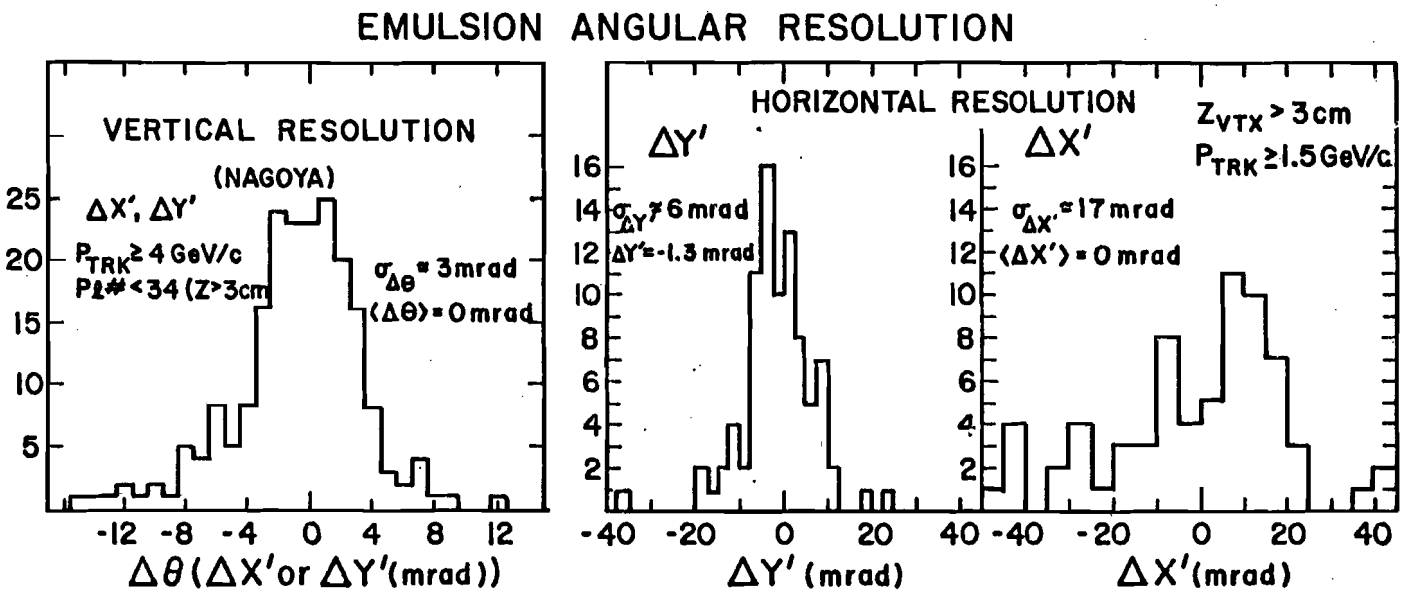

Figure 41. Emulsion Track Angular Resolution

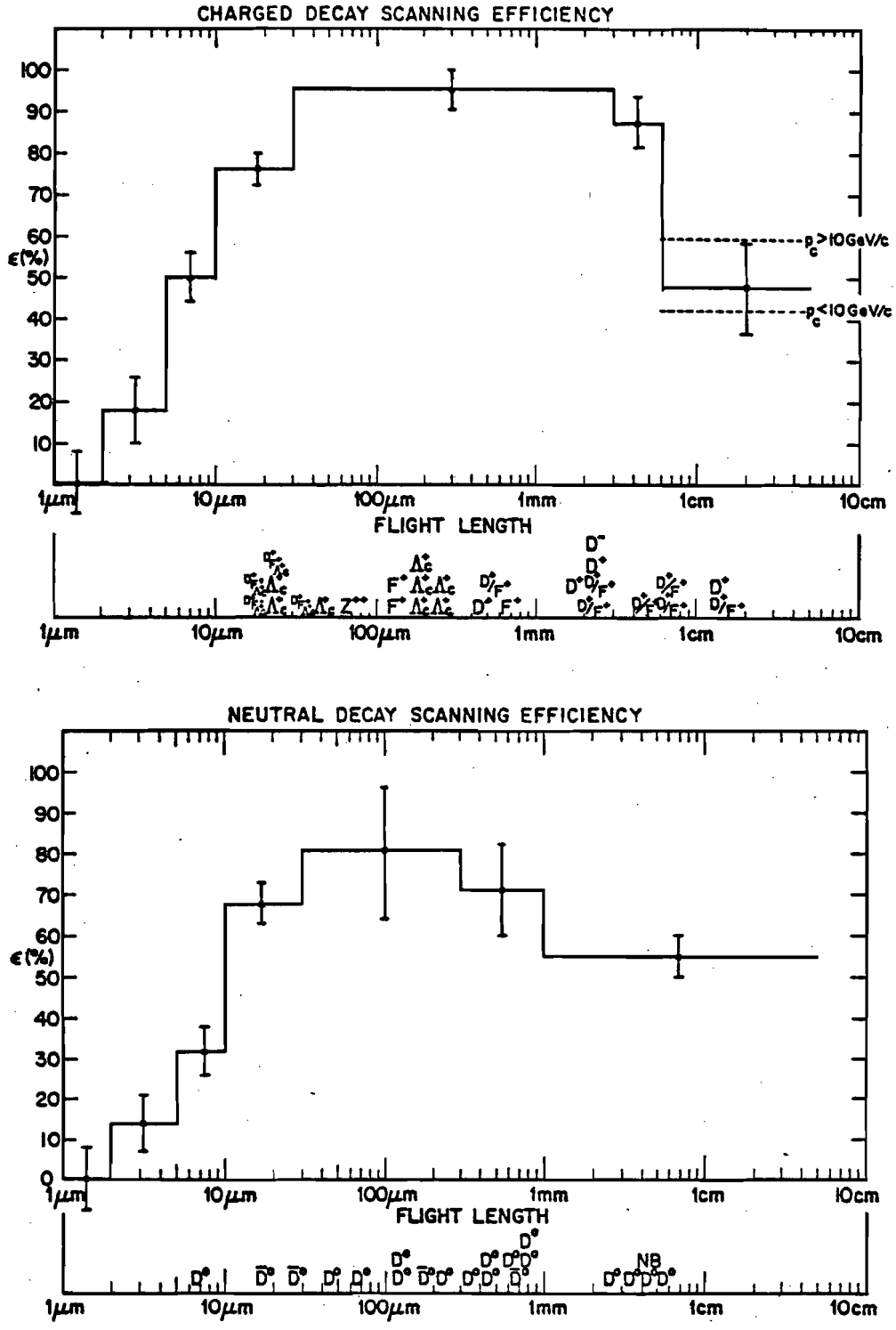

Figure 42.

Charged and Neutral Decay Scanning Efficiencies; Flight Lengths of Charmed Particles

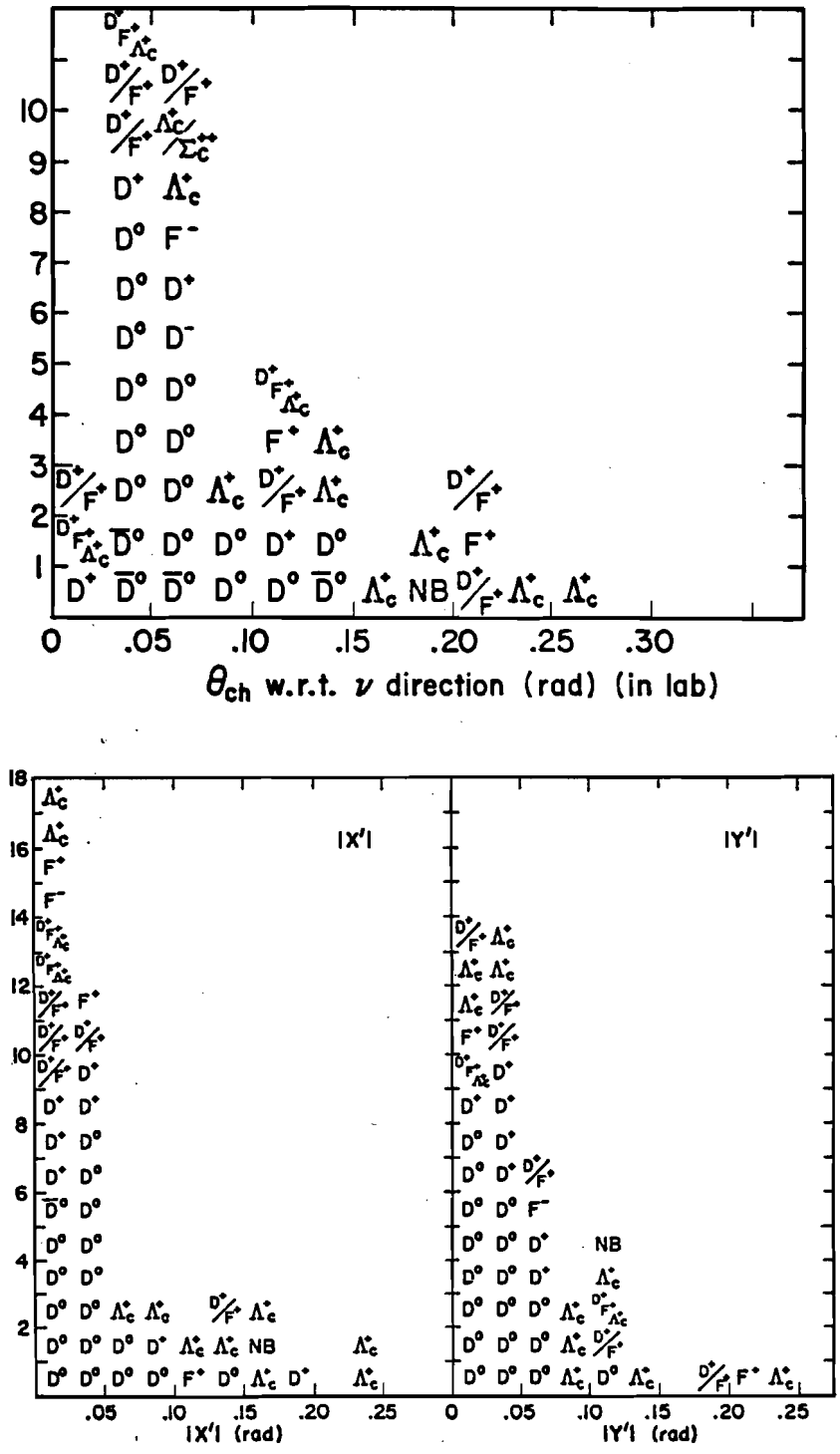

Figure 43. Charm Production Angle

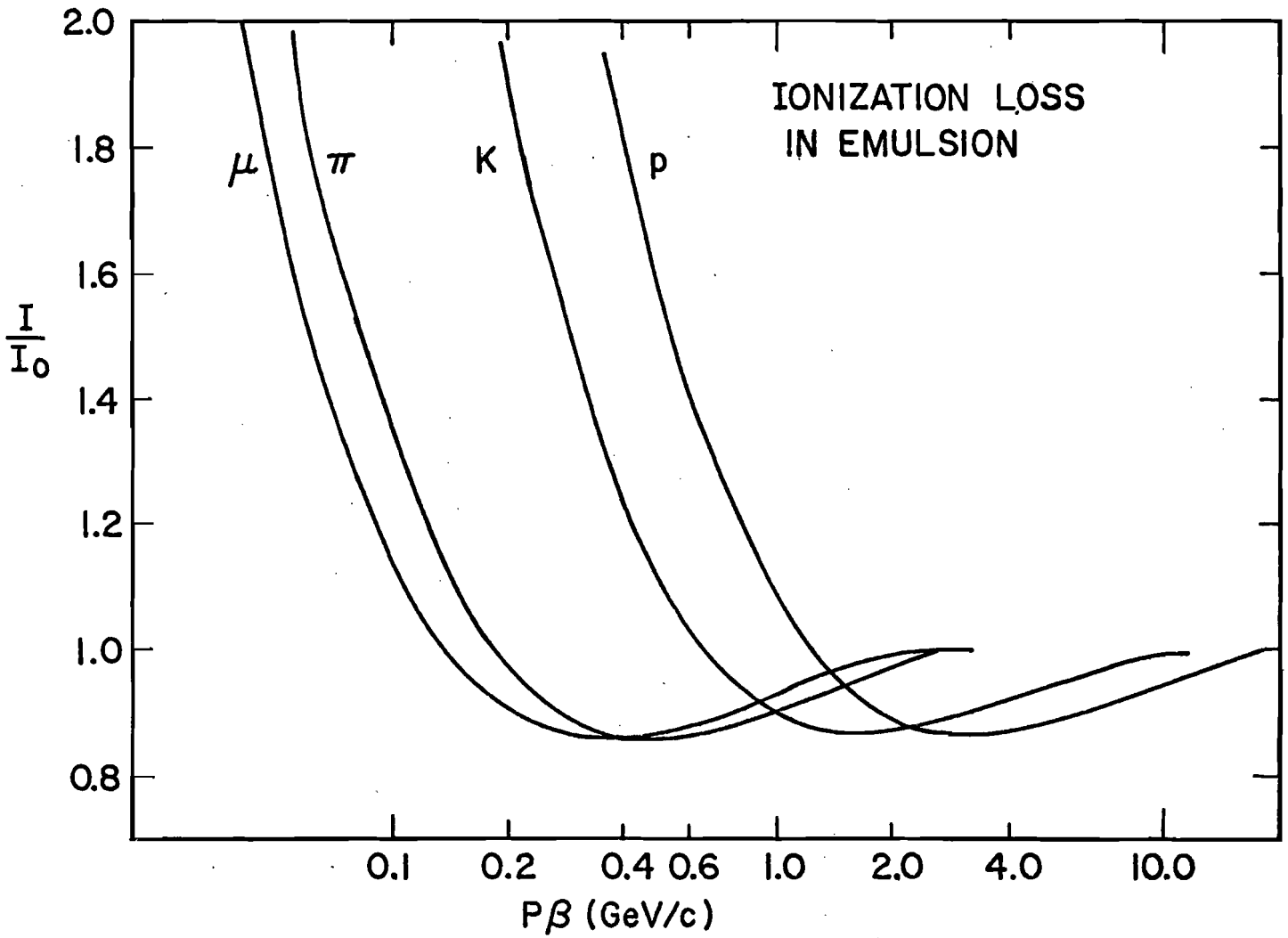

Figure 44. I/I_o vs. $P\beta$

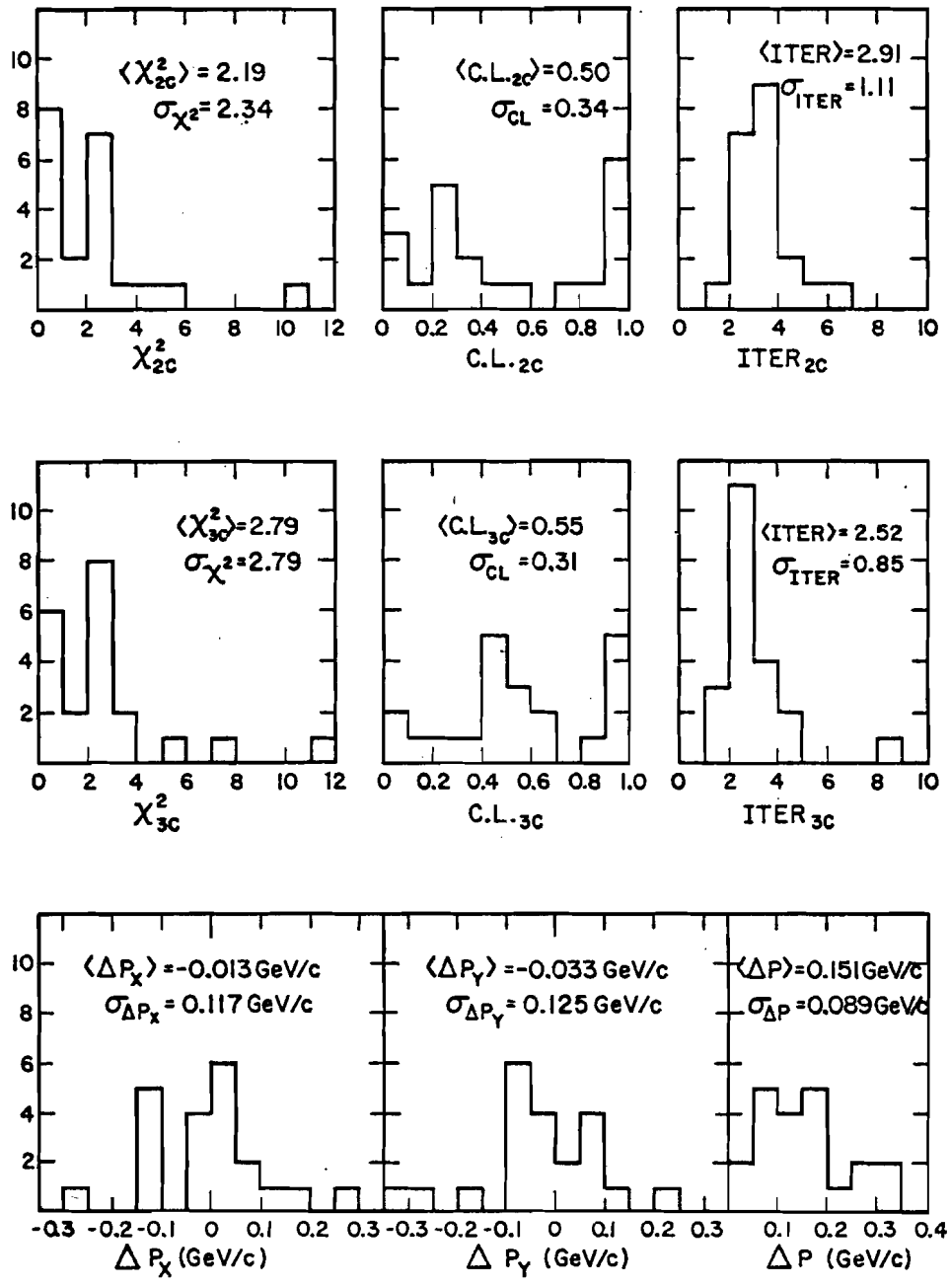

Figure 45.

χ^2, C.L., ΔP_x, ΔP_y, ΔP Distributions for Charm Decays

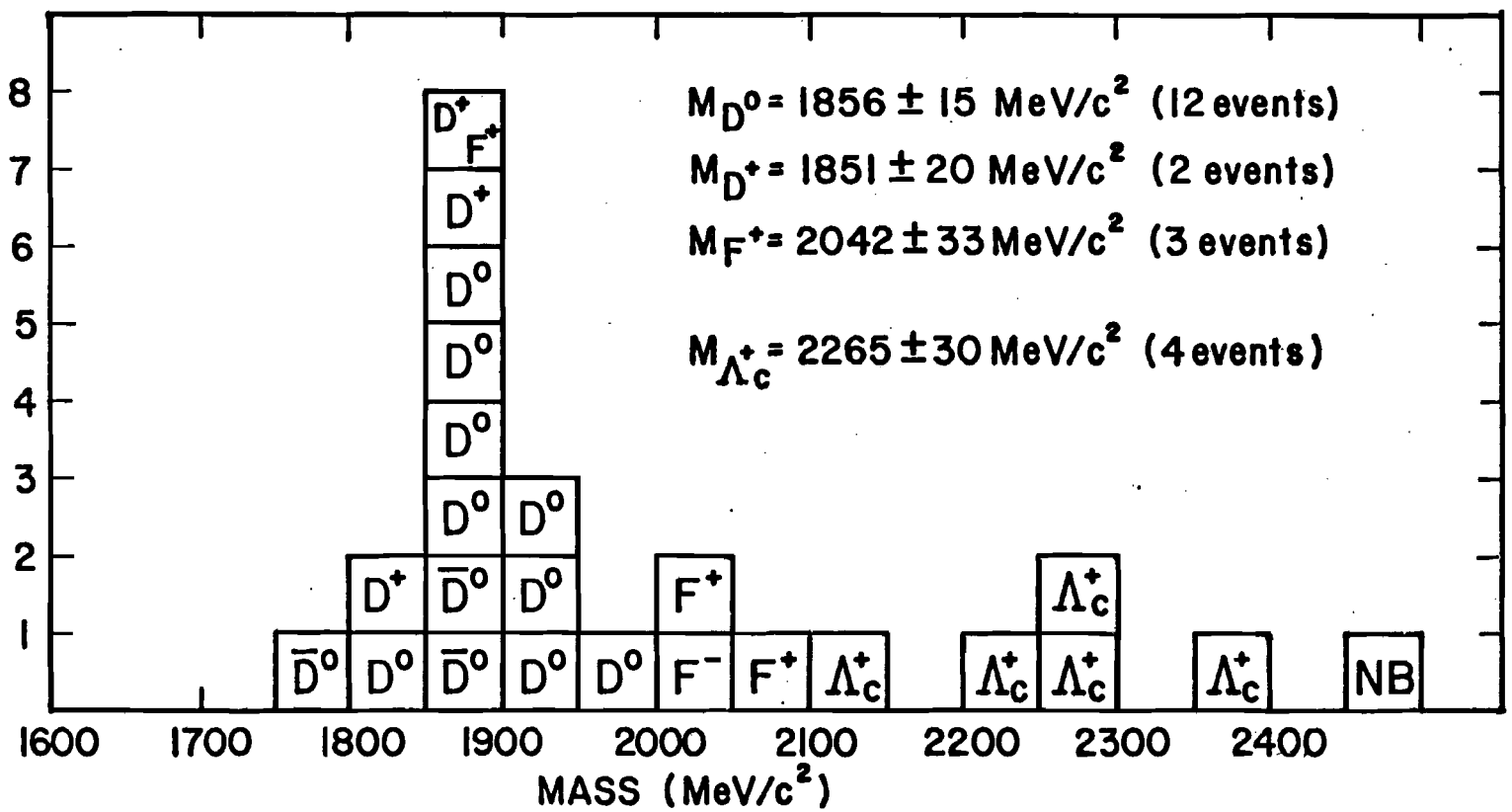

Figure 46. Charmed Particle Masses

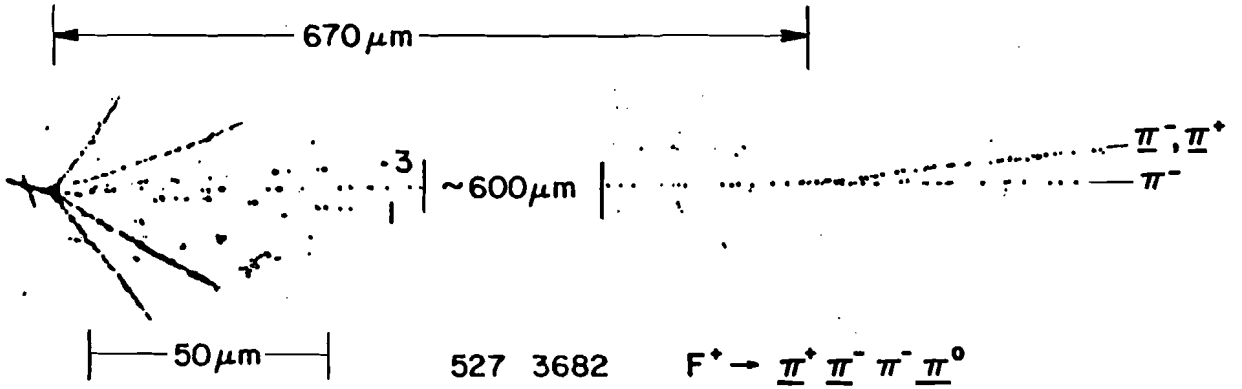

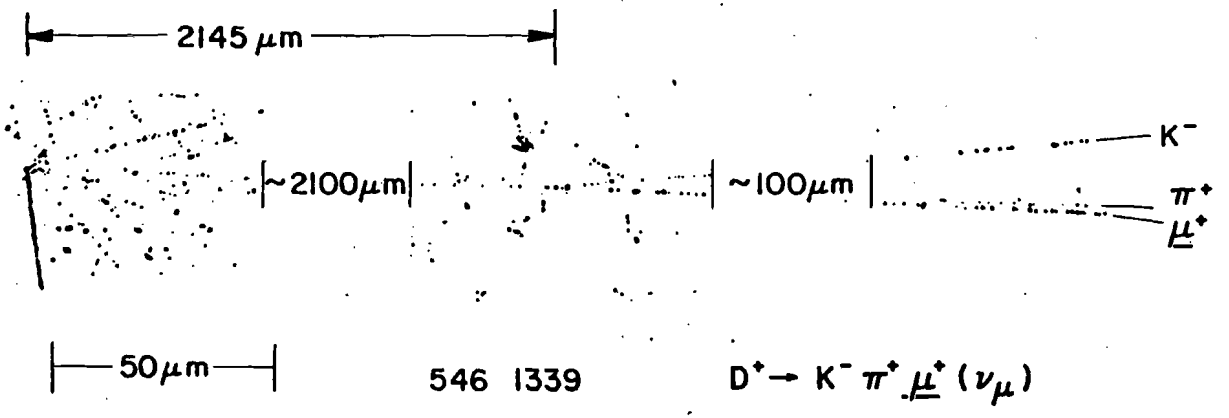

Figure 47. Photo-Micrographs of Event 546-1339 and Event 527-3682

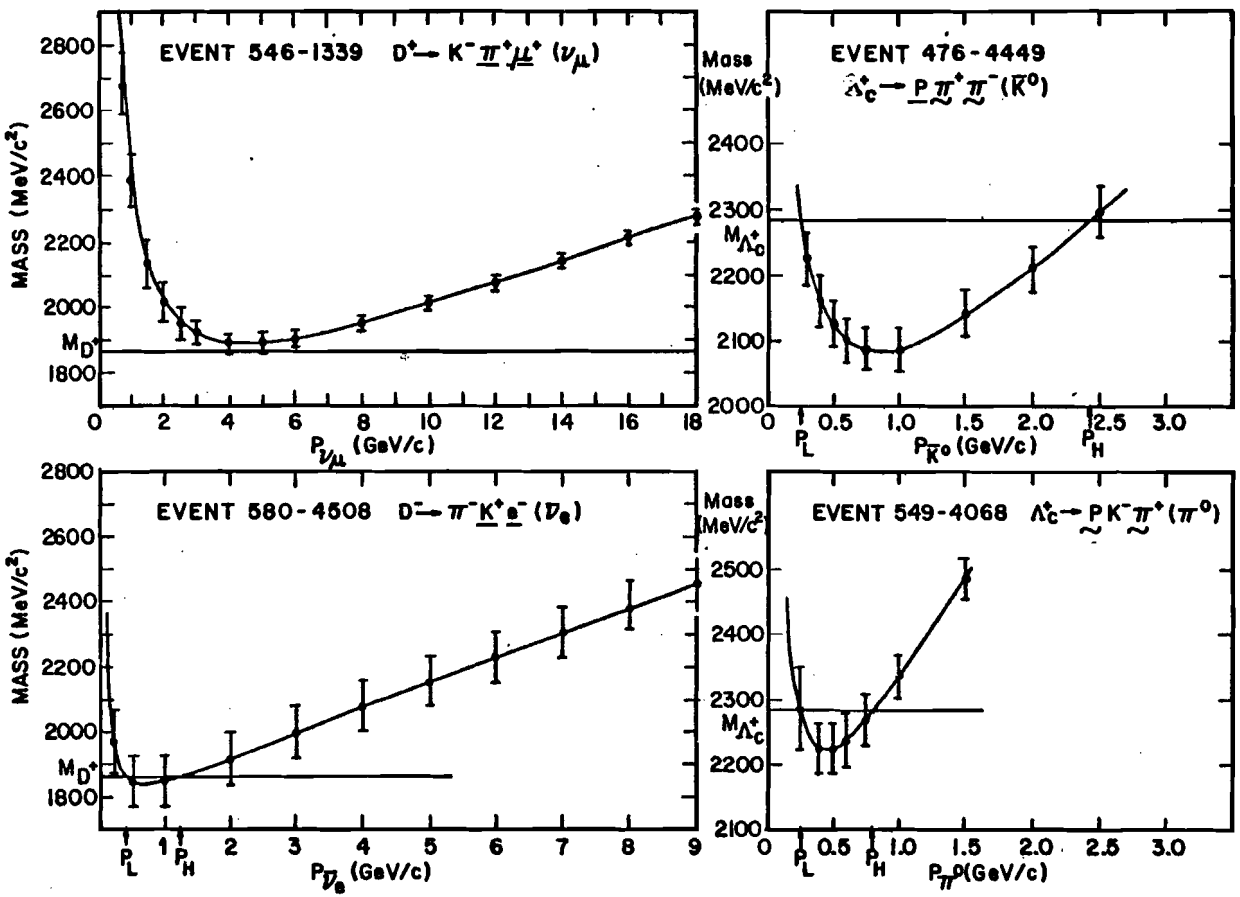

Figure 48. -1C Curves for Events with a Missing Neutral

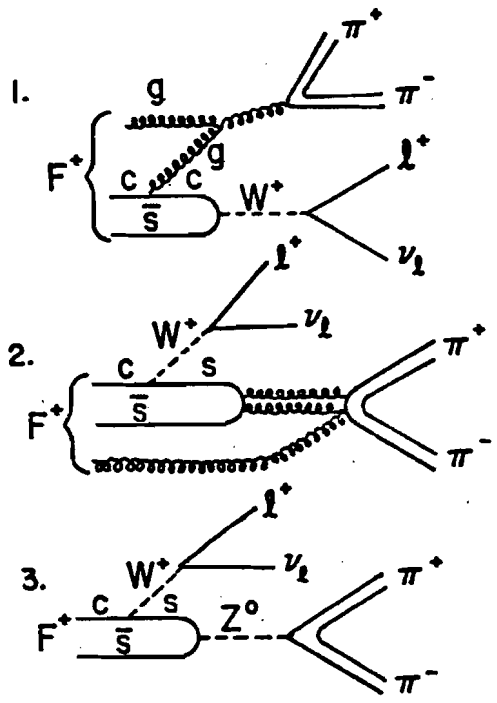

$c\bar{s}$ annihilation to $\ell^+\nu_\ell$ (color singlet)
gluon bremstrahlung
$g + ng \rightarrow \pi^+\pi^-$

Zweig supressed
$c \rightarrow s$ W−radiation
$s\bar{s}$ annihilation
(color singlet or non-singlet)

"2nd order" Weak process
$s\bar{s}$ weak annihilation
(color singlet)
extremely small contribution

Figure 49.

F^+ Background for Semi-Leptonic D^+ Decays:

$F^+ \rightarrow \pi^+\pi^-\ell^+(\nu_\ell)$ Decay Diagrams

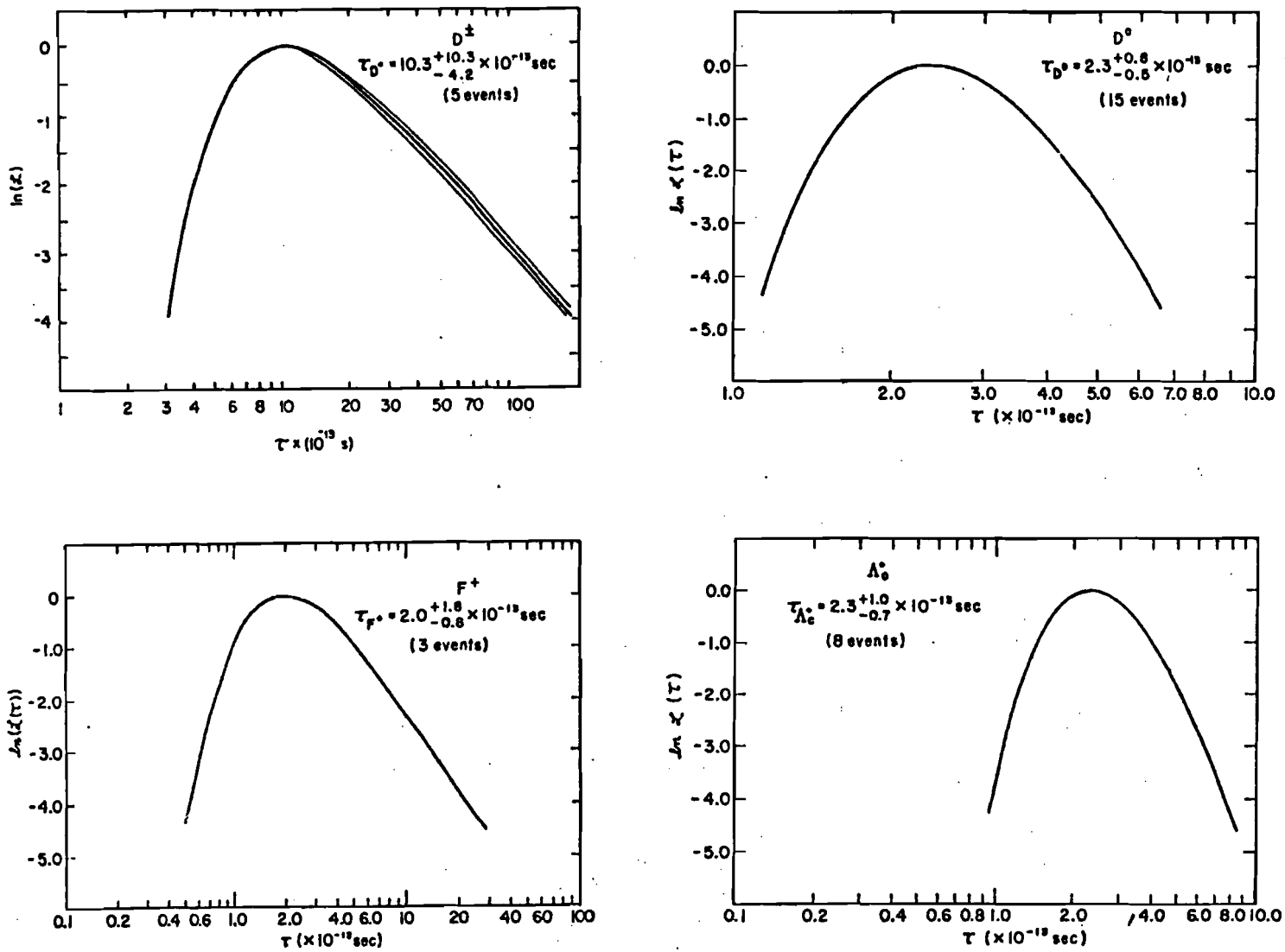

Figure 50. D^+, D^0, F^+, Λ_c^+ $\ln \mathscr{L}(\tau)$ vs. τ

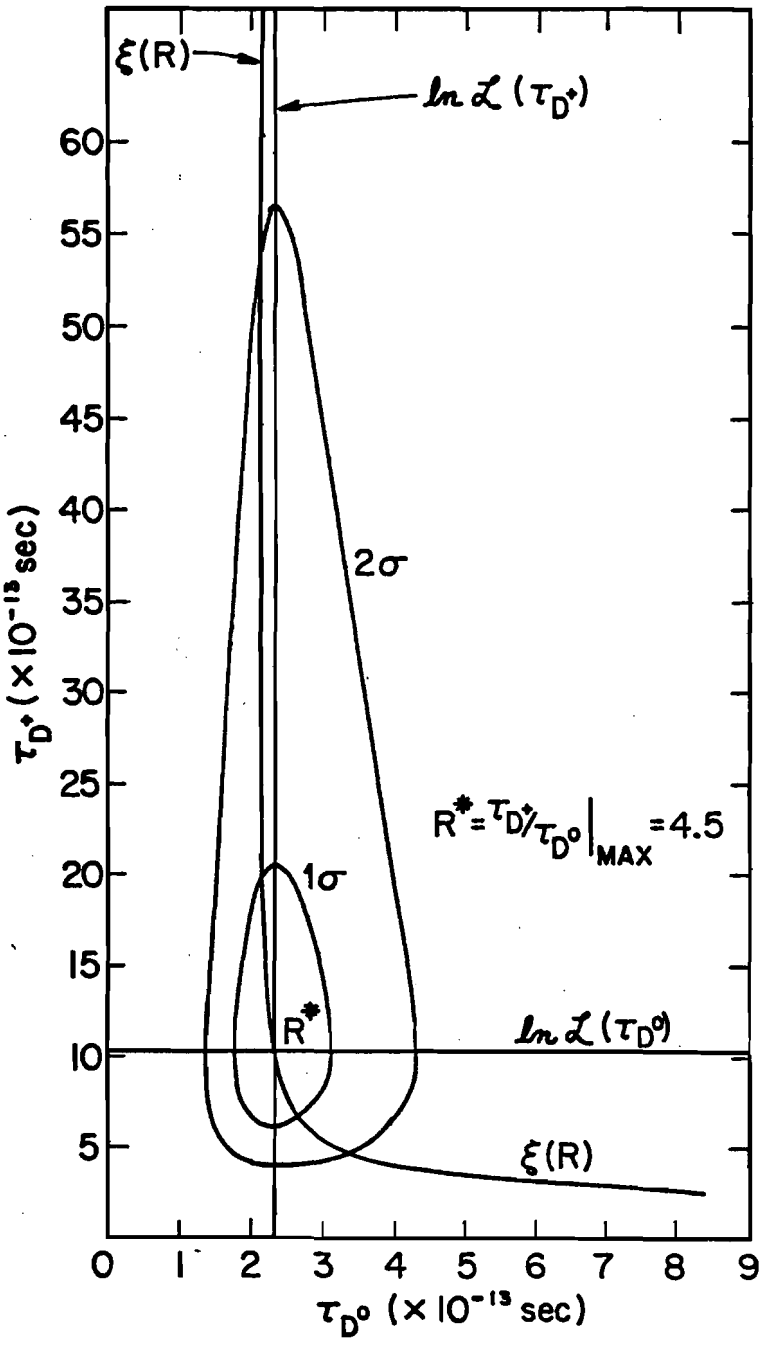

Figure 51. D^+/D^0 Lifetime Ratio:

1 and 2 S.D. Contours

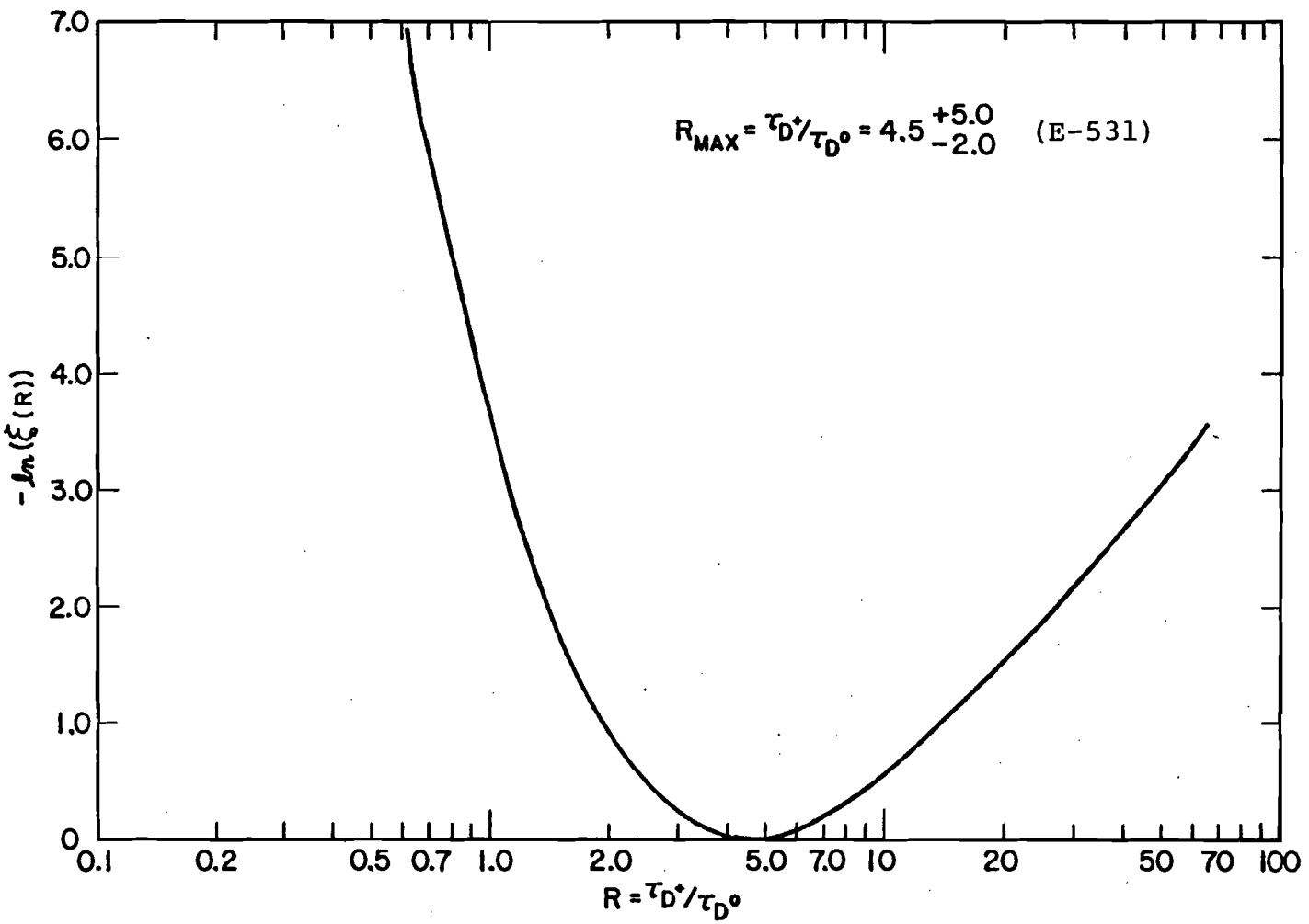

Figure 52. Likelihood Function $\xi(R)$ for D^+/D^0 Lifetime Ratio

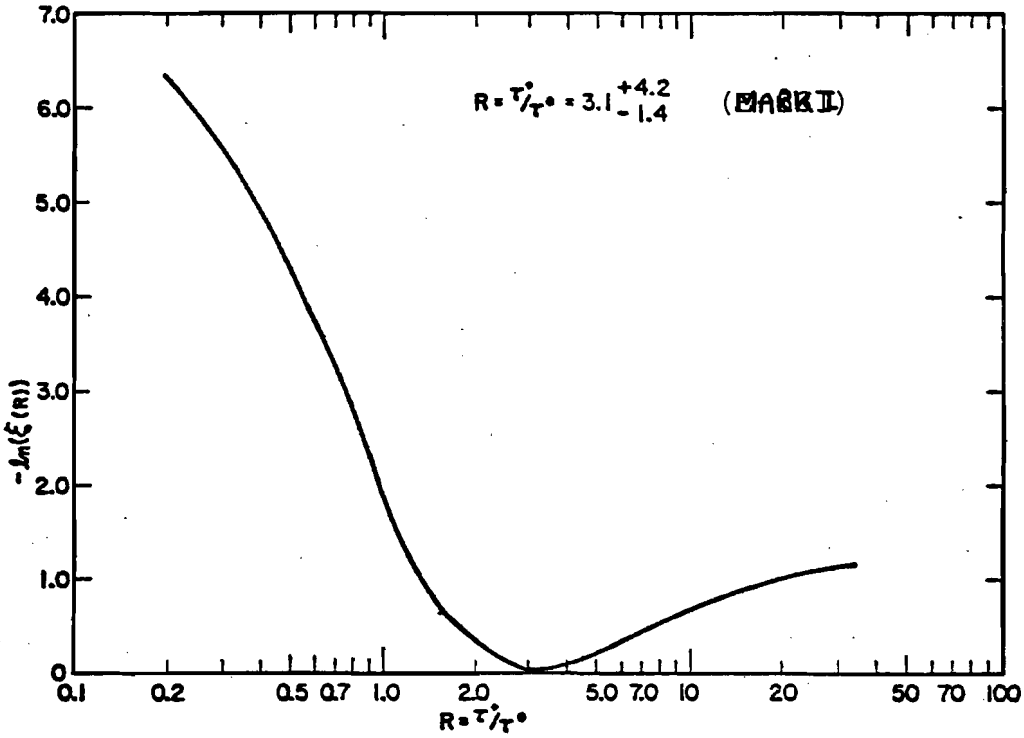

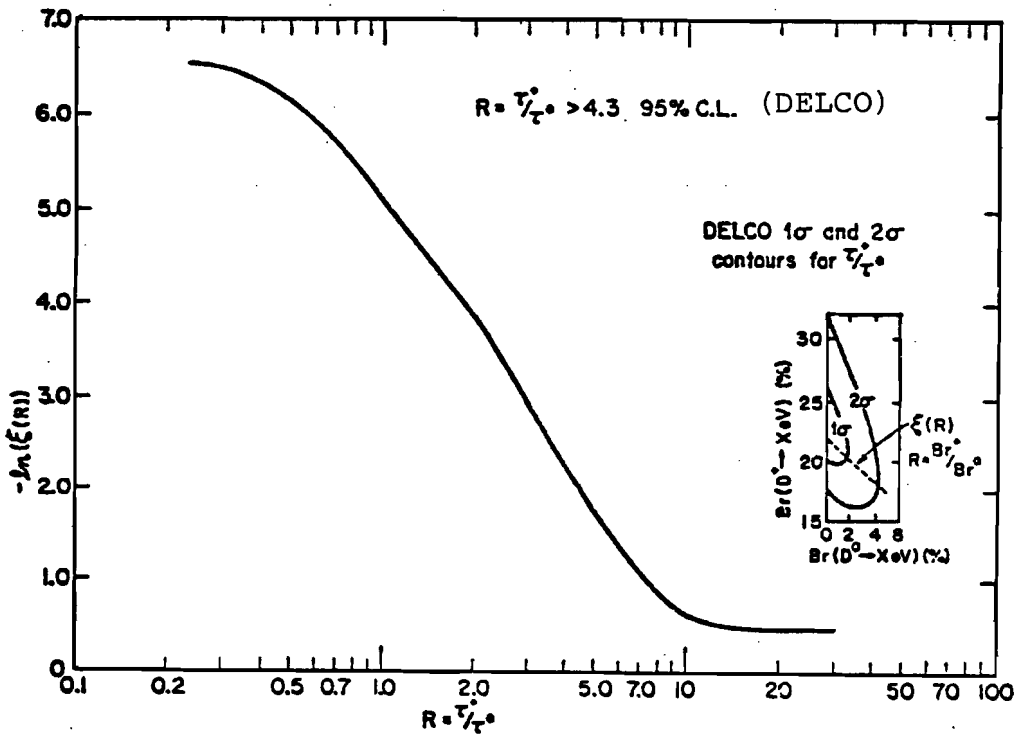

Figure 53. Likelihood Functions $\xi(R)$ for D^+/D^0 Lifetime Ratio: Mk. II and DELCO

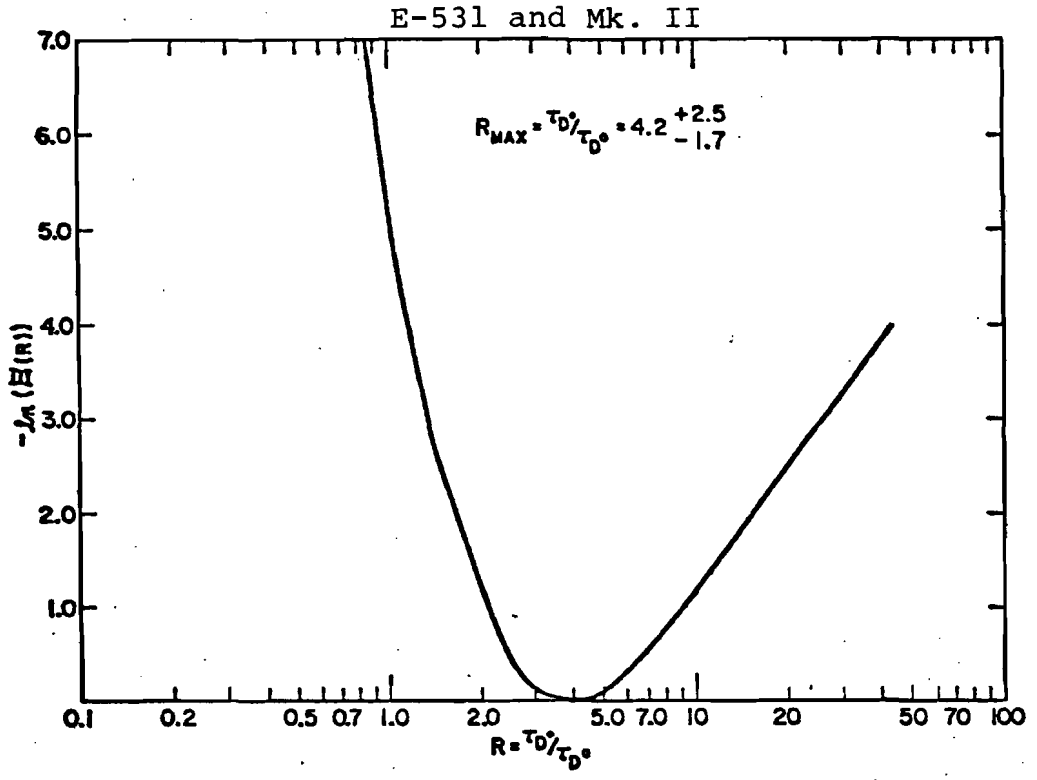

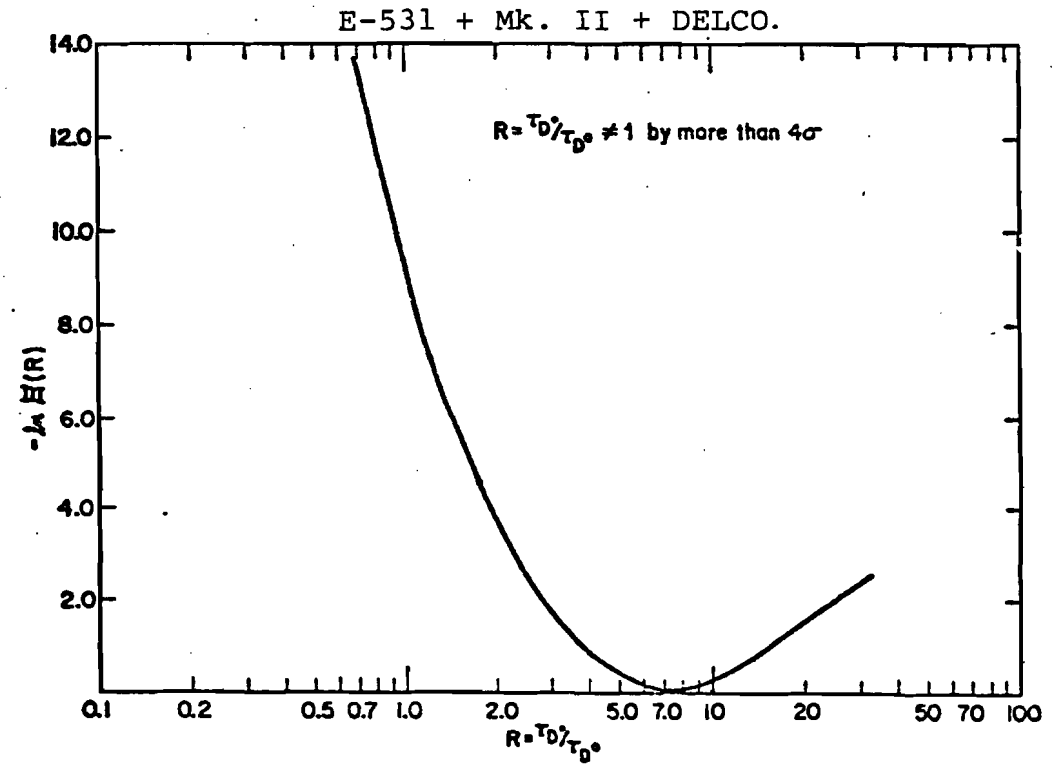

Figure 54. Combined Likelihood Functions $\Xi(R)$ for D^+/D^0 Lifetime Ratio: E-531, Mk. II and DELCO

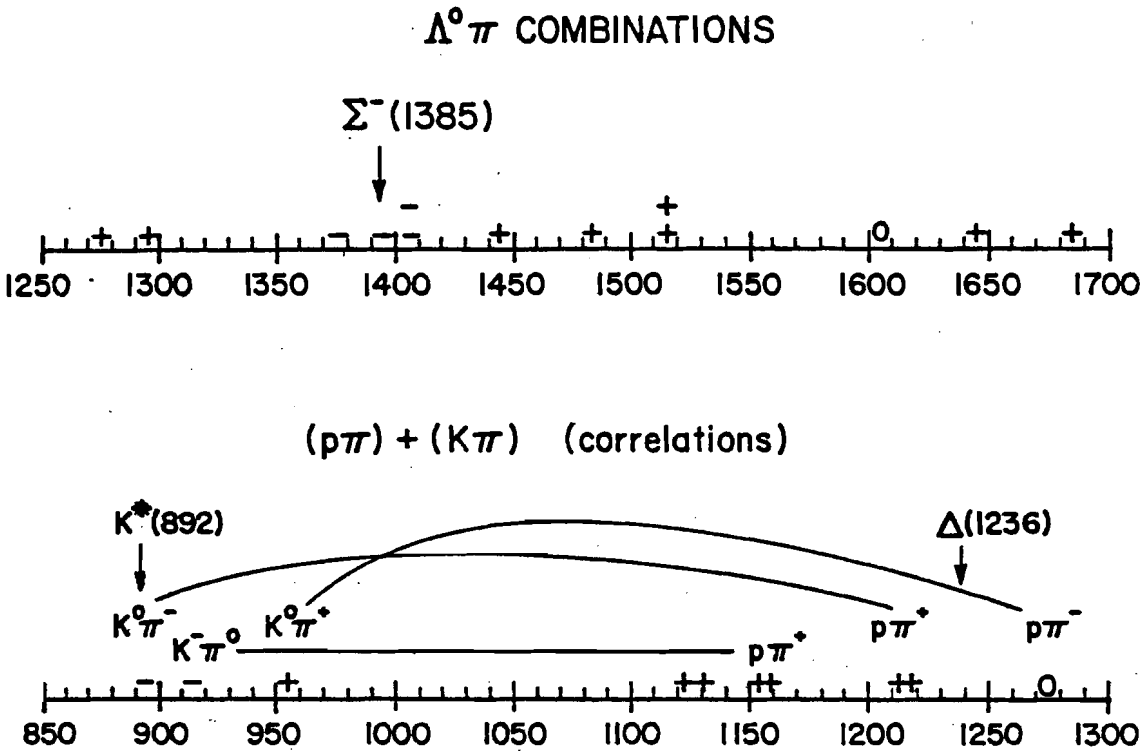

Figure 55.
Λ_c^+ Decay: $\Lambda^0-\pi^\pm$, $(p-\pi^\pm)(K^{-,0}-\pi^\pm)$ Mass Combinations

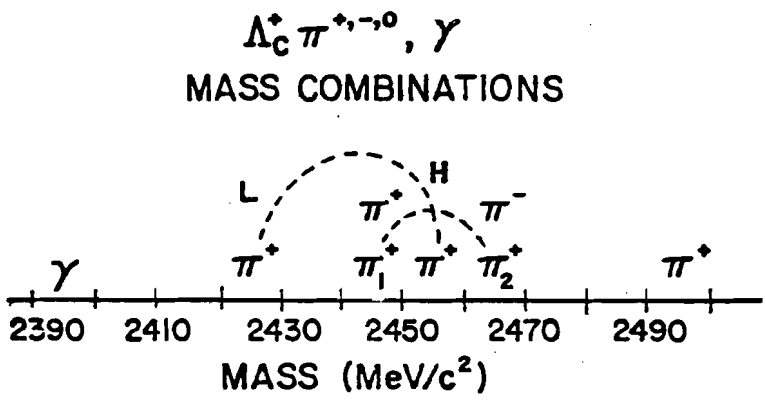

Figure 56. $\Lambda_c^+-\pi^{\pm,0}$ Mass Combinations

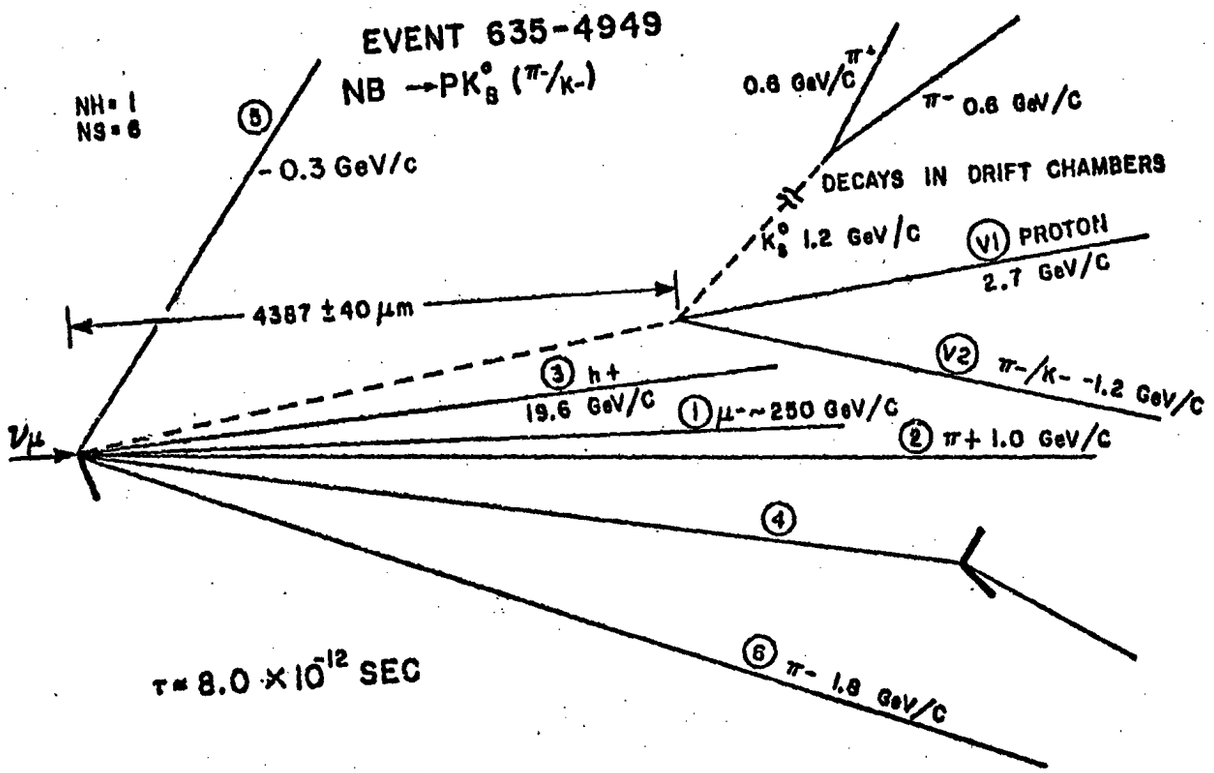

Figure 57. Event 635-4949

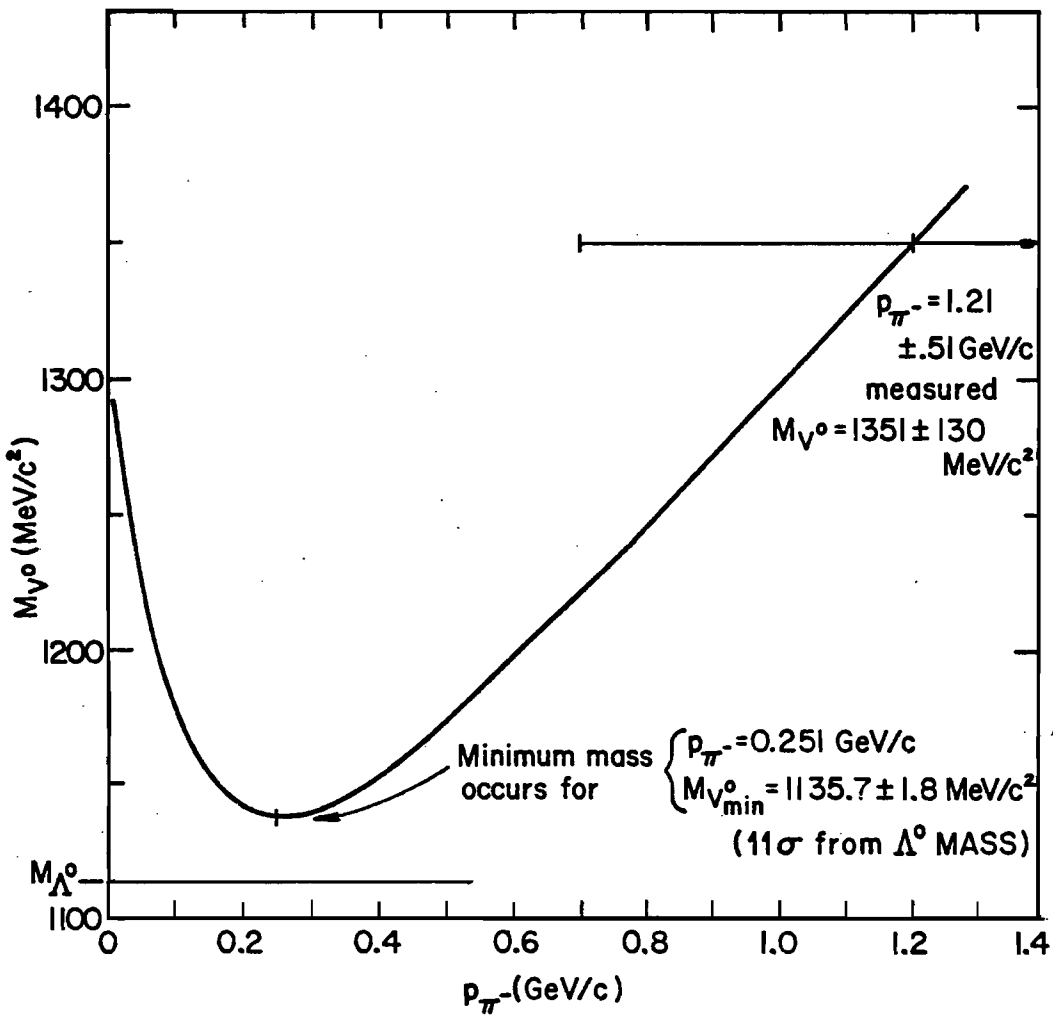

Figure 58. -1C Curve for $V^o \rightarrow p\ \pi^-$ (V_1 - V_2)

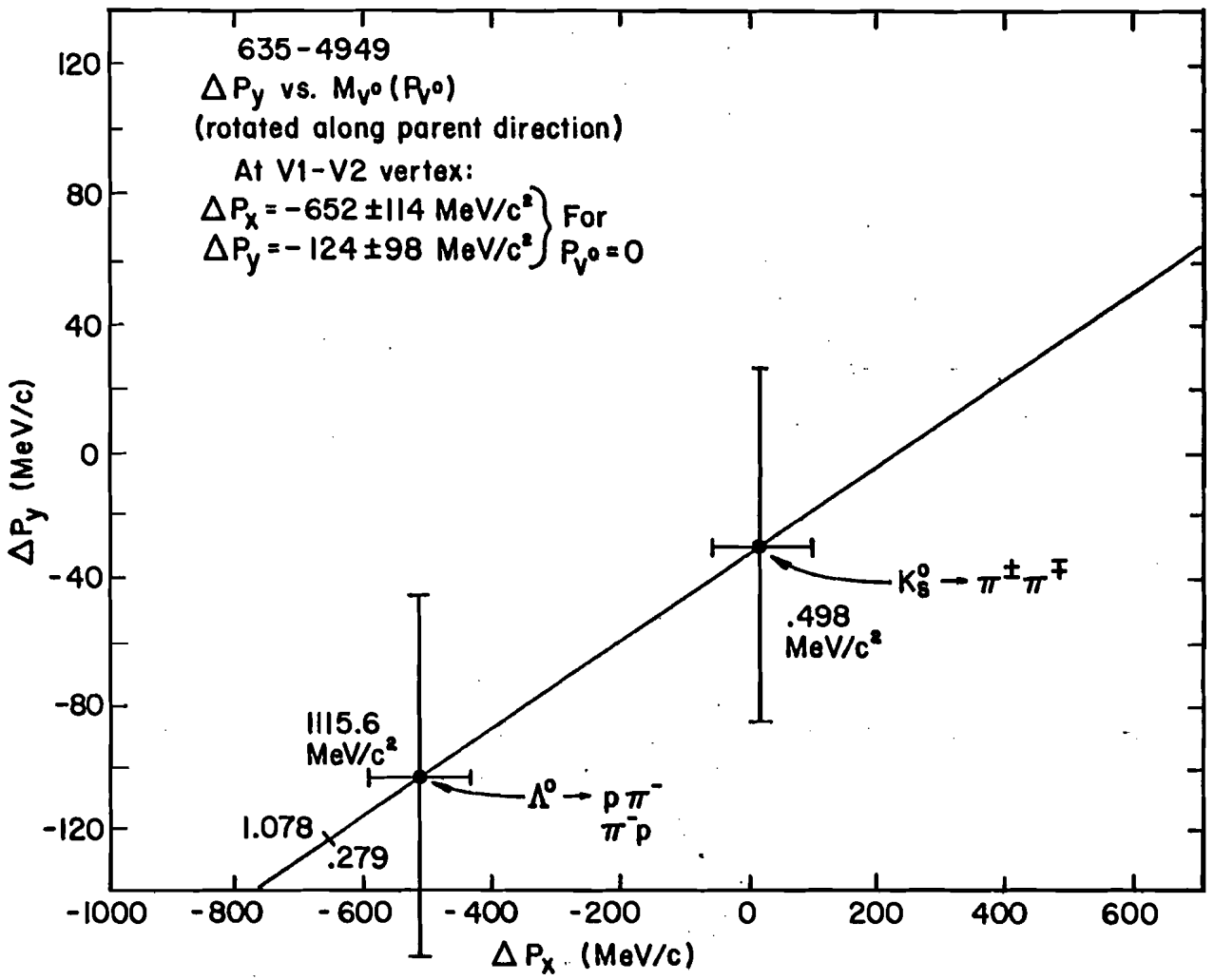

Figure 59. ΔP_x, ΔP_y vs. $M_{V^0}(P_{V^0})$

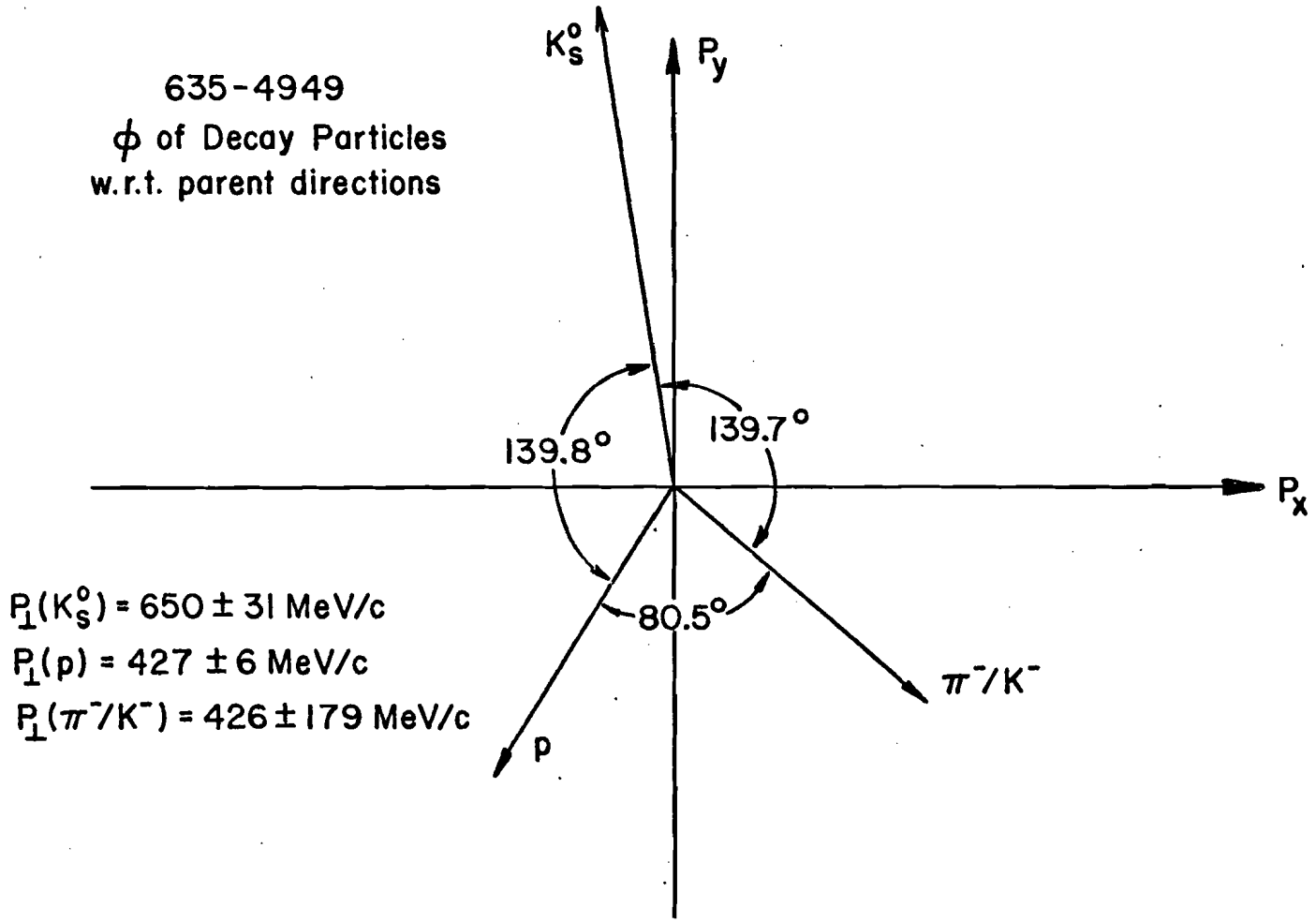

Figure 60. ϕ of Decay Particles

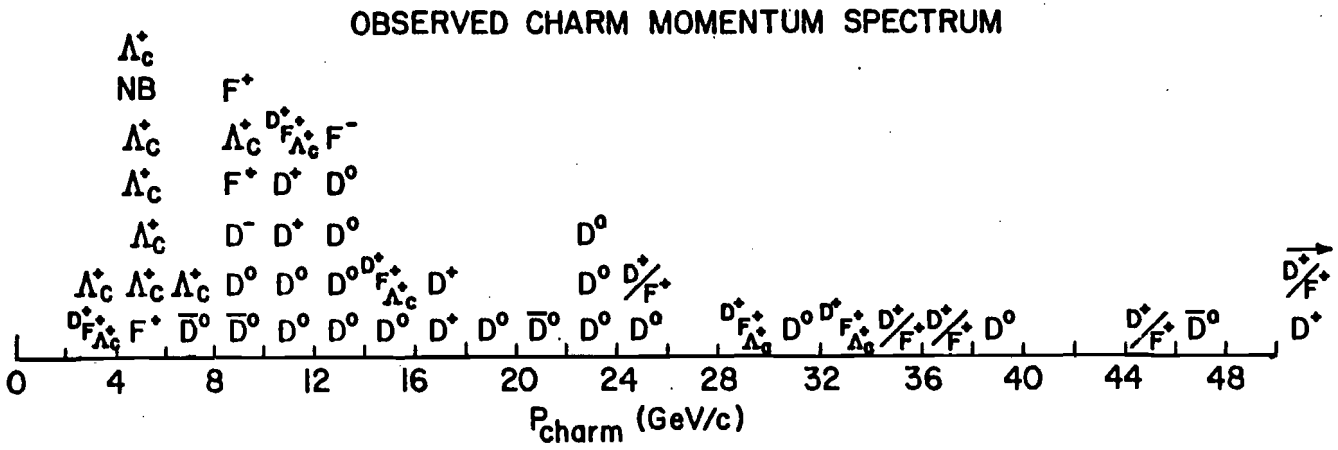

Figure 61. Charmed Particle Momentum Spectrum

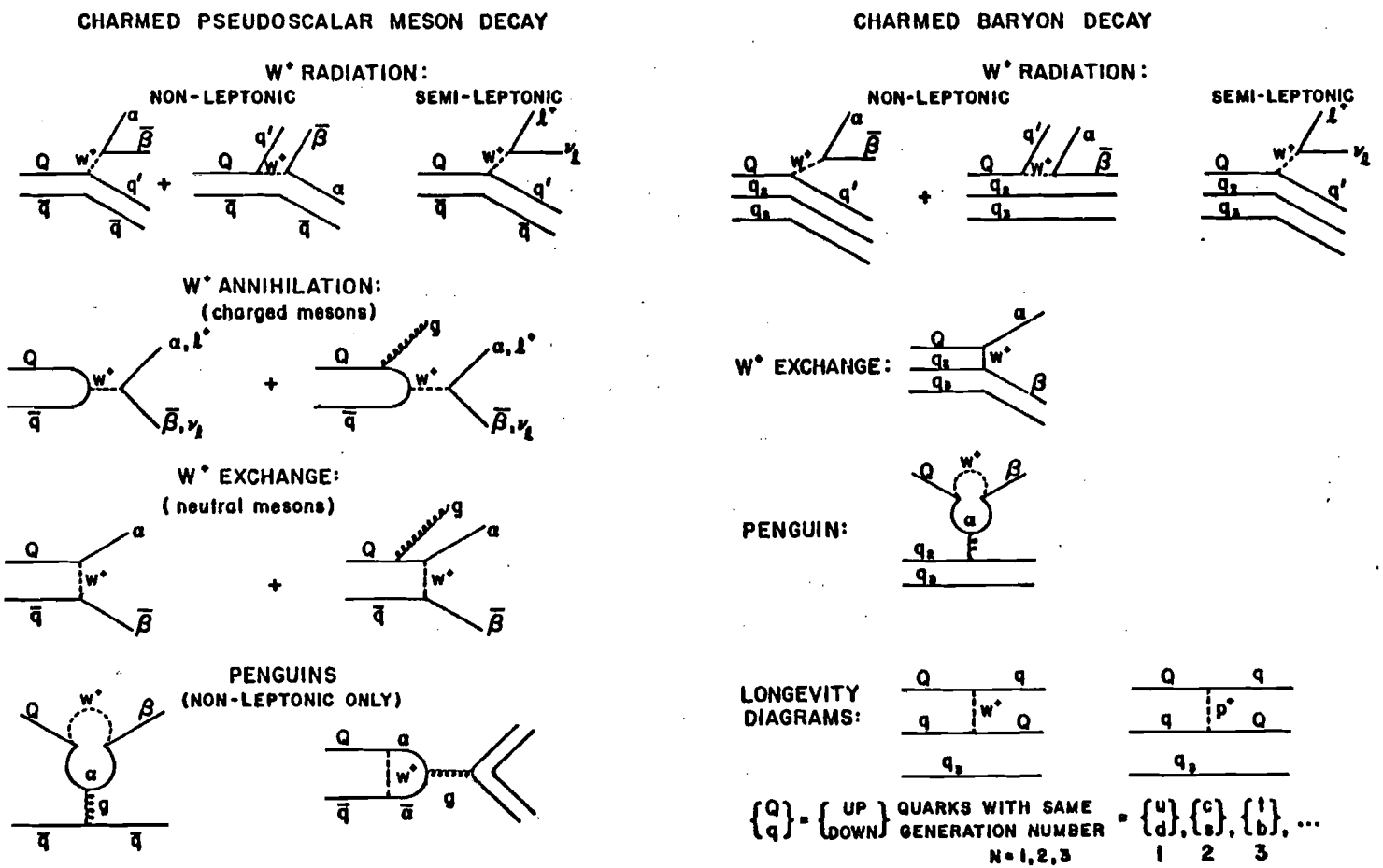

Figure 62. Weak Decays of Charmed Mesons and Baryons

TABLE 23
CHARM CANDIDATE EVENT SUMMARY SHEETS

RUN 476 RECORD 4449
OTT 000 NH 20 NS 12
LAST DONE ON 81/04/30.
2 VERTICES

NUMBER	TYPE	X	Y	Z
1	1	-8.435	-6.661	1.090
2	2	2.8	2.6	27.5

TOTAL CALORIMETER ENERGY IS 18.66 GEV
.44 14.70 2.96 .58 IN COLUMNS 1,2,3,4
TOTAL LEAD GLASS ENERGY IS 5.56 GEV
15 EMULSION TRACKS

	PRODUCTION		EXIT				
TRACK	DX/DZ	DY/DZ	DX/DZ	DY/DZ	I/I0	1/PBETA	V
1	.318	.109	.318	.109			
	.005	.005	.005	.005			
2	-.055	-.039	-.055	-.039			
	.002	.002	.002	.002			
3	.216	.269	.216	.269			
	.005	.005	.005	.005			
4	.115	-.090	.115	-.090			
	.003	.003	.003	.003			
5	-.072	.123	-.072	.123			
	.003	.003	.003	.003			
6	.022	.220	.022	.220			
	.004	.004	.004	.004			
7	.014	.089	.014	.089			
	.002	.002	.002	.002			
8	.428	1.295	.428	1.295			
	.015	.015	.015	.015			
9	.585	.546	.585	.546			
	.010	.010	.010	.010			
10	-.301	.464	-.301	.464			
	.007	.007	.007	.007			
11	-.527	.369	-.527	.369			
	.008	.008	.008	.008			
12	.100	.094					2
	.018	.018					
12-1	1.513	-.092	1.513	-.092	1.30	5.555	
	.017	.017	.017	.017	.04	1.500	
12-2	-.306	-.806	-.306	-.806	1.05	3.850	
	.010	.010	.010	.010	.03	1.000	
12-3	.159	.224	.140	.235			
	.004	.004	.004	.004			

20 SPECTROMETER TRACKS

TRACK	DX/DZ	DY/DZ	1/P	Q	UP	DN	CHISQ	ID	EPBG	BETA	V	XMISS	YMISS	F
1	.291	.147	4.349	1	12	8	.262	000010	0.00	.152	1	-.127	.009	0
			.057							.036				
2	-.045	-.033	.015	-1	10	8	.353	000004	.42	-.034	1	-.046	-.042	0
			.005							.044				
3	.210	.260	1.010	1	12	8	.385	000100	.41	.261	1	-.065	-.030	0
			.014							.037				
4	.122	-.088	.321	1	9	7	1.000	000136		-.085	1			0
			.007							1.000				
5	-.051	.098	2.099	-1	12	6	1.152	000014	.12	.022	1	.028	-.050	0
			.028							.023				
6								000136			1			
7	.034	.086	2.692	1	12	8	.162	000014	0.00	.075	1	.138	-.062	0
			.035							.028				
8								000136			1			
9	.577	.518	2.064	-1	10	0	.529	000136	0.00	0.000	1	-.085	.065	0
			.350							1.300				
10	-.297	.521	2.241	1	10	0	2.145	000136	0.00	0.000	1	-.126	.046	0
			.350							1.000				
11								000136			1			
12								040000			1			
12-1				1				000010			2			0
12-2				-1				000010			2			0
12-3	.156	.257	.393	1	11	8	1.889	000100	.31	.032	2	-.116	-.104	1
			.007							1.000				
U-1	-.067	-.045	1.820	-1	12	7	1.838	000100	.02	.505	1	.290	.185	0
			.024							.063				
G-1	.057	.030	.583	0		39		000001	1.72		1	0.000	0.000	0
	.015	.015	.062						.18					
G-2	.180	-.093	1.501	0		55		000001	.67		1	0.000	0.000	0
	.015	.015	.257						.11					
G-3	.057	-.093	1.469	0		57		000001	.63		1	0.000	0.000	0
	.015	.015	.249						.12					
G-4	.180	-.155	.909	0		63		000001	1.10		1	0.000	0.000	0
	.015	.015	.121						.15					

0 LINES OF AUXILLIARY TRACK INFORMATION
0 LINES OF COMMENTS

```
RUN  493 RECORD   1235
EOB   36 NH  3 NS  4
LAST DONE ON  81/05/08.
  3 VERTICES
NUMBER TYPE    X       Y       Z
   1     1   -6.913   6.712    .684
   2     2   -425.0  -132.0  2203.0
   3     1   -6.869   6.608   1.392
TOTAL CALORIMETER ENERGY IS  25.74 GEV
   3.08   6.25   1.62  14.79 IN COLUMNS 1,2,3,4
TOTAL LEAD GLASS ENERGY IS  21.33 GEV
  7 EMULSION TRACKS
          PRODUCTION        EXIT
 TRACK   DX/DZ  DY/DZ  DX/DZ  DY/DZ   I/I0  1/PBETA  V
  1       .082   .056   .082   .056
          .009   .004   .009   .004
  2      -.325   .005  -.325   .005
          .014   .007   .014   .007
  3      -.193  -.060                 0.96           2
          .011   .005                  .06
 3-1      .058  -.149                 1.01    0.555  3
          .011   .005                  .05    0.095
 3-2     -.304   .035  -.250   .044  0.96
          .013   .006   .013   .006  0.06
 3-3     -.120   .017  -.116  -.015  1.01
          .010   .004   .010   .004   .07
  4       .046  -.340   .046  -.340
          .015   .007   .015   .007
 13 SPECTROMETER TRACKS
 TRACK   DX/DZ  DY/DZ   1/P   Q UP DN CHISQ   ID    EPBG  BETA V XMISS YMISS F
  1       .092   .065   .138 -1 11  8  .420 000004  6.35 -.006 1 -.000  .000 0
                         .005                                .013
  2      -.325   .009   .335 -1 11  8  .553 000100  0.00  .047 1 -.081  .021 0
                         .007                                .016
  3      -.191  -.060  0.075  1       2.000 070000            1
          006    .002   .011
 3-1                                         000136            2            0

 3-2     -.266   .039  1.386  1 11  7  .204 000136  0.00 0.000 2 -.121 -.024 1
                         .019                                1.000
 3-3     -.102  -.022   .254 -1 12  6  .186 000130  3.05 0.000 2 -.060 -.011 1
                         .006                                1.000
  4       .013  -.371  1.398 -1  8  0  .126 000136  0.00 0.000 1  .076 -.045 0
                         .350                                1.000
E1-1      .075   .031   .913  1 12  8  .284 000002  1.50 -.016 1 -.071 -.031 0
                         .013                                 .015
E1-2      .069   .027   .187 -1 10  8  .541 000002  6.46 -.014 1 -.010  .009 0
                         .006                                1.000
 U-1     -.068   .068  2.422  1 12  6  .229 000010  0.00  .072 1 -.041 -.090 0
                         .032                                 .024
 U-2     -.054   .148  2.153  1 12  6 1.974 000010  0.00  .063 1 -.413  .303 0
                         .028                                 .022
 G-1      .044   .045   .107  0    21       000001  9.38       1 0.000 0.000 0
          .015   .015   .005                           .43
 G-2     -.079  -.017   .387  0    32       000001  2.59       1 0.000 0.000 0
          .015   .015   .034                           .23
  0 LINES OF AUXILLIARY TRACK INFORMATION
  1 LINES OF COMMENTS
TRACK 3-1 INTERACTS IN EMULSION PRODUCING A NH=19, NS=0 SHOWER
```

```
RUN  498 RECORD   4985
CCU  000 NH  0 NS  6
LAST DONE ON  81/05/08.
  3 VERTICES
NUMBER TYPE     X       Y       Z
   1     1   16.351   4.247   1.455
   2     2     -2.5    23.8   180.0
   3     1   16.351   4.247   5.455
TOTAL CALORIMETER ENERGY IS   9.57 GEV
    .50   6.95   1.17    .96 IN COLUMNS 1,2,3,4
TOTAL LEAD GLASS ENERGY IS   2.38 GEV
 11 EMULSION TRACKS
          PRODUCTION        EXIT
 TRACK   DX/DZ  DY/DZ  DX/DZ  DY/DZ   I/I0  1/PBETA  V
  1       .180   .360   .180   .360   0.93
          .016   .007   .016   .007    .04
  2      -.014   .132                              2
          .018   .009
 2-1     -.105   .158  -.105   .158
          .011   .005   .011   .005
 2-2      .011   .119   .018   .111   1.02
          .010   .004   .010   .004    .04
 2-3     -.188  -.357  -.200  -.325   0.86
          .016   .007   .016   .007    .04
  3       .061   .043   .061   .043
          .009   .004   .009   .004
  4       .044  -.062   .044  -.062   1.00
          .009   .004   .009   .004    .04
  5      -.315  -.128  -.315  -.128
          .015   .007   .015   .007
  6       .090  -.352   .090  -.352
          .015   .007   .015   .007
 0L       .013   .182                              3
          .003   .003
 L-1      .002   .178   .002   .178
          .011   .005   .011   .005
 L-2      .186   .241   .186   .241
          .014   .006   .014   .006
 15 SPECTROMETER TRACKS
 TRACK   DX/DZ  DY/DZ   1/P   Q UP DN CHISQ   ID    EPBG  BETA V XMISS YMISS F
  1       .180   .360  3.143  1 11  0 1.139 000136  0.00 0.000 1 -.007 -.060 0
                        .350                                1.000
  2      -.042   .127  0.119  1       2.900 040000            1            0
          .004   .003   .001
 2-1     -.109   .156   .315  1 11  8  .308 000010   .25 -.013 2  .013  .002 1
                        .006                                 .011
 2-2      .018   .111   .599 -1 12  7  .409 000010   .29  .004 2 -.008 -.009 1
                        .009                                 .017
 2-3     -.188  -.345  1.695  1 12  0 1.568 000136  0.00 0.000 2  .008 -.069 1
                        .350                                1.000
  3                                          000136            1

  4       .044  -.062   .066 -1 11  8  .766 000004   .38  .030 1 -.005 -.008 0
                        .005                                 .018
  5      -.316  -.127   .570 -1 11  8 1.012 000010   .57  .007 1 -.031  .026 0
                        .009                                 .012
  6                                          000136            1

 0L                                          000200            1            0

 L-1                                         000136            1

 L-2                                         000136            1

 U-1     -.116   .114  1.272 -1 10  6 2.379 000134  0.00 0.000 1  .095 -.021 0
                        .017                                1.000
 U-2      .039   .072  1.344  1 12  8  .126 000014   .26  .027 1  .045 -.024 0
                        .018                                 .016
 U-3     -.324  -.118  3.816 -1 12  6  .637 000134  0.00 0.000 1  .059 -.078 0
                        .050                                1.000
 G-1     -.021   .189  3.226  0     2       000001   .31       1 0.000 0.000 0
          .015   .015   .811                              .08
 0 LINES OF AUXILLIARY TRACK INFORMATION
 0 LINES OF COMMENTS
```

```
RUN  499 RECORD   4713
NGY  615 NH  6 NS  6
LAST DONE ON  81/08/07.
  3 VERTICES
NUMBER TYPE     X        Y        Z
   1     1    8.943   -8.899    1.587
   2     2    -59.0     31.0    360.0
   3     1    9.268   -7.413    5.609
TOTAL CALORIMETER ENERGY IS  16.34 GEV
   1.78   3.83   4.38   6.34 IN COLUMNS 1,2,3,4
TOTAL LEAD GLASS ENERGY IS    .94 GEV
  6 EMULSION TRACKS
          PRODUCTION        EXIT
 TRACK   DX/DZ  DY/DZ   DX/DZ  DY/DZ   I/I0  1/PBETA  V
   1      .001  -.015    .001  -.015
          .002   .002    .002   .002
   2     -.165   .086                              2
          .016   .009
  2-1    -.331  -.115   -.331  -.115
          .005   .005    .005   .005
   3      .027   .314    .027   .314
          .005   .005    .005   .005
   4     -.523   .646   -.523   .646
          .010   .010    .010   .010
   5      .901   .722    .901   .722
          .013   .013    .013   .013
  9 SPECTROMETER TRACKS
 TRACK   DX/DZ  DY/DZ    1/P   Q UP DN CHISQ    ID    EPBG  BETA V XMISS YMISS F
   1      .001  -.015    .003 -1 12  8  .798 000004   .51 -.021 1 -.002  .005 0
                         .005                                .018
   2     -.164   .088    .237  1        2.350 040000            1            0
          .003   .003    .003
  2-1    -.332  -.116    .385  1 10  7  .789 000036  0.00 -.006 2 -.009  .002 1
                         .007                                .017
   3      .015   .333   1.861  1 12  8  .403 000010  0.00  .002 1  .011 -.009 0
                         .025                                .018
   4                                          000136            1

   5                                          000136            1

  0L      .091   .404    .559  0             000200            2            1
          .006   .006    .009
 L-1      .592  1.051   3.794 -1 10  0  .768 000136  0.00 0.000 1-2.020-2.769 0
                         .350                               1.000
 L-2      .052   .352    .604  1 12  7  .405 000100  0.00  .112 1  .100  .081 0
                         .009                                .010
  0 LINES OF AUXILLIARY TRACK INFORMATION
  1 LINES OF COMMENTS
LAMBDA-C FIT IS WITH A 0-C FIT TO SIGMA-0 GOES TO LAMBDA-0, GAMMA
```

```
RUN  502 RECORD    354
NGY  194 NH  0 NS  3
LAST DONE ON  81/05/08.
  3 VERTICES
NUMBER TYPE     X        Y        Z
   1     1   15.000   -4.862   1.384
   2     2      4.1      1.1    66.0
   3     1   15.027   -4.854   1.803
TOTAL CALORIMETER ENERGY IS  27.30 GEV
  13.99  10.78    .81   1.71 IN COLUMNS 1,2,3,4
TOTAL LEAD GLASS ENERGY IS   7.30 GEV
 10 EMULSION TRACKS
          PRODUCTION        EXIT
 TRACK   DX/DZ  DY/DZ  DX/DZ  DY/DZ   I/10  1/PBETA  V
  1      -.063  -.001  -.063  -.001
          .002   .002   .002   .002
  2       .062   .016                              2
          .003   .002
 2-1      .063   .020                1.00    0.885  3
          .002   .002                 .10     .350
I2-1-1    .480  -.362   .480  -.362  0.91    6.667
          .008   .008   .008   .008   .05    3.000
I2-1-2   -.176  -.575  -.176  -.575  1.28    2.857
          .008   .008   .008   .008   .06    2.424
 2-2     -.239  -.112  -.239  -.112  0.90    1.300
          .004   .004   .004   .004   .05     .255
  3       .190   .013   .190   .013  0.82    1.316
          .003   .003   .003   .003   .05     .366
 E1-1    -.414   .119  -.414   .119
          .006   .006   .006   .006
 E1-2    -.433   .166  -.433   .166
          .006   .006   .006   .006
 18 SPECTROMETER TRACKS
 TRACK   DX/DZ  DY/DZ   1/P   Q UP DN CHISQ   ID     EPBG  BETA V XMISS YMISS P
  1      -.063  -.007   .016  1 10  7  .597 000004   .48 -.062 1 -.018 -.009 0
                        .005                                .021
  2       .062   .020         2             100000            1             0
                        .005                                .021
 2-1      .064   .020         1             000020            2             1

I2-1-1                                      000010            3

I2-1-2  -.173  -.594   .560  1 11  0  .722 000020  0.00 0.000 3 -.017  .259 0
                        .350                              1.000
 2-2    -.242  -.096   .030 -1 11  7 1.787 000030   .53 -.040 2 -.063 -.005 1
                        .005                              1.000
  3      .194   .007   .071  1  8  8 1.468 000132  0.00 -.016 1 -.157  .047 0
                        .005                               .020
 E1-1   -.413   .112   .034  1 10  7  .663 000002   .27  .009 1  .034 -.006 0
                        .005                               .013
 E1-2   -.413   .112   .034  1 10  7  .663 000002   .27  .009 1  .034 -.006 0
                        .005                               .013
 U-1    -.237  -.135   .001  1 10  8 1.285 000130   .62 -.041 1 -.035 -.019 0
                        .005                              1.000
 U-2    -.072   .054   .551 -1 12  0 1.365 000136  0.00 0.000 1  .062 -.053 0
                        .350                              1.000
 G-1    -.072   .078   .856  0    29        000001  1.17       1 0.000 0.000 0
         .015   .015   .111                             .15
 G-2     .114   .016  1.019  0    35        000001   .98       1 0.000 0.000 0
         .015   .015   .144                             .14
 G-3     .052   .016  2.101  0    36        000001   .48       1 0.000 0.000 0
         .015   .015   .426                             .10
 G-4    -.010   .016  1.533  0    37        000001   .65       1 0.000 0.000 0
         .015   .015   .266                             .11
 G-5     .052  -.046  2.822  0    45        000001   .35       1 0.000 0.000 0
         .015   .015   .664                             .08
 G-6    -.010  -.046   .610  0    46        000001  1.64       1 0.000 0.000 0
         .015   .015   .067                             .18
  0 LINES OF AUXILLIARY TRACK INFORMATION
  1 LINES OF COMMENTS
MAGNET OFF EVENT
```

```
RUN  512 RECORD   5761
NGY   75 NH  0 NS  4
LAST DONE ON  81/05/08.
  2 VERTICES
NUMBER TYPE    X       Y       Z
   1     1  -14.953  -1.168    .400
   2     2    12.0    13.0   457.0
TOTAL CALORIMETER ENERGY IS   5.28 GEV
   0.00   0.00   4.52    .76 IN COLUMNS 1,2,3,4
TOTAL LEAD GLASS ENERGY IS   7.49 GEV
  7 EMULSION TRACKS
          PRODUCTION        EXIT
 TRACK   DX/DZ  DY/DZ  DX/DZ  DY/DZ   I/I0  1/PBETA  V
  1       .001  -.012   .001  -.012
          .002   .002   .002   .002
  2       .026  -.028                              2
          .004   .004
 2-1      .053   .085   .083   .061
          .003   .003   .003   .003
 2-2      .071  -.133   .088  -.136
          .003   .003   .003   .003
 2-3      .071  -.206   .042  -.193
          .004   .004   .004   .004
  3      -.108   .194  -.094   .185
          .004   .004   .004   .004
  4       .441  1.482   .441  1.482
          .016   .016   .016   .016
 12 SPECTROMETER TRACKS
 TRACK   DX/DZ  DY/DZ   1/P   Q UP DN CHISQ   ID     EPBG  BETA V XMISS YMISS F
  1       .001  -.012  0.000  1 10  8 2.722 000004   .44 -.030 1 -.037  .017 0
                        .005                            .049
  2       .031  -.030   .097  1       6.260  030000          1            0
          .002   .002   .001
 2-1      .085   .069   .380 -1 12  8  .157 000030   .41  .006 2 -.003 -.024 1
                        .007                            .013
 2-2      .089  -.141   .299  1 11  8  .960 000030   .52 -.004 2 -.040  .043 1
                        .006                            .012
 2-3      .038  -.198   .521  1 12  7 1.211 000010   .21  .009 2  .018  .074 1
                        .009                            .014
  3      -.089   .193   .750 -1 12  8  .881 000014   .26  .011 1 -.027 -.058 0
                        .011                            .015
  4                                          000136          1

 U-1     -.047   .038  3.485  1 12  7  .266 000136  0.00 0.000 1 -.111  .063 0
                        .046                           1.000
 G-1     -.137   .170  1.193  0    16        000001   .84       1 0.000 0.000 0
          .015   .015   .182                            .13
 G-2     -.014   .109  1.031  0    23        000001   .97       1 0.000 0.000 0
          .015   .015   .147                            .14
 G-3      .048   .047   .388  0    31        000001  2.58       1 0.000 0.000 0
          .015   .015   .034                            .22
 G-4     -.014   .047  1.721  0    32        000001   .58       1 0.000 0.000 0
          .015   .015   .316                            .11
 0 LINES OF AUXILLIARY TRACK INFORMATION
 0 LINES OF COMMENTS
```

```
RUN  522 RECORD   2107
OSK  130 NH 14 NS  4
LAST DONE ON  81/05/08.
  2 VERTICES
NUMBER TYPE    X       Y       Z
   1     1    6.530  12.690   1.395
   2     2     41.0  1660.0 13600.0
TOTAL CALORIMETER ENERGY IS  27.32 GEV
   1.13  19.56   4.91   1.72 IN COLUMNS 1,2,3,4
TOTAL LEAD GLASS ENERGY IS  21.32 GEV
  7 EMULSION TRACKS
          PRODUCTION        EXIT
 TRACK   DX/DZ  DY/DZ   DX/DZ  DY/DZ   I/T0  1/PBETA  V
  1       .061   .132    .061   .132
          .010   .005    .010   .005
  2       .003   .122                              2
          .006   .003
 2-1     -.002   .136   -.002   .136
          .010   .005    .010   .005
 2-2     -.012   .072   -.012   .072
          .009   .004    .009   .004
 2-3     -.065   .057   -.065   .057
          .009   .004    .009   .004
  3       .087   .072    .087   .072
          .010   .004    .010   .004
  4      -.021  -.067   -.021  -.067
          .009   .004    .009   .004
 25 SPECTROMETER TRACKS
 TRACK   DX/DZ  DY/DZ    1/P   Q UP DN CHISQ   ID     EPBG  BETA V XMISS YMISS F
  1       .059   .136    .659  1 10  8 1.047 000134   .54  .116 1  .042 -.075 0
                         .010                                1.000
  2       .003   .122          1             070000            1            0

 2-1     -.002   .135    .061  1 10  7 1.453 000130   .40  .013 2  .010  .006 1
                         .005                                1.000
 2-2      .024   .061   1.015  1 12  7  .646 000014   .37  .012 2 -.152  .019 1
                         .014                                 .022
 2-3     -.044   .060    .223 -1 11  6 2.477 000120   .99  .033 2  .001  .039 1
                         .006                                 .025
  3       .087   .072    .211 -1 11  7  .638 000100   .75  .031 1  .039 -.026

  4      -.020  -.067    .014 -1 11  8 1.531 000130 11.82 0.000 1 -.018 -.092 0
                         .005                                1.000
 U-2      .141   .038   2.220  1 12  6 2.375 000134   .03 0.000 1 -.083  .081 0
                         .029                                1.000
 U-3      .118   .101   1.592  1 12  6 2.074 000134   .03  .233 1  .133 -.112 0
                         .021                                1.000
 U-4     -.054  -.082   3.552 -1 10  0 1.044 000136  0.00 0.000 1  .085 -.079 0
                         .350                                1.000
 U-5      .028  -.047   1.024  1 12  8  .903 000136  1.16  .036 1 -.206 -.069 0
                         .014                                 .014
 U-6      .092  -.007   1.385  1 12  6 1.616 000134   .02  .038 1 -.046 -.051 0
                         .019                                1.000
 U-7     -.103   .081    .805 -1 12  7 2.339 000016  1.39 -.022 1  .317  .102 0
                         .012                                 .021
 U-8     -.174  -.044   1.913 -1 12  6  .851 000136   .67 0.000 1  .093  .010 0
                         .025                                1.000
 U-9      .060  -.071    .242 -1  9  7 2.783 000100  4.23  .038 1  .256 -.235 0
                         .006                                 .013
 G-1      .121   .120   3.087  0     1        000001   .32       1 0.000 0.000 0
          .015   .015    .759                             .08
 G-2      .121   .058   1.327  0     9        000001   .75       1 0.000 0.000 0
          .015   .015    .214                             .12
 G-3     -.003   .058   1.679  0    11        000001   .60       1 0.000 0.000 0
          .015   .015    .305                             .11
 G-4     -.003  -.004   2.068  0    20        000001   .48       1 0.000 0.000 0
          .015   .015    .416                             .10
 G-5      .121  -.066    .316  0    27        000001  3.16       1 0.000 0.000 0
          .015   .015    .025                             .25
 G-6     -.003  -.066    .088  0    29        000001 11.35       1 0.000 0.000 0
          .015   .015    .004                             .47
 G-7     -.065  -.066   3.182  0    30        000001   .31       1 0.000 0.000 0
          .015   .015    .795                             .08
 G-8     -.127  -.066   2.629  0    31        000001   .38       1 0.000 0.000 0
          .015   .015    .597                             .09
 G-9     -.065  -.314   3.170  0    65        000001   .32       1 0.000 0.000 0
          .015   .015    .790                             .08
 0 LINES OF AUXILLIARY TRACK INFORMATION
 0 LINES OF COMMENTS
```

```
RUN  527 RECORD   3682
KOB    3 NH  7 NS  5
LAST DONE ON  81/05/08.
  2 VERTICES
NUMBER TYPE,   X       Y       Z
   1     1   -4.763   8.235   2.033
   2     2     8.0   -33.7   670.0
TOTAL CALORIMETER ENERGY IS  22.09 GEV
    .58   3.52  11.54   6.45 IN COLUMNS 1,2,3,4
TOTAL LEAD GLASS ENERGY IS  10.76 GEV
  6 EMULSION TRACKS
          PRODUCTION        EXIT
 TRACK    DX/DZ  DY/DZ  DX/DZ  DY/DZ   I/I0  1/PBETA  V
  1       -.022   .027  -.022   .027   1.00
           .008   .004   .008   .004    .06
  2        .012  -.050                 0.94           2
           .008   .004                  .07
 2-1      -.041  -.114  -.036  -.115   1.10
           .010   .005   .010   .005    .06
 2-2       .345  -.076   .362  -.080   0.98
           .015   .007   .015   .007    .05
 2-3      -.240  -.058  -.240  -.056   1.30
           .013   .006   .013   .006    .22
  3        .018  -.128   .018  -.128
           .010   .005   .010   .005
 13 SPECTROMETER TRACKS
 TRACK    DX/DZ  DY/DZ   1/P   Q UP DN CHISQ   ID     EPBG  BETA V XMISS YMISS F
  1       -.012   .030   .034  1 10  8  .667 000004  1.55  .001 1  .002 -.006 0
                         .005                                .013
  2        .020  -.053   .082 -1        2.270 020000            1            0
           .005   .003   .002
 2-1      -.048  -.109   .187 -1 12  8  .143 000130  2.33 -.007 2  .001  .002 1
                         .006                                .014
 2-2       .317  -.063   .663 -1 12  7  .559 000016  0.00  .018 2 -.018 -.014 1
                         .010                                .016
 2-3      -.248  -.060   .895  1 11  8  .260 000016  0.00  .020 2 -.021  .019 1
                         .013                                .017
  3        .026  -.127   .195  1 11  8 1.038 000030  3.75 -.014 1 -.022  .003 0
                         .006                                .014
 U-1      -.596  -.399  1.399 -1 10  0  .735 000136  0.00 0.000 1 -.172 -.019 0
                         .350                               1.000
 G-1       .089   .033   .401  0    20        000001  2.49       1 0.000 0.000 0
           .015   .015   .036                          .22
 G-2       .027   .033   .843  0    21        000001  1.19       1 0.000 0.000 0
           .015   .015   .108                          .15
 G-3       .027  -.029  1.458  0    30        000001   .69       1 0.000 0.000 0
           .015   .015   .246                          .12
 G-4      -.035  -.092   .536  0    40        000001  1.87       1 0.000 0.000 0
           .015   .015   .055                          .19
 G-5      -.035  -.154   .943  0    49        000001  1.06       1 0.000 0.000 0
           .015   .015   .128                          .14
 G-6       .152  -.216   .482  0    55        000001  2.08       1 0.000 0.000 0
           .015   .015   .047                          .20
  0 LINES OF AUXILLIARY TRACK INFORMATION
  0 LINES OF COMMENTS
```

```
RUN  529 RECORD    271
NGY  423 NH  0 NS  5
LAST DONE ON  81/08/07.
  2 VERTICES
NUMBER TYPE    X       Y       Z
   1    1     .012  -4.798    .346
   2    2    -71.0  -147.0  2542.0
TOTAL CALORIMETER ENERGY IS  38.05 GEV
   1.03  18.46  17.18   1.38 IN COLUMNS 1,2,3,4
TOTAL LEAD GLASS ENERGY IS  11.64 GEV
  8 EMULSION TRACKS
          PRODUCTION        EXIT
 TRACK   DX/DZ  DY/DZ  DX/DZ  DY/DZ   I/I0  1/PBETA  V
  1       .032   .045   .032   .045
          .002   .002   .002   .002
  2      -.028  -.058                              2
          .002   .002
 2-1     -.087  -.005  -.087  -.005
          .002   .002   .002   .002
  3       .165  -.129   .165  -.129
          .004   .004   .004   .004
  4      -.254   .437  -.254   .437
          .007   .007   .007   .007
 0I      -.028  -.060
          .002   .002
 I0-1    -.010  -.058  -.010  -.058
          .002   .002   .002   .002
 I0-2     .043  -.068   .043  -.068
          .002   .002   .002   .002
 12 SPECTROMETER TRACKS
 TRACK   DX/DZ  DY/DZ   1/P   Q UP DN CHISQ   ID    EPBG  BETA V XMISS YMISS F
  1       .031   .045   .018 -1  8  8  .307 000004   .44  .003 1 -.009 -.010 0
                        .005                                .013
  2                           1             070000            1             0

 2-1     -.088   .002   .160  1  9  7 1.286 000130   .36  .011 2  .017 -.043 1
                        .005                                .010
  3       .165  -.129   .489 -1 12  8  .341 000010   .00 -.003 1  .016  .012 0
                        .008                                .015
  4      -.254   .437  2.633 -1 10  0 2.435 000136  0.00 0.000 1  .268 -.083 0
                        .350                               1.000
 0I                           0             000001            1             0

 I0-1    -.020  -.044  3.440 -1  8  0 5.644 000136  0.00 0.000 3  .118 -.033 0
                        .350                               1.000
 I0-2     .028  -.070  2.759 -1 12  6  .702 000016  0.00  .030 3 -.080  .036 0
                        .036                                .026
 U-1     -.139  -.043  1.127 -1 12  8  .413 000016  8.79  .013 1  .328 -.092 0
                        .015                                .014
 G-1     -.012  -.047   .120  0    48        000001  8.32       1 0.000 0.000 0
          .015   .015   .006                            .40
 G-2     -.135  -.047  2.364  0    50        000001   .42       1 0.000 0.000 0
          .015   .015   .509                            .09
 G-3     -.012  -.108  1.086  0    57        000001   .92       1 0.000 0.000 0
          .015   .015   .158                            .13
  0 LINES OF AUXILLIARY TRACK INFORMATION
  0 LINES OF COMMENTS
```

```
RUN  533 RECORD   7152
NGY  644 NH  5 NS  6
LAST DONE ON  81/08/07.
  2 VERTICES
NUMBER TYPE    X       Y       Z
   1     1    5.285  -7.179    .645
   2     2    100.0    52.0  5245.0
TOTAL CALORIMETER ENERGY IS  51.60 GEV
    .41  38.78  11.02   1.39 IN COLUMNS 1,2,3,4
TOTAL LEAD GLASS ENERGY IS  10.18 GEV
  5 EMULSION TRACKS
          PRODUCTION        EXIT
 TRACK   DX/DZ  DY/DZ  DX/DZ  DY/DZ   I/IO  1/PBETA  V
  1       .019   .010                                2
          .002   .002
 1-1     -.023  -.084  -.023  -.084
          .002   .002   .002   .002
  2      -.043   .049  -.043   .049
          .002   .002   .002   .002
  3      -.033   .016  -.033   .016
          .002   .002   .002   .002
  4      0.000  -.060  0.000  -.060
          .002   .002   .002   .002
 15 SPECTROMETER TRACKS
 TRACK   DX/DZ  DY/DZ   1/P   Q UP DN CHISQ   ID    EPBG  BETA V XMISS YMISS F
  1                           1              070000            1              0

 1-1     -.019  -.082   .207  1  7  8 2.068 000130   .59  .002 2 -.148  .043 1
                        .006                                 1.000
  2      -.040   .053   .112 -1 10  8  .879 000004  5.36 -.632 1 -.006 -.008 0
                        .005                                 1.000
  3      -.031   .015   .207 -1 10  8  .511 000132  5.29 -.597 1  .002  .001 0
                        .006                                 1.000
  4       .000  -.058   .087  1  9  8  .861 000130  1.79 -.512 1 -.002 -.025 0
                        .005                                 1.000
 U-1      .007  -.052  3.578  1 12  7  .526 000136  0.00 0.000 1 -.218  .007 0
                        .047                                 1.000
 U-2     -.009   .016  3.706  1 12  6  .591 000136  0.00 0.000 1 -.110  .110 0
                        .048                                 1.000
 U-3     -.022   .051  3.674  1 12  6  .601 000136  0.00 0.000 1 -.106  .018 0
                        .048                                 1.000
 U-4      .045  0.000   .814  1 11  6 1.359 000000  1.36 -.662 1 -.005  .043 0
                        .012                                  .039
 G-1      .007   .034   .296  0    38        000001  3.38       1 0.000 0.000 0
          .015   .015   .023                          .26
 G-2     -.055   .034  1.722  0    39        000001   .58       1 0.000 0.000 0
          .015   .015   .316                          .11
 G-3      .130  -.027   .922  0    45        000001  1.08       1 0.000 0.000 0
          .015   .015   .124                          .15
 G-4      .007  -.027  1.710  0    47        000001   .58       1 0.000 0.000 0
          .015   .015   .313                          .11
 G-5      .069  -.089  2.163  0    55        000001   .46       1 0.000 0.000 0
          .015   .015   .445                          .10
 G-6      .007  -.089  2.362  0    56        000001   .42       1 0.000 0.000 0
          .015   .015   .508                          .09
  0 LINES OF AUXILLIARY TRACK INFORMATION
  0 LINES OF COMMENTS
```

```
RUN  546 RECORD   1339
KOB    8 NH  7 NS  5
LAST DONE ON  81/07/14.
  2 VERTICES
NUMBER TYPE    X       Y       Z
   1     1   -8.722   2.706    .588
   2     2   -62.0  -110.0  2145.0
TOTAL CALORIMETER ENERGY IS  11.57 GEV
   0.00   0.00   4.65   6.92 IN COLUMNS 1,2,3,4
TOTAL LEAD GLASS ENERGY IS   5.09 GEV
 11 EMULSION TRACKS
          PRODUCTION        EXIT
 TRACK   DX/DZ  DY/DZ  DX/DZ  DY/DZ   I/I0  1/PBETA  V
  1       .195  -.341   .195  -.341
          .016   .007   .016   .007
  2      -.085  -.335  -.085  -.335
          .015   .007   .015   .007
  3      2.489  -.320  2.489  -.320
          .080   .040   .080   .040
  4      2.545  -.311  2.545  -.311
          .080   .040   .080   .040
  5      -.014  -.052                            2
          .008   .004
 5-1     -.024  -.159  -.024  -.159   0.99
          .011   .005   .011   .005   0.04
 5-2      .016  -.038   .016  -.038   1.08
          .008   .004   .008   .004   0.04
 5-3      .094  -.032   .094  -.032   1.03
          .009   .004   .009   .004    .04
  6      -.165   .079  -.165   .079
          .011   .005   .011   .005
  7      -.221   .215  -.221   .215
          .014   .006   .014   .006
  8      1.398   .891  1.398   .891
          .044   .020   .044   .020
 16 SPECTROMETER TRACKS
 TRACK   DX/DZ  DY/DZ   1/P   Q UP DN CHISQ   ID    EPBG  BETA V XMISS YMISS F
  1       .233  -.400   .224  1 10  0  .407 000136  0.00 0.000 1 -.105  .096 0
                        .350                                1.000
  2                                          000136            1

  3                                          000136            1

  4                                          000136            1

  5                                          700000            1

 5-1     -.023  -.160   .258 -1 11  8  .534 000130   .86  .013 2 -.023  .019 1
                        .006                                1.000
 5-2      .017  -.038   .213  1 11  7  .578 000004  2.83  .009 2 -.008 -.003 1
                        .006                                .011
 5-3      .094  -.032   .308  1 10  8  .810 000130   .57 -.021 2 -.024 -.001 1
                        .006                                .014
  6                                          000136            1

  7      -.172   .216   .148 -1 11  8  .398 000004  0.00  .020 1 -.026 -.007 0
                        .005                                .016
  8                                          000136            1

 U-1     -.120   .080   .618  1 11  7  .622 000010   .30 -.009 1 -.034  .089 0
                        .009                                .016
 U-2      .536   .820   .036  1 11  0 1.649 000136  0.00 0.000 1 -.210 -.123 0
                        .350                                1.000
 U-3      .009  -.295   .624 -1 10  0  .187 000136  0.00 0.000 1 -.078 -.068 0
                        .350                                1.000
 G-1     -.003  -.046   .423  0    40        000001  2.37       1 0.000 0.000 0
          .015   .015   .038                             .22
 G-2     -.003  -.169  2.123  0    58        000001   .47       1 0.000 0.000 0
          .015   .015   .433                             .10
 0 LINES OF AUXILLIARY TRACK INFORMATION
 0 LINES OF COMMENTS
```

```
RUN  547 RECORD   3192
OCU  000 NH  1 NS 11
LAST DONE ON  81/07/14.
  3 VERTICES
NUMBER TYPE     X        Y        Z
   1     1    6.600    6.480    .895
   2     2     -4.2    -20.3    185.0
   3     2   -273.0   1194.0 17100.0
TOTAL CALORIMETER ENERGY IS  16.00 GEV
    .57   6.40   7.34   1.69 IN COLUMNS 1,2,3,4
TOTAL LEAD GLASS ENERGY IS   5.48 GEV
 15 EMULSION TRACKS
          PRODUCTION        EXIT
 TRACK   DX/DZ   DY/DZ   DX/DZ   DY/DZ    I/I0   1/PBETA  V
  1      -.040    .277   -.040    .277
          .013    .006    .013    .006
  2      -.081    .225   -.081    .225
          .013    .006    .013    .006
  3      -.002    .092   -.002    .092
          .009    .004    .009    .004
  4       .241    .047    .241    .047
          .013    .006    .013    .006
  5      -.005   -.050   -.005   -.050
          .008    .004    .008    .004
  6       .046   -.052    .046   -.052
          .009    .004    .009    .004
  7      -.124   -.068   -.124   -.068
          .010    .005    .010    .005
  8      -.096   -.115   -.096   -.115
          .011    .005    .011    .005
  9      -.023   -.110                                  2
          .011    .005
 9-1      .084    .478    .084    .478   0.97    2.632
          .018    .008    .018    .008   0.04     .667
 9-2     -.007    .066                   1.01    0.385  3
          .010    .005                   0.04    0.144
I9-2-1    .200   -1.800   .200  -1.800
          .047    .021    .047    .021
 9-3     -.021   -.218   -.021   -.218   0.95    0.263
          .012    .005    .012    .005   0.04    0.094
 10       .234   -.199    .234   -.199
          .014    .006    .014    .006
 11       .443   -.205    .443   -.205
          .018    .008    .018    .008
 18 SPECTROMETER TRACKS
 TRACK   DX/DZ   DY/DZ    1/P   Q UP DN CHISQ   ID     EPBG   BETA V XMISS YMISS F
  1                                             000136            1

  2                                             000136            1

  3      -.002    .092    .063 -1 10  8 1.086 000004   .36   .032 1 -.024 -.020 0
                           .005                                .019
  4       .240    .048   1.640  1 12  8  .324 000014   .21   .014 1 -.062 -.039 0
                           .022                                .017
  5       .007   -.071    .210 -1  9  7 2.677 000030  1.72 -.016 1 -.035  .112 0
                           .006                                .020
  6                                             000136            1

  7                                             000136            1

  8      -.096   -.116    .573 -1 11  7  .497 000136   .66 -.181 1 -.019 -.025 0
                           .009                                .021
  9                                             070000            1

 9-1      .088    .479    .088 -1 11  0 1.548 000136  0.00 0.000 2  .053 -.023 0
                           .350                              1.000
 9-2                                            000136            2
I9-2-1                                          000136            3

 9-3                                            000136            2

 10       .234   -.200   1.046  1 12  8  .852 000014   .07 -.004 1  .026  .069 0
                           .014                                .020
 11       .443   -.205   3.570  1 12  8  .852 000100   .00  .634 1  .026  .069 0
                           .050                                .028
 G-1     -.065    .109    .776  0    12        000001  1.29        1 0.000 0.000 0
          .015    .015    .096                          .16
 G-2      .058   -.077    .814  0    37        000001  1.23        1 0.000 0.000 0
          .015    .015    .103                          .16
 G-3     -.004   -.200   1.544  0    56        000001   .65        1 0.000 0.000 0
          .015    .015    .269                          .11
  0 LINES OF AUXILLIARY TRACK INFORMATION
  2 LINES OF COMMENTS
TRACK 9-1 HITS POLE
TRACK 9-2 INTERACTS TO PRODUCE A NH=6 NS=1 SHOWER..
```

```
RUN  549 RECORD   4068
NGY  151 NH  4 NS  8
LAST DONE ON  81/06/26.
  2 VERTICES
NUMBER TYPE    X       Y       Z
   1     1     .918 -10.361   1.711
   2     2    -5.0     0.5    21.0
TOTAL CALORIMETER ENERGY IS  15.47 GEV
    .46   2.59   3.72   8.70 IN COLUMNS 1,2,3,4
TOTAL LEAD GLASS ENERGY IS    .78 GEV
  7 EMULSION TRACKS
          PRODUCTION        EXIT
 TRACK   DX/DZ  DY/DZ  DX/DZ  DY/DZ   I/IO  1/PBETA  V
  1       .067   .067   .067   .067
          .002   .002   .002   .002
  2      -.236   .025                              2
          .025   .025
 2-1      .097  -.129   .094  -.119   1.10    1.176
          .003   .003   .003   .003    .06     .337
 2-2     -.339   .451  -.354   .364   1.31    1.587
          .007   .007   .007   .007    .07     .560
 2-3     3.756-10.321                         -21.097
          .100   .300                            .312
  3      -.126  -.034  -.126  -.034
          .003   .003   .003   .003
  4      -.358   .004  -.324  -.006
          .005   .005   .005   .005
  5      -.059  -.595  -.055  -.544
          .007   .007   .007   .007
  8 SPECTROMETER TRACKS
 TRACK   DX/DZ  DY/DZ   1/P   Q UP DN CHISQ   ID    EPBG  BETA V XMISS YMISS F
  1       .066   .068   .089 -1 12  7 1.147 000004   .51  .002 1  .015 -.015 0
                        .005                                .011
  2      -.236   .025         1            070000            1             0

 2-1                                       000136            2

 2-2     -.320   .468   .837  1 12  0 1.770 000100  0.00 0.000 2 -.040 -.002 1
                        .350                                1.000
 2-3    -3.756 10.321-21.097  1            000010            2             1
                        .312
  3      -.132  -.034   .269  1 12  8  .256 000120   .26  .026 1 -.014 -.010 0
                        .006                                .013
  4                                        000136            1

  5      -.112  -.494  1.981  1 11  0  .842 000136  0.00 0.000 1  .025 -.147 0
                        .350                                1.000
  0 LINES OF AUXILLIARY TRACK INFORMATION
  3 LINES OF COMMENTS
TRACK 2-3 GOES BACKWARD IN THE LAB FRAME
TRACK 2-2 IS IDENTIFIED AS PROTON BY I/IO
TRACK 2-3 IS IDENTIFIED AS PI+ FROM PI-MU-E CHAIN
```

```
RUN  563 RECORD   5269
KOB  002 NH  4 NS  6
LAST DONE ON  81/08/07.
  2 VERTICES
NUMBER TYPE    X        Y        Z
   1     1   -3.292   3.493   1.280
   2     2   -727.0 -1247.0  6600.0
TOTAL CALORIMETER ENERGY IS  66.03 GEV
    .57   4.52  53.25   7.69 IN COLUMNS 1,2,3,4
TOTAL LEAD GLASS ENERGY IS   3.77 GEV
  7 EMULSION TRACKS
          PRODUCTION        EXIT
 TRACK   DX/DZ  DY/DZ  DX/DZ  DY/DZ   I/IO  1/PBETA  V
   1     -.004  -.255  -.004  -.255
          .013   .006   .013   .006
   2     -.110  -.189                              2
          .013   .006   .013   .006
  2-1    -.429  -.037  -.399  -.035
          .016   .007   .016   .007
   3     -.021  -.100  -.021  -.100
          .010   .004   .010   .004
   4     -.105  -.080  -.105  -.080
          .010   .005   .010   .005
   5      .047   .025   .047   .025
          .008   .004   .008   .004
   6     -.122   .035  -.122   .035
          .010   .005   .010   .005
  9 SPECTROMETER TRACKS
 TRACK   DX/DZ  DY/DZ   1/P   Q UP DN CHISQ   ID     EPBG  BETA V XMISS YMISS F
   1     -.010  -.262   .711 -1 12  7  .673 000014   .17  .003 1  .028  .116 0
                         .011                                .021
   2                          1            070000            1             0

  2-1    -.404  -.040  1.106  1 12  0 1.990 000136  0.00 0.000 2  .098 -.085 1
                         .350                                1.000
   3     -.004  -.098   .042 -1 11  7 3.011 000004   .44  .022 1  .002  .012 0
                         .005                                .021
   4     -.099  -.086   .714  1 12  8  .283 000014   .30 -.005 1 -.017  .053 0
                         .011                                .019
   5      .015   .022   .071  1 11  6 3.094 000130   .85 -.020 1 -.032  .017 0
                         .005                                .012
   6     -.110   .035   .407 -1 10  8  .735 000030   .43  .017 1  .021  .030 0
                         .007                                .015
 U-1     -.111  -.042  1.430 -1 12  7 1.324 000136   .85 0.000 1  .114  .001 0
                         .019                                1.000
 G-1      .015   .071   .903  0    21        000001  1.11       1 0.000 0.000 0
          .015   .015   .120                             .15
  0 LINES OF AUXILLIARY TRACK INFORMATION
  0 LINES OF COMMENTS
```

```
RUN  567 RECORD   2596
KOB  027 NH  6 NS  6
LAST DONE ON  81/08/07.
  2 VERTICES
NUMBER TYPE    X       Y       Z
   1     1   -9.074   6.423   2.086
   2     2    16.8    -1.8   175.0
TOTAL CALORIMETER ENERGY IS   8.58 GEV
   1.88   0.00   4.98   1.72 IN COLUMNS 1,2,3,4
TOTAL LEAD GLASS ENERGY IS   2.45 GEV
  7 EMULSION TRACKS
          PRODUCTION        EXIT
 TRACK   DX/DZ  DY/DZ  DX/DZ  DY/DZ   I/I0  1/PBETA  V
   1      .019   .088   .019   .088
          .009   .004   .009   .004
   2     -.239   .028  -.239   .028
          .013   .006   .013   .006
   3      .096  -.010                              2
          .010   .005
  3-1     .466   .023   .466   .023
          .018   .008   .018   .008
   4      .024  -.072   .024  -.072
          .009   .004   .009   .004
   5     -.240  -.112  -.240  -.112
          .013   .006   .013   .006
   6      .305  -.157   .305  -.157
          .015   .007   .015   .007
 10 SPECTROMETER TRACKS
 TRACK   DX/DZ  DY/DZ   1/P   Q UP DN CHISQ   ID     EPBG  BETA V XMISS YMISS F
   1      .019   .089   .177 -1  9  8  .298 000004   .33  .004 1  .005 -.003 0
                         .006                                .013
   2     -.282   .023  2.632 -1 10  6 1.000 000014  0.00  .013 1  .000  .000 0
                         .030                                .059
   3      .096  -.010   .173  1       0.280 040000            1            0
                         .003
  3-1     .387  -.026   .598  1 10  7  .805 000100   .25  .111 2  .006  .009 1
                         .009                                .015
   4      .009  -.066   .371  1 12  0 3.927 000136  0.00 0.000 1  .076 -.016 0
                         .350                               1.000
   5     -.237  -.117  1.341 -1 12  0 2.751 000136  0.00 0.000 1  .005 -.034 0
                         .350                               1.000
   6      .275  -.133  1.012 -1 10  7  .851 000016  0.00  .010 1  .008  .013 0
                         .014                                .019
  0K     -.034   .000   .323  0             000120            2            1
          .050   .200   .014                                .019
 G-1     -.062  -.015  2.968  0    32       000001   .34       1 0.000 0.000 0
          .015   .015   .716                             .08
 G-2     -.062  -.077  2.238  0    41       000001   .45       1 0.000 0.000 0
          .015   .015   .469                             .09
 G-3     -.124  -.139  1.731  0    51       000001   .58       1 0.000 0.000 0
          .015   .015   .319                             .11
  0 LINES OF AUXILLIARY TRACK INFORMATION
  1 LINES OF COMMENTS
0K IS FROM EXCESS IN CALORIMETER
```

```
RUN  580 RECORD   4508
NGY   93 NH  3 NS  4
LAST DONE ON  81/07/14.
  3 VERTICES
NUMBER TYPE     X        Y        Z
   1     1   12.478   -4.194    1.800
   2     2     -8.0   -107.0   2305.0
   3     2   -735.0  -1162.0   7000.0
TOTAL CALORIMETER ENERGY IS  14.55 GEV
    .91   3.86   1.18   8.59 IN COLUMNS 1,2,3,4
TOTAL LEAD GLASS ENERGY IS   7.08 GEV
  8 EMULSION TRACKS
          PRODUCTION        EXIT
 TRACK   DX/DZ  DY/DZ  DX/DZ  DY/DZ   I/I0  1/PBETA  V
  1      -.003  -.049                                2
          .003   .003
 1-1      .062  -.038   .064  -.041
          .002   .002   .002   .002
 1-2      .075  -.213   .084  -.210
          .004   .004   .004   .004
 1-3     -.267  -.027  -.253  -.027   0.95
          .004   .004   .004   .004   0.06
  2       .033  -.196   .033  -.196
          .003   .003   .003   .003
  3      -.105  -.166                                3
          .003   .003
 3-1     -.024  -.205  -.024  -.205
          .004   .004   .004   .004
  4       .044   .211   .044   .211
          .004   .004   .004   .004
 11 SPECTROMETER TRACKS
 TRACK   DX/DZ  DY/DZ   1/P   Q UP DN CHISQ   ID    EPBG  BETA V XMISS YMISS F
  1                                          070000            1

 1-1      .065  -.043   .233 -1 12  8  .444 000032  5.70 -.011 2 -.016 -.000 1
                        .006                                .017
 1-2      .081  -.221   .823 -1 12  0  .975 000136  0.00 0.000 2 -.029  .000 1
                        .350                               1.000
 1-3     -.274  -.032   .654  1 12  8  .342 000020   .17  .057 2 -.005  .045 1
                        .010                                .021
  2       .010  -.206  4.148 -1 12  0 2.326 000136  0.00 0.000 1  .192  .022 0
                        .350                               1.000
  3                                          000136            1

 3-1     -.033  -.217   .986  1 12  0  .492 000136  0.00 0.000 3 -.051 -.003 1
                        .350                               1.000
  4       .044   .219   .149  1 10  7 1.709 000004   .27  .005 1  .030  .050 0
                        .005                                .015
 G-1      .135   .135  2.955  0    17        000001   .34       1 0.000 0.000 0
          .015   .015   .711                            .08
 G-2     -.052   .010  3.149  0    38        000001   .32       1 0.000 0.000 0
          .015   .015   .782                            .08
 G-3      .073  -.052   .188  0    45        000001  5.31       1 0.000 0.000 0
          .015   .015   .011                            .32
  0 LINES OF AUXILLIARY TRACK INFORMATION
  0 LINES OF COMMENTS
```

```
RUN  597 RECORD   1851
NGY  253 NH  0 NS  5
LAST DONE ON  81/07/14.
  2 VERTICES
NUMBER TYPE     X        Y        Z
   1     1   12.797   -9.408   1.629
   2     2    -13.5     -0.3    129.0
TOTAL CALORIMETER ENERGY IS  10.38 GEV
   2.81   2.21   3.65   1.71 IN COLUMNS 1,2,3,4
TOTAL LEAD GLASS ENERGY IS   1.53 GEV
  8 EMULSION TRACKS
          PRODUCTION        EXIT
 TRACK   DX/DZ  DY/DZ  DX/DZ  DY/DZ   I/I0  1/PBETA  V
   1     -.105  -.002                                2
          .018   .013
  1-1    -.091  -.078  -.091  -.078
          .003   .003   .003   .003
  1-2    -.070   .027  -.070   .027
          .002   .002   .002   .002
  1-3     .089   .114   .089   .114
          .003   .003   .003   .003
   2      .022   .503   .022   .503
          .007   .007   .007   .007
   3      .410   .353   .410   .353
          .007   .007   .007   .007
   4      .225  -.627   .225  -.627
          .008   .008   .008   .008
   5      .080  -.302   .080  -.302
          .005   .005   .005   .005
 10 SPECTROMETER TRACKS
 TRACK   DX/DZ  DY/DZ   1/P   Q UP DN CHISQ   ID    EPBG  BETA V XMISS YMISS F
   1                                          070000            1

  1-1    -.096  -.080   .462  1 12  8  .771 000020   .48  .025 2 -.021 -.018 1
                        .008                                .011
  1-2    -.072   .018   .658 -1 11  6 1.983 000010   .39  .012 2 -.010  .082 1
                        .010                                .013
  1-3     .096   .119   .392  1 11  7 1.921 000010   .28 -.000 2 -.090 -.073 1
                        .008                                .013
   2                                          000136            1

   3      .347   .290   .789 -1 10  0 1.506 000136  0.00 0.000 1 -.017 -.019 0
                        .350                                1.000
   4                                          000136            1

   5      .096  -.237   .773  1  8  0 1.886 000136  0.00 0.000 1 -.056 -.015 0
                        .350                                1.000
  0K     -.303  -.009   .326  0             000120  0.00 0.000 2             1
          .015   .015   .204                                1.000
 U-1     -.380   .636   .105 -1 11  0 1.943 000136  0.00 0.000 1  .291 -.219 0
                        .350                                1.000
  0 LINES OF AUXILLIARY TRACK INFORMATION
  1 LINES OF COMMENTS
0K IS AN ASSUMED K0-LONG WHICH INTERACTS IN PBG AND CALORIMETER
```

```
RUN  598 RECORD   1759
NGY  224 NH  1 NS  2
LAST DONE ON  81/07/14.
  2 VERTICES
NUMBER TYPE     X        Y        Z
   1     1     .481  -10.008   1.968
   2     2   -171.7    -80.7  1792.0
TOTAL CALORIMETER ENERGY IS  21.72 GEV
   2.44   1.24  14.16   3.89 IN COLUMNS 1,2,3,4
TOTAL LEAD GLASS ENERGY IS   3.89 GEV
  5 EMULSION TRACKS
          PRODUCTION        EXIT
 TRACK   DX/DZ  DY/DZ   DX/DZ  DY/DZ    I/I0  1/PBETA  V
  1       .161   .051    .161   .051
          .003   .003    .003   .003
  2      -.096  -.045                                  2
          .003   .003
 2-1     -.130   .011   -.125   .014
          .003   .003    .003   .003
 2-2     -.118  -.063   -.111  -.055
          .003   .003    .003   .003
 2-3      .100  -.084    .102  -.081
          .003   .003    .003   .003
  8 SPECTROMETER TRACKS
 TRACK   DX/DZ  DY/DZ    1/P   Q UP DN CHISQ    ID     EPBG  BETA V XMISS YMISS F
  1       .162   .051    .085  -1 12  8 1.168 000004   .31  .003 1 -.012 -.003 0
                        .005                                  .023
  2      -.095  -.042    .057   1        2.270 010000            1             0
          .002   .002    .001
 2-1     -.125   .013    .159  -1 11  8  .820 000130  1.07 -.020 2  .021  .005 1
                        .005                                  .062
 2-2     -.111  -.054    .134   1 12  7 1.897 000130   .97 -.039 2 -.009 -.014 1
                        .005                                  .076
 2-3      .102  -.082    .646   1 12  8  .244 000034   .28 -.046 2 -.037 -.002 1
                        .010                                  .079
 G-1     -.140  -.067   1.729   0    59        000001   .58       1 0.000 0.000 0
          .015   .015    .318                             .11
 G-2      .046  -.129   2.580   0    64        000001   .39       1 0.000 0.000 0
          .015   .015    .580                             .09
 G-3     -.016  -.129   2.968   0    65        000001   .34       1 0.000 0.000 0
          .015   .015    .716                             .08
  0 LINES OF AUXILLIARY TRACK INFORMATION
  0 LINES OF COMMENTS
```

```
RUN  602 RECORD   2032
OTT  000 NH 10 NS  4
LAST DONE ON  81/07/14.
  4 VERTICES
NUMBER TYPE    X        Y        Z
   1     1   -6.920  -11.720    1.350
   2     2      4.5    -27.8    280.0
   3     2  -1340.0   2950.0  28000.0
   4     2    670.0   -260.0   4000.0
TOTAL CALORIMETER ENERGY IS  11.74 GEV
   4.49   0.00   3.21   4.05 IN COLUMNS 1,2,3,4
TOTAL LEAD GLASS ENERGY IS   1.04 GEV
 10 EMULSION TRACKS
          PRODUCTION        EXIT
 TRACK   DX/DZ  DY/DZ  DX/DZ  DY/DZ   I/I0  1/PBETA  V
   1      .003   .008   .003   .008
          .002   .002   .002   .002
   2      .016  -.099                              2
          .002   .002
  2-1    -.048   .106                              3
          .005   .005
I2-1-1   -.107   .166  -.107   .166
          .003   .003   .003   .003
  2-2     .271  -.188   .271  -.188
          .005   .005   .005   .005
  2-3    -.125  -.594  -.125  -.594
          .008   .008   .008   .008
   3      .204  -.059   .204  -.059
          .004   .004   .004   .004
   4     -.408  -.024  -.408  -.024
          .006   .006   .006   .006
 E1-1     .166  -.061   .166  -.061
          .003   .003   .003   .003
 E1-2     .168  -.069   .168  -.069
          .003   .003   .003   .003
 15 SPECTROMETER TRACKS
 TRACK   DX/DZ  DY/DZ   1/P   Q UP DN CHISQ   ID    EPBG  BETA V XMISS YMISS F
   1      .003   .007   .052 -1  9  8 1.686 000004  .63   .005 1 -.002 -.006 0
                        .005                                .015
   2                         1             070000            1             0

  2-1                    .483  1             000100            2             1
                         .025
I2-1-1   -.107   .166    .565  1 12  8  .722 000100  .26   .116 3 -.066 -.019 0
                         .009                                .019
  2-2     .259  -.168   2.552 -1  8  0 4.163 000136  0.00 0.000 2 -.006 -.108 1
                         .350                              1.000
  2-3                                        000136            2

   3      .204  -.059    .679 -1 12  7  .531 000014  .06  -.017 1  .031 -.079 0
                         .010                                .026
   4                                         000136            1

 E1-1     .204  -.059    .679 -1 12  7  .531 000002  .06  -.017 4  .031 -.079 0
                         .010                                .026
 E1-2                         1             000002            4             0

 U-1     -.131   .138   1.603 -1  8  0 3.224 000136  0.00 0.000 1  .091  .021 0
                         .350                              1.000
 U-2      .237  -.116   1.619 -1  8  0  .670 000136  0.00 0.000 1 -.093 -.033 0
                         .350                              1.000
 U-3      .222  -.071   5.368 -1  8  0  .261 000136  0.00 0.000 1  .223 -.133 0
                         .350                              1.000
 U-4     -.118  -.227    .116 -1 10  0  .212 000136  0.00 0.000 1  .153 -.292 0
                         .350                              1.000
 U-5      .281   .050   1.681  1 11  6 1.461 000136  .29   .799 1 -.328  .182 0
                         .022                                .013

   0 LINES OF AUXILLIARY TRACK INFORMATION
   4 LINES OF COMMENTS
 2-1 SCATTERS AFTER 37 PLATES
 MOMENTUM FOR 2-1 = MOMENTUM OF I2-1-1 +300 MEV FOR ELASTIC SCATTER
 VERTEX FOR E-PAIR IS GUESSED AT FROM DESCRIPTION OF "SEVERAL PLATES"
 TRACK U-5 SEEMS TO BE A DEUTERON!
```

```
RUN  610 RECORD   4088
NGY  343 NH  2 NS  2
LAST DONE ON  81/07/14.
  3 VERTICES
NUMBER TYPE    X        Y       Z
   1     1  -12.508   -.003   1.548
   2     2     43.3    23.3   216.0
   3     1   -6.500   0.800  27.000
TOTAL CALORIMETER ENERGY IS   1.54 GEV
   0.00   0.00   0.00   1.54 IN COLUMNS 1,2,3,4
TOTAL LEAD GLASS ENERGY IS   1.35 GEV
  5 EMULSION TRACKS
          PRODUCTION        EXIT
 TRACK   DX/DZ  DY/DZ   DX/DZ  DY/DZ    I/I0  1/PBETA  V
  1      -.119  -.110   -.119  -.110
          .003   .003    .003   .003
  2       .236   .123                                  2
          .007   .007
 2-1      .169  -.140    .169  -.140
          .004   .004    .004   .004
 2-2     -.079  1.331   -.079  1.331            5.882
          .015   .015    .015   .015            1.000
 2-3      .387   .901    .387   .901            3.125
          .011   .011    .011   .011            1.230
  8 SPECTROMETER TRACKS
 TRACK   DX/DZ  DY/DZ    1/P   Q UP DN CHISQ    ID     EPBG  BETA V XMISS YMISS F
  1      -.118  -.110    .126 -1 12  8  .860 000004   .27 -.011 1 -.011  .009 0
                         .005                                .019
  2       .222   .115    .212  1        5.960 040000            1            0
                         .001
 2-1      .187  -.137    .676  1 12  7  .505 000014   .38  .008 2  .009  .008 1
                         .010                                .015
 2-2                                            000136            2

 2-3      .353   .943   3.058  1 12  0  .666 000136  0.00 0.000 2  .124 -.127 1
                         .350                                1.000
 0L       .227   .063    .370  0              000200            2            1
          .010   .010    .041
 L-1      .252   .035    .472  1  0  8        000100   .62  .061 3
                         .010                                .020
 L-2     -.526  -.004  10.000 -1  0  8        000010  0.00 0.000 3            0
                        4.000                                1.000
  0 LINES OF AUXILLIARY TRACK INFORMATION
  1 LINES OF COMMENTS
LAMDA-0 IS MADE FROM DOWNSTREAM SEGMENTS,P FROM BEND ANGLE
```

```
RUN  635 RECORD   4949
NGY  258 NH  1 NS  6
LAST DONE ON  81/05/31.
  4 VERTICES
NUMBER TYPE    X        Y        Z
   1     1   -2.858  -10.423    1.853
   2     2    680.7   -506.6   4304.0
   3     2  -1720.0   4470.0   9000.0
   4     1    1.009  -12.795    5.902
TOTAL CALORIMETER ENERGY IS  25.39 GEV
    .23  21.76   3.40   0.00 IN COLUMNS 1,2,3,4
TOTAL LEAD GLASS ENERGY IS   2.48 GEV
 10 EMULSION TRACKS
          PRODUCTION        EXIT
 TRACK   DX/DZ  DY/DZ  DX/DZ  DY/DZ   I/I0  1/PBETA  V
   1     -.024   .044  -.023   .044
          .002   .002   .002   .002
   2     -.068   .044  -.066   .054
          .002   .002   .002   .002
   3      .063  -.069   .063  -.067
          .002   .002   .002   .002
   4     -.190   .497                 1.11            3
          .007   .007                  .06
  4-1    3.740   .544  3.740   .544
          .060   .060   .060   .060
   5     1.384  -.153  1.279  -.091   0.98
          .015   .015   .015   .015    .05
   6     -.407  -.498  -.411  -.154
          .008   .008   .008   .008
  0V      .158  -.118                              2
          .004   .004
  V-1     .099   .027   .088   .025
          .003   .003   .003   .003
  V-2    -.231  -.199  -.249  -.181   0.91
          .005   .005   .005   .005    .05
 13 SPECTROMETER TRACKS
 TRACK   DX/DZ  DY/DZ   1/P   Q UP DN CHISQ   ID     EPBG  BETA V XMISS YMISS F
   1     -.023   .044   .002 -1  9  7 1.795 000004   .52  .000 1 -.001 -.007 0
                         .005                                .014
   2     -.069   .048   .975  1 12  8  .616 000014   .16  .002 1 -.015  .026 0
                         .014                                .017
   3      .063  -.070   .048  1 10  7 1.124 000130  1.38  .024 1 -.006  .010 0
                         .005                              1.000
   4                                          000136            1

  4-1                                         000136            3

   5                                          000136            1

   6     -.408  -.160   .351 -1 12  0  .252 000136  0.00 0.000 1  .008  .008 0
                         .350                              1.000
  0V      .154  -.118   .216  0       10.510 100000            1            0
          .002   .002   .001
  V-1     .090   .023   .362  1 11  8  .466 000100   .35  .055 2  .007 -.006 1
                         .007                                .015
  V-2    -.244  -.188  5.025 -1 11  0       000136  0.00 0.000 2            1
                         .350                              1.000
  0K      .970  -.554   .928  0             000020  0.00 0.000 2            1
          .004   .004   .005                              1.000
  K-1    1.322  -.061                       000010  0.00 0.000 4            1
  -       .005   .005                                      1.000
  K-2     .653 -1.000                       000010  0.00 0.000 4            1
          .005   .005                                      1.000
  0 LINES OF AUXILLIARY TRACK INFORMATION
  2 LINES OF COMMENTS
THIS IS A NEUTRAL BARYON DECAY
TRACK 4 UNDERGOES A NH=2, NS=1 INTERATION IN EMULSION PLATE 1

 0K IS PER SE
```

```
RUN  638 RECORD   9417
NGY  648 NH  1 NS  3
LAST DONE ON  81/07/14.
  2 VERTICES
NUMBER TYPE     X        Y       Z
   1     1  -16.342  -1.316    .533
   2     2     -0.3   -28.1   132.0
TOTAL CALORIMETER ENERGY IS   6.06 GEV
    .26   1.21   4.08    .51 IN COLUMNS 1,2,3,4
TOTAL LEAD GLASS ENERGY IS   6.22 GEV
  7 EMULSION TRACKS
          PRODUCTION        EXIT
 TRACK   DX/DZ  DY/DZ  DX/DZ  DY/DZ   I/I0  1/PBETA  V
  1      -.002  -.213                              2
          .005   .015
 1-1      .041  -.045   .041  -.045
          .002   .002   .002   .002
 1-2     -.009  -.046  -.009  -.046
          .002   .002   .002   .002
 1-3     -.174  -.275  -.174  -.275
          .005   .005   .005   .005
  2       .046   .231   .046   .231
          .004   .004   .004   .004
  3     -1.124   .284 -1.124   .284
          .013   .013   .013   .013
  4      -.614  -.506  -.614  -.506
          .009   .009   .009   .009
 15 SPECTROMETER TRACKS
 TRACK   DX/DZ  DY/DZ   1/P   Q UP DN CHISQ   ID    EPBG  BETA V XMISS YMISS F
  1      -.004  -.204   .168  1       2.610 020000             1            0
                        .001
 1-1      .045  -.044   .560  1 11  7  .615 000020   .67  .054 2 -.137 -.033 1
                        .009                                .014
 1-2     -.018  -.037   .448 -1 12  8  .691 000100   .50  .063 2 -.043 -.060 1
                        .008                                .012
 1-3     -.183  -.290   .548  1 10  0  .923 000136  0.00 0.000 2 -.049 -.005 1
                        .350                               1.000
  2       .048   .235   .117 -1 10  8  .529 000130   .39  .002 1 -.057 -.031 0
                        .005                                .012
  3                                          000136            1

  4                                          000136            1

 U-1      .065  -.866  1.424 -1 10  0 1.081 000136  0.00 0.000 1 -.379 -.029 0
                        .350                               1.000
 U-2      .085  -.192  5.794 -1 10  0 1.698 000136  0.00 0.000 1 -.047  .238 0
                        .350                               1.000
 U-3      .370  -.392  2.523  1 12  0 1.796 000136  0.00 0.000 1  .046 -.058 0
                        .350                               1.000
 U-4      .147  -.092   .281 -1  9  7 2.778 000132  3.50  .045 1 -.032  .082 0
                        .006                                .036
 G-1     -.002   .048  3.309  0    32        000001   .30       1 0.000 0.000 0
          .015   .015   .843                             .08
 G-2      .244  -.013  3.115  0    37        000001   .32       1 0.000 0.000 0
          .015   .015   .770                             .08
 G-3      .059  -.013  2.486  0    40        000001   .40       1 0.000 0.000 0
          .015   .015   .549                             .09
 G-4      .182  -.075   .322  0    47        000001  3.10       1 0.000 0.000 0
          .015   .015   .026                             .25
  0 LINES OF AUXILLIARY TRACK INFORMATION
  3 LINES OF COMMENTS
EMULSION TRACK 4 IS GRAY
TOF ON 2-1 IS IN DOUBT, PROBABLY IS K-
DB SAYS THAT TOF START PULLED EARLY BY E-M SHOWER IN TOF1
```

```
RUN  650 RECORD   6003
NGY  129 NH  0 NS  7
LAST DONE ON  81/07/14.
  2 VERTICES
NUMBER TYPE    X       Y       Z
   1     1    9.105  -8.745   1.843
   2     2    -6.7    -1.5    40.0
TOTAL CALORIMETER ENERGY IS   5.63 GEV
   3.36   1.66    .33    .27 IN COLUMNS 1,2,3,4
TOTAL LEAD GLASS ENERGY IS   1.75 GEV
 10 EMULSION TRACKS
          PRODUCTION        EXIT
 TRACK   DX/DZ  DY/DZ  DX/DZ  DY/DZ   I/I0  1/PBETA  V
   1      .043  -.077   .043  -.077
          .002   .002   .002   .002
   2     -.034  -.069  -.034  -.069
          .002   .002   .002   .002
   3     -.167  -.038                            2
          .038   .015
  3-1    -.397   .121  -.397   .121
          .006   .006   .006   .006
  3-2    -.220  -.256  -.211  -.255   0.80    1.250
          .005   .005   .005   .005   0.05    0.570
  3-3    -.387  -.308  -.410  -.309   0.89    2.630
          .007   .007   .007   .007   0.05    0.950
   4     -.041   .035  -.041   .035
          .002   .002   .002   .002
   5      .319   .319   .319   .319
          .006   .006   .006   .006
   6      .368   .127   .368   .127
          .005   .005   .005   .005
   7     -.285   .152  -.285   .152
          .005   .005   .005   .005
 14 SPECTROMETER TRACKS
 TRACK   DX/DZ  DY/DZ   1/P   Q UP DN CHISQ   ID    EPBG  BETA V XMISS YMISS F
   1      .043  -.077   .068 -1 11  7  .496 000004   .73  .007 1  .004  .006 0
                        .005                                .014
   2     -.032  -.070   .425 -1 12  8  .503 000034   .73  .017 1 -.008  .005 0
                        .007                                .014
   3     -.182  -.057   .175  1       3.890 040000          1            0
          .003   .003   .009
  3-1    -.391   .114   .845  1 12  7  .816 000016  0.00 -.005 2 -.006 -.014 1
                        .012                                .021
  3-2                                       000136          2

  3-3                                       000136          2

   4     -.071   .066  2.710  1 12  7  .554 000014  0.00  .062 1 -.015 -.009 0
                        .036                                .023
   5      .321   .329   .800  1 12  6  .264 000100  0.00  .214 1  .002 -.014 0
                        .012                                .013
   6      .380   .138  1.233  1 11  8  .206 000136  0.00 0.000 1 -.038  .017 0
                        .017                               1.000
   7                                        000136          1

   0L    -.018   .071   .407  0        .727 000200          2            1
          .002   .002   .006
  L-1    -.041   .051   .604  1 12  8 2.581 000100   .75  .124 3  .052 -.022 0
                        .009                                .013
  L-2                        -1            000136          3            0

  U-1    -.416   .114  3.763 -1 12  7  .597 000006   .19  .030 1  .228 -.031 0
                        .049                                .031
 0 LINES OF AUXILLIARY TRACK INFORMATION
 0 LINES OF COMMENTS
```

```
RUN  656 RECORD   2631
NGY  149 NH  6 NS  5
LAST DONE ON  81/07/10.
  2 VERTICES
NUMBER TYPE     X        Y        Z
   1     1  -16.877    .676    1.094
   2     2      8.0    22.6    530.0
TOTAL CALORIMETER ENERGY IS  26.07 GEV
    .21     .22  25.65   0.00 IN COLUMNS 1,2,3,4
TOTAL LEAD GLASS ENERGY IS  10.92 GEV
  8 EMULSION TRACKS
          PRODUCTION        EXIT
 TRACK   DX/DZ  DY/DZ  DX/DZ  DY/DZ   I/I0  1/PBETA  V
  1      -.031  -.042  -.031  -.042
          .002   .002   .002   .002
  2      -.048  -.044  -.048  -.044
          .002   .002   .002   .002
  3       .015   .043                              2
          .002   .004
 3-1      .018   .030   .022   .031
          .002   .002   .002   .002
 3-2      .027   .053   .026   .054
          .002   .002   .002   .002
 3-3     -.225   .001  -.239   .004
          .004   .004   .004   .004
  4      -.436   .142  -.436   .142
          .006   .006   .006   .006
  5      2.719  1.268  2.719  1.268
          .030   .030   .030   .030
 14 SPECTROMETER TRACKS
 TRACK   DX/DZ  DY/DZ   1/P   Q UP DN CHISQ   ID     EPBG  BETA V XMISS YMISS F
  1      -.031  -.042  0.000  1 11  8 1.079 000004   .76  .001 1  .007  .002 0
                        .005                                .026
  2      -.047  -.043   .317 -1 10  8 0.607 000130  0.33  .027 1  .011  .005 0
                        .007                                1.000
  3       .016   .043   .031  1       1.304 070000            1            0
                        .001
 3-1      .018   .034   .087  1 11  7 1.493 000130  4.27  .009 2  .041 -.034 1
                        .005                                .014
 3-2      .027   .055   .047 -1  9  8 1.353 000130  4.60 -.005 2 -.024  .003 1
                        .005                                .016
 3-3     -.239   .014  1.355  1 11  0  .362 000136  0.00 0.000 2  .075 -.003 1
                        .350                                1.000
  4      -.400   .113  2.514  1 10  0 1.140 000136  0.00 0.000 1 -.018 -.017 0
                        .350                                1.000
  5                                            000136            1

 G-1      .064   .156  2.919  0    13        000001   .34       1 0.000 0.000 0
          .015   .015   .698                            .08
 G-2      .126   .094   .325  0    21        000001  3.07       1 0.000 0.000 0
          .015   .015   .026                            .25
 G-3     -.060   .094  1.318  0    24        000001   .76       1 0.000 0.000 0
          .015   .015   .212                            .12
 G-4      .126   .032  1.229  0    30        000001   .81       1 0.000 0.000 0
          .015   .015   .191                            .13
 G-5      .002   .032   .299  0    32        000001  3.34       1 0.000 0.000 0
          .015   .015   .023                            .26
 G-6      .002  -.153  2.986  0    59        000001   .33       1 0.000 0.000 0
          .015   .015   .722                            .08
  0 LINES OF AUXILLIARY TRACK INFORMATION
  0 LINES OF COMMENTS
```

```
RUN  663 RECORD   7758
NGY  317 NH  0 NS  6
LAST DONE ON  81/07/10.
  2 VERTICES
NUMBER TYPE     X        Y        Z
   1     1  -16.922    -.860    1.524
   2     2    -53.0    -32.0 12960.0
TOTAL CALORIMETER ENERGY IS  55.50 GEV
   2.31    .61  49.49    3.09 IN COLUMNS 1,2,3,4
TOTAL LEAD GLASS ENERGY IS  27.27 GEV
  9 EMULSION TRACKS
          PRODUCTION        EXIT
 TRACK   DX/DZ  DY/DZ  DX/DZ  DY/DZ    I/I0  1/PBETA  V
   1     -.004  -.003                                 2
          .002   .002
  1-1     .000  -.008   .003  -.011
          .002   .002   .002   .002
  1-2    -.018  -.009  -.018  -.012
          .002   .002   .002   .002
  1-3    -.016   .001  -.016   .004
          .002   .002   .002   .002
   2      .021  -.010   .021  -.010
          .002   .002   .002   .002
   3     -.061  -.003  -.061  -.003
          .002   .002   .002   .002
   4      .046   .091   .046   .091
          .003   .003   .003   .003
   5     -.012   .114  -.012   .114
          .003   .003   .003   .003
   6     -.058   .213  -.058   .213
          .004   .004   .004   .004
 16 SPECTROMETER TRACKS
 TRACK   DX/DZ  DY/DZ   1/P    Q UP DN CHISQ   ID     EPBG  BETA V XMISS YMISS F
   1                          1            070000                1              0

  1-1     .003  -.012   .041  1 12  6 1.866 000136 22.29  .008 2  .010  .043 0
                        .007                                1.000
  1-2    -.019  -.012   .027 -1  9  8 2.264 000136 22.29 -.103 2  .025  .007 1
                        .005                                 .029
  1-3    -.018   .003   .065  1  8  8 1.162 000132 24.40  .001 2  .020  .024 1
                        .005                                1.000
   2      .022  -.011   .009  1  8  7 1.601 000004 19.92 -.072 1  .006 -.019 0
                        .005                                1.000
   3     -.078  -.005   .481 -1 11  8  .575 000136  2.54 -.048 1  .006  .000 0
                        .008                                1.000
   4      .051   .087   .444  1 11  8  .756 000132  3.05 -.089 1 -.030  .054 0
                        .008                                1.000
   5                                       000136            1

   6     -.074   .222   .587  1 11  8  .522 000032  0.00  .005 1 -.019  .184 0
                        .009                                 .021
 U-1     -.011   .015  2.365  1 10  0 3.525 000136  0.00 0.000 1  .126 -.146 0
                        .350                                1.000
 U-2     -.085   .010  1.337 -1 12  6 2.089 000136 19.98  .032 1  .136  .153 0
                        .018                                1.000
 G-1      .002   .107  1.813  0    23        000001   .55       1 0.000 0.000 0
          .015   .015   .342                              .10
 G-2      .126   .045   .926  0    30        000001  1.08       1 0.000 0.000 0
          .015   .015   .125                              .15
 G-3      .002   .045   .475  0    32        000001  2.11       1 0.000 0.000 0
          .015   .015   .046                              .20
 G-4      .002  -.017   .057  0    41        000001 17.59       1 0.000 0.000 0
          .015   .015   .002                              .59
 G-5     -.060  -.017   .629  0    42        000001  1.59       1 0.000 0.000 0
          .015   .015   .070                              .18
  0 LINES OF AUXILLIARY TRACK INFORMATION
  1 LINES OF COMMENTS

  THERE IS MUCH UNCERTAINTY IN TRUE SOLUTION FOR 1-1
```

```
RUN  665 RECORD   2113
NGY  380 NH  2 NS  5
LAST DONE ON  81/07/10.
  2 VERTICES
NUMBER TYPE     X        Y        Z
   1     1  -10.967 -11.365    .407
   2     2      0.6    -0.6    33.0
TOTAL CALORIMETER ENERGY IS   7.84 GEV
   0.00   4.35   2.24   1.25 IN COLUMNS 1,2,3,4
TOTAL LEAD GLASS ENERGY IS   1.89 GEV
  8 EMULSION TRACKS
          PRODUCTION        EXIT
 TRACK   DX/DZ  DY/DZ  DX/DZ  DY/DZ   I/I0  1/PBETA  V
   1     -.021  -.034  -.021  -.034
          .002   .002   .002   .002
   2      .018  -.018                              2
          .010   .010
  2-1     .142   .110   .142   .110
          .003   .003   .003   .003
  2-2    -.189   .043  -.189   .043   0.84    1.724
          .003   .003   .003   .003    .05     .500
  2-3    -.061  -.357  -.061  -.357   0.87
          .005   .005   .005   .005    .05
   3      .140   .328   .140   .328
          .005   .005   .005   .005
   4     -.381  -.408  -.381  -.408
          .007   .007   .007   .007
   5     -.512  -.252  -.512  -.252
          .007   .007   .007   .007
 13 SPECTROMETER TRACKS
 TRACK   DX/DZ  DY/DZ   1/P   Q UP DN CHISQ    ID    EPBG  BETA V XMISS YMISS F
   1     -.024  -.036   .057 -1  8  7 2.673 000004   .22 -.002 1  .068  .040 0
                         .005                              .012
   2                          1             070000            1             0

  2-1     .149   .103   .807  1 11  7 1.029 000014   .44  .009 2 -.140  .036 1
                         .012                              .015
  2-2    -.186   .051  1.145  1 10  0 1.000 000014  0.00 0.000 2 -.030 -.014 1
                         .350                              1.000
  2-3    -.068  -.365  1.930 -1 11  0 1.075 000014  0.00 0.000 2  .021  .047 1
                         .350                              1.000
   3      .136   .341   .466 -1 12  7 1.008 000010  0.00  .004 1  .020 -.000 0
                         .008                               .013
   4                                            000136            1

   5                                            000136            1

 U-1      .157  1.116  1.935  1 12  0  .488 000136  0.00 0.000 1 -.373 -.189 0
                         .350                              1.000
 U-2      .435  -.134   .891 -1 11  0  .920 000136  0.00 0.000 1 -.007  .008 0
                         .350                              1.000
 U-3      .112  1.103  3.508 -1 11  0  .398 000136  0.00 0.000 1  .247  .090 0
                         .350                              1.000
 G-1     -.169   .130  1.354  0    34        000001   .74       1 0.000 0.000 0
          .015   .015   .220                              .12
 G-2      .138   .068  2.726  0    38        000001   .37       1 0.000 0.000 0
          .015   .015   .630                              .08
  0 LINES OF ADXILLIARY TRACK INFORMATION
  1 LINES OF COMMENTS
2-2 AND 2-3 ARE IDENTIFIED FROM I/I0 IN EMULSION
```

```
RUN  665 RECORD   4023
NGY  289 NH  0 NS  8
LAST DONE ON  81/07/14.
  2 VERTICES
NUMBER TYPE     X        Y        Z
   1     1   12.040   -7.210    2.130
   2     2   -157.0   -308.0   6820.0
TOTAL CALORIMETER ENERGY IS  20.00 GEV
   2.00  13.84   3.42    .74 IN COLUMNS 1,2,3,4
TOTAL LEAD GLASS ENERGY IS  16.59 GEV
 11 EMULSION TRACKS
          PRODUCTION        EXIT
 TRACK   DX/DZ  DY/DZ   DX/DZ  DY/DZ    I/I0  1/PBETA  V
   1      .148  -.051    .148  -.051
          .003   .003    .003   .003
   2      .095   .019    .095   .019
          .002   .002    .002   .002
   3      .066   .021    .066   .021
          .002   .002    .002   .002
   4     -.023  -.045                              2
          .002   .002
  4-1     .005  -.090    .005  -.090
          .002   .002    .002   .002
  4-2    -.055  -.002   -.055  -.002
          .002   .002    .002   .002
  4-3    -.156   .087   -.156   .087
          .003   .003    .003   .003
   5     -.080   .453   -.080   .453
          .006   .006    .006   .006
   6      .661   .241    .661   .241
          .008   .008    .008   .008
   7    -1.760   .670  -1.760   .670
          .020   .020    .020   .020
   8     -.638  -.399   -.638  -.399
          .008   .008    .008   .008
 25 SPECTROMETER TRACKS
 TRACK   DX/DZ  DY/DZ    1/P   Q UP DN CHISQ    ID    EPBG  BETA V XMISS YMISS F
   1      .145  -.059    .422  1 12  8  .471 000134   .79 -.037 1  .061  .022 0
                         .007                                1.000
   2      .095   .014    .399 -1 12  7  .433 000130  1.12 -.443 1  .013 -.009 0
                         .007                                1.000
   3      .064   .017    .027 -1  9  7 1.555 000004   .80  .010 1  .004  .008 0
                         .005                                 .016
   4                          1             070000            1             0

  4-1     .005  -.090    .172 -1 11  8  .638 000136   .34 -.036 2 -.016  .001 1
                         .005                                 .021
  4-2    -.055  -.001    .122  1  9  7 1.977 000130  4.09 -.001 2 -.005 -.015 1
                         .005                                 .023
  4-3    -.157   .085    .684 -1 12  7  .924 000016  5.45  .000 2 -.114  .006 1
                         .010                                 .024
   5     -.059   .445   1.574 -1 11  0  .462 000136  0.00 0.000 1 -.099  .119 0
                         .350                                1.000
   6                                          000136            1             0

   7                                          000136            1             0

   8     -.616  -.391   1.621 -1 11  0 1.736 000136  0.00 0.000 1 -.083 -.280 0
                         .350                                1.000
 U-1     -.005  -.069    .982  1 12  7  .385 000136  1.13 -.380 1 -.004  .035 0
                         .014                                 .423
 U-2     -.365   .084   2.284  1 12  0 1.098 000136  0.00 0.000 1  .044 -.046 0
                         .350                                1.000
 U-3     -.544   .303   1.079 -1 12  7  .206 000016  0.00 -.005 1  .060 -.034 0
                         .015                                 .018
 G-1     -.048   .097    .974  0    29        000001  1.03       1 0.000 0.000 0
          .015   .015    .135                             .14
 G-2     -.111   .097    .287  0    30        000001  3.49       1 0.000 0.000 0
          .015   .015    .022                             .26
 G-3      .076   .035   3.055  0    36        000001   .33       1 0.000 0.000 0
          .015   .015    .748                             .08
 G-4     -.048   .035    .683  0    38        000001  1.46       1 0.000 0.000 0
          .015   .015    .079                             .17
 G-5     -.111   .035   2.221  0    39        000001   .45       1 0.000 0.000 0
          .015   .015    .464                             .09
 G-6      .139  -.027   3.112  0    44        000001   .32       1 0.000 0.000 0
          .015   .015    .769                             .08
 G-7     -.048  -.027    .908  0    47        000001  1.10       1 0.000 0.000 0
          .015   .015    .121                             .15
 G-8     -.111  -.027   1.511  0    48        000001   .66       1 0.000 0.000 0
          .015   .015    .260                             .11
 G-9     -.173  -.027   3.142  0    49        000001   .32       1 0.000 0.000 0
          .015   .015    .780                             .08
 G-10     .139  -.090    .728  0    53        000001  1.37       1 0.000 0.000 0
          .015   .015    .087                             .16
 G-11    -.048  -.090    .485  0    56        000001  2.06       1 0.000 0.000 0
          .015   .015    .047                             .20
  0 LINES OF AUXILLIARY TRACK INFORMATION
  1 LINES OF COMMENTS
DECAY IS NOT VISIBLE, COULD BE AN INTERACTION
```

```
RUN  670 RECORD     12
NGY  457 NH  4 NS  4
LAST DONE ON  81/07/10.
  2 VERTICES
NUMBER TYPE    X       Y       Z
   1     1    2.070 -11.840   1.850
   2     2     11.4    -3.3   155.6
TOTAL CALORIMETER ENERGY IS   3.65 GEV
    .27   1.66   0.00   1.72 IN COLUMNS 1,2,3,4
TOTAL LEAD GLASS ENERGY IS   1.71 GEV
  9 EMULSION TRACKS
          PRODUCTION        EXIT
 TRACK   DX/DZ  DY/DZ  DX/DZ  DY/DZ   I/I0  1/PBETA  V
  1       .021  -.050   .021  -.050
          .002   .002   .002   .002
  2       .073  -.021                              2
          .007   .002
 2-1      .126  -.248   .126  -.248   1.18    1.300
          .004   .004   .004   .004    .06     .930
 2-2      .195  -.201   .195  -.201   1.49    1.887
          .004   .004   .004   .004    .08     .700
 2-3     2.592 11.093  2.592 11.093   1.02
          .115   .115   .115   .115    .06
  3      -.346   .383  -.346   .383
          .007   .007   .007   .007
  4       .604   .867   .604   .867
          .012   .012   .012   .012
 U1       .079   .003   .079   .003
          .002   .002   .002   .002
 E1-1     .024   .107   .024   .107
          .003   .003   .003   .003
 10 SPECTROMETER TRACKS
 TRACK   DX/DZ  DY/DZ   1/P   Q UP DN CHISQ   ID    EPBG  BETA V XMISS YMISS F
  1       .023  -.050   .190 -1  9  8 1.174 000004   .31 -.007 1 -.034  .013 0
                        .006                                .017
  2                           1             070000            1            0

 2-1      .125  -.235  1.847  1 12  0 1.238 000100  0.00 0.000 2 -.019  .035 1
                        .350                                1.000
 2-2                                       000120            2

 2-3                                       000136            2

  3                                        000136            1

  4                                        000136            1

 U1       .079   .003  1.224  1 12  8  .827 000100   .03  .348 1  .122 -.024 0
                        .017                                .013
 E1-1     .024   .107  1.702  1 12  7  .679 000016   .66 -.002 1  .064 -.017 0
                        .023                                .019
 U-1     -.038   .125  3.611 -1 10  0 2.408 000136  0.00 0.000 1  .237  .072 0
                        .350                                1.000
  0 LINES OF AUXILLIARY TRACK INFORMATION
  1 LINES OF COMMENTS
TRACKS 2-1 AND 2-2 ARE IDENTIFIED FROM I/I0 IN EMULSION
```

```
RUN  671 RECORD   2642
NGY  459 NH  7 NS  4
LAST DONE ON  81/07/14.
  2 VERTICES
NUMBER TYPE     X        Y        Z
   1     1   -1.690  -11.290   1.330
   2     2   -281.0    95.0   2326.0
TOTAL CALORIMETER ENERGY IS   4.84 GEV
    .26   1.87   1.04   1.67 IN COLUMNS 1,2,3,4
TOTAL LEAD GLASS ENERGY IS   1.51 GEV
  6 EMULSION TRACKS
          PRODUCTION        EXIT
 TRACK   DX/DZ  DY/DZ  DX/DZ  DY/DZ   I/I0  1/PBETA  V
   1     -.122   .042                              2
          .003   .003
  1-1    -.132   .121  -.144   .101
          .003   .003   .003   .003
  1-2    -.151   .068  -.152   .080
          .003   .003   .003   .003
  1-3     .389   .702   .437   .554   1.83
          .009   .009   .009   .009    .09
   2      .193   .148   .193   .148
          .004   .004   .004   .004
   3      .025  -.061   .025  -.061
          .002   .002   .002   .002
 11 SPECTROMETER TRACKS
 TRACK   DX/DZ  DY/DZ   1/P   Q UP DN CHISQ   ID    EPBG  BETA V XMISS YMISS F
   1                          1             070000              1           0

  1-1    -.159   .114  1.044  1 10  8  .721 000014  0.00  .022 2  .143 -.038 1
                       .014                                  .018
  1-2    -.152   .080   .925 -1 12  7  .099 000014   .29  .018 2  .075 -.021 1
                       .013                                  .015
  1-3     .477   .663  8.440  1 12  0 1.137 000136  0.00 0.000 2 -.334 -.267 1
                       .350                                 1.000
   2      .193   .148   .504  1 12  7  .604 000100   .29  .078 1  .034  .009 0
                       .008                                  .012
   3      .025  -.061   .058 -1 12  8 1.752 000004   .30 -.003 1  .020  .030 0
                       .005                                  .020
  U-1    -.341   .226   .822 -1  9  0  .306 000136  0.00 0.000 1  .142 -.334 0
                       .350                                 1.000
  U-2     .095  -.127  4.571 -1  8  0 5.150 000136  0.00 0.000 1-2.552 1.941 0
                       .350                                 1.000
  U-3    -.531  -.152  1.868 -1 10  0 2.964 000136  0.00 0.000 1 -.108 -.187 0
                       .350                                 1.000
  U-4    -.574  -.262 12.329 -1  8  0 2.824 000136  0.00 0.000 1 -.053  .723 0
                       .350                                 1.000
  G-1    -.122   .006  2.417  0    50        000001   .41       1 0.000 0.000 0
          .015   .015   .526                              .09
 0 LINES OF AUXILLIARY TRACK INFORMATION
 0 LINES OF COMMENTS
```